

ABSTRACT

Title of Dissertation: RADIATION SYNTHESIS OF IONIC
LIQUID POLYMER ELECTROLYTE
MEMBRANE FOR HIGH
TEMPERATURE FUEL CELL
APPLICATIONS

Kevin Robert Mecadon, Doctor of
Philosophy, 2020

Dissertation directed by: Professor Mohamad Al-Sheikhly,
Department of Material Sciences and
Engineering

The purpose of this thesis was to design, synthesize and analyze innovative anhydrous fuel cell membranes that can operate at temperatures above 100°C. Operating at this higher temperature region improves performance and reliability of fuel cells: increasing proton mobility, enhancing reaction kinetics, increasing catalysis activity and reducing carbon monoxide poisoning. Traditional polymer electrolyte membrane fuel cells (PEMFCs) do not operate efficiently above 100°C because water is used as a proton conductive medium through the Grotthuss hopping mechanism. Through substituting

water with protic ionic liquids and grafting onto fluorocarbon films, a new proton conductive network solid state PEM has been developed. These membranes can perform at high temperature above 100°C. Polymers were selected for grafting based on the following properties: high proton conductivity, low electrical conductivity, high mechanical properties, high chemical resistance, and high temperature and humidity stability.

The method used to synthesize these anhydrous polymer electrolyte membranes (PEMs) was radiation grafting using heterocyclic protic ionic liquid monomers and fluorocarbon substrates. PEMs were prepared at the Medical Industrial Radiation Facilities (MIRF) at the National Institute of Standards and Technology (NIST). MIRF is a 10.5 MeV electron beam accelerator, which was used to radiate the fluorocarbon substrate and then indirectly graft heterocyclic protic ionic liquids to create PEMs. After synthesis, the extent and uniformity of PEM composition was analyzed using FTIR microscopy, SEM/EDS, SANS and their proton conductivity as measured by EIS.

Through this research, indirect radiation grafting was shown to covalently bond ionic liquids onto fluorocarbon substrates to synthesize PEMs. The resulting ionic liquid PEMs showed proton conductivities greater than 10^{-3} S/cm above 100°C that behaved independent of humidity. The ionic liquid PEMs also demonstrated a positive correlation of increasing proton conductivity with increasing temperatures above 100°C even after the PEMs are dehydrated. The chemical properties and structure of the grafted ionic liquids greatly affects the proton conductive mechanisms present in the PEMs. These trends found through the course of this research will help the development of future anhydrous PEM with higher proton conductivity, performance, and reliability.

RADIATION SYNTHESIS OF IONIC LIQUID POLYMER ELECTROLYTE
MEMBRANE FOR HIGH TEMPERATURE FUEL CELL APPLICATIONS

by

Kevin Mecadon

Dissertation submitted to the Faculty of the Graduate School of the
University of Maryland, College Park, in partial fulfillment
of the requirements for the degree of
Doctor of Philosophy

2019

Advisory Committee:

Professor Mohamad Al-Sheikhly, Chair

Dr. Joseph Robertson

Professor Eric D. Wachsman

Professor Lourdes G. Salamanca-Riba

Professor Gary A. Pertmer, Dean Representative

© Copyright by
Kevin Robert Mecadon
2019

Acknowledgements

This thesis represents the accumulation of 6 years of scientific research which could not be completed without the collaboration and support of many people. First, I would like to specially acknowledge my advisor **Professor Mohamad Al-Sheikhly**. His guidance, knowledge, and continued belief in my abilities as a student and researcher allowed me to complete this body of work.

I would also like to thank my committee members: **Dr. Joseph Robertson**, **Professor Eric D. Wachsman**, **Professor Lourdes Salamanca-Riba** and **Professor Gary Pertmer**, for their scientific review and helping me to think critically about my research.

My sincere thank you to researchers from the National Institute of Standards and Technology including **Dr. Fred Bateman**, **Dr. Lonnie Cumberland**, **Dr. Ileana Pazos** of the Radiation Physics Department for the use of the linear accelerator, Co-60 irradiator, and electron paramagnetic resonance facilities. Special thanks to **Dr. Joseph Robertson**, **Dr. Yaw Obeng**, **Dr. Marcus Bleuel** for sharing their time, guidance and expertise for this research.

Members of the Al-Sheikhly lab group throughout my tenure have also been instrumental in the completion of this work. I would like to thank **Dr. Zois Tsinas** for his instruction and guidance with the use of scanning electron microscopy, Fourier transform infrared spectroscopy, and numerous other characterization techniques. **Dr. Ileana Pazos** for her assistance with irradiations of PEM samples and for her help with the electron paramagnetic spectroscopy work. **Dr. Travis Deitz** for great discussions on radiation

and polymer grafting. Many thanks to my fellow group members including, **Dr. Najlaa Hassan, Azadeh Farzaneh and Matt LeBlanc** for their valuable scientific discussions.

Thank you to undergraduates **Megan Lilly, Monica Cardenas and Michael Floccare** for their assistance with sample preparation and useful discussions concerning experimental development.

Thank you to **Jonathan Hummel** at The Maryland NanoCenter for his training on the scanning electron microscope.

Thank you to 3M Company, **Michael Yandrasits**, for testing my PEM samples and providing 3M reference samples used for EIS measurements.

This research was funded and supported by the Nuclear Regulatory Commission (NRC) through the NRC Nuclear Education Grant Program under the federal grant number NRC-HQ-12-G-38-0023.

I would also like to thank the staff of the University of Maryland Materials Science and Engineering Department, including **Michael McNicholas, Olivia Noble, Ginette Villeneuve, Jenna Bishop, Kay Morris, and Novy Choi** for their assistance. I especially would like to thank **Dr. Kathleen Hart** and **N. Adaire Parker** for their expert guidance and welcome suggestions towards achieving my educational goals.

Last but certainly not least, I would like to express my appreciation for my family, to my mother and father, **Verna and Mark Mecadon** for their continued love and support throughout my entire tenure here at the University of Maryland. To my Grandfather, **Robert H. Hutzler**, who instilled a love of problem solving and engineering mindset and who continues to this day to inspire me.

Table of Contents

Acknowledgements.....	ii
Table of Contents	iv
List of Figures	viii
List of Tables	xv
List of Abbreviations	xvi
1.0 Introduction.....	1
1.1 History of Hydrogen Fuel Cell Development.....	1
1.1.1 Milestones in Fuel Cell development	2
1.1.2 Hydrogen as a Renewable Energy Source	6
1.2 Polymer Electrolyte Membrane Fuel Cell Operation	6
1.2.1 Mechanisms of Proton Conductivity	8
1.3 Disadvantages of Current PEMFC.....	13
1.4 Application of Radiation on Materials.....	16
1.4.1 History of Radiation Treatment on Materials	17
1.4.2 Radiation Physics.....	18
1.4.3 Radiation Chemistry	34
1.4.4 Radiation Grafting Methods	37
1.5 Alternative High Temperature Fuel Cell Designs	39
2.0 Chemistry of Proton Conductive Ionic Liquid Membrane	43
2.1 Ionic Liquids	43
2.1.1 Acidic Ionic Liquids	45
2.1.2 Proton Conductive Ionic Liquids	50
2.2 Polymer substrate for radiation grafting	51

2.3	Design of Protic Ionic Liquid Membranes.....	55
3.0	Experimental Methods and Approach	59
3.1	Material Design.....	59
3.1.1	Substrate Selection.....	59
3.1.2	Proton Conductive Ionic liquid.....	62
3.2	Radiation Chemistry/Grafting.....	63
3.3	Analysis Techniques	68
3.3.1	Electron Paramagnetic Resonance (EPR).....	69
3.3.2	Degree of Grafting	71
3.3.3	Cross-Section Microtome Sample Preparation	72
3.3.4	Fourier Transform Infrared Spectroscopy (FTIR)	73
3.3.5	Scanning Electron Microscopy and Energy-Dispersive X-ray Spectrometry	73
3.3.6	Proton Conductivity - Electrochemical Impedance Spectroscopy.....	74
3.4	Small Angle Neutron Scattering	89
4.0	Results and Discussion	92
4.1	EPR Analysis of Free Radicals in Fluorocarbon Substrates.....	92
4.1.1	EPR Analysis of FEP	93
4.1.2	EPR Analysis of PCTFE.....	98
4.1.3	EPR Analysis of PVF.....	102
4.2	Radiation Grafting Results.....	106
4.2.1	Direct Radiation Grafting Synthesis	106
4.2.2	Indirect Radiation Grafting Synthesis.....	109
4.2.3	Indirect Radiation Grafting Parameters	111
4.3	PEM Composition Analysis.....	117
4.3.1	SEM/EDS Cross-section Analysis.....	117
4.3.2	Ramman Spectroscopy.....	153
4.3.3	FTIR/ATR Measurements	153

4.4	Proton Conductivity of PEM	161
4.4.1	Two Point Parallel Plate Capacitor Probe EIS Analysis.....	162
4.4.2	Four Point Probe EIS Analysis	171
4.4.3	Distribution of Relaxation Time (DRT) and Equivalent Circuit Model Analysis of EIS Data.....	182
4.5	SANS Measurements	191
5.0	Conclusion and Future Plan	194
5.1	Conclusions.....	194
5.1.1	PEM design.....	194
5.1.2	PEM Synthesis	194
5.1.3	PEM Performance	200
5.2	Contributions to Science	202
5.3	Future Work	203
Appendix A: EIS Proton Conductivity Measurements and Equivalent Circuit Modeling		
	207
	8122016FEP-12	213
	8112016PCTFE-12	218
	8122016PVF-12.....	221
	PCB 2-Point Probe Summary	225
	Au 2-Point Probe Analysis.....	227
	3M 825EW Control	227
	9102018FEP-13	229
	8112016PCTFE-16	233
	9102018PVF-13	235
	Au 2-Point Probe Summary: 5-vinylpyridine.....	238

9122018FEP-2Na.....	239
3222017PVF-1a	244
Au 2-Point Probe Summary: 4-vinylpyrimidine.....	246
4-Pt Point Probe	247
3M 825EW Control	247
322017FEP-1b	250
3222017PCTFE-3c	252
322017PVF-1e	254
Pt 4-Point Probe Summary: Humidity	257
Pt 4-Point Probe Summary: Temperature	257
Results/Discussion EIS Analysis	258
Appendix B: DRT Analysis of EIS Data	260
List of References	278

List of Figures

Figure 1.1: First Fuel Cell developed by William Robert Grove.[6]	2
Figure 1.2- Future projected development of hydrogen fuel market[3]	5
Figure 1.3: Basic description of hydrous proton transport in PEM and catalysis reactions at the anode and cathode.[5]	7
Figure 1.4: Mechanisms of Proton conductivity in Nafion: (a) Vehicular Mechanism (b) Grotthuss Mechanism and (c) Surface Mechanism.[24].....	8
Figure 1.5: Mechanisms of Proton Conductivity in Nafion (a) Mechanisms (b)Proton conductivity electrochemical circuit model [26]	10
Figure 1.6- Proton conductivity of Nafion as a function of relative humidity of vapor phase showing the contribution of Grotthuss, Surface and Vehicular proton conductive mechanism. [26].....	11
Figure 1.7- Hydronium ion complexes found in water (a) Hydronium ion (b) Zundel Ion (c) Egon ions	12
Figure 1.8- Reactions at Platinum Catalytic Electrode: (a) Hydrogen Adsorption (b) Carbon Monoxide Poisoning	15
Figure 1.9- Carbon monoxide fractional coverage of Pt electrodes as a function of temperature and carbon monoxide concentration [38]	16
Figure 1.10- Ionizing radiation track in condensed matter and its interactions [47]	19
Figure 1.11- Radiolysis of Water: physical and chemical interaction [49]	21
Figure 1.12- Dominant Gamma radiation interactions with matter dependent on photon energy and atomic number of target[47].....	23
Figure 1.13- Events in the photoelectric scattering process [51]	23
Figure 1.14 Events that occur in Compton scattering[51]	25
If a gamma ray has energy higher than 1.022 MeV, it may interact with matter by a process called pair production.[51] The photon, passing near the nucleus of an atom, is subjected to strong field effects from the nucleus. The photon may undergo a mass-energy conversion forming positron and electron pair. As depicted in Figure 1.15.[51]	26
Figure 1.15- Events that occur in pair production[51].....	26
Figure 1.16- Gamma radiation attenuate through materials. [52].....	28

Figure 1.17 -Element Mass Attenuation Coefficient[52].....	29
Figure 1.18 - Penetration of gamma ray in water produced by a Cobalt-60 source [45]..	30
Figure 1.19 -Electron interactions with matter (a) electron beam traveling through vacuum (b) Inelastically scattering producing secondary electrons (c) elastically scattering off the nucleus of an atom [53]	31
Figure 1.20 - Penetration of electron beam in water [55]	33
Figure 1.21 - Irradiated polymer chains undergo two competing reactions; scission and cross-linking. Dominance is based on radiation conditions and chemical properties of the polymer.	35
Figure 1.22 - Simplified structure of a grafted copolymer consisting of a polymer A backbone and polymer B side chains.....	36
Figure 1.23 -Direct Radiation Grafting Method: ionic liquid monomer and substrate are irradiated together	38
Figure 1.24 -Indirect Radiation Grafting Method: ionic liquid monomer added after substrate is irradiated	38
Figure 1.25 - Microstructure comparison of PEM: (left) Nafion™ and (right) sulfonated polyetherketone; chemical properties of nanochannels and their effect on proton conductivity[69].....	40
Figure 1.26 -Proton Conductivity of heterocyclic protic ionic liquids[69].....	42
Figure 2.1 - Ionic liquid types: Aprotic, Protic and Zwitterionic and their applications[88].....	44
Figure 2.2 - Example of Protic Ionic Liquid: Imidazole proton conductivity can occur by H ⁺ exchange of near neighbors which act as both proton donors and acceptors.[88]	45
Figure 2.3 - Sub-groups of Bronsted acid ionic liquids (BAILs); protic acidic ionic liquids (PAILs) [90].....	46
Figure 2.4 - Relationship between pKa and boiling point for ionic liquid systems [91] ..	47
Figure 2.5 : Heterocyclic Amine Protic Ionic Liquid and their pKa values	51
Figure 2.6 - Fluorocarbon polymers with available sites for radiation grafting.	52
Figure 2.7 -Mechanical Properties: (a) Tensile Strength and (b)Elongation at break for Fluoropolymers that have been irradiate with gamma radiation. [104].....	55

Figure 2.8- Different ways ionic liquids can be incorporated into polymer membranes[88]	56
Figure 2.9 -Radiation Grafting Reactions: 4-vinylpyridine onto FEP substrate.....	57
Figure 2.10- Depiction of Microstructure of radiation grafted 4-vinylpyrindine to FEP PEM.	58
Figure 3.1- Chemical structure of fluorocarbon substrates FEP, PCTFE and PVF.....	61
Figure 3.2- Ionic liquids investigated in this research	63
Figure 3.3: (Top) Electron beam accelerator “MIRF” at NIST; (bottom) Diagram of radiation sample setup: Electron beam (yellow), sample chamber (pink) and sample (green).[108]	64
Figure 3.4: Indirect Radiation Grafting Competing Reactions; (1) Polymerization (2) Grafting (3) Cross-linking (4) Oxidation.....	65
Figure 3.5: Overview of indirect radiation grafting procedure used to synthesize PEM	67
Figure 3.6: Grafting Front Model: Cross-section View of Indirect Radiation Grafting [113].....	68
Figure 3.7: 2-point probe EIS test cells: (a) 2-point probe PCB gold plated electrode (b) 2-point probe gold electrode	77
Figure 3.8: 4-point probe EIS test cells (a) 4- point probe platinum wire electrodes (b) 4-point probe high temperature PCB cell Cu/Ni/Pt plated wire electrode.....	78
Figure 3.9: PCB 2-point probe measurement of 3M 825EW control at 80°C; (a) Nyquist Plot (b) Bode Plots; (red line) EIS data (green line) simplified circuit model fit.	80
Figure 3.10- (a) Equivalent circuit model of 2-point Au parallel plate capacitor test cell (b) diagram of EIS measurements 2-point probe cell: (yellow) electrodes (blue) PEM (c) Simplified circuit model.	81
Figure 3.11: Limiting frequency range of 2-point parallel plate capacitor probe EIS measurements (black). Threshold frequency range simulated for C_{PEM} of 60pF predicted for the PCB 2-point probe and Cdl 5uF.	83
Figure 3.12: 4-point probe analysis 3M Company 825EW Control at 60°C, 20% R.H.; (a) Nyquist Plot (b) Bode Plots; (red line) EIS data (green line) simplified circuit model fit.....	85

Figure 3.13: (a) Equivalent circuit model of 4-point Pt wire test cell (b) Diagram of EIS measurement 4-point probe cell (c) Simplified circuit model.	87
Figure 3.14: Limiting frequency range of 4-point wire probe EIS measurements (black). Threshold frequency range simulated for C_{PEM} of 0.25 pF predicted for the 4-point probe and Cdl 0.5uF.....	89
Figure 3.10- SANS beam line at NIST[124].....	90
Figure 3.11- SANS measurement of Nafion Membrane showing the proton conductive water cylinder nanostructure and ionomer structure within the PEM[121].....	91
Figure 4.1- 1 st derivative EPR spectrum of irradiated FEP substrate treated with MIRF set at 10.5MeV electron beam, 50 kGy dose at a 1000 kGy/hr dose rate.	94
Figure 4.2- Free radicals generated by radiation treatment of FEP	96
Figure 4.3- FEP free radical decay: (a) Area of EPR absorption spectrum vs. time. (b) Free radical decay of irradiated FEP thin films fit with a 2 nd order reaction decay in red.	97
Figure 4.4- 1 st derivative of EPR spectrum of irradiated PCTFE substrate treated with the MIRF set at 10.5 MeV electron beam, 50 kGy Dose at a 1000 kGy/hr. dose rate.	99
Figure 4.5 - Free radicals generated by radiation treatment of PCTFE	100
Figure 4.6- PCTFE free radical decay: (a) Area of EPR absorption spectrum vs. time. (b) Free radical decay of irradiated PCTFE thin films fit with a 2 nd order reaction decay in red.	101
Figure 4.7- 1 st derivative EPR spectrum of irradiated PVF substrate treated with the MIRF set at 10.5MeV electron beam, 50kGy dose at a 1000kGy/hr. dose rate.	103
Figure 4.8- Free Radicals generated by radiation treatment of PVF	104
Figure 4.9- PVF free radical decay: (a) Area of EPR absorption spectrum vs. time. (b) Free radical decay of irradiated PVF thin films fit with a 2 nd order reaction decay in red.	105
Figure 4.10: Direct Radiation Grafting Procedure-Radicals were generated in both ionic liquid monomer and substrate which caused competing reactions which prevented grafting.....	108
Figure 4.11: Indirect radiation grafting process.....	109

Figure 4.12: Indirect radiation grafting 4-vinylpyridine onto FEP, monomer was added 15 mins after radiation treatment PHT (n=2).....	112
Figure 4.13 -Indirect grafting of 4-vinylpyridine onto FEP, free radicals were preserved under dry ice, monomer added after 6 hrs. (n=3)	113
Figure 4.14: Indirect radiation grafting 4-vinylpyridine onto PCTFE (n=2).....	114
Figure 4.15: Indirect radiation grafting 4-vinylpyridine onto PVF (n=2)	115
Figure 4.16- Indirect grafting of 4-vinylpyridine onto PVF, free radicals were preserved under dry ice, monomer added after 6 hrs. (n=3)	116
Figure 4.17- SEM Image of FEP substrate	119
Figure 4.18- EDS of FEP substrate.....	119
Figure 4.19- SEM image of sample 20180910 FEP-10a	121
Figure 4.20- EDS of center of cross-section for sample 20180910 FEP-10a	121
Figure 4.21- (a) Three SEM/EDS line scans across the cross-section of sample 20180910 FEP-10a and corresponding test area results for (b) red (c) green (d) blue.....	125
Figure 4.22- SEM image of sample 20180910FEP-11a	126
Figure 4.23- EDS from center of sample 20180910FEP-11a cross-section	126
Figure 4.24- (a) Three SEM/EDS line scans across the cross-section of sample 20180910 FEP-11a and corresponding test area results for (b) red (c) green (d) blue.....	130
Figure 4.25- SEM Image of untreated PCTFE substrate	131
Figure 4.26- EDS of untreated PCTFE substrate.....	131
Figure 4.27- SEM image of Sample 8112016PCTFE-16	133
Figure 4.28- EDS of Sample 8112016PCTFE-16.....	133
Figure 4.29- (a) Three SEM/EDS line scans across the cross-section of sample 8112016PCTFE-16 and corresponding test area results for (b) red (c) green (d) blue...	136
Figure 4.30- SEM Cross-section of Sample 3222017PCTFE-3c	137
Figure 4.31- EDS of Sample 3222017PCTFE-3c.....	138
Figure 4.32- (a) Three SEM/EDS line scans of Sample 3222017PCTFE-3c cross-section and corresponding test area results for (b) red (c) green (d) blue.....	141
Figure 4.33- SEM image of PVF substrate	142
Figure 4.34- EDS PVF substrate.....	142
Figure 4.35- SEM of Sample 20180910PVF-10b cross-section.....	144

Figure 4.36 -EDS of Sample 20180910PVF-10b cross-section	144
Figure 4.37 -(a) Three SEM/EDS line scans of Sample 20180910PVF-10b cross-section and corresponding test area results for (b) red (c) green (d) blue.	147
Figure 4.38 -SEM cross-section of 3222017PVF-1a (black bar is 50um).....	148
Figure 4.39 -EDS of sample 3222017PVF-1a	149
Figure 4.40 - (a) Three SEM/EDS line scans of sample 3222017PVF-1a cross-section and corresponding test area results for (b) red (c) green (d) blue.....	152
Figure 4.41 : FTIR analysis of (a) FEP substrates acid treated (b) 8122016FEP-9 PEM synthesis with 4-vinylpyridine and acid treatments for proton conductivity measurements.	155
Figure 4.42 : FTIR analysis of (a) PCTFE substrates acid treated (b) 8112016PCTFE-9 PEM synthesis with 4-vinylpyridine and acid treatments for proton conductivity measurements.....	158
Figure 4.43 : FTIR analysis of (a) PVF substrates acid treated (b) 8122016PVF-9 PEM synthesis with 4-vinylpyridine and acid treatments for proton conductivity measurements.	160
Figure 4.44 - 2-point Probe Parallel Plate Capacitor Test Cells: (a) PCB test cell gold plated electrode (b) Teflon conductivity test cell with gold electrodes	163
An example of the EIS spectrums of samples using 2-Point Probe Parallel Plate Electrode Test Cells is shown below in Figure 4.45 for sample 81212016PVF-12 grafted with 4-vinylpyrimidine. The simplified circuit model shown in Figure 3.10c was used to analyze this data. The R_{PEM} was determined to be 20.12 Ω . The proton conductivity of this ionic liquid PEM was calculated as 1.14E-2 S/cm.	163
Figure 4.46 -EIS proton conductivity vs. temperature PCB 2-Point Parallel Plate Capacitor Test Cell: (black) 3M 825EW Control, 4-vinylpyridine PEM: (red) 81212016FEP-12, (green) 8112016PCTFE-12, (blue) 81212016PVF-12; samples were acid treated with 5% HNO_3 , $n = 1$	165
Figure 4.48 : Conductivity data of 4-vinylpyridine grafted onto fluorocarbon films:	172
(black) FEP-14: 60.17% grafting, (red) PCTFE-8: 37.7% grafting, (blue) PVF-12: 280% grafting, (green) 3M 825EW standard control.....	172

Figure 4.49: 5-vinylpyrimidine 50.5% grafting on PVF-1d and acid treated: (black) 5% nitric acid, (red) 5% sulfuric acid, (blue) 5% phosphoric acid, (green) 3M 825EW standard control.....	173
Figure 4.50: 4-point probe EIS test cells (a) PCB 4-point probe Cell Cu/Ni/Pt plated (b) 4- point probe platinum wires	175
Figure 4.52: EIS Proton conductivity as a function of relative humidity at 80°C treated with 5% HNO ₃ : (black) 3M 825EW Control; PEM were grafted with 5-vinylpyrimidine: (red) 3222017FEP-1b, (green) 322017PCTFE-3c, (blue) 3222017PVF-1e, n = 3.....	181
Figure 4.53 - EIS proton conductivity as a function of temperature without humidity control treated with 5% HNO ₃ : (black) 3M 825EW Control; PEM grafted with 5-vinylpyrimidine: (red) 3222017FEP-1b, (green) 322017PCTFE-3c, (blue) 3222017PVF-1e, n = 3	181
Figure 4.54- SANS measurement of PVF grafted with 50.5% 5-vinylpyrimidine: (gray) untreated PVF film (Yellow) radiation grafted PVF with 5-vinylpyrimidine (blue) wet radiation grafted PVF with 5-vinylpyrimidine (red) 5% nitric acid treated radiation grafted PVF with 5-vinylpyrimidine DI water treated.....	192
Figure 5.1: Indirect radiation grafting process.....	195
Figure 5.2: Chemical Structure of heterocyclic amine ionic liquids that can be used for PEMFC applications	204

List of Tables

Table 1.1: Proton Transport Mechanism Step Times and Distances in Nafion [26]	11
Table 1.2: Sources of Impurities that Affect Hydrogen Fuel Cell operation [35]	14
Table 1.3: Bond Dissociation Energies for Fluorocarbon Polymers[48]	20
Table 2.1- The proton free energy level diagram for Ionic Liquids formed from strong acids and bases to yield neutral ionic liquid products.[91]	48
Table 2.2: Material Properties of Fluorocarbon Substrates [57],[66],[100],[101],[102],[103]......	53
Table 4.1: Indirect radiation grafting results of 4-vinyl pyridine onto fluorocarbon substrates varying ionic liquid monomer concentration	111
Table 4.2: Indirect radiation grafting 4-vinylpyridine and 5-vinylpyrimidine onto fluorocarbon substrates at high dose rates	117
Table 4.3: EDS Atomic composition analysis of FEP Substrate	120
Table 4.4: EDS atomic analysis of sample 20180910 FEP-10a.....	121
Table 4.5: EDS analysis from center of 20180910FEP-11a cross-section	127
Table 4.6: EDS atomic analysis of untreated PCTFE.....	132
Table 4.7: EDS analysis of atomic composition of Sample 8112016PCTFE-16	134
Table 4.8: EDS analysis of Sample 3222017PCTFE-3c atomic composition.....	138
Table 4.9: EDS analysis of untreated PVF atomic composition	143
Table 4.10: EDS analysis of Sample 20180910PVF-10b atomic composition	145
Table 4.11: EDS analysis of sample 3222017PVF-1a atomic composition	149
Table 4.12: Conductivity Results of 2-point Au Parallel Plate Cell	170
Table 4.13: EIS conductivity Data 4-Point Surface probe Pt Wire.....	178
Table 5.1: Comparison of Substrate-Dominant free radical structure after radiation treatment and decay rate.	197
Table 5.2: Summary of SEM/EDS measurements	199

List of Abbreviations

FC	Fuel Cell
PEM	Polymer Electrolyte Membrane
DoG	Degree of Grafting
EPR	Electron Paramagnetic Resonance
SEM	Scanning Electron Microscopy
EDS	Energy Dispersive X-Ray Spectroscopy
ATR	Attenuated total reflectance
FTIR	Fourier transform infrared spectroscopy
pK _a	Acid dissociation constant
MIRF	Medical, Industrial Radiation Facility
NIST	National Institute of Standards and Technology
NASA	National Air and Space Administration
EIS	Electrochemical Impedance Spectroscopy
SANS	Small Angle Neutron Scattering
LET	Low Energy Transfer
HET	High Energy Transfer
FCEV	Fuel Cell Electric Vehicles
PCB	Printed Circuit Board
PHT	Post Heat Treatment
CPE	Constant Phase Element
PPC	Parallel Plate Capacitor

1.0 Introduction

The purpose of this thesis was to design, synthesize and analyze innovative anhydrous fuel cell membranes that operate at temperatures above 100°C. Operating at this higher temperature region improves performance and reliability of polymer electrolyte membrane fuel cells (PEMFCs): increasing proton mobility, enhancing reaction kinetics, increasing catalysis activity and reducing carbon monoxide poisoning. Traditional PEMFCs do not operate efficiently above 100°C because water is used as a proton conductive medium through the Grotthuss hopping mechanism. It has become common to substitute water with ionic liquids for high temperature electrochemical reactions[1]. Through substituting water with protic ionic liquids and radiation grafting them onto fluorocarbon films, a new proton conductive network solid state PEM has been developed. These membranes can perform at high temperature above 100°C. Polymers were selected for grafting based on the following properties: high proton conductivity, low electrical conductivity, high mechanical properties, high chemical resistance, and high temperature and humidity stability.[2]

1.1 History of Hydrogen Fuel Cell Development

Fuel cells were developed to replace traditional combustion engines because they operate cleaner, have a higher operating efficiency and use renewable fuel sources. Carbon emissions produced by combustion of fossil fuels have a significant impact on the environment and are contributors to global warming.[3],[4] The ratio of hydrogen to carbon in fuel has a significant impact on the amount of carbon biproducts in their emissions. The longer the hydrocarbon chains in fuel, the higher the energy density but the lower the combustion efficiency. Hydrogen

gas produces water as a biproduct which makes it a considerably cleaner energy source.

Hydrogen power sources are plentiful because it can be produced from water through electrolysis making it a renewable energy source. The maximum theoretical efficiency of hydrogen fuel cells is 85% which is considerably higher than combustion engines at 37%. [5] The following section will discuss the history of hydrogen fuel cell research and development.

1.1.1 Milestones in Fuel Cell development

The first hydrogen fuel cell was developed in 1838 by William Robert Grove [6]. Grove mixed hydrogen and oxygen in the presence of an electrolyte and was able to produce electricity and water. This marked the first-time gases were demonstrated in an electrochemical reaction. The first fuel cell is shown below in Figure 1.1.

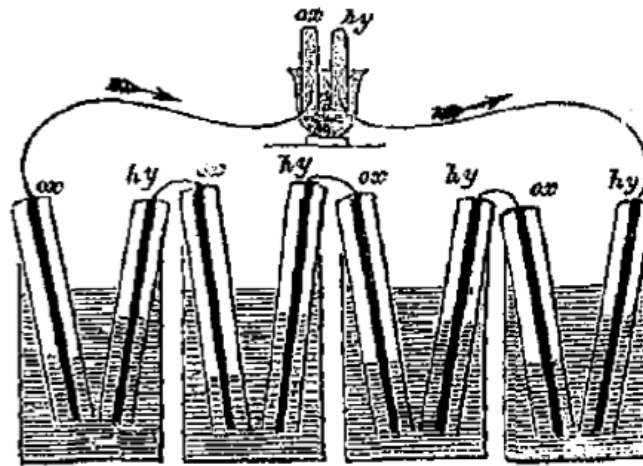


Figure 1.1: First Fuel Cell developed by William Robert Grove.[6]

However, this technology was not pursued as an electrical power source until 1889, when Ludwig Mond and Charles Langer attempted to build an apparatus using air and coal gas to produce electricity.[7] They called their invention a “fuel cell”. Their design was the first time a

porous proton conductive membrane, PEM, was used in fuel cells. Catalyst poisoning of coal gas on platinum electrodes prevented them from successfully producing a reliable fuel cell. It also could not compete with the emerging combustion engines and automobiles in the early 1900s.[8]

In the 1920s, fuel cell researchers in Germany developed the carbonate cycle and then developed the first solid oxide fuel cells (SOFC). The first ceramic SOFC was created in 1937 by E. Baur and H. Z. Preis and operated at 1000°C.[9] In 1932, Francis Thomas Bacon pioneered the development of cheaper more economical fuel cells. He developed the first fuel cell that converted hydrogen and oxygen directly into electricity through an electrochemical reaction. His fuel cell used an alkaline electrolyte (KOH solution) in a matrix for proton conductivity.[10] However this electrolyte, could be poisoned by carbon dioxide so only high purity oxygen and hydrogen could be used. He later developed an inexpensive, less corrosive nickel electrode to replace the more expensive porous platinum electrodes. These nickel electrodes required operating temperatures above 200°C. In 1959 Francis Thomas Bacon demonstrated a five-kilowatt fuel cell that powered an electric welder. His design became famously named the "Bacon Cell" and became a cornerstone for future fuel cell design.[10]

Leonard Niedrach and Willard Tomas Grubb in 1958 developed the first modern PEMFC by depositing Pt onto an ion exchange membrane at General Electric.[11][12] These early PEMFC were hydrogen base and could not operate for long times and had low reliability. In 1959, Harry Karl Ihrig, an engineer for the Allis - Chalmers Manufacturing Company, demonstrated a tractor that was the first vehicle powered by a fuel cell. [6] During the 1960s, General Electric developed and manufactured fuel cell systems to generate electric power for NASA's Gemini and Apollo space capsules.[13] Today, NASA continues to use fuel cells to

power space exploration due to their multi-functional applications including: high power efficiency, fuel storage density, and the ability to produce water which is essential for the crew life support.

The first commercial use of fuel cells in vehicles began in the 1990s. The first bus powered by a fuel cell was designed in 1993, and several fuel-cell cars have been developed and built in Europe and in the United States.[12],[14] Daimler-Benz and Toyota launched the first prototype fuel cell powered cars in 1997. Honda introduced the first mass produced fuel cell car in 2007.[8] These hydrogen fuel cells were only available for testing and leased from dealerships. The first commercially available fuel cell electric vehicles (FCEV) was introduced in 2013 by Hyundai (Tucson) followed by Toyota (Mirai) in 2015.[15]

Today automobile engines contribute about 20 % of global warming based on their carbon dioxide emissions. [16] In order to mitigate the effects of global warming, rapid development and adoption of hydrogen fuel cells by industry is necessary for cleaner energy source availability in the future. By 2050, the global energy demand is expected to double and renewable energy sources are expected to fill this need and play a larger role in society. Figure 1.2 shows the projected develop of the hydrogen fuel cell industry over the next 30 years as the technology becomes available to consumers. [16]

Projected Growth of Hydrogen Fuel Industry from Today to 2050

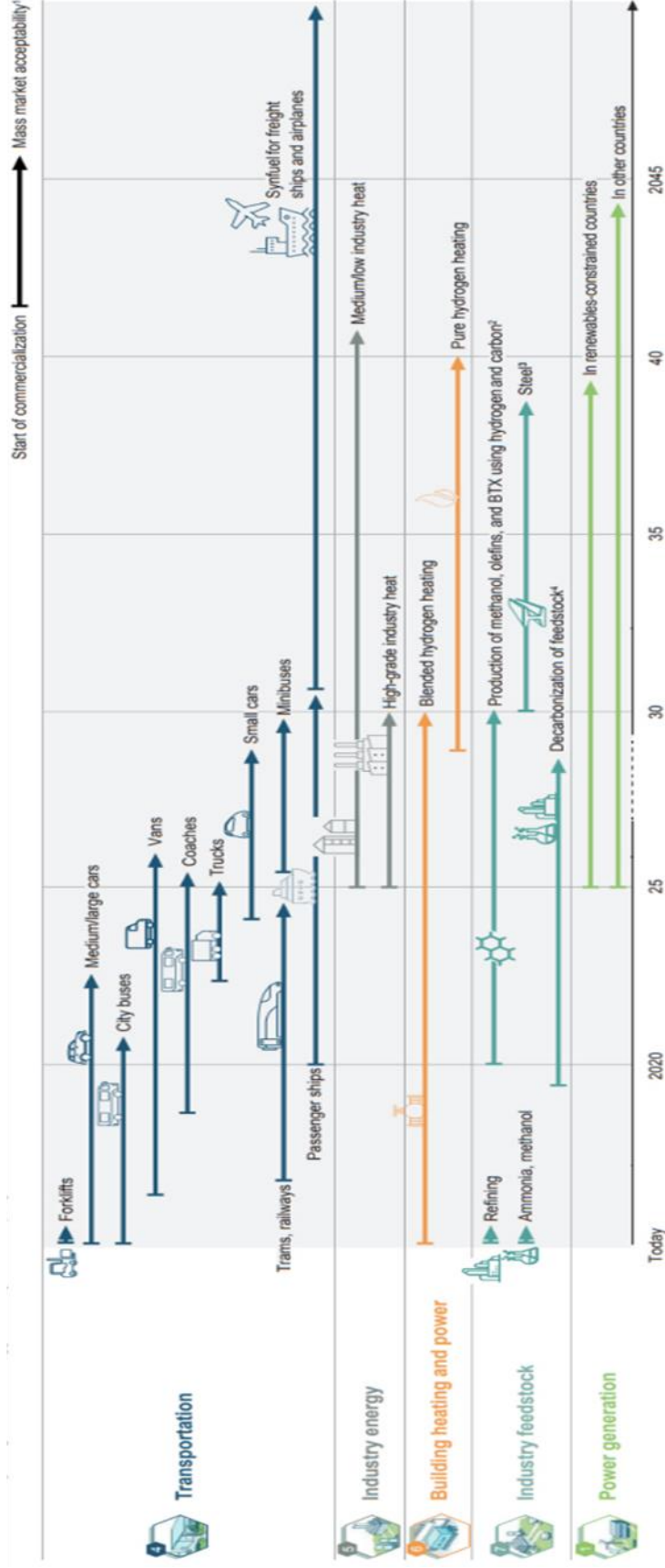


Figure 1.2-Future projected development of hydrogen fuel market[3]

1.1.2 Hydrogen as a Renewable Energy Source

There is continued interest in developing alternative polymer fuel cell membranes to improve their operating efficiency at higher temperatures. Since the 1960s, there has been a shift in technology from combustion engines to renewable energy sources such as hydrogen fuel cells. The purity of hydrogen used in these fuel cells varies based on the source. Most hydrogen is produced as a bi-product from the refining of fossil fuels.[17][18][19] These sources of hydrogen produce contaminants that impacts fuel cell efficiency.

Hydrogen gas can also be produced by electrolysis utilizing environmentally friendly renewable energy sources such as wind and solar. In addition, hydrogen gas is produced in large quantities through radiolysis of water in nuclear power plants and next generation plants are being designed to produce hydrogen in large quantities anticipating future energy applications as a replacement for fossil fuels. [20],[21],[22] These methods produce high purity hydrogen gas. However, the current production level of hydrogen cannot replace the energy demand for hydrocarbon fuels. Alternative hydrogen production sources, as well as improving fuel cell efficiencies are being studied to meet future energy needs.

1.2 Polymer Electrolyte Membrane Fuel Cell Operation

A polymer electrolyte membrane fuel cell (PEMFC) relies on a proton conducting membrane to convert the chemical potential of hydrogen combustion into electrical power. Fuel cells operate by separating the redox reactions at the electrodes by using a PEM, creating a flow of electrons to generate power.[5],[23] PEM allow for the transport of protons while also acting as a gas barrier between hydrogen and oxygen, preventing uncontrolled combustion. The PEM proton conducting capabilities define the power, efficiency and performance of a fuel cell.

Figure 1.3, depicts the operation of a traditional PEMFC in which water is used as the medium for proton transport from anode to cathode.

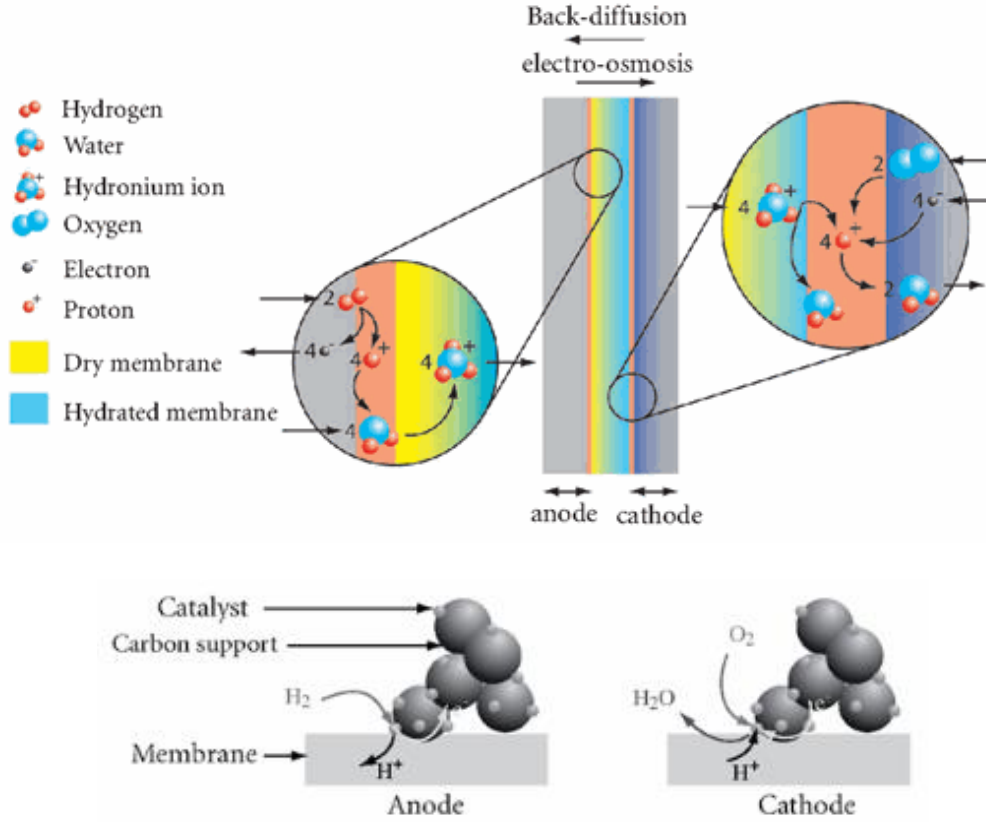
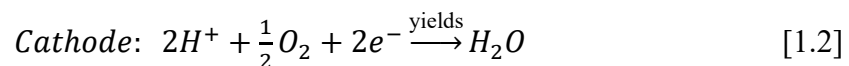
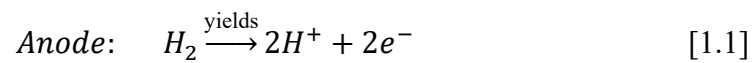


Figure 1.3: Basic description of hydrous proton transport in PEM and catalysis reactions at the anode and cathode.[5]

The diagram above describes how a triple phase interface between hydrogen gas (H₂), platinum catalyst (Pt) and the proton conductive membrane are required for fuel cell operation. The redox reactions of hydrogen that occur at the anode and cathode within the PEMFC are shown below in Equation 1.1 and Equation 1.2 respectively.



Since water is the transport medium for protons in a traditional PEMFC, operating temperature and humidity have a significant impact on their proton conductivity and functional performance.

1.2.1 Mechanisms of Proton Conductivity

There are three mechanisms for proton transport in PEM; the Vehicular mechanism, the Grotthuss mechanism and the Surface mechanism. The three mechanisms are depicted in Figure 1.4.

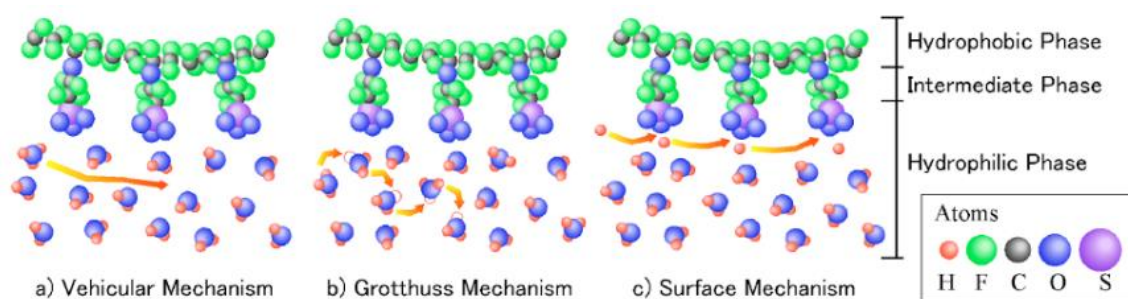


Figure 1.4: Mechanisms of Proton conductivity in Nafion: (a) Vehicular Mechanism (b) Grotthuss Mechanism and (c) Surface Mechanism.[24]

The dominate mechanism depends on the structure and hydration of the amorphous hydrophilic phase of the PEM membrane. The dominate mechanism will also have the lowest activation energy for proton transport.[25] It has been shown by S. Tsushima et al. that the Grotthuss mechanism is the dominate mechanism for proton conductivity in traditional PEMs such as Nafion membranes.[26] The Nafion membranes use water for proton transport. The fluoropolymers with sulfonate side chains create a network of proton conductive water nano-channels.[24] Figure 1.5a shows how the proton conductivity occurs in Nafion. Figure 1.5b shows how the proton conductivity through the PEM is the combination of the 3 mechanisms in parallel.[26] Table 1.1 shows the step distance, time and diffusion coefficients of the three

proton transport mechanisms modeled for Nafion. These values can be used in the Einstein-Smoluchowski random walk equation, shown below in Equation 1.3, to determine the hydrogen diffusion constant for the proton transport mechanisms.

$$D_{H^+} = \frac{l^2}{\kappa \tau_D} \quad [1.3]$$

Where D_{H^+} is the hydrogen diffusion constant (m^2/s), l is the average step distance (m), τ_D average step time (s) and κ is the random walk dimension constant (2, 4, 6) for (1, 2, 3) dimensions respectively. As shown in Table 1.1 the Grotthuss mechanism has the highest diffusion coefficient $7.225\text{E-}09 \text{ m}^2/\text{s}$ of the proton conductive mechanisms for Nafion. Figure 1.6 supports this by showing that the Grotthuss mechanism contributes the most to the proton conductivity in Nafion™. This is supported by the PEM pore structure in which temperature, water content and electric field are the main factors that influence the proton conductivity mechanism[27].

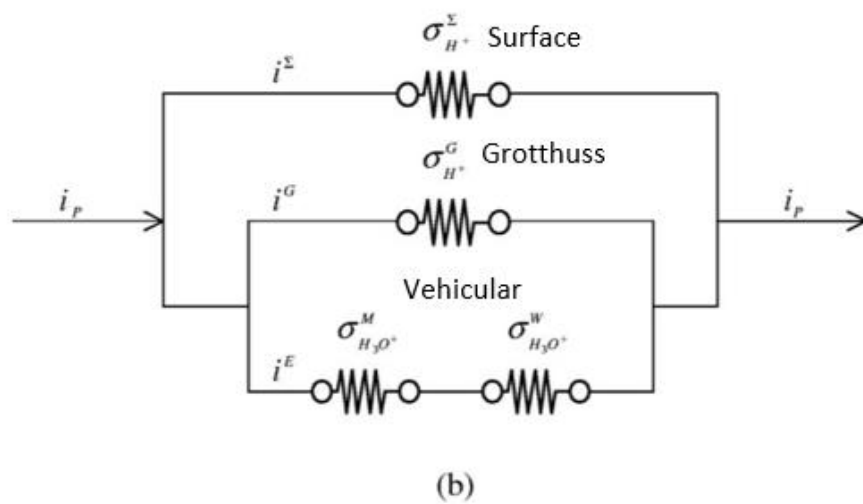
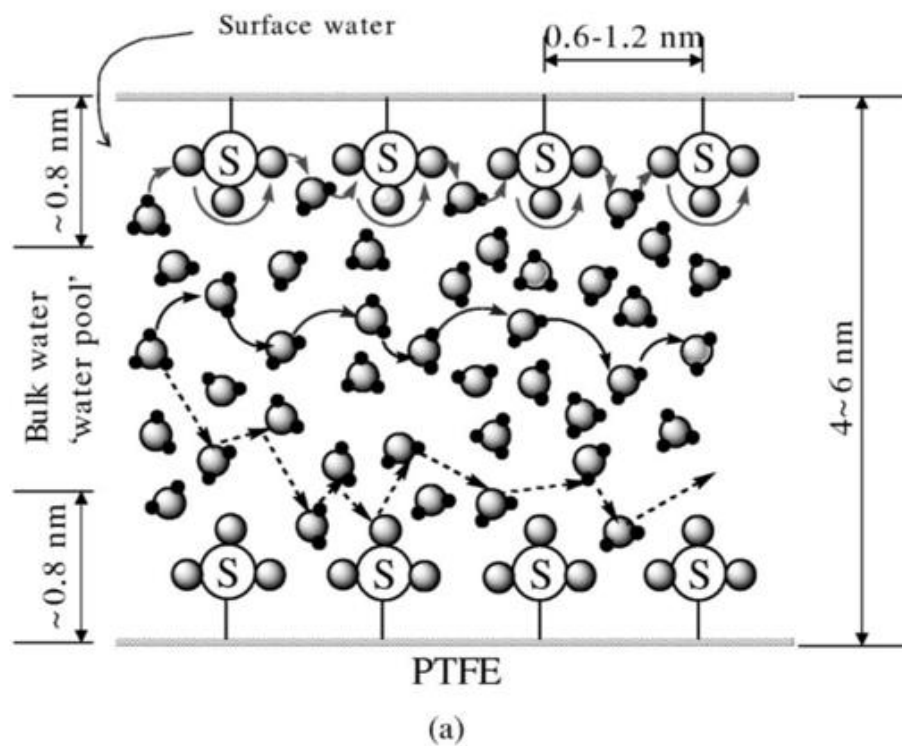


Figure 1.5: Mechanisms of Proton Conductivity in Nafion (a) Mechanisms (b) Proton conductivity electrochemical circuit model [26]

Table 1.1: Proton Transport Mechanism Step Times and Distances in Nafion [26]

	Surface	Grotthuss	En Masse
	Diffusion	Diffusion	Diffusion
Step Time(s)	1.61E-09	1.50E-12	5.78E-12
Step Distance (nm)	0.255	0.255	0.280
Hydrogen			
Diffusion	6.731E-12	7.225E-09	2.261E-09
Coefficient(m ² /s)			

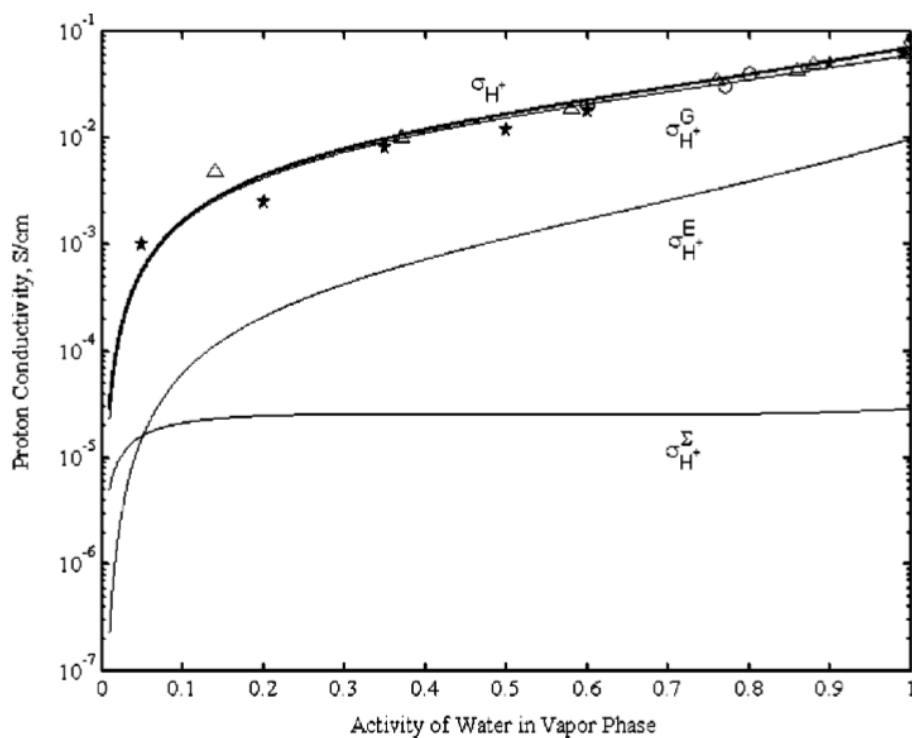


Figure 1.6-Proton conductivity of Nafion as a function of relative humidity of vapor phase showing the contribution of Grotthuss, Surface and Vehicular proton conductive mechanism.

[26]

The hydronium ion (H_3O^+) shows unexpectedly high mobility through aqueous systems compared to dissolved cations.[28] This mobility is attributed to a proton hopping mechanism where protons can hop between neighboring water molecules. There are conflicting theories on the behavior of the hydronium ion complex in water and its involvement in proton hopping.[29],[30] A combination of proton hopping between Hydronium ions (H_3O^+), Zundel ions (H_5O_2^+) and Eigen ions (H_9O_4^+) contribute to high proton mobility in water. Figure 1.7 shows the chemical structure of hydronium ion complexes in water. The hopping occurs through the formation and breaking of coordination bonds within the hydronium water complex. The proton hopping model for conductivity in water is also known as the Grotthuss mechanism.[31]

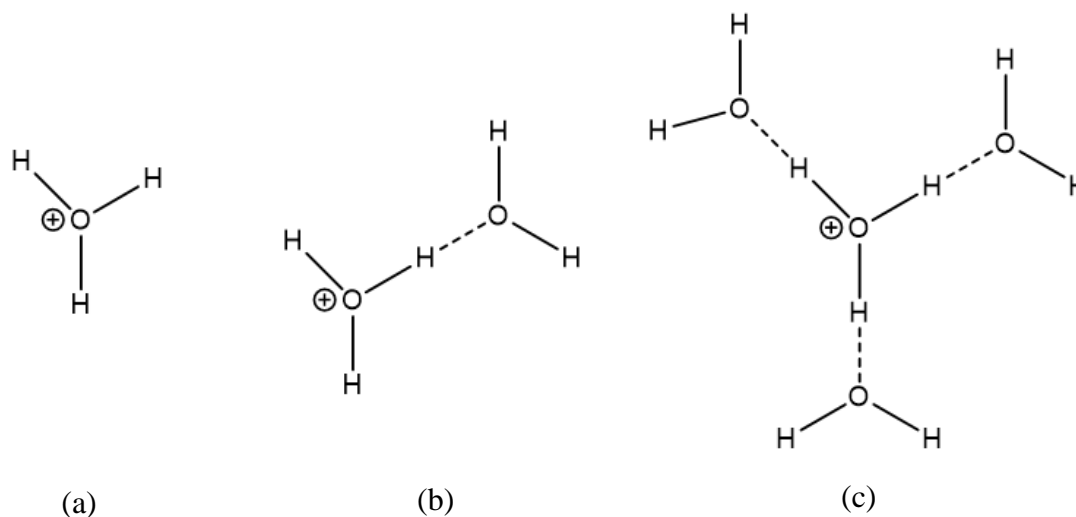


Figure 1.7-Hydronium ion complexes found in water (a) Hydronium ion (b) Zundel Ion (c)

Eigen ions

Proton conductivity in fuel cells is driven by the concentration gradient (diffusion) and chemical potential gradient (migration) between the anode and cathode according to the Nernst-Planck Equation 1.4 shown below.[32]

$$J_i(x) = -D_i \left(\frac{dC_i(x)}{dx} \right) + \left(\frac{-z_i F}{RT} D_i C_i \frac{d\phi(x)}{dx} \right) + C_i v(x) \quad [1.4]$$

The Nernst-Planck equation indicates the flux $J(x)$ of a species i (in this case protons), where

$-D_i \left(\frac{dC_i(x)}{dx} \right)$ is the diffusion component driven by a concentration gradient across the membrane.

$\left(\frac{-z_i F}{RT} D_i C_i \frac{d\phi(x)}{dx} \right)$ is the migration of protons driven by the presence of an electrochemical potential gradient across the membrane. $C_i v(x)$ is the convection component due to mixing which is not present in PEMFC. In a PEMFC system, there is a concentration gradient of protons with a high concentration at the anode where hydrogen is oxidized and a low concentration at the cathode where hydrogen is reduced. In PEMFC systems, there is also an electrochemical potential which is driving the proton to migrate between the two electrodes.

The electrical current generated by fuel cells is limited by the proton transport within PEMs and because fuel cells serve mainly as high current/low voltage devices, efficiency of proton transport heavily affects their power output. The industrial standard PEM is Nafion, which is based on polymerizing perfluorosulfonic acid and was developed by Dupont in the 1960s.[33] The sulfonic acid ionmers in Nafion bind water within the PEM lattice. At high temperatures the membranes dehydrate resulting in reduced conductivity. None-the-less, Nafion has demonstrated reliability for fuel cell applications with an operating life of 60,000 hours at an operating temperature of 80°C.[34]

1.3 Disadvantages of Current PEMFC

During PEMFC operation, impurities in the hydrogen fuel including (CO, CO₂, H₂S and NH₃) and in the oxygen/air intake (NO₂, NO₃, SO₂, SO₃, CO and CO₂) will impact performance

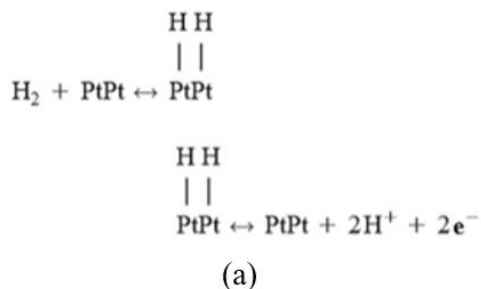
and operation life.[35] Table 1.2 list the sources of impurities that effect hydrogen fuel cell operation.

Table 1.2: Sources of Impurities that Affect Hydrogen Fuel Cell operation [35]

Impurity source	Typical contaminant
Air	N_2 , NO_x (NO, NO_2), SO_x (SO_2 , SO_3) NH_3 , O_3
Reformate hydrogen	CO, CO_2 , H_2S , NH_3 , CH_4
Bipolar metal plates (end plates)	Fe^{3+} , Ni^{2+} , Cu^{2+} , Cr^{3+}
Membranes (Nafion [®])	Na^+ , Ca^{2+}
Sealing gasket	Si
Coolants, DI water	Si, Al, S, K, Fe, Cu, Cl, V, Cr
Battlefield pollutants	SO_2 , NO_2 , CO, propane, benzene
Compressors	Oils

Impurities may be introduced to hydrogen fuel by their production method. Figure 1.8a shows the platinum catalysis reactions at the electrodes that occur under normal fuel cell operations. Figure 1.8b shows how carbon monoxide contaminates can bind to the electrodes, blocking the hydrogen and proton transfer from the electrode to the electrolyte. These impurities react with the Pt catalytic electrodes by reducing their active surface area, preventing the oxidation and reduction reactions of hydrogen. These impurities adsorb onto the surface of platinum, blocking the formation of platinum hydride (Pt-H) which is an intermediate step for oxidizing hydrogen gas H_2 into protons (H^+) at the anode. [35],[36],[37]

Hydrogen Adsorption and Oxidation at Catalytic Platinum Electrode



Carbon Monoxide Poisoning at Platinum Electrode

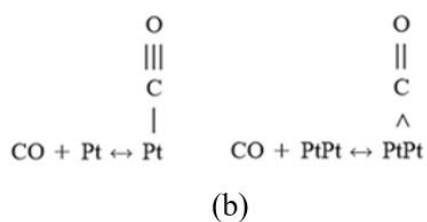


Figure 1.8-Reactions at Platinum Catalytic Electrode: (a) Hydrogen Adsorption (b) Carbon Monoxide Poisoning

Carbon monoxide impurities can be produced within the PEMFC by carbon dioxide reacting with the hydrogen fuel, in concentrations as low as 20-50ppm.[38] It has been demonstrated by Q. Li et al. that carbon monoxide tolerance can be increased and Pt poisoning can be prevented by increasing the PEM operating temperature.[38] Figure 1.9 shows the carbon monoxide fractional coverage of Pt electrodes as a function of temperature and carbon monoxide concentration. However, to operate at these higher temperatures, water needs to be substituted as the proton conducting medium, since PEMs utilizing water would dehydrate and lose their proton conductivity. Higher temperatures enable fuel cells to operate more efficiently by enhancing reaction kinetics, increasing catalysis activity and reducing carbon monoxide poisoning of the electrodes.[36],[39]

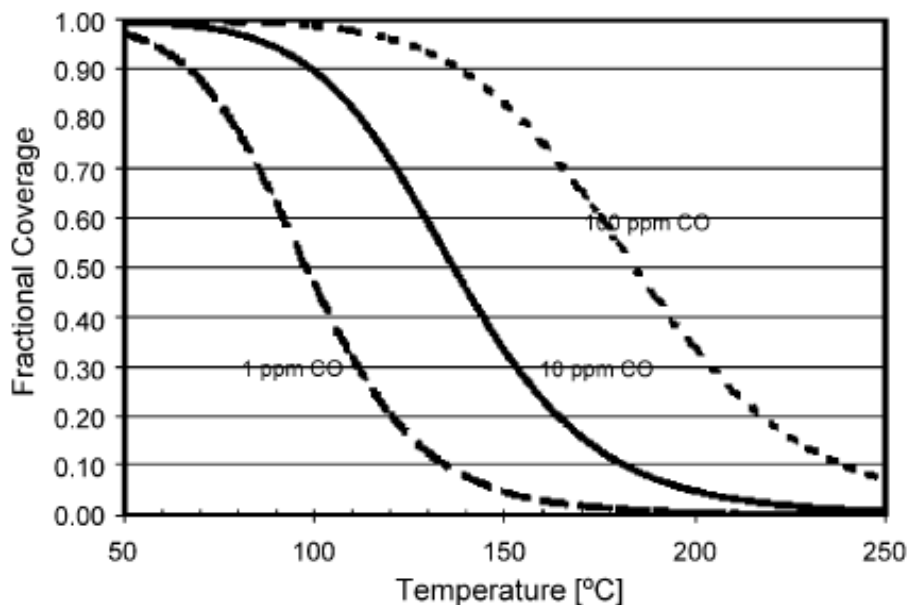


Figure 1.9- Carbon monoxide fractional coverage of Pt electrodes as a function of temperature and carbon monoxide concentration [38]

1.4 Application of Radiation on Materials

Radiation is frequently used in the polymer industry to synthesize, functionalize and alter material properties through free radical generation. Examples include radiation induced cross-linking, polymerization, curing, sterilization, and grafting. Radiation crosslinking is used to increase the mechanical properties of polymers. Applications include insulation of power cables, artificial joints replacement and o-rings. Radiation polymerization provides finer controls over initiation and degree of polymerization without relying on chemical additives. Radiation curing is used in a wide range of coatings inks adhesives and composites. Radiation sterilization is used in the food packaging and medical industry to decontaminate items before use. Radiation grafting can be used to modify chemically resistant polymers such as fluoropolymers and is used

to synthesize polymer functionalized grafted groups. Today, radiation treatments are widely used by industry for the synthesis, modification and sterilization of polymers. This thesis will focus on the radiation grafting techniques for the preparation of novel PEM for fuel cell applications.[40],[41],[42],[43],[44]

1.4.1 History of Radiation Treatment on Materials

Radiation chemistry explores different types of radiation energy and its physical and chemical effect on materials. The history of radiation chemistry can be traced back to the discovery of X-rays by Roentgen in 1895 and radioactivity by Becquerel in 1896.[45] These independent discoveries happened with the observation of changes in materials when exposed to radioactive elements. The types of radiation discovered by Becquerel and Roentgen rendered air electrically conductive and activated photographic emulsions. [45] This became the foundation of X-ray imaging which uses the difference in density of bone and soft tissue to create contrast in photographic film. These discoveries lead more researchers to explore the effects of radiation on various materials. A notable milestone was research conducted by Marie and Pierre Curie, who discovered and isolated the elements radium and polonium in 1898. This provided researchers access to a stable and controlled source of radiation for further experimentation. The exploration of the fundamental science behind radioactive materials eventually led to a greater understanding of ionizing radiation's effect on molecules and atoms.[45] The development of nuclear reactors in the 1940s revealed polymers were especially susceptible to radiation and a new branch of science, radiation chemistry, was recognized.

The development of radiation sources and treatments had a significant impact on the polymer industry which began to develop after World War II.[46] However, it was not until the 1950s

that effects of radiation on materials were understood at a molecular level and applied to polymers. High energy ionizing radiation systems were constructed including electron beams and gamma cells which could be used to apply controlled radiation treatments.[45] These advancements were significant milestones which opened radiation chemistry for industrial applications including development and design of polymers. Radiation can be used to modify the material properties of polymers. However, applying optimized radiation treatment parameters is necessary for controlled reactions.

1.4.2 Radiation Physics

Radiation is divided into different types: alpha, beta, gamma, proton and neutron. Each of these radiation types will interact with materials differently depending on their charge, mass and energy. If the radiation energy is high enough, it will ionize the electrons from atoms as it interacts with materials. If the radiation particles are large, they can collide with atoms, displace them, and physically change the structure of the atomic lattice. This can cause highly ordered crystalline materials to become amorphous over time. Radiation types can further be broken down into high energy transfer (HET), which deposit their energy quickly and low energy transfer (LET) which deposit their energy slowly within the material. The interactions of radiation and materials are also dependent on the material properties of the target substrate including composition, density and environment.

In order to use radiation to create chemical changes in materials, the energy transfer from the applied radiation must be high enough to ionize the electrons from the targeted material. As shown in Figure 1.10, when ionizing radiation passes through a material it creates a primary ionization track which is 2 nm in diameter. [47]

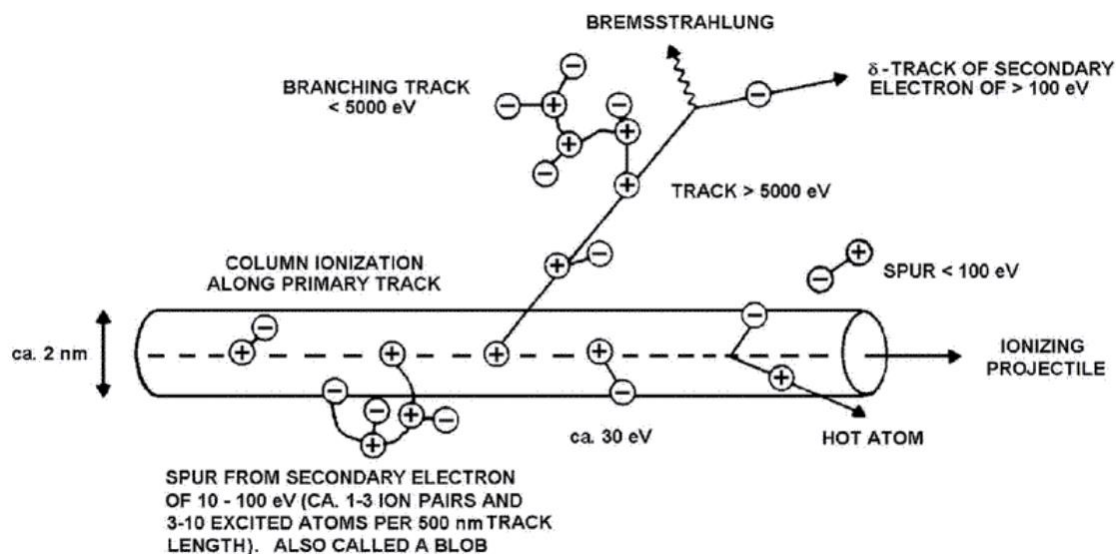


Figure 1.10-Ionizing radiation track in condensed matter and its interactions [47]

Electrons ionized by radiation have a variety of kinetic energies, the greater their energy the further from the primary ionization track they will travel. Electrons with low energy will form spurs, which are areas of excited atoms. Electrons ionized by radiation are also known as secondary electrons.[47] If secondary electrons have enough energy, they can branch off, causing further ionization events in surrounding atoms, eventually resulting in an ionization cascade. Within polymers, atoms are covalently bonded and after ionization, the atoms in the polymer chains become positively charged, reaching an excited and unstable energy state. To reach a lower energy state, a covalent bond breaks in the polymer causing the chain to become neutral but also forming lone electron pair free radicals. The breaking of covalent bonds in this way is called radiation induced scission. These scissions can occur along the backbone of the polymer or in functional groups along the backbone chain. The bond dissociation energy required for polymer bond scission are shown in Table 1.3. The weaker the bonds, the greater

probability of undergoing radiation induced scission.[48] The chemical structure of the polymer can control which bonds break and where free radicals are generated.

Table 1.3: Bond Dissociation Energies for Fluorocarbon Polymers[48]

Bond	ΔH_{BDE} [kJ/mol]
C–C	370–420
C–H	430–450
C–F	480–520

The effect of radiation with materials is comprised of physical and chemical interactions as the ionizing radiation passes through the material. The radiation treatment of aqueous solutions is important for the modification of polymers. In aqueous systems, most of the sample mass is water and radiation induced reactions are driven by the radiolysis of water. Figure 1.11 shows the radiation interaction with water over time and the physical and chemical interactions. [49]

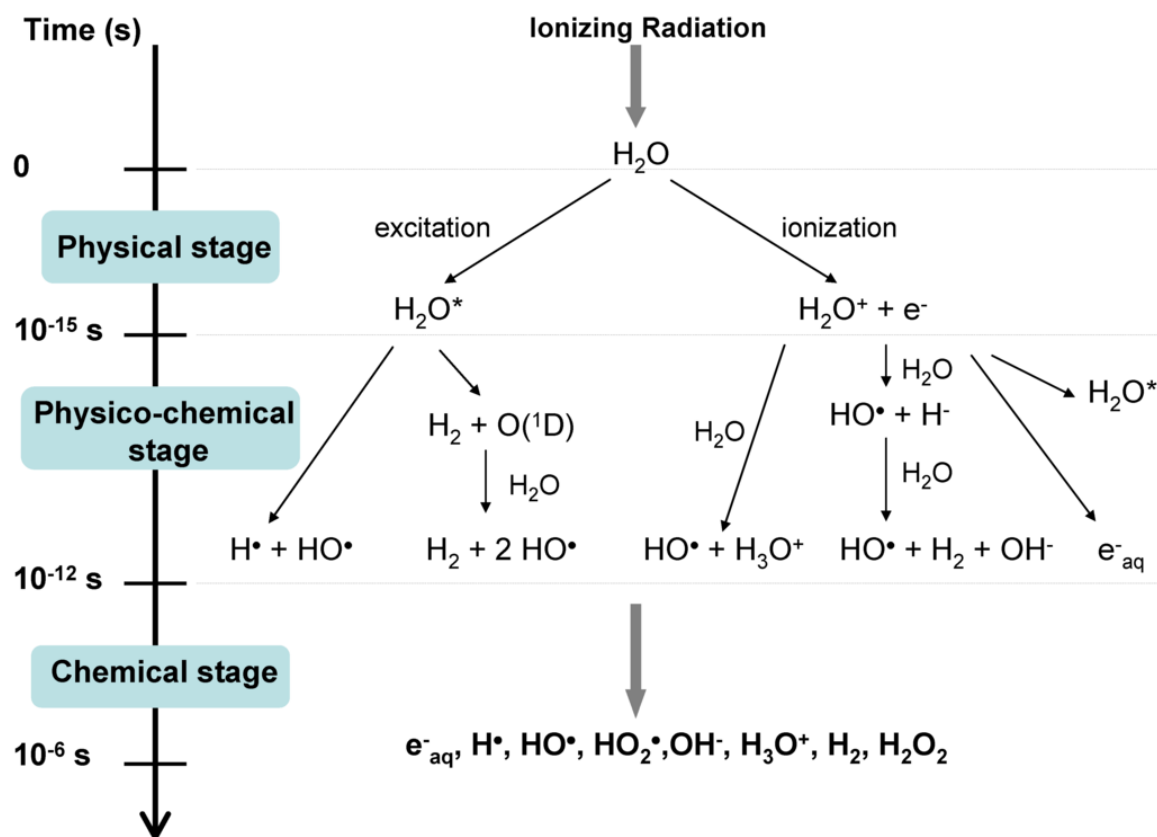


Figure 1.11- Radiolysis of Water: physical and chemical interaction [49]

The chemical interactions of radiation occur by free radicals produced as a result of bond scissions. The number of free radicals produced during a radiation treatment is proportional to the radiation dose. Dose is defined as the ratio of energy deposited per unit mass of the material. The SI unit for dose is the gray (Gy) which is equal to J/kg. The dose rate (Gy/s) at which radiation is applied greatly effects the equilibrium concentration of free radicals and the rate of the subsequent chemical reactions. [45],[50] Primarily, gamma sources or electron beams are used for industrial modification of polymers due to their high penetration, allowing for uniform treatment. As such, only beta and gamma radiation treatments will be discussed as a part of this research.

1.4.2.1 Gamma Radiation

Gamma radiation are high energy photons that are produced by unstable nuclei of atoms as they decay to a more stable state. Cobalt-60 (Co-60) is an artificially produced gamma source which is commonly used by industry for radiation treatments. Co-60 produces gamma rays with energies of 1.17 MeV and 1.33 MeV.[43] Gamma rays are photons and have sufficient energy to ionize electrons from atoms in materials. Gamma rays are electrically neutral. Unlike charged particles, they do not lose energy through coulombic interactions with electrons. This allows gamma rays the ability to travel a considerable distance in air before interacting with denser materials, leading to partial or total transfer of photon energy to electron energy. These secondary electrons deposit all their energy in the material gradually through a LET interaction. Photons are far more penetrating than charged particles of similar energy and can only be shielded by materials with high electron density such as lead.

Gamma rays interact with materials through three primary mechanisms: photoelectric effect, Compton scattering and pair production.[43],[45] The dominant interaction is dependent on the energy of the photon and atomic number of the material, as shown below in Figure 1.12.[47]

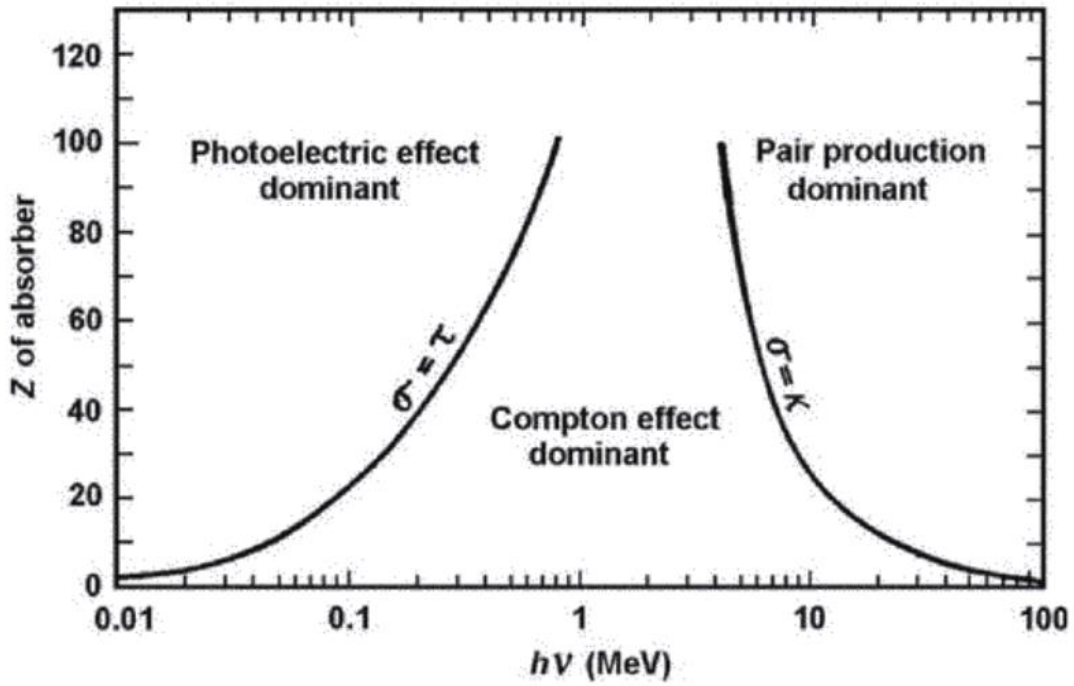


Figure 1.12-Dominant Gamma radiation interactions with matter dependent on photon energy and atomic number of target[47].

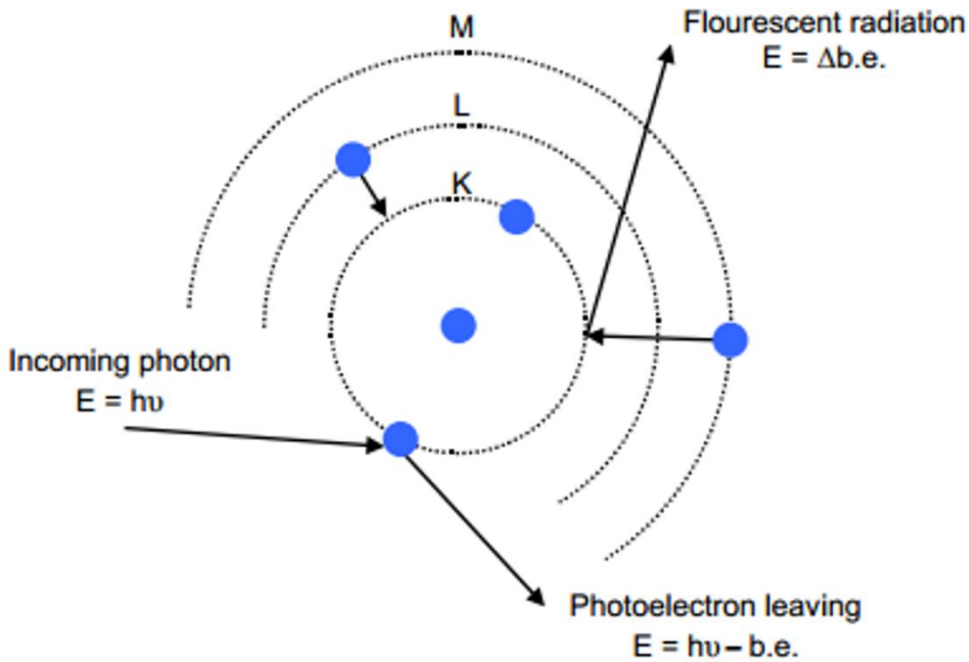


Figure 1.13-Events in the photoelectric scattering process [51]

In the photoelectric effect, the photon is absorbed by an atom causing an energetic photoelectron to be ejected from its orbital. The photoelectric effect is shown in Figure 1.13. The photoelectron appears with an energy (E_γ) given by the Equation 1.5 below, where $h\nu$ is the energy of the photon and $E_{b.e.}$ is the binding energy or ionization energy of the electron. [51]

$$E_\gamma = h\nu - E_{b.e.} \quad [1.5]$$

High energy x-rays and gamma rays have sufficient energy to ionize electrons in material. In the photoelectric effect, most of the energy is transmitted to the ionized electron. The photoelectric effect predominates when photon have relatively low energy and are interacting with high atomic number materials which have lower binding energies.

For Compton scattering, the incoming gamma-ray photon is deflected through an angle θ with respect to its original direction. Figure 1.14 depicts the photon-electron interaction that occurs during Compton scattering. The photon transfers a portion of its energy to the electron (assumed to be initially at rest), which is then known as a recoil electron, or a Compton electron. All angles of photon scattering are possible in this mechanism. The energy transferred to the electron can vary from zero to a large fraction of the gamma-ray energy. [51]

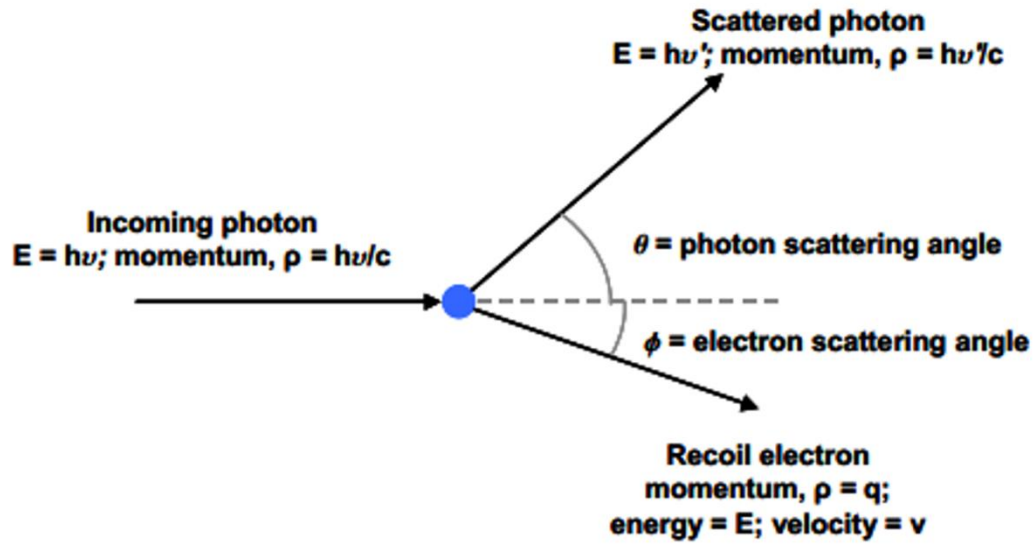


Figure 1.14 Events that occur in Compton scattering[51]

The energy transferred from the photon with energy ($h\nu$) to the electron in the atom during Compton scattering can be calculated through equations 1.6, 1.7 and 1.8 below:

$$h\nu' = h\nu \frac{1}{1 + \alpha(1 - \cos\theta)} \quad [1.6]$$

$$E_e = h\nu \frac{\alpha(1 - \cos\theta)}{1 + \alpha(1 - \cos\theta)} \quad [1.7]$$

$$\alpha = \frac{h\nu}{m_0c^2} \quad [1.8]$$

For these equations, the photon scatters at angle θ , $h\nu'$ is the energy of the photon after scattering and E_e is the energy of the electron ionized from the atom. As a part of these calculations, α is the ratio of $h\nu$ (the energy of the incident photon) to m_0c^2 , the rest mass energy of the electron which equals 0.511MeV. This is the predominant interaction mechanism for gamma-ray energies, typical of radioisotope sources. It is the most dominant interaction mechanism in low atomic number (Z) materials such as polymers. [51]

If a gamma ray has energy higher than 1.022 MeV, it may interact with matter by a process called pair production.[51] The photon, passing near the nucleus of an atom, is subjected to strong field effects from the nucleus. The photon may undergo a mass-energy conversion forming positron and electron pair. As depicted in Figure 1.15.[51]

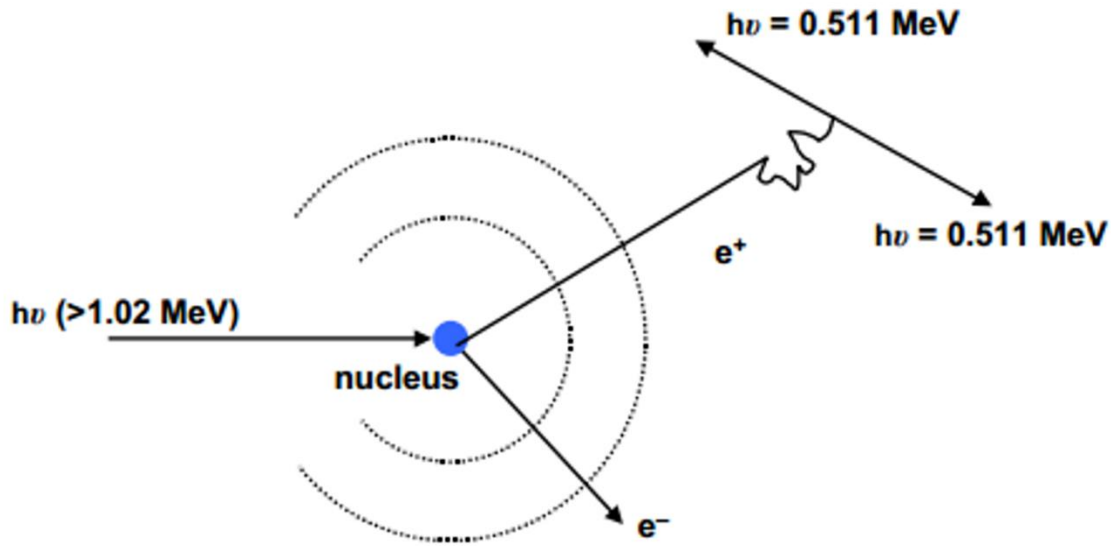


Figure 1.15-Events that occur in pair production[51]

The minimum energy of 1.022MeV is required because it is the energy of formation of the positron-electron pair. The remaining energy of the photon is converted into kinetic energy which is split between the positron electron pair. Equation 1.9 show the energy transfer of the photon to the electron positron pair.

$$h\nu - 1.022 = E_{positron} + E_{electron} \quad [1.9]$$

The scattering nucleus absorbs a small amount of kinetic energy and does not change significantly from this event. The probability of pair production occurring is related to the energy of the photon and is proportional to the atomic number squared. [51]

Each of these three interactions cause the gamma ray to lose part of its energy as it travels through the material as it ionizes secondary electrons in its path. The rate at which this energy is lost and the ability of the material to act as a shield is reflected by the attenuation constant (μ), which is determined by Equation 1.10.

$$\mu = \frac{N\sigma\rho}{A} \quad [1.10]$$

In this equation, N is Avogadro's number, σ is the reaction cross-section, ρ is the density of the material and A is the atomic mass of the material. The value (μ) correlates to the electron density of the material which impacts the frequency of interactions occurring. The total attenuation of gamma rays through materials due to scattering and absorption can be determined by Equation 1.11.

$$I = I_0 e^{-\mu L} \quad [1.11]$$

For Equation 1.11, I_0 is the initial intensity of the gamma radiation, μ is the attenuation constant and L is the thickness of the material. [52] A diagram of this interaction is shown below in Figure 1.16.

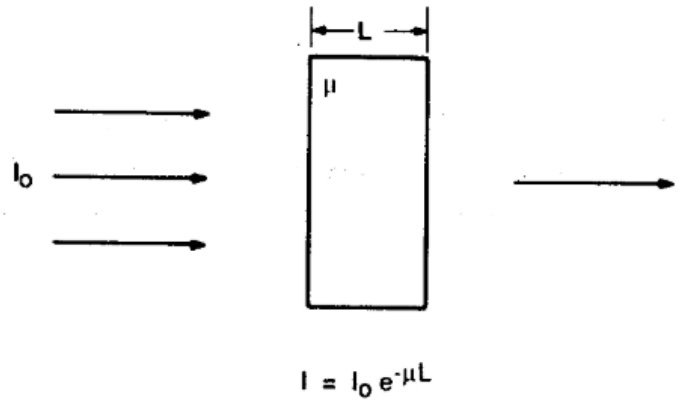


Figure 1.16- Gamma radiation attenuate through materials. [52]

The mass attenuation coefficient which is the attenuation coefficient divided by the density for select elements are shown below in Figure 1.17. [52] The mass attenuation coefficient is used to predict the number of interactions the applied radiation will have with a material. It will determine the rate that energy is transferred, from gamma ray to the material and how well the material can shield gamma radiation.

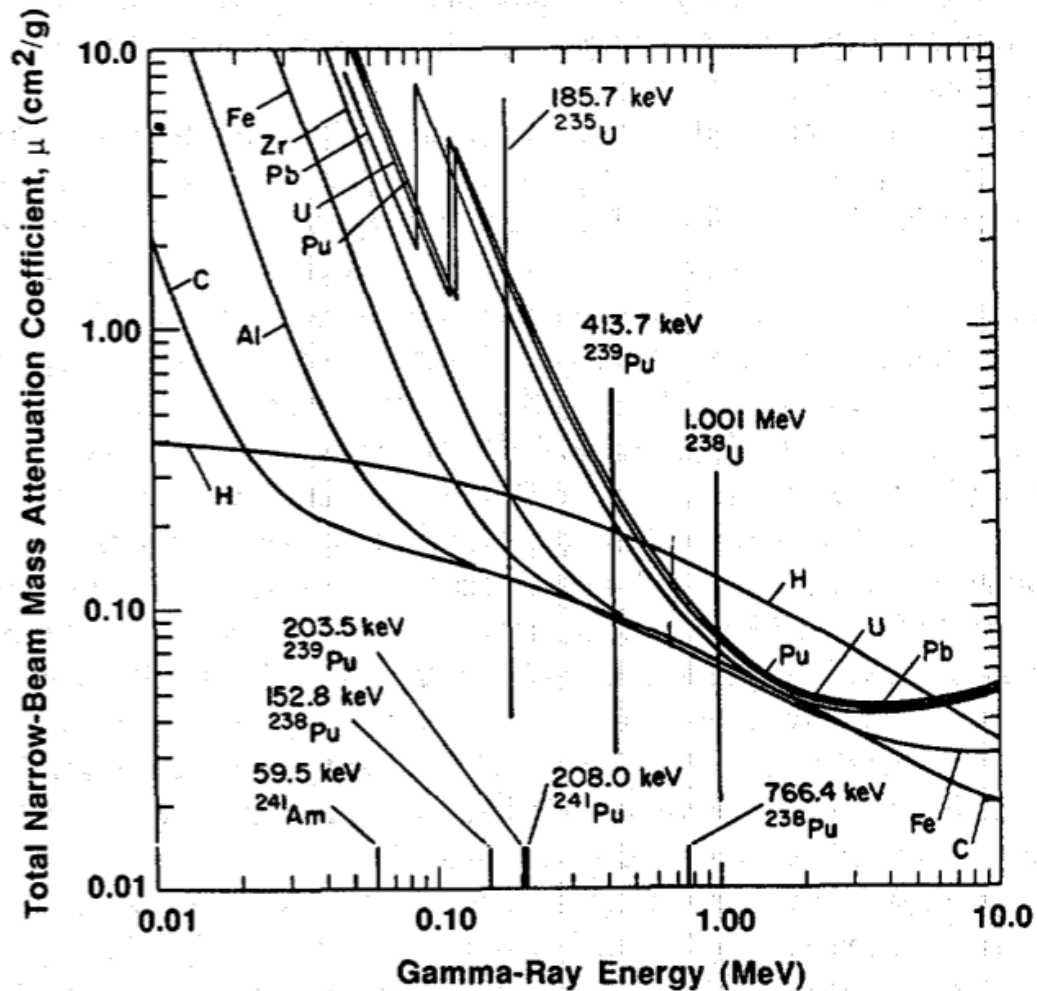


Figure 1.17-Element Mass Attenuation Coefficient[52]

For example, in Figure 1.17, Lead (Pb) has a high mass attenuation coefficient and is frequently used as shielding for gamma radiation. Whereas polymers, which are mostly composed of carbon and hydrogen have a low mass attenuation, allowing the gamma radiation gradually and uniformly deposit its energy in the material. The penetration of gamma radiation from a Cobalt-60 source into water is shown in Figure 1.18. Polymers are considered water equivalent materials because of their similar density and chemical structure. The high penetration makes gamma radiation a useful treatment method to modify bulk properties of polymers.

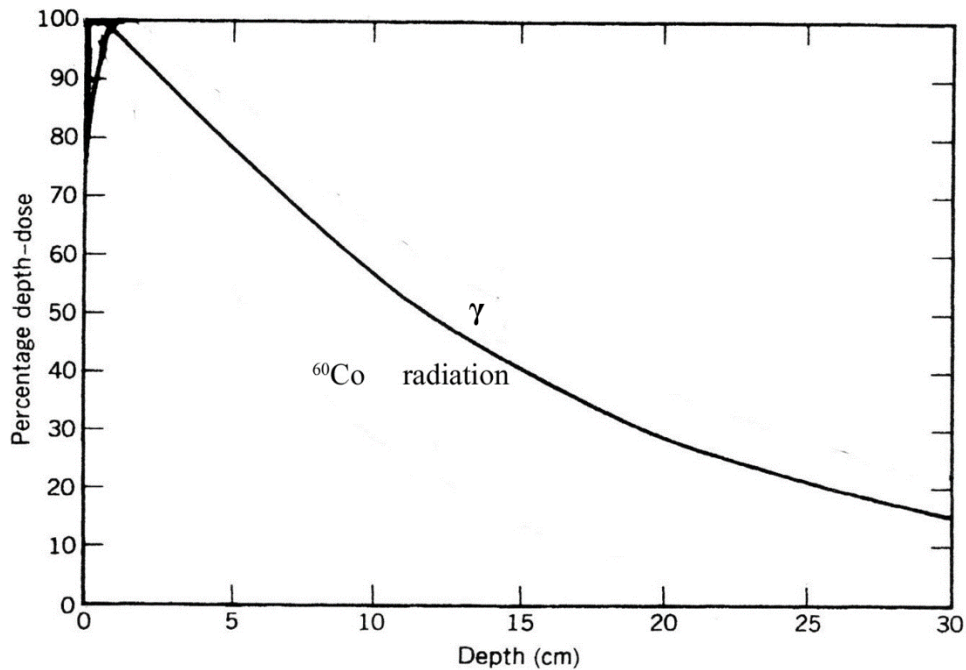


Figure 1.18- Penetration of gamma ray in water produced by a Cobalt-60 source [45]

1.4.2.2 Beta Radiation

Beta (β) radiation is a flux of high energy electrons which can be produced through radioactive nuclear decay or generated electrically with an accelerator. Beta radiation has the mass of an electron and a negative charge of $1-$. This negative charge means the radiation coulombic interactions occur with electrons as it traverses the target material. The small mass and negative charge gives beta radiation a LET allowing the electrons to penetrate deep into materials without displacing atoms. The interaction events of high energy electrons with matter are depicted in Figure 1.19. These high energy electrons will interact with atoms in two ways. Inelastically with the electron cloud producing secondary electrons, as shown in Figure 1.19b. Elastically, with the nucleus scattering as shown in Figure 1.19c. The only way for an electron to not scatter is by traveling in a vacuum. The path of electron beam is shown in Figure 1.19a.[53]

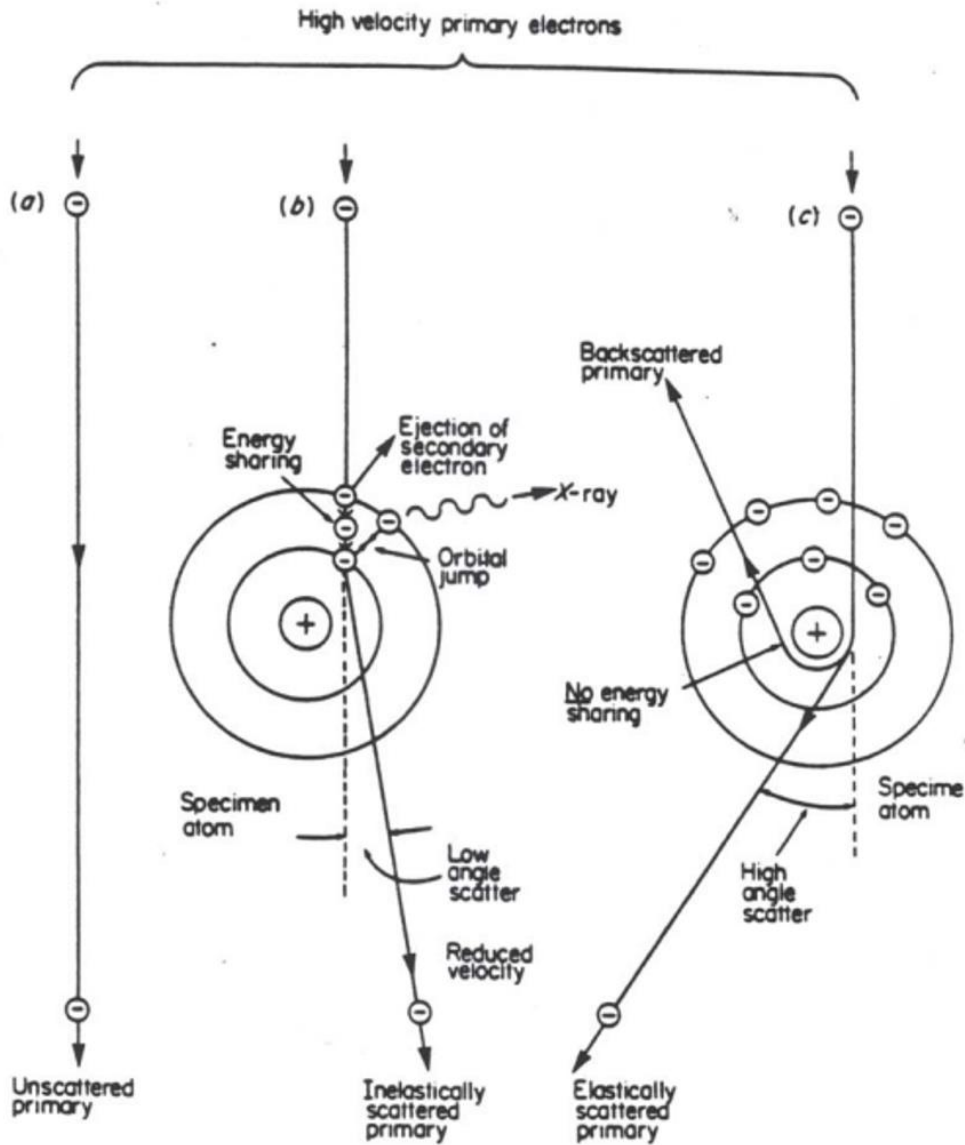


Figure 1.19-Electron interactions with matter (a) electron beam traveling through vacuum (b) Inelastically scattering producing secondary electrons (c) elastically scattering off the nucleus of an atom [53]

Of these two interactions, inelastic is much more common, which causes ionization events and produce secondary ionized electrons. These secondary electrons in turn interact with the

material producing an electron cascade. In the case of polymers, the ionized polymer chains will then undergo scissions which form free radicals allowing chemical reactions to occur.

Most industrial electron beams operate between 0.1-10 MeV for polymer production.[54] They are used for the modification of polymer systems. The frequency of ionization interaction is dependent on electron density of the target and materials. Materials with higher atomic numbers, have a greater ability to stop β particles which decreases the radiation depth of penetration. This dependence of penetration depth on the material properties of the target is based on the Bethe equation. This equation models the stopping power, rate of energy loss (J/m) by an electron as it travels through a material (Equation 1.12).

$$-\left(\frac{dE}{dx}\right) = \frac{2\pi N e^4 Z}{m_e v^2} \left[\ln \frac{m_e v^2 E}{2I^2(1-\beta^2)} - (2\sqrt{1-\beta^2} - 1 + \beta^2) \ln 2 + 1 - \beta^2 + \frac{1}{8}(1 - \sqrt{1-\beta^2})^2 \right] \quad (1.12)$$

In Equation 1.12, v is the velocity of the electrons, c is the velocity of light, β is the ratio of electron velocity to the speed of light, I is the mean electron ionization energy for the target material, N is the packing factor, e is the charge of an electron, m_e is the rest mass of an electron, and Z is the atomic number of the target material[45]. Figure 1.20 shows the penetration of an electron beam in water as a function of the energy level of the accelerated electron.

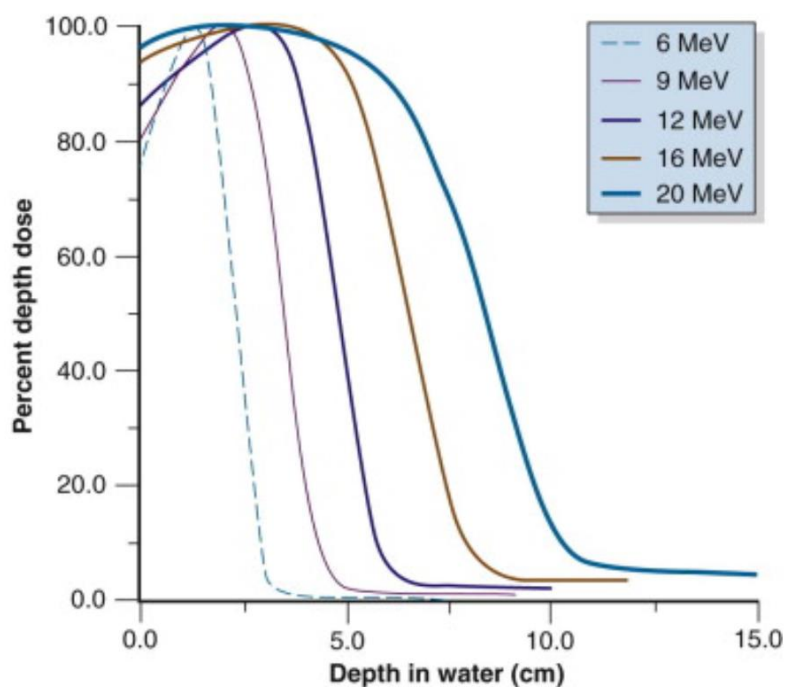


Figure 1.20- Penetration of electron beam in water [55]

As the electron loses its energy and slows down, it is transferring energy into the material, causing ionization. It also produces bremsstrahlung which is electromagnetic radiation.

An advantage of β radiation is it can be generated through the use of electronic means such as a Van de Graaff generator or linear accelerator (LINAC). These devices use electrical potentials to collect and accelerate packets of electrons to high velocities at a target substrate. The operation of these devices will be discussed in the experimental section of this thesis. This dissertation utilized a LINAC to generate 10.4 MeV high energy electrons for radiation grafting of the ionic liquids to fluorocarbon substrates to synthesis novel PEM designed for high temperature fuel cell applications. This thesis will evaluate the use of beta radiation, high energy electrons accelerated in a linear accelerator (LINAC) to synthesize PEM samples.

1.4.3 Radiation Chemistry

When polymers are irradiated, there are two significant competing reactions; cross-linking in which bonds are created between neighboring polymer chains and scission where bonds in the polymer are broken. Figure 1.21 depicts radiation induced scission and cross-linking reactions and how they modify the polymer structure. Radiation yield (G-values) are used to describe the chemical changes that occur in materials and is proportional to the applied dose. The units of radiation yield are usually given in molecules/100eV or the SI unit of $\mu\text{mol/J}$. [45] Based on their structure, some polymers are more susceptible to radiation. The ratio of G-cross-linking (G_c) and G-scission (G_s) can be used as indicator of a polymers radiation resistance and whether it will strengthen or degrade after radiation treatment. This ratio (G_c/G_s) greatly effects the radiation behavior and resistance of a polymer as shown in Figure 1.21. [56],[57] The free radicals generated during radiation treatment are active sites for grafting and can be used to functionalize the polymers for specific applications. Furthermore, the type, intensity and environment of the radiation treatment can affect the physical, chemical and material properties of polymers.

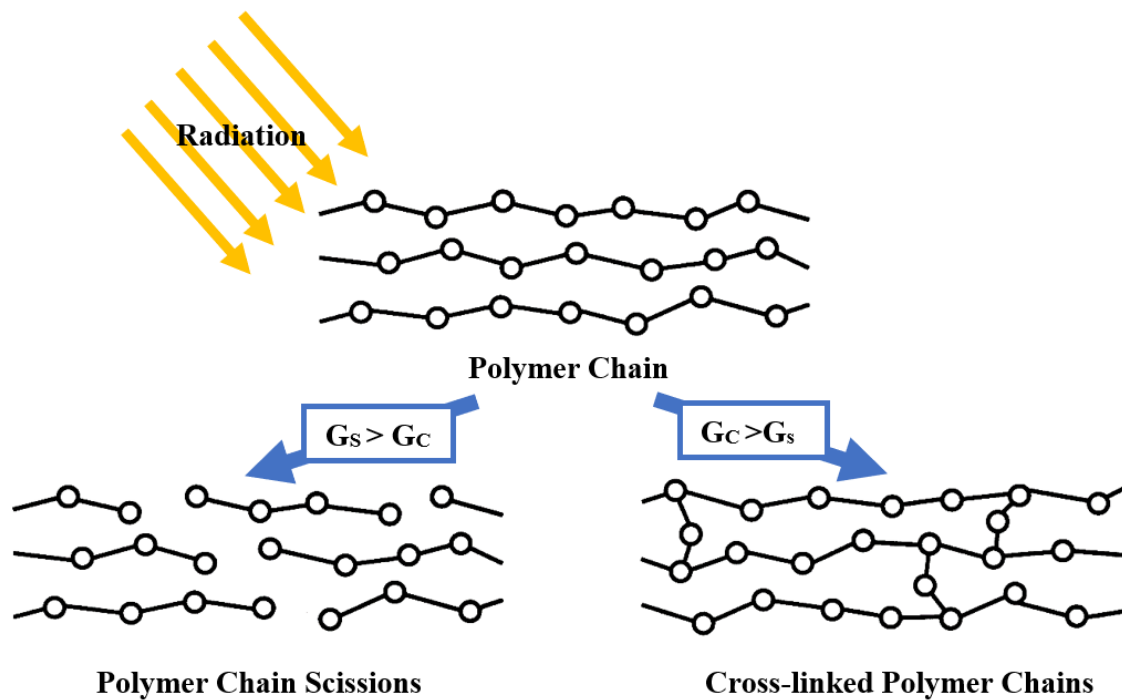


Figure 1.21- Irradiated polymer chains undergo two competing reactions; scission and cross-linking. Dominance is based on radiation conditions and chemical properties of the polymer.

The mechanical strength of the bulk polymer is proportional to the chain length and can be decreased if the number of back bone scissions are substantial. The free radicals can act as sites for chemical and cross-linking reactions, which allows the properties of the material to be further modified.

Radiation grafting is a method using ionizing radiation to generate free radicals which act as sites to chemically bond one polymer onto the matrix of another polymer. An example of a branched co-polymer is depicted in Figure 1.22, where polymer B was grafted onto the backbone of polymer A.

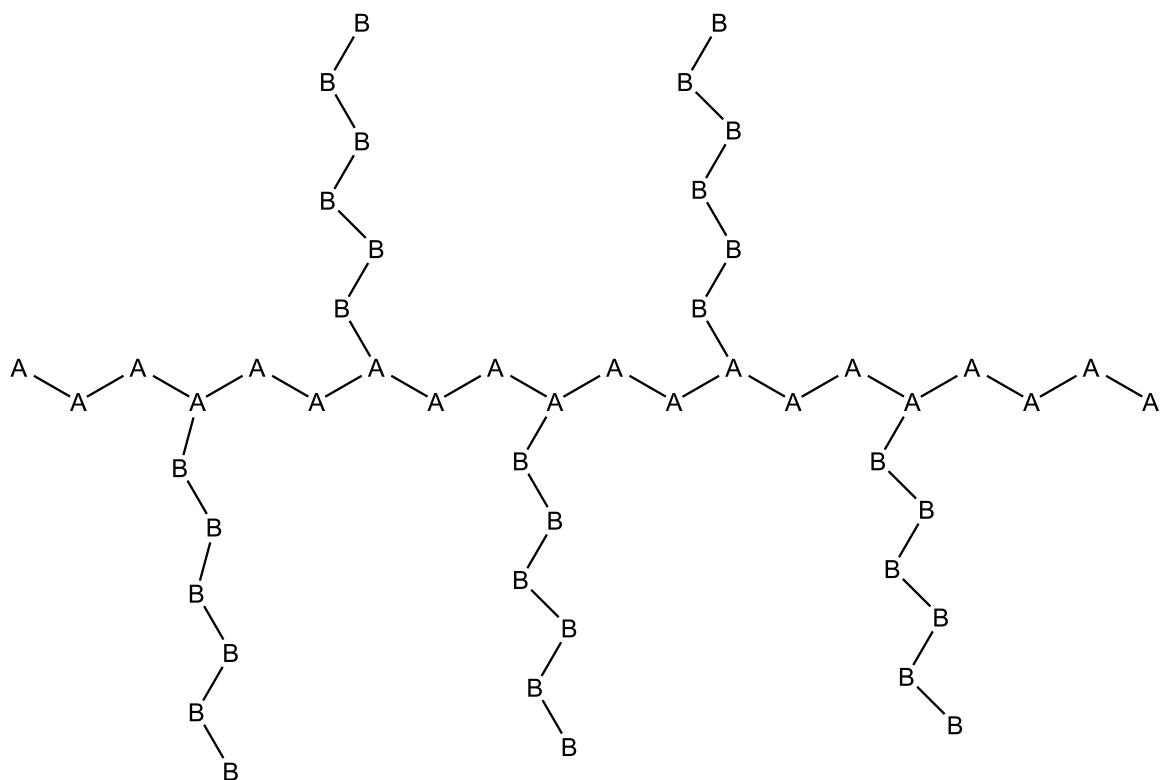


Figure 1.22- Simplified structure of a grafted copolymer consisting of a polymer A backbone and polymer B side chains.

When free radicals produced by ionizing radiation are used as grafting sites for monomer solutions, branching polymer chains are produced on the surface and in amorphous regions of the irradiated polymer. Radiation grafting is commonly used to create composite polymers with modified material properties that are an amalgamation of the two polymers. The composite material properties will take on the mechanical properties of the backbone polymer and the chemical properties of the side chain polymer.[40]

This grafting technique has been used in a number of industries to improve various characteristics of the substrate material, including hydrophilicity, biocompatibility, and electrical conductivity. The technology has been used for a number of different applications including the

fabrication of fuel cell membranes, fire-retardant materials and ion exchange membranes.[58],[59],[60],[61]

1.4.4 Radiation Grafting Methods

There are significant benefits to utilizing radiation grafting over chemical methods to generate modified co-polymers. Radiation grafting is versatile since most polymers will form free radicals when placed in ionizing radiation, thereby producing grafting sites for the formation of copolymer chains. No initiator or additives are required to start or limit the reaction. As such, additional materials are not affecting the chemistry of the grafted polymer. The degree of grafting can be controlled by changing the radiation treatment conditions. Radiation grafting does not require heating the system which allows grafting of volatile monomers. There are two methods of radiation grafting, direct and indirect, which are depicted in Figure 1.23 and Figure 1.24 respectively.[62],[63],[64]

Through the course of this research, polymers were synthesized using beta radiation to graft proton conductive ionic liquids onto fluorocarbon substrates. The high mechanical, chemical resistant and thermal stability properties of the fluorocarbon backbone combined with the ionic liquid branches act as a proton conductive medium for high temperature applications. A copolymer produced with these properties can be utilized in PEM for fuel cells operating at temperatures above 100°C.

Direct Radiation Grafting Procedure

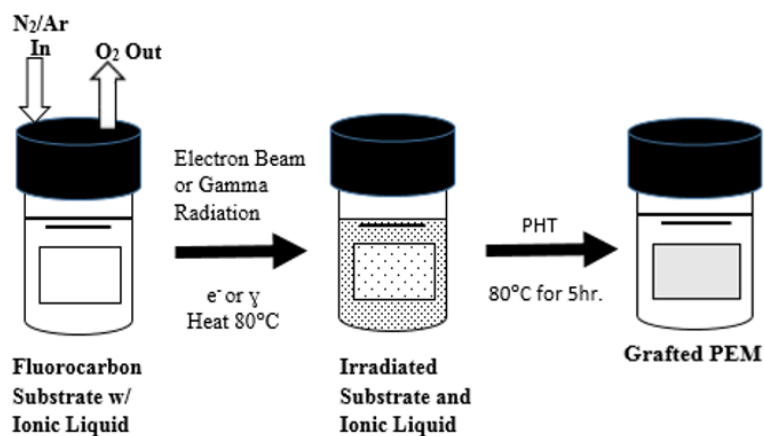


Figure 1.23 -Direct Radiation Grafting Method: ionic liquid monomer and substrate are irradiated together

Indirect Radiation Grafting Procedure

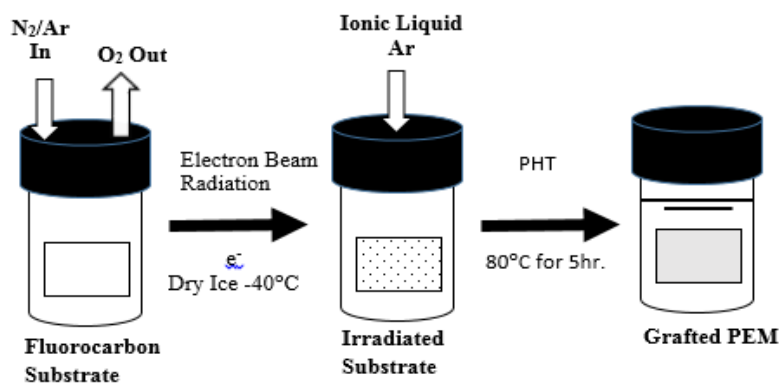


Figure 1.24-Indirect Radiation Grafting Method: ionic liquid monomer added after substrate is irradiated

1.5 Alternative High Temperature Fuel Cell Designs

PEM have been designed incorporating sulfuric acid and phosphoric acid to replace water as the proton transport medium to increase their operating temperature.[65] Because hydrogen fuel cells produce water, acid could leach from these membranes affecting the proton conductivity of the system and their reliability. The acid vapor runoff from the system can also cause corrosion of components in the fuel cell system.

Radiation grafted ionomers have been evaluated as candidates for use in fuel cells to replace Nafion membranes for improved performance.[61] Radiation grafting of styrene onto FEP followed by sulfonation treatment has been performed to produce styrene sulfonic acid PEM[62][66]. These membranes had good proton conductivity but poor mechanical properties.[67]–[68] Acidic chemicals are usually added with high temperature treatments which can significantly damage the PEM, affecting their reliability. A comparison of the microstructure of a sulfonated membrane and Nafion is shown in Figure 1.25. The diameter of the nanochannels and the pKa of the functional groups affects the high temperature proton conductivity properties of PEM. [69] To improve the reliability of these PEM and to prevent their degradation, a one-step radiation grafting procedure has been studied, which will attach the ionic functional groups directly onto fluorocarbon membranes.[61] The resulting membranes showed improved proton conductivity without a significant decrease in reliability.

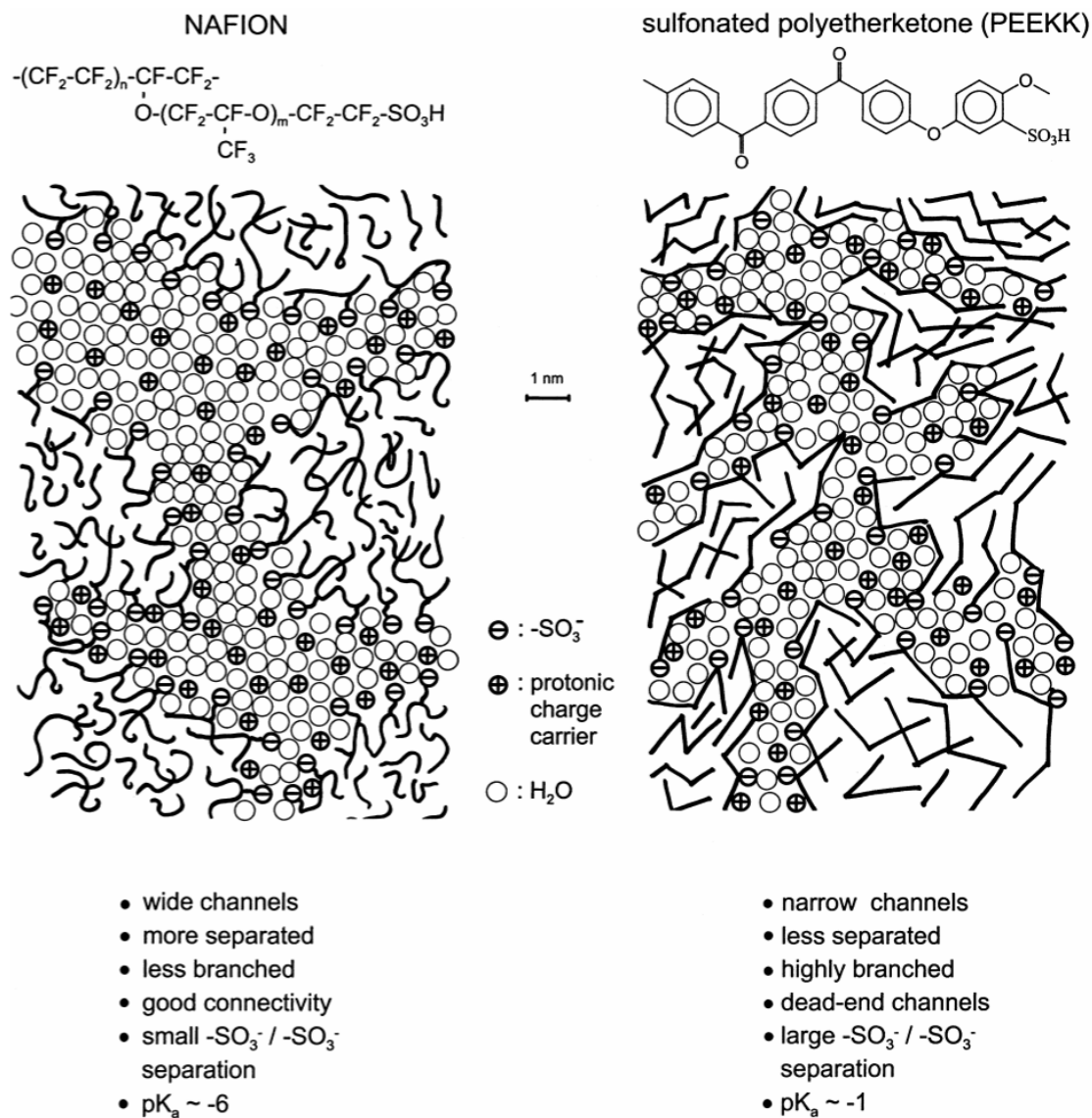


Figure 1.25- Microstructure comparison of PEM: (left) Nafion™ and (right) sulfonated polyetherketone; chemical properties of nanochannels and their effect on proton conductivity[69]

The addition of ionic liquids to PEM as a means of proton conductivity has been investigated to create anhydrous, high temperature solid state systems.[70],[71],[72],[73],[74],[75],[76],[77] Ionic liquids were shown to have a positive correlation with proton

conductivity and temperature allowing PEMFCs to operate above the 100°C threshold.[78]

Proton conductivity of ionic liquids have been shown to be tied to their mobility and viscosity, with higher degrees of freedom producing higher conductivity.[79] To stabilize ionic liquids within PEMs, free radical polymerization was used to covalently graft the ionic liquid. While previous ionic liquid membranes have been fabricated by filling or mixing the ionic liquids into the porous membrane, the technique of free radical chain polymerization has recently been utilized for fabricating ionic liquid fuel cell membranes. Imidazole groups are covalently attached to the polymer substrate to prevent loss of conductivity due to volatilization.[80]

Polymers of ionic liquids such as poly-4-vinylpyridine, poly-2-vinylpyridine, polyvinylimidazoline and polybenzimidazole have also been combined with strong acids to generate PEM.[81],[82],[83] Figure 1.26 shows how heterocyclic amine ionic liquid systems exhibit high proton conductivity at high temperatures. [69] They also can compete with traditional PEM such as Nafion™ and membranes that use sulfonate groups for proton conductivity.

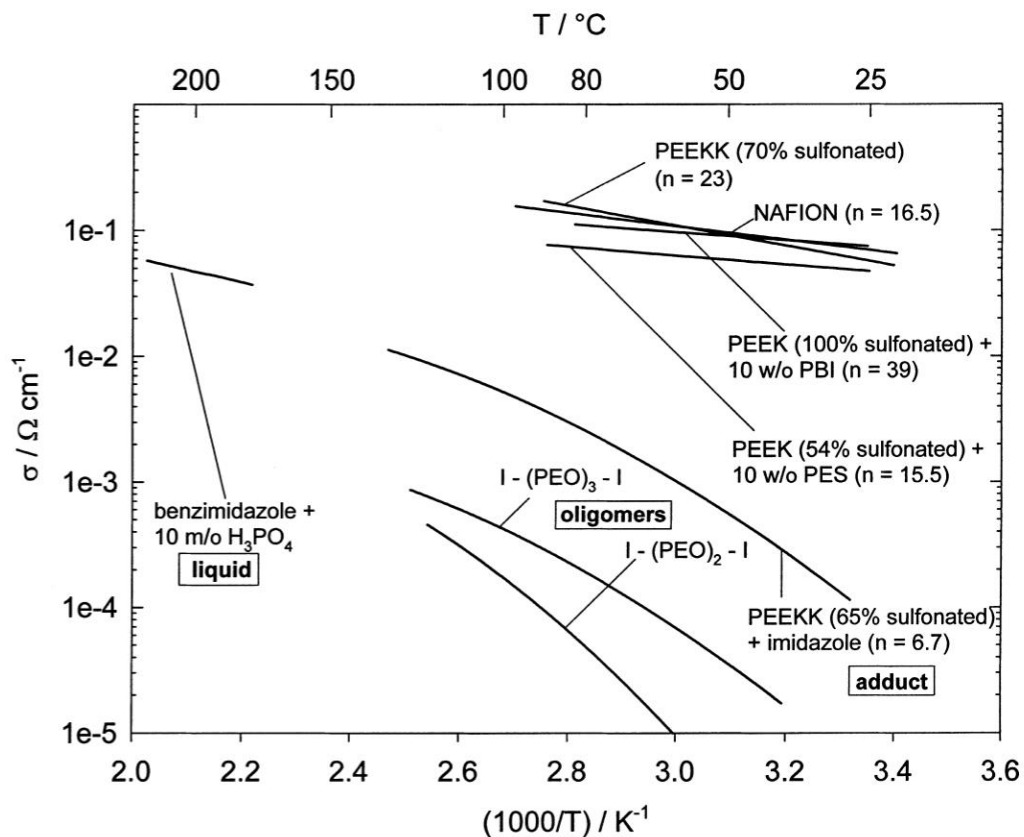


Figure 1.26-Proton Conductivity of heterocyclic protic ionic liquids[69]

Ionic liquids have been incorporated into Nafion and fluorocarbon membranes to improve proton conductivity, but radiation induced grafting of ionic liquids to fluoropolymers has not been thoroughly investigated.[84],[85],[86],[87] Through the course of this research, radiation grafting of ionic liquids onto fluorocarbon substrates will be reported along with performance testing at high temperatures (120°C). The following chapter will discuss further application of ionic liquids as proton conductive functional groups.

2.0 Chemistry of Proton Conductive Ionic Liquid Membrane

This chapter will explore the theory and chemistry supporting the development of proton conductive ionic liquid membranes for fuel cell applications. The properties, suitability and selection of proton conductive ionic liquids and polymer substrate for radiation grafting are presented. In traditional fuel cell membranes, water or ionic liquids are used as the conductive medium. However, for high temperature operation above 100°C, water is not a suitable medium because of evaporation in the membrane which decreases conductivity. To design membranes that have high proton conductivity at high temperatures, water needs to be substituted with another medium capable of conducting protons. Ionic liquids are able to play this role and act as charge carriers which will create stable conductive membrane systems that function at higher temperatures. It is critical to select a polymer substrate that is chemically resistant, can tolerate high temperatures and can create enough radiation induced grafting sites to allow proton transfer through the membrane.

2.1 Ionic Liquids

Ionic liquids cover a broad range of compounds that can be neutral or charged. They are liquid at room temperature where the molecules contain charged functional groups with strong electrostatic forces. The ability to create a flow of charge makes them useful as solvents to moderate electrochemical reactions. Preferred properties of ionic liquids are:

- high ionic, electron and proton conductivity
- low vapor pressure
- high electrochemical stability
- high thermal stability
- high decomposition temperatures.[88]

There are three main types of ionic liquids based on their charge interactions; aprotic, protic and zwitterionic.

The first type, aprotic ionic liquids are incapable of acting as a proton donor meaning that there is no charge transfer between the anion and cation groups. As a result, the charges are fixed and conductivity occurs through diffusion. The second type, protic ionic liquids are created through proton transfer between the anion and cation. The presence of this proton transfer makes protic ionic liquids suitable to create proton conductive systems. The third type, Zwitterionic ionic liquids are created when the cation and anion are present in the same molecule. These different types of ionic liquids are shown below in Figure 2.1.

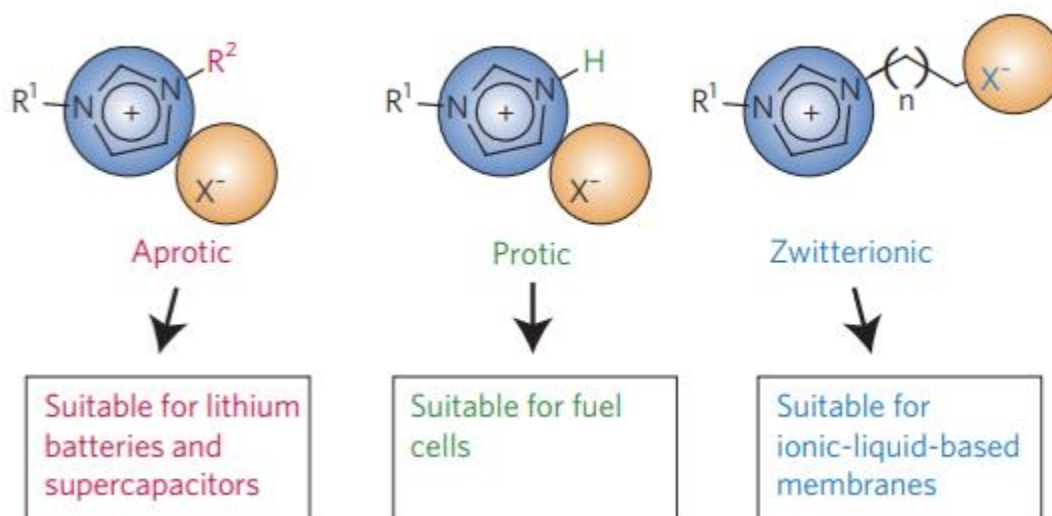


Figure 2.1- Ionic liquid types: Aprotic, Protic and Zwitterionic and their applications[88]

Ionic liquids are commonly used in electrochemical systems as electrolyte or solvent to facilitate redox reactions. However, only protic ionic liquids are suitable for solid state proton conductivity for fuel cell application.

As shown in Figure 2.2, protic ionic liquids similar to water are able to exchange hydrogen with neighboring cyclic amine groups.

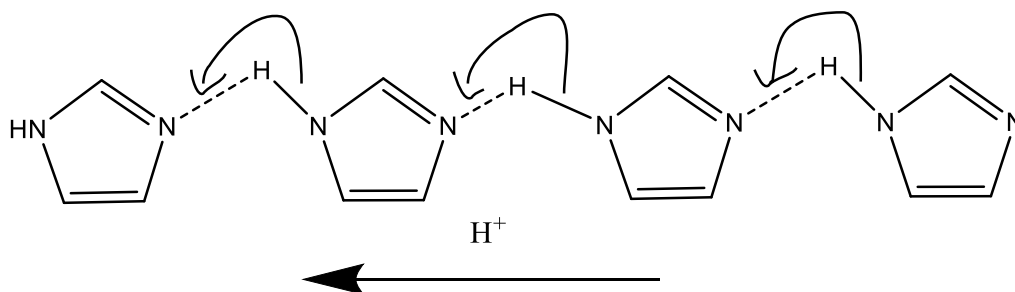


Figure 2.2- Example of Protic Ionic Liquid: Imidazole proton conductivity can occur by H^+ exchange of near neighbors which act as both proton donors and acceptors.[88]

A major objective of this research was to study acidic protic ionic liquids and their proton exchange properties to create a solid-state proton conductive network within PEM. Protic ionic liquids have functional groups that can accept and release protons and therefore can be used for proton transport.[89] The other types of ionic liquids, aprotic and zwitterionic, either have no available sites to accept and release protons or form a complex that prohibit diffusion and grafting. As such they were not studied for this research project.

2.1.1 Acidic Ionic Liquids

Acidic ionic liquids are low melting ionic salts with acidic characteristics.[90] There are two types of acidic ionic liquids, Bronsted acid ionic liquids and Lewis acid ionic liquids. Lewis acid ionic liquids are electron acceptors giving acidic properties and Bronsted acid ionic liquids are acidic as a proton donor. Lewis acids are not considered for fuel cell applications in PEMs which require protons to be exchanged.

The type of Bronsted acid ionic liquids can be further classified based on the location of the acidic proton in the ionic liquid structure. Refer to Figure 2.3 for sub groups. [90]

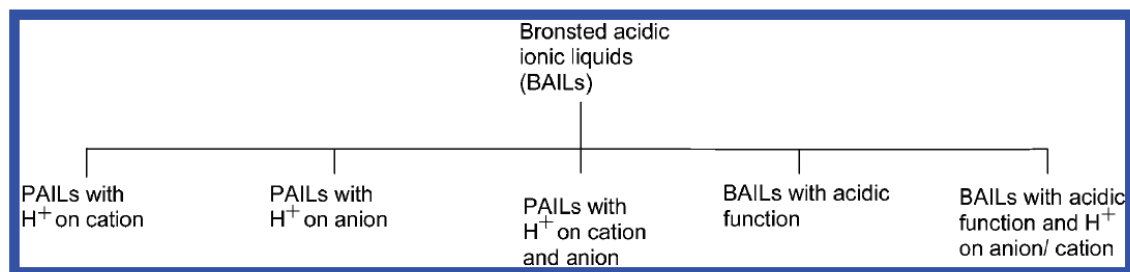


Figure 2.3- Sub-groups of Bronsted acid ionic liquids (BAILs); protic acidic ionic liquids (PAILs) [90]

Of these Bronsted acid sub-groups, heterocyclic amine protic ionic liquids are classified as PAILS with H⁺ on cation and anion with application in fuel cells as an electrolyte.[90]

Ionic liquids are used for high temperature electrochemical applications. The boiling point of an ionic liquid determines the operating temperature range. The boiling point of protic ionic liquids is dependent on the proton transfer from acid to the base. The relationship between boiling point and proton conductivity is shown in Figure 2.4. The ionic liquids that have higher boiling temperatures (T_b), have greater ΔpK_a values for the ionic liquid cation and anion, which should result in lower proton conductivity.

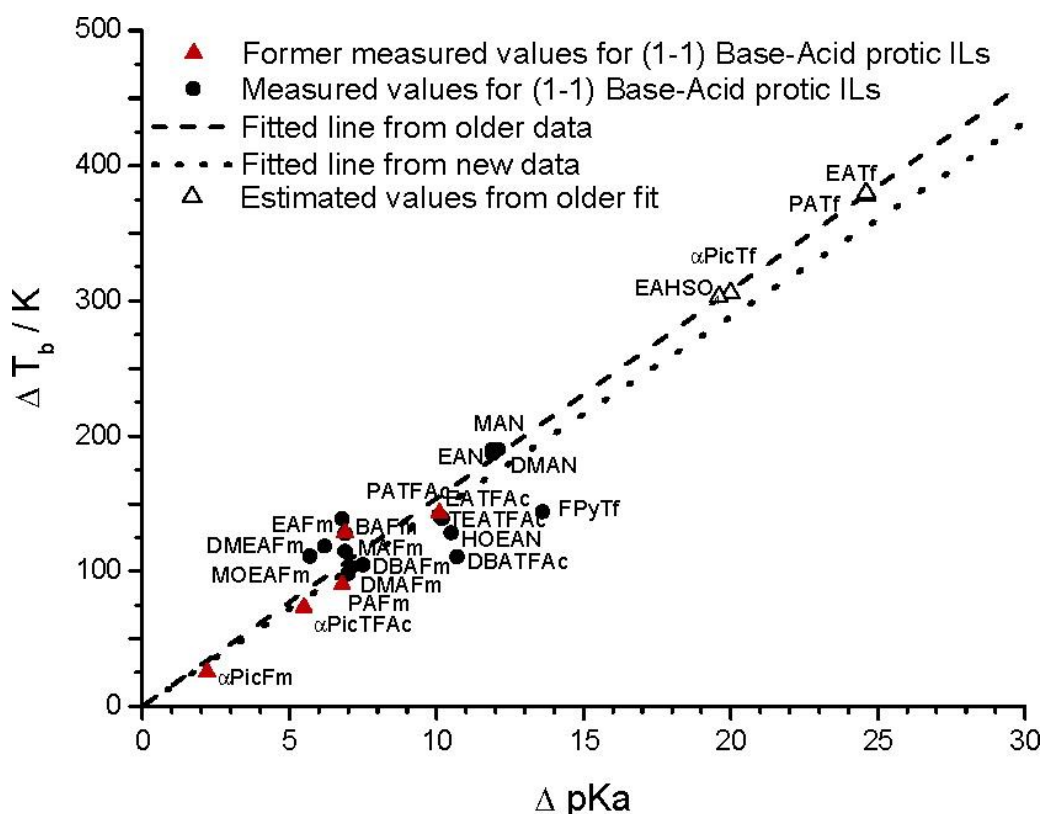


Figure 2.4- Relationship between pKa and boiling point for ionic liquid systems [91]

The pKa value relates to the free energy (ΔG) of a proton transfer from the Bronsted acid to water and is depicted by Equation 2.1[91]:

$$\Delta G = -RT \ln K_a \quad [2.1]$$

R is the gas constant, T is temperature, K_a is the acid dissociation constant. This equation can be related to the activation energy for proton conductivity in anhydrous ionic liquid systems. The pH is a measure of available free protons in a system, the lower the pH the higher the concentration of $[H^+]$ in the PEM. In fuel cell operation, the pH level is driven by a hydrogen gas reaction at the platinum catalysis electrode. When the pH of the system is equal to the pK_a of the ionic liquid, 50% of the ionic liquid monomers will be protonated. The greater the difference in the ΔpK_a values of the cation (acidic) and anion (basic) ionic liquids, the greater

the activation energy for proton conductivity.[92],[93],[94] The relationship between ΔpK_a and proton conductivity in a protic ionic liquid system is shown by Equation 2.2:

$$\Delta G = RT\Delta pK_a \quad [2.2]$$

The pK_a values of protic ionic liquids are shown in Table 2.1 and how they relate to the activation energy of proton conductivity for a variety of ionic liquids. The higher the activation energy the greater the barrier and lower the proton conductivity. This barrier can be overcome by increasing the operating temperature in which thermal energy is on the order of the activation energy. However, by design it is better to select ionic liquids that would create a system with the lowest activation energy for proton conductivity.[95]

Table 2.1-The proton free energy level diagram for Ionic Liquids formed from strong acids and bases to yield neutral ionic liquid products.[91]

	Occupied	Vacant	pK _a	E (eV)
	HNO ₃	NO ₃ ⁻	-1.30	0.08
	CF ₃ COOH	CF ₃ COO ⁻	-0.25	0.01
	H ₃ O ⁺	H ₂ O	0	0
	H ₃ PO ₄	H ₂ PO ₄ ⁻	2.12	-0.13
	3,4,5-trifluoroanilineH ⁺	3,4,5-trifluoroaniline	2.62	-0.15
	1,2,4-1H-triazoleH ⁺	1,2,4-1H-triazole	3.00	-0.18
	HF	F ⁻	3.20	-0.19
	HCOOH	HCOO ⁻	3.75	-0.22
	anilineH ⁺	aniline	4.60	-0.27
	CH ₃ COOH	CH ₃ COO ⁻	4.75	-0.28
	pyridineH ⁺	pyridine	5.23	-0.31
	ImH ⁺	Im	6.99	-0.41
	hydrazineH ⁺	hydrazine	7.96	-0.47
	Me ₂ ImH ⁺	Me ₂ Im	8.38	-0.50
	NH ₄ ⁺	NH ₃	9.23	-0.55
	Me ₃ NH ⁺	Me ₃ N	9.80	-0.58
	EtNH ₃ ⁺	EtNH ₂	10.63	-0.63
	Et ₃ NH ⁺	Et ₃ N	10.72	-0.63
	Et ₂ NH ₂ ⁺	Et ₂ NH	10.80	-0.64
	Bu ₂ NH ₂ ⁺	Bu ₂ NH	11.25	-0.67
	H ₂ O	OH ⁻	14	-0.83

0.71eV

Neutral Electrolytes

In order to lower the ΔpK_a of PEM, Bronsted acid ionic liquids were grafted onto PEMs to create a network for proton conductivity. A barrier to proton hopping in this model is structural due to the spacing of the grafted ionic liquids groups and the limited degrees of freedom of the ionic liquid. The ionic liquids need to be present in sufficient density to allow proton conductivity between neighboring functional groups.

The activation energy directly effects the proton conductivity in PEM through the Arrhenius equation shown in Equation 2.3.

$$\sigma \text{ (S/cm)} = \sigma_0 * e^{-\frac{E_a}{kT}} \quad [2.3]$$

In Equation 2.3, σ_0 is the pre-exponential constant, E_a is the activation energy of proton conductivity, k is the Boltzmann constant and T is temperature. Equation 2.3 shows the interrelationship between proton activation energy, operating temperature and proton

conductivity of PEM. However, this model assumes that there is only a single barrier to proton conductivity and that it is not affected by temperature. This might not be the case for PEM where the proton conductivity is affected by the configuration of the grafted ionic liquid groups. In summary, the activation energy of proton conductivity in the PEM will be affected by amount and density of grafted protic ionic liquid monomer, the pK_a of ionic liquid and the microstructure of the PEM.

2.1.2 Proton Conductive Ionic Liquids

Heterocyclic amine protic acidic ionic liquids such as imidazole, pyrazole, triazole and benzimidazole have been studied as suitable proton solvents to replace water in PEMFC.[70][87],[96],[97] Selecting suitable protic ionic liquids for PEM application is based on the proton conductivity of the protic ionic liquids. Conductivity is reflected in the dissociation constants (pK_a) between the proton donor and acceptor within the system. The greater the potential energy difference between these two states, the lower the proton conductivity. The energy to oscillate between these two energy states can be improved by a higher operating temperature of the membranes.

A goal of this research is to determine the relationship between pK_a of protic ionic liquids and their conductivity behavior in PEM. The heterocyclic amine protic ionic liquids which have been established in literature as having high proton conductivity at high temperatures, and selected for further study were; 4-vinylpyridine and 5-vinylpyrimidine.[80],[96],[97] The chemical structure of the two protic ionic liquids are shown in Figure 2.5.

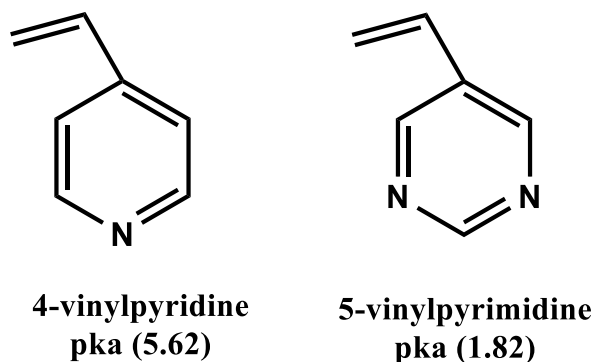


Figure 2.5: Heterocyclic Amine Protic Ionic Liquid and their pKa values

These protic ionic liquids were chosen since their structures are symmetric and have vinyl groups suitable for radiation grafting to a polymer substrate to create PEM. The monomer symmetry will decrease the activation energy for proton transfer between grafted ionic liquid groups.[25],[78]

2.2 Polymer substrate for radiation grafting

Proton conductive membranes prepared by radiation grafting are composed of two materials; a polymer substrate and protic ionic liquid. Polymers were evaluated that have thermal properties to withstand the environment of high temperature fuel cell operation. Fluoropolymers such as polytrifluoroethylene (PTFE), fluorinated ethylene-co-propylene (FEP), polyvinyl fluoride (PVF), polyvinyl difluoride (PVDF), polyfluoroacrylate (PFA) and polychlorotrifluoroethylene (PCTFE) are chemically resistant polymers with high melting temperatures, high glass transition temperatures and low electrical conductivity.[98]

After primary radiation studies, the polymers FEP, PCTFE and PVF were selected for further research because their functional groups gave them a higher degree of radiation resistance.[99] The repeating structure of the fluorocarbon polymers are depicted in Figure 2.6. See Table 2.2 for a comparison of their physical and chemical properties.

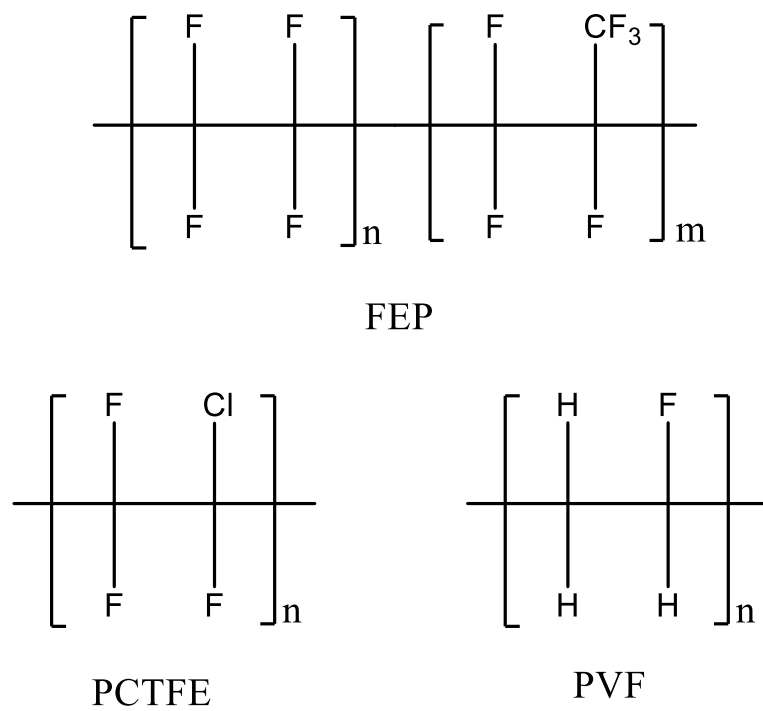


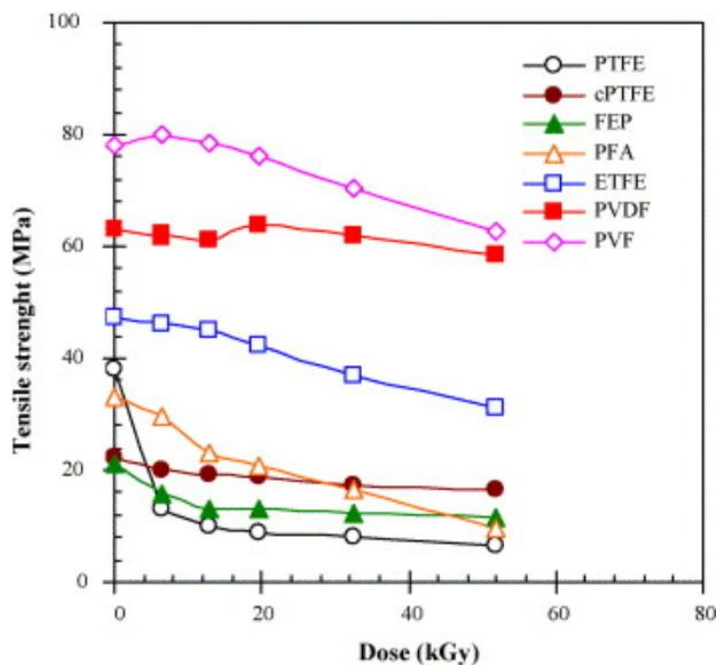
Figure 2.6- Fluorocarbon polymers with available sites for radiation grafting.

Table 2.2: Material Properties of Fluorocarbon Substrates [57],[66],[100],[101],[102],[103]

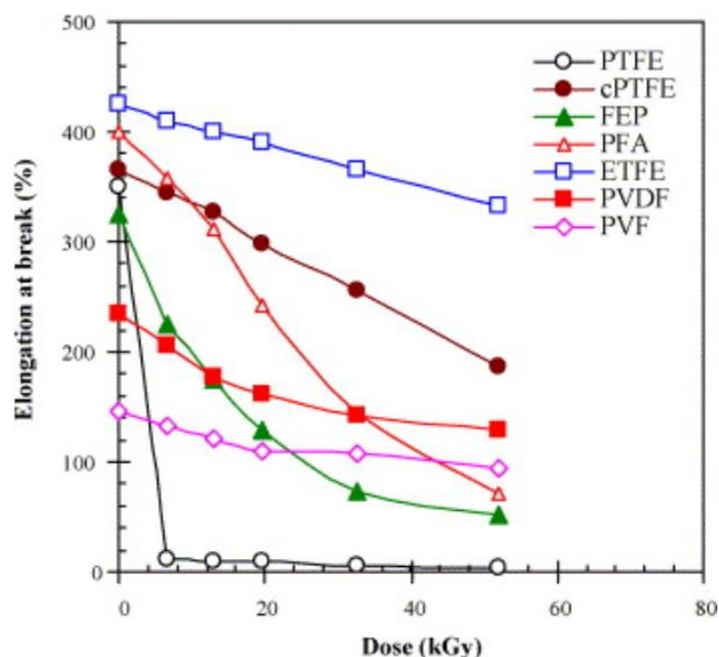
Material Properties	FEP	PCTFE	PVF
Mechanical Properties			
Film Thickness	25 μm	23.5 μm	25 μm
Ultimate Tensile Strength	22 MPa	76-141 MPa	55.2-110.4 MPa
Yield Strength	12 MPa	100 MPa	33.8-41.4 MPa
Elastic Modulus	480 MPa	1.31-1.55 GPa	2.07-2.62 GPa
% Elongation	300%	100-150%	90-250%
Density	2.15 g/cm	2.11 g/cm ³	1.37-1.72 g/cm ³
Molecular Weight	250-600 kg/mol	75-150 kg/mol	100-500 kg/mol
% Crystallinity	50-75%	40-65%	20-60%
Thermal Properties			
Melting Point	260-280°C	211°C	193°C
Glass Transition Temperature	80°C	45°C	41°C
Thermal Expansion	9.4 X 10 ⁻⁵ /K	7x 10 ⁻⁵ /K	5.04 X 10 ⁻⁵ /K
Dimensional Stability	0.72%	12%	4%
Electrical Properties			
Dielectric Constant	1.93-2.02	2.50-2.60	8.5-11
Dissipation Factor	0.0002-0.0007	0.02	0.014-0.042
Volume Resistance	>1X10 ¹⁸ ohm.cm	>1X10 ¹⁸ ohm.cm	4X10 ¹⁴ ohm.cm
Chemical Properties			
Chemical Resistance	No Visible Effect (Acid, Bases, Solvent)	No Visible Effect (Acid, Bases, Solvent)	No Visible Effect (Acid, Bases, Solvent)
Gas Permeability	10 ³ *cm ³ /m ² x24hrxatm		
Carbon Dioxide	25.9	0.0259	17.2
Hydrogen	34.1	0.0341	90
Nitrogen	5	0.005	0.39
Oxygen	11.6	0.0116	5
Radiation Properties			
G Scission	4	0.67	1.8-4.0
G Crosslinking	1.2	-	3.0-8.0
G Gas	0.8	0.11	4.5

The fluorocarbon substrates provide the backbone structure of the PEM. J. Chen et al. studied mechanical properties of fluorocarbon polymers to determine good candidates for radiation

grafting substrates.[104] Mechanical properties: ultimate tensile strength and elongation at break were measured for increasing radiation dose, as shown in Figure 2.7. However, it is important to note that PEM are not being selected solely based on their mechanical properties. PTFE degrades significantly under radiation treatment because all the scissions occur along the polymer back bone. This is shown in Figure 2.7a as the ultimate tensile strength decreased significantly with radiation dose. It is also shown in Figure 2.7b as the elongation at break approaches zero at 5 kGy dose. The mechanical properties of polymers are tied to backbone chain length. In comparison, the change of mechanical properties of FEP films are affected less by the radiation dose. The greater radiation resistance of FEP is due to the $-CF_3$ group which protects the backbone. The elongation at break is expected to increase with radiation dose due to cross-linking reactions and is not necessarily associated with the degradation of the polymer.



(a)



(b)

Figure 2.7-Mechanical Properties: (a) Tensile Strength and (b)Elongation at break for Fluoropolymers that have been irradiate with gamma radiation. [104]

2.3 Design of Protic Ionic Liquid Membranes

In order to have high proton conductivity in PEM there needs to be uniform grafting within the membrane structure. The microstructure of the ionic liquid in the membrane will therefore significantly impact the proton conductivity in the polymer chain. Protic ionic liquid monomers are covalently bonded onto the polymer substrate via free radical induced radiation grafting. Figure 2.8 shows different ways ionic liquids can be incorporated into polymer membranes. [88],[105]

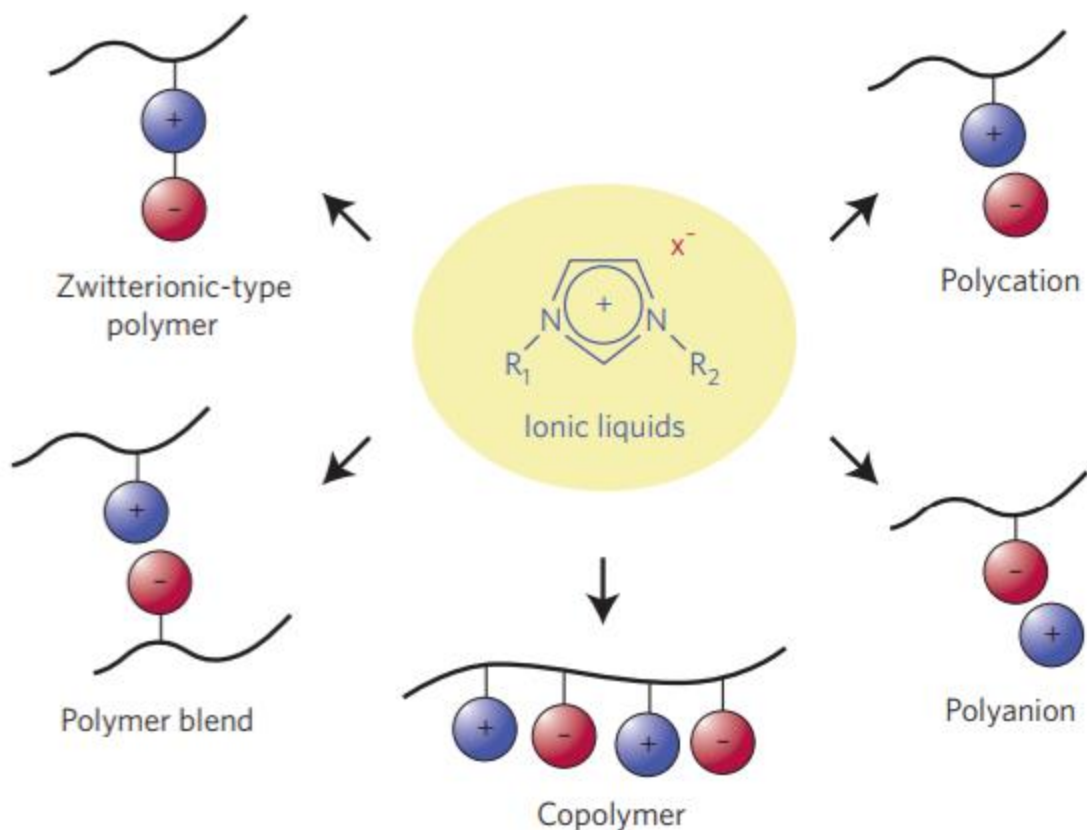


Figure 2.8- Different ways ionic liquids can be incorporated into polymer membranes[88]

While there are different ways ionic liquids can be incorporated into PEM, the polycation structure was chosen since the proton conductivity happens between the available acidic protic ionic liquid cation groups. Radiation grafting experiments were conducted to attach 4-vinylpyridine and 5-vinylpyrimidine monomers onto fluorocarbon substrates including FEP, PCTFE and PVF. Radiation generated free radicals react with vinyl groups of ionic liquids forming a covalent bond and grafting the ionic liquids into the membrane. The grafting site remains active and polymerizes the ionic liquid forming a branching copolymer structure, this process is shown in Figure 2.9.

Free Radical Polymerization Reaction 4-Vinylpyridine onto FEP

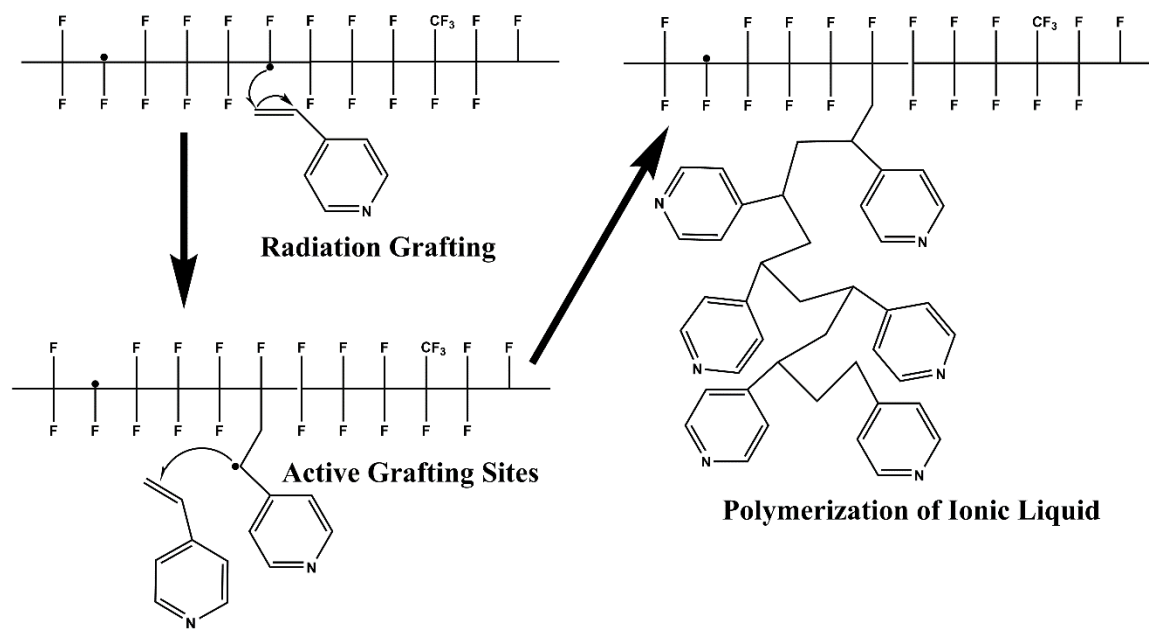


Figure 2.9 -Radiation Grafting Reactions: 4-vinylpyridine onto FEP substrate

Ionic liquids will only graft in amorphous regions of the polymer where they are able to diffuse into the membrane. A depiction of the microstructure of the grafted PEM is shown in Figure 2.10.

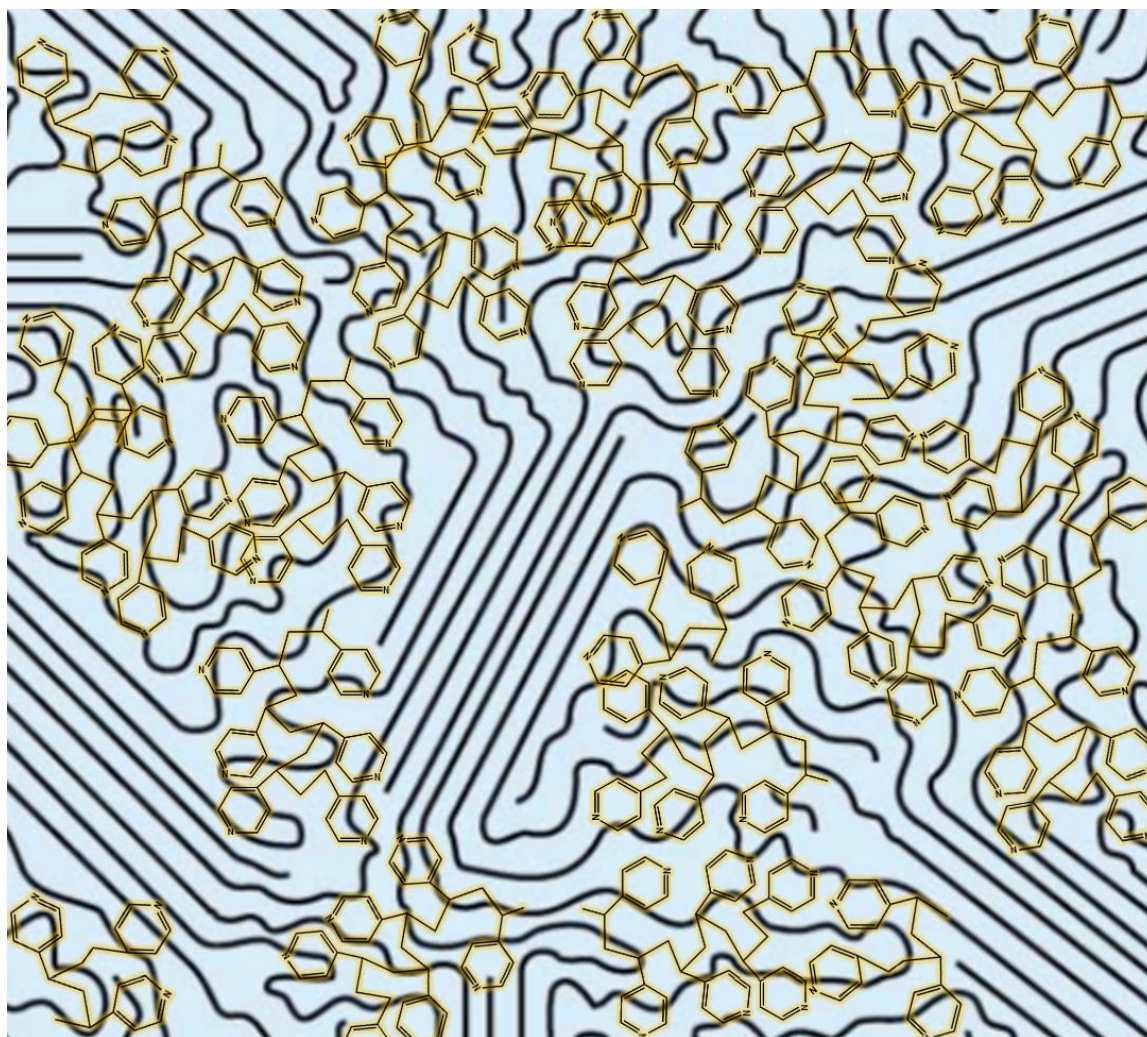


Figure 2.10- Depiction of Microstructure of radiation grafted 4-vinylpyridine to FEP PEM.

As discussed in this chapter, the selected materials demonstrate the capability for radiation grafting and proton conductivity with suitable mechanical properties and chemical stability at varying temperature and humidity conditions. The method used to synthesis these anhydrous PEM are discussed further in chapter 3 and are evaluated in chapter 4.

3.0 Experimental Methods and Approach

The research objective for this thesis was to design, synthesize, analyze and test innovative fuel cell membranes that function at temperatures above 100°C. Through substituting water with protic ionic liquids and radiation grafting onto fluorocarbon films, new proton conductive network solid state PEM have been prepared. The PEM were investigated and the inter-relationship between chemical and physical properties including conductivity measurements were used to assess applicability as fuel cell membranes. This chapter discusses the approach and methodology for preparation and testing the grafted solid state PEMs.

3.1 Material Design

The research goal was to design PEM for fuel cell applications capable of operating at temperatures above 100°C. Higher temperatures enable fuel cells to operate more efficiently by enhancing the reaction kinetics, increasing catalysis activity and reducing carbon monoxide poisoning of the electrodes[106]. However, operating above the boiling point of water leads to dehydration of the membrane and loss of proton conductivity unless a different transport mechanism is in place. PEM were prepared with select properties in order to achieve this goal. The PEM were designed to have high proton conductivity, low electrical conductivity, high mechanical properties, high chemical resistance, and high temperature and humidity stability. To produce fuel cell membranes with these properties, fluorocarbon substrates were combined with protic ionic liquids through radiation grafting.

3.1.1 Substrate Selection

The two material components of the fuel cell membranes are; the fluorocarbon substrates and the ionic liquids monomers. The substrate material serves as the foundation of the PEM. Polymers were evaluated that have thermal properties to withstand the environment of high

temperature fuel cell operation. Fluoropolymers such as polytrifluoroethylene (PTFE), fluorinated ethylene-co-propylene (FEP), polyvinyl fluoride (PVF), polyvinyl difluoride (PVDF), polyfluoroacrylate (PFA) and polychlorotrifluoroethylene (PCTFE) are chemically resistant with high melting points, high glass transition temperatures and low electrical conductivity.[98] After primary radiation studies, the polymers FEP, PCTFE and PVF were selected for further research because their functional groups gave them a higher degree of radiation resistance.[99] The chemical structure of these fluorocarbon membranes are depicted in Figure 3.1. When these polymers were exposed to radiation, their functional groups offer some protection to the polymer backbone by preventing radiation degradation. This allows for long lived free radicals that can be used as grafting sites without significantly degrading their mechanical properties. The fluorocarbon membranes selected for this research project were:

- FEP thin membranes, 25 μ m, purchased from CS Hyde
- PVF thin membranes, 25 μ m, purchased from Goodfellows
- PCTFE thin membranes, 23.5 μ m, provided by Honeywell.

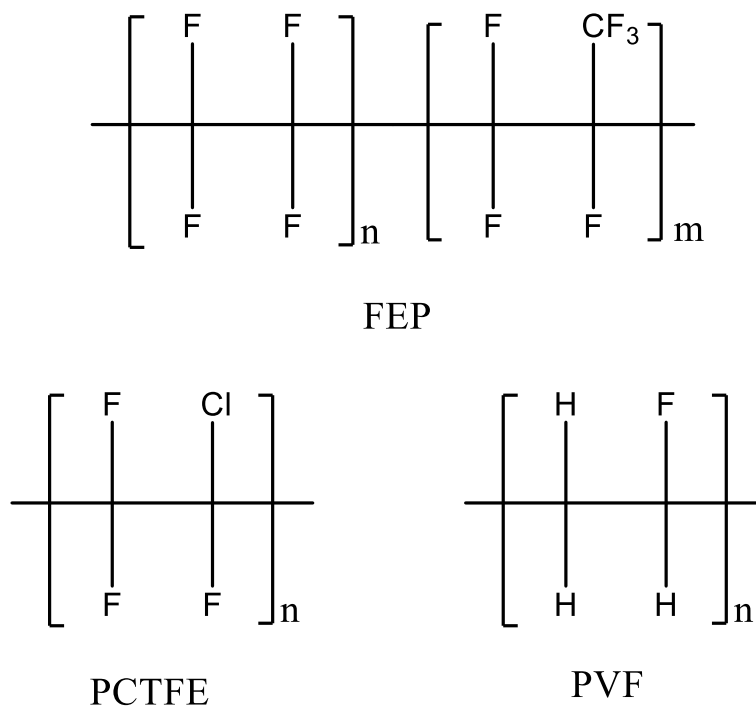


Figure 3.1-Chemical structure of fluorocarbon substrates FEP, PCTFE and PVF

Nylon based polymers were initially investigated. Nylon 4/6 has a melting temperature of 220°C and is used as a barrier for anaerobic systems.[107] The polymer has a higher permeability for water, can exclude oxygen, and has internal hydrogen bonding that can be used for proton transport. These Nylon materials are able to keep their structure at high temperatures, as well as act as gas barriers, making them ideal scaffolding materials for ionic liquids for PEMFC application. However, Nylons are polyamides, which degrade under acidic conditions making them unreliable for long term operation in fuel cells. When Nylon samples were acid treated for conductivity testing, they degraded into solution and as a result were not pursued further for this research. The selected fluorocarbon substrates have good compatibility with radiation grafting and testing conditions being studied.

3.1.2 Proton Conductive Ionic liquid

The fluorocarbon based PEM substrates require functional groups to be added for proton conductivity. In order to achieve proton conductivity at temperatures above 100°C, it was important to replace water with another medium that could transport protons. This research supports that protic ionic liquids are suitable for this role because they have functional groups that can accept and donate protons and remain stable at elevated temperatures. Ionic liquids are appropriate for proton transport in fuel cells because they exhibit high ionic conductivity, low vapor pressure, high electrochemical stability and high decomposition temperatures which would make them suitable for the high temperature fuel cell environment. The conductivity of protic ionic liquids are dependent on their pK_a values. It is important to note, environmental pH can affect the ionic liquids ability to accept and donate a proton and must be controlled. Ideally, the pH value should be the same across the proton conductive system to reduce barriers for conductivity. To achieve this, ionic liquid monomer having multiple proton sites with equivalent bond energies (symmetrical amine sites) were used, creating structural alignment as a lattice for proton conductivity. The ionic liquid monomers were also selected based on chemical properties such as having either a vinyl or allyl group with a double bond to allow covalent bonding to the irradiated substrate. Figure 3.2 shows the ionic liquids that were selected and investigated for proton conductivity throughout this project. Grafting the ionic liquid to the substrate will reduce the degrees of freedom of the ionic liquid, however the proton conductivity is due to proton hopping and not charge transport. As such, proton conductivity is not reliant on the mobility of the ionic liquid in this system. Radiation grafting ionic liquid PEM produced a more robust film that was stable with reliable performance.

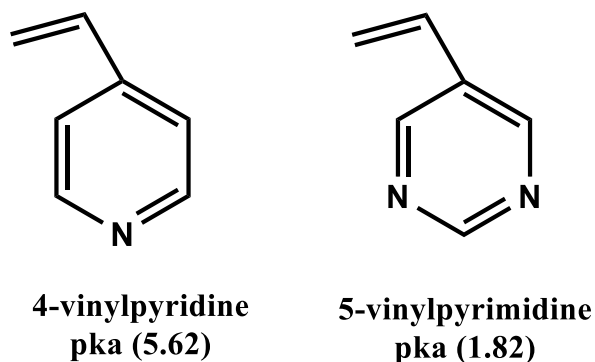


Figure 3.2-Ionic liquids investigated in this research

3.2 Radiation Chemistry/Grafting

The Medical Industrial Radiation Facilities (MIRF) at the National Institute of Standards and Technology (NIST) was the facility used to radiation graft heterocyclic protic ionic liquids onto fluorocarbon substrates to create each PEM. The MIRF is a 10MeV electron beam accelerator with a pulse rate of 120 pulses/sec and average pulse current of 100 μ A. Radiation grafting was used to treat the bulk substrate and required no chemical additions, solvents or additives to generate free radicals.[108]

As shown in Figure 3.3, samples were placed on a turntable to allow for treatment of multiple samples and to ensure a uniform radiation treatment. Electron paramagnetic resonance (EPR) Kodak® alanine dosimetry strips were used to calibrate the electron beam treatments in accordance with ISO/ASTM 51607.[109] The sample position and the gun current were adjusted to control the dose rate and applied dose for each radiation treatment.

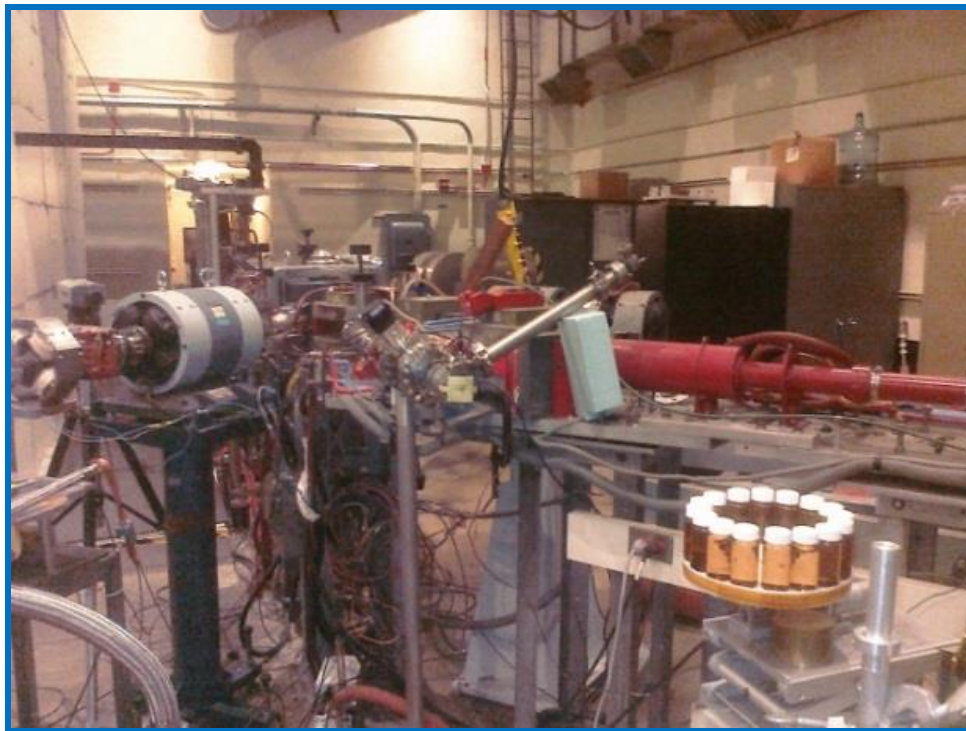


Figure 3.3: (Top) Electron beam accelerator “MIRF” at NIST; (bottom) Diagram of radiation sample setup: Electron beam (yellow), sample chamber (pink) and sample (green).[108]

The MIRF is a high energy ionizing radiation source utilized to treat the fluorocarbon substrate samples. The radiation treatment results in scissions and the generation of free radicals. The radiation induced free radicals were used to graft the protic ionic liquids directly onto the polymer substrate. The competing reactions of this process are depicted in Figure 3.4.

Indirect Grafting Reactions FEP with 4-Vinylpyridine

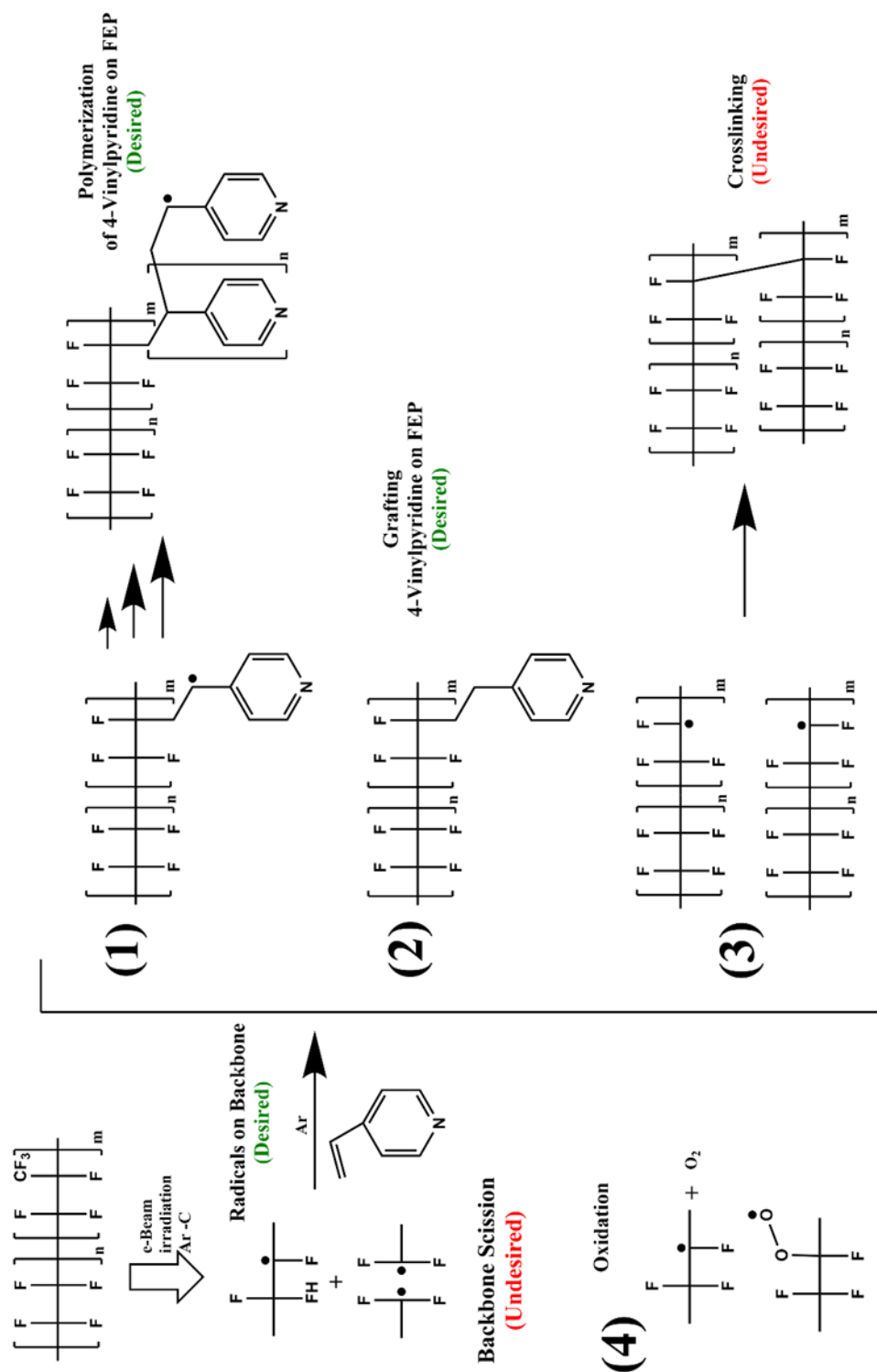


Figure 3.4: Indirect Radiation Grafting Competing Reactions; (1) Polymerization (2) Grafting (3) Cross-linking (4) Oxidation

Figure 3.4 shows an example (FEP and 4-vinylpyridine) and the reactions involved for indirect radiation grafting treatment of the PEM samples. Following sample irradiation, radicals are formed along the backbone of the polymer through either defluorination or chain scission.[110] Carbon centered free radicals in fluoropolymers have higher stability than in hydrocarbons polymers due to their lower mobility along the backbone of the chains which is reflected in a greater time to 50% free radical concentration in EPR studies.[111]:[112] This longer free radical decay is due to the greater steric hindrance of fluorine versus hydrogen in the carbon backbone. During radiation treatment, dry ice was used to preserve generated radicals by reducing their mobility by cooling the samples to temperatures below -40 °C. By testing a range of radiation parameters, it was determined that higher dose rates produced higher and more uniform grafting. However, the dose levels were optimized for each specific protic ionic liquid.

After the samples were irradiated and cooled, the monomers were added in an inert environment and placed in an oven for a post heat treatment (PHT) at 80°C for 5 hrs. The heat treatment temperature was selected to be above the glass transition temperature of the grafted polymers to allow uniform diffusion and grafting. However, the higher the temperature, the greater the radical mobility and probability of undesired cross-linking. These competing reactions during heat treatment are reflected in Figure 3.4. The indirect grafting synthesis experiments were performed under an inert atmosphere by bubbling the samples with Argon and using a glove bag for the protic ionic liquid addition. The Argon purge was performed to prevent oxygen from reacting with the free radicals generated in the fluorocarbon substrate. This reaction will form peroxy radicals leading to backbone scission. This is unfavorable because backbone scission will decrease the molecular weight of the membrane leading to a loss in

mechanical properties and functionality as PEM. The indirect radiation grafting procedure is depicted below in Figure 3.5.

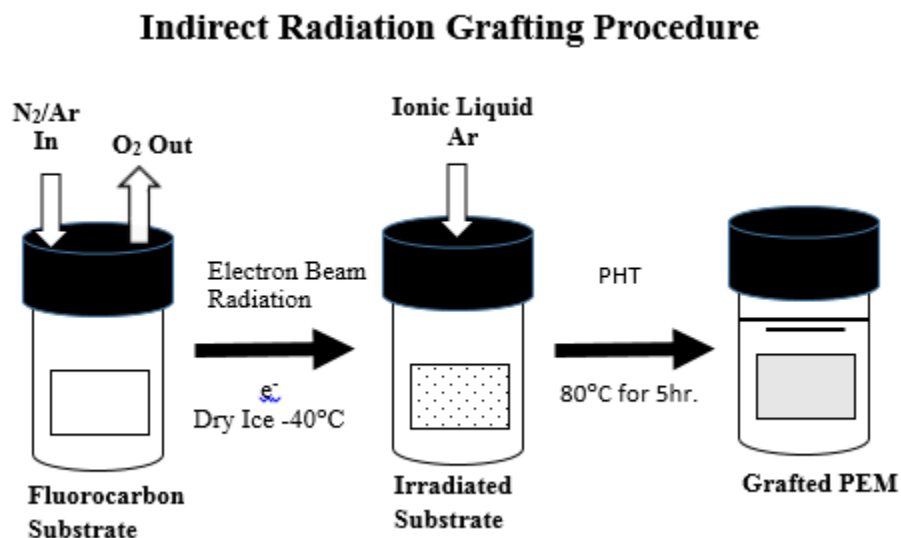


Figure 3.5: Overview of indirect radiation grafting procedure used to synthesize PEM

Grafting with beta radiation is a proven and widely used method that requires no catalyst and can be performed at almost any temperature with little or no solvents or additives. The radiation parameters must be optimized to achieve bulk radiation grafting and create a uniform structure throughout the depth of the PEM. The degree of grafting was controlled by the radiation dose, dose rate and temperature. During this synthesis, bulk grafting occurred by the grafting front model depicted in Figure 3.6.[113]

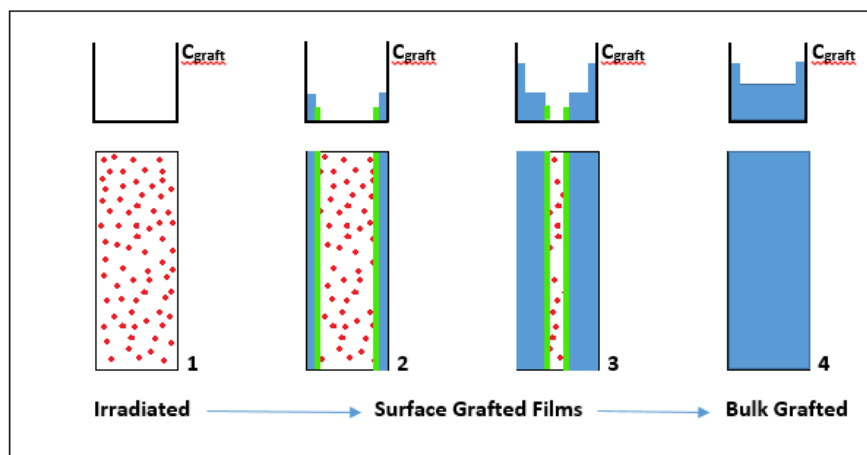


Figure 3.6: Grafting Front Model: Cross-section View of Indirect Radiation Grafting [113]

According to the grafting front model, shown in Figure 3.6, (1) radiation generates free radicals, active sites for grafting, which are represented as red dots. (2) Grafting was initiated at the surface by polymerization of monomers in solution. (3) Further grafting of active sites within the irradiated film required diffusion of monomers through the already grafted polymer zone. Over time, the grafting front, depicted in green, moves from the surfaces to the center of the membrane. Further grafting increased the concentration of monomer in the membrane. (4) Grafting for an extend time yields homogeneously grafted films with uniform concentration grafted over the entire film thickness. The use of radiation-induced grafting for membrane fabrication has been successful in a wide range of applications. Since, ionizing radiation penetrates the entire depth of the substrate material, fuel cell membranes can be fabricated in such a way that the ion-conducting monomer is evenly embedded within the substrate polymer.

3.3 Analysis Techniques

Analysis techniques were used to evaluate the synthesis parameters of the PEM and determine those that would best promote grafting reactions to ensure a high density ionic liquid network

within the membrane. After the PEMs were synthesized using radiation grafting, it was important to determine the membrane composition and evaluate their proton conductivity for fuel cell operation.

3.3.1 Electron Paramagnetic Resonance (EPR)

Electron paramagnetic spectroscopy is a technique that can be applied to measure the amount and type of lone pair electrons (free radicals) in radiation treated materials. Free radicals are short lived but can play a role in many chemical processes such as photosynthesis, oxidation, catalysis and polymerization reactions. Electrons have a spin, causing them to generate their own magnetic field. When unpaired electrons are placed in a magnetic field, they will align parallel to the magnetic field. During EPR measurements, the samples are exposed to microwaves which are adsorbed by the aligned, unpaired electrons causing the electrons to orientate anti-parallel to the magnetic field by changing their spin direction. The amount of energy or microwave frequency required to flip the spin of the free radical electron is described by the following Equation 3.1. [114]

$$\Delta E = \hbar\nu = g\mu_0 B \quad [3.1]$$

In Equation 3.1 above, ΔE is the energy required to flip the spin of the free radical electron, \hbar is the reduced Planck's constant, 1.055×10^{-34} Js, ν is the frequency of the microwave, g is the g-factor of the free radical which is dependent on the type of free radical, μ_0 is the Bohr magneton (9.264×10^{-24} J/T), and B is the magnitude of the applied magnetic field in gauss. In order to collect EPR spectra, a constant microwave frequency was applied to the sample and the absorption recorded while a variable magnetic field was applied. The first derivative of the absorption spectrum is reported as an EPR spectrum, because the g-factors and type of free

radicals present are more evident. Free radicals are affected by localized nuclear spins on neighboring atoms which create their own magnetic fields and impact free radical behavior. This is known as a hyperfine interaction and causes the absorption peak to split, showing the presence of free radicals.[114]

In this study, free radicals were used as grafting sites to attach protic ionic liquids onto the fluorocarbon substrates. Understanding the chemistry and reactivity of these free radicals in the fluorocarbon polymers was key to the successful synthesis of PEM samples. EPR measurements were also performed in order to verify the hold time of the fluorocarbon membranes (FEP, PCTFE and PVF) after radiation treatment and prior to monomer addition.

As a control, EPR was performed on irradiated and ungrafted fluorocarbon substrate to determine the type of free radicals generated and their rate of decay. The sites of these free radicals are potential grafting sites and their behavior is important to understand the quality of the grafting. EPR spectroscopy measurements were performed to determine the concentration, decay rate and type of free radicals produced during radiation treatment. These measurements are important especially for indirect radiation grafting where there is a time delay between radiation treatment and monomer addition. The protic ionic liquid were added immediately after radiation treatment, however it was important to know the time dependency of free radical decay.

The following procedure was used to prepare EPR samples. The fluorocarbon substrates were irradiated at MIRF with a 10.5 MeV electron beam to 50 kGy dose at 300 kGy/hr. dose rate. These radiation treatment parameters reflect the indirect grafting treatments used during this research. The substrate membrane samples were irradiated in an inert argon atmosphere under dry ice temperatures -40°C. After radiation treatment the samples were moved to a glove bag which was then purged with Argon. Samples were transferred to quartz EPR tubes and

sealed. The oxygen level was reduced in the samples and in post radiation treatments because oxygen rapidly reacts with free radicals to form peroxy radicals, which would change the free radical behavior. This would affect the EPR measurements and confound the measurement of free radicals produced by indirect radiation grafting. The samples were then placed on dry ice to be transported to the EPR laboratory at NIST to be analyzed. The dry ice conditions reduced the mobility of the free radicals, decreasing the probability of cross-linking reaction and preserving them for EPR analysis.

EPR spectroscopy measurements were carried out at NIST on a Bruker instrument. The following instrument parameters were used: microwave frequency of 9.822 GHz, microwave power of 0.6362 mW, frequency modulation of 100 kHz, modulation amplitude of 5 G, receiver gain of 50, center field at 3480 G, sweep width of 300 G, data conversion time of 40.96 ms and time constant of 20.48 ms at room temperature 25 °C. The intensity of the peaks in the EPR spectrum is directly correlated to the concentration of free radical electrons within the sample. These EPR experiments were conducted in order to determine the free radical decay time inside fluorocarbon substrates and validate the indirect radiation grafting method used to synthesis PEM. These experiments were also conducted to improve the understanding of the grafting mechanism and physical and chemical structure of the grafting sites.

3.3.2 Degree of Grafting

The synthesized PEMs were analyzed to evaluate the amount of monomer that grafted on the substrate. The presence of grafting was determined using the gravimetric formula, Equation 3.2. The initial mass (M_i) of fluorocarbon substrates and the final mass (M_f) of the PEM was used to determine the degree of grafting from the radiation synthesis.

$$\text{Degree of Grafting} = \frac{M_F - M_i}{M_i} * 100 \quad [3.2]$$

These results were used to evaluate the process parameters of the radiation treatment and optimize the percent grafting. The degree of grafting provides a scale to access the synthesis of the PEM and extent of ionic liquid polymerized to the substrate.[63],[64],[115] Unfortunately, these measurements do not give information on the extent or uniformity of grafting which is important for the preparation and functionality of conductive membranes. Uniformity of grafting was further determined by cross-section measurements using FTIR and SEM/EDS.

3.3.3 Cross-Section Microtome Sample Preparation

Cross-section of grafted samples were prepared for FTIR and SEM/EDS by first imbedding the membranes using epoxy resin. Silicon molds were used to shape the epoxy for easy release of the samples after curing. The membrane samples were cut and added to the surface after the molds were half filled with epoxy and allowed to cure. The rest of the mold was then filled with epoxy to completely encapsulate the sample and a second cure step performed. The epoxy samples were removed from the molds and precut to expose the cross-section of the membrane. The samples were then mounted in a Leica microtome and cut perpendicular into 1-25 μm thick slices. Samples were cut into a water bath to prevent curling. The samples were mounted on gold plated microscope slides and place on a hot plate set to 120°C to dry. The hydrostatic pressure caused the sample to adhere flush on the slide surface. These cross-section samples were used to measure the extent of ionic liquid grafting in the membrane and the uniformity of composition.

3.3.4 Fourier Transform Infrared Spectroscopy (FTIR)

FTIR measures the absorption of infrared light due to resonance with bond vibration modes. The synthesis of grafted PEM can be confirmed by FTIR measurements using attenuated total reflectance (ATR). Each spectrum will be taken from 72-100 scans measured with a resolution of 2 cm^{-1} . FTIR utilizes bond resonance vibration modes in the infrared region to identify the chemical composition of samples. A comparison of the FTIR-ATR spectrum before and after radiation grafting treatments were used to show the chemical changes that occur in the PEM. These FTIR measurements can only evaluate the membranes on the surface. FTIR microscopy techniques were used to measure the extent of grafting by scanning the cross-section of PEM. Cross-sections of membranes were prepared using techniques described above in Section 3.3.3. For this measurement to be successful, the cross-sections need to be approximately $1\text{-}25\mu\text{m}$ in thickness to prevent saturation of the absorption spectrum.

3.3.5 Scanning Electron Microscopy and Energy-Dispersive X-ray Spectrometry

Scanning electron microscopy and energy-dispersive X-ray spectrometry (SEM/EDS) was used to investigate the surface and cross-section of the PEM. Membranes were prepared for this measurement by imbedding them in epoxy, cross-sectioning and finely polishing. The SEM images will demonstrate if the membranes have a uniform density and composition showing uniformity of grafting, but not extent of grafting because the resolution between carbon and nitrogen in the EDS is very poor. As such, there is not enough contrast with nitrogen to determine the extent of grafting of ionic liquid monomers being studied. However, a significant change in the carbon to fluorine ratio in the PEM contributed by grafting was identified through this method. The elemental ratio was used to estimate the extent and uniformity of grafting.

This technique was also used to accurately determine the thickness of the membranes for conductivity measurements.[62]

3.3.6 Proton Conductivity - Electrochemical Impedance Spectroscopy

Electrochemical impedance spectroscopy (EIS) provides insight into electrochemical systems and is commonly used for evaluation of material coatings, batteries, fuel cells, solar cells, sensors and biochemical applications.[116] EIS was used to measure the impedance of the 2-point and 4-point test cells and to determine the proton conductivity of ionic liquid PEM membranes. During EIS measurement, the impedance of the system is measured as a function of frequency according to Equation 3.3:

$$Z(\omega) = \frac{V(t)}{I(t)} = \frac{V_0 \sin(\omega t)}{I_0 \sin(\omega t + \theta)} \quad (3.3)$$

In this equation, (V) is the AC voltage and (I) is the AC current. During EIS measurements, the phase shift (θ) between the AC signals is measured to determine the resistance real (Z') and the reactance imaginary component (iZ'') for impedance.[116] The interrelationship between impedance real and imaginary components is shown in Equations 3.4, 3.5, 3.6:

$$Z(\omega) = Z' + iZ'' \quad (3.4)$$

$$Z' = Z \cos(\theta) \quad (3.5)$$

$$Z'' = Z \sin(\theta)i \quad (3.6)$$

To analyze the EIS data, the real and imaginary components were evaluated on a Nyquist plot Z' versus Z'' . The frequency dependence of the EIS data was evaluated using Bode plots for ω versus Z and ω versus θ . [116] An equivalent circuit model that represents both the test cell and the sample were fit to the EIS data to separate the components of the electrochemical system. It is important to note that there are multiple equivalent circuits that can fit the same data and that

the equivalent circuit should be derived from the system being studied. There were two important electrochemical systems to be modeled during the EIS measurements; charge transfer at the electrodes and the charge transport in the PEM. Resistors were used to model the resistance to flow of charge in the membrane and capacitors were used to model variable flow of charge with frequency. The following sections discuss the electrochemical equivalent circuit models used for the 2-point and 4-point probe measurements. The values extracted from the equivalent circuit model were used to determine the proton conductivity of the ionic liquid PEM synthesized during this research.

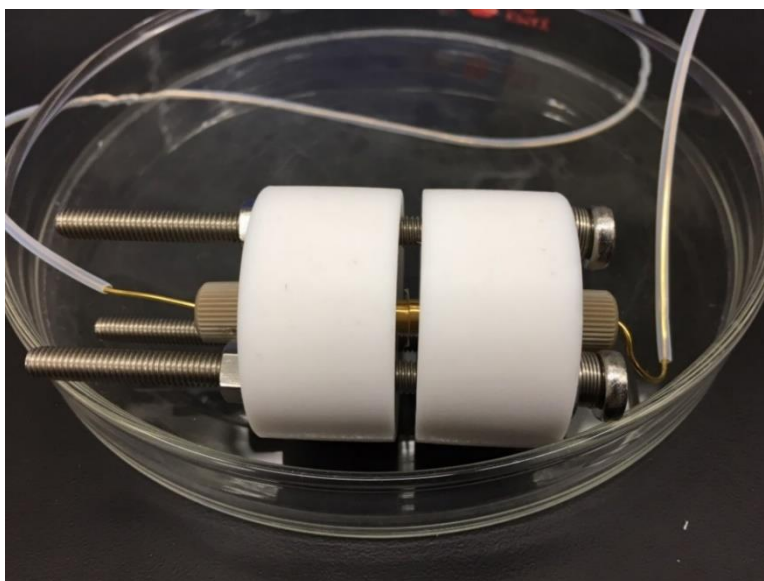
3.3.6.1 EIS Testing Parameters

For the 2-point and 4-point probe test cells, the proton conductivity of PEM was measured by EIS using a Solartron Modulab XM ECS potentiostat. The proton conductivity was measured by applying a low alternating current (AC) signal, either voltage (10mV) potentiostatic or current (1 μ A) galvanostatic at varying frequencies and then measuring the system response.[116] For PEM, a phase shift between the AC signal and response was expected due to double layer capacitance and redox reaction kinetics of proton transport at the electrodes. Measurements were taken across the frequency range of 10^6 to 1 Hz and EIS spectrum were analyzed using equivalent circuit models to determine the proton conductivity in the membrane. It was important to monitor all components that were in parallel with this measurement sample. If the impedances of these components became significantly lower than the impedance of the PEM, then the conductivity of the membrane would not be accurately determined. Both 2-point probe and 4-point probe test cells shown in Figure 3.7 and Figure 3.8, were utilized to study proton conductivity through the membrane and across the surface of the membrane respectively.

Samples for EIS testing were prepared based on the 3M Company standard procedure. PEMs were cut into strips and boiled in deionized water for 30 minutes to remove residual ions. The PEMs were then protonated by an acid treatment with 5% by volume of either HNO_3 , H_2SO_4 or H_3PO_4 at 50°C for 1 hour. The membranes were double rinsed with deionized water to remove residual acid. PEM was mounted in the test cells, shown in Figure 3.7 and Figure 3.8, which are EIS probes designed to measure the bulk and surface conductivity of the membrane.[117] For PEMFC functionality, the bulk proton conductivity through the membrane must be demonstrated. The 4-point probe test method assumes that surface conductivity and conductivity through the film will be the same if the electrodes are spaced far enough apart. A study was conducted with Nafion by Z. Xie et al. and it was shown that the closer the electrodes, the greater the discrepancy between the 2-point probe and 4-point probe measurements.[118] This was attributed to the geometry of the test cell design.[117] In my research it was determined to use a 2-point parallel plate capacitor probe since it would be more representative of fuel cell operation as it measures conductivity through the thickness of the membrane. However, 4-point surface probe measurements were also conducted because it is the 3M Company industrial standard test. Also, the geometry of the 4-point probe test allows for more accurate impedance measurements of membranes with higher proton conductivities by controlling the electrode spacing.

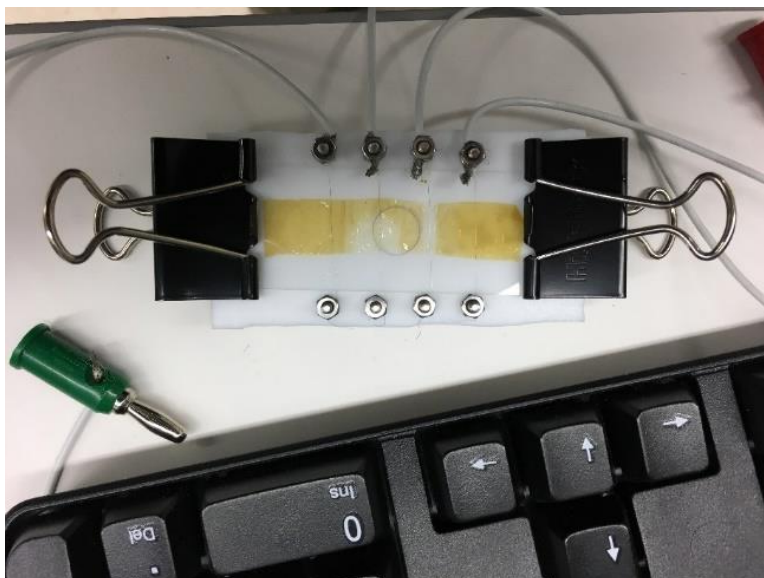


(a)

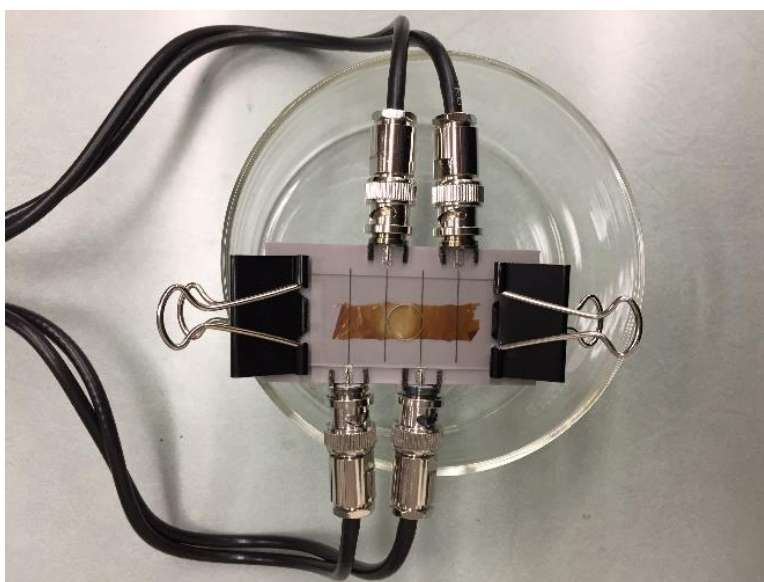


(b)

Figure 3.7: 2-point probe EIS test cells: (a) 2-point probe PCB gold plated electrode (b) 2-point probe gold electrode



(a)



(b)

Figure 3.8: 4-point probe EIS test cells (a) 4- point probe platinum wire electrodes (b) 4-point probe high temperature PCB cell Cu/Ni/Pt plated wire electrode

3.3.6.2 2-Point Probe Analysis

Figure 3.7a shows the 2-point probe printed circuit board (PCB) design to measure proton conductivity through the thickness of the membrane. This was the initial cell design used for measurements utilizing gold plated copper electrodes. Design changes were made to make the 2-point probe measurements more reproducible as shown in Figure 3.7b. These changes included: a solid gold electrode and wire leads, and mounting the membrane using compression to ensure a constant interface between the electrodes and membrane. The data from both 2-point probe designs are presented, and represent the body of data collected. The 2-point probe measurements were conducted with the EIS potentiostatic mode applying an AC voltage of 10 mV to the electrodes and measuring the current response. For the test cell shown in Figure 3.7a, the electrodes were 1cm in diameter and had a surface area of 0.785 cm^2 . For the test cell shown in Figure 3.7b, the electrodes were smaller, 0.5 cm in diameter with a surface area of 0.196 cm^2 , decreasing the capacitance and increasing its impedance. The higher impedance of this test cell allowed membranes with lower proton conductivities to be accurately measured. The test PEMs were placed between the parallel plates of the 2-point probe tests cells. The electrodes spacing was controlled by the membrane thickness which varied with the degree of grafting. Thickness values for the membranes were measured using a micrometer with an accuracy of $0.1\mu\text{m}$.

The equivalent circuit model selected to describe the electrochemical system for the 2-point probe measurement was based on the test cell design and data obtained by measuring the 3M control sample, see Figure 3.9. The data shown in red was analyzed by fitting an equivalent circuit model shown in green using a Nyquist plot, (Figure 3.9a) and Bode plots (Figure 3.9b). The simplified circuit model that was used for data assessment to describe the 2-point probe test cell and 3M membrane is depicted in Figure 3.10.

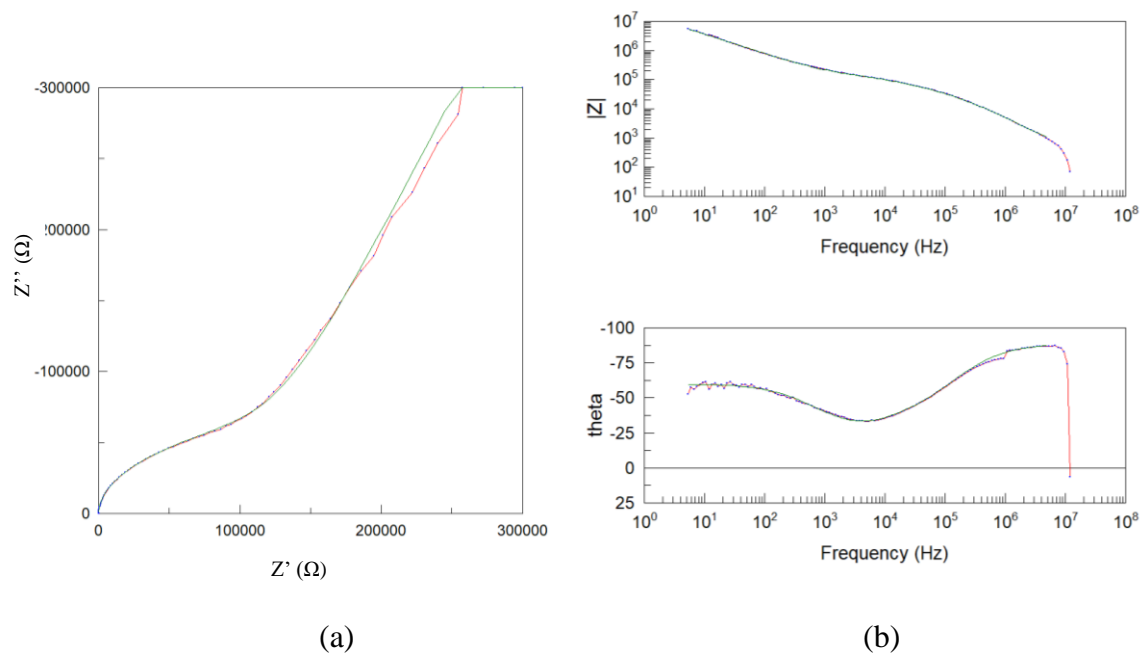
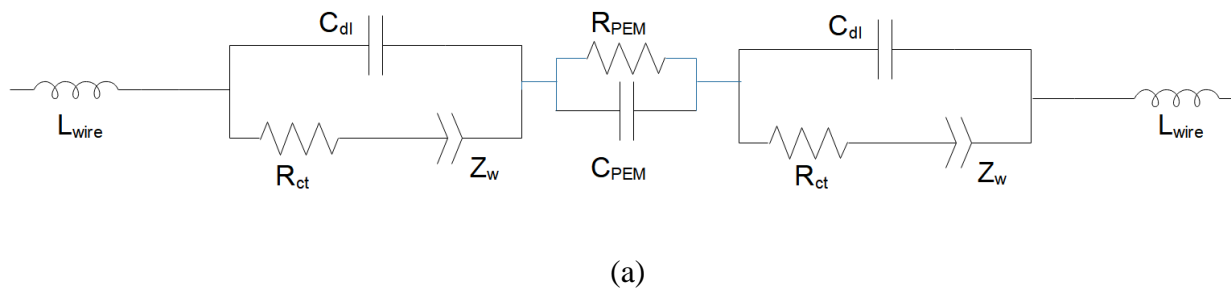
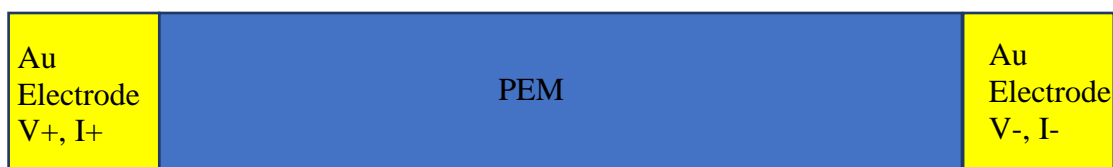


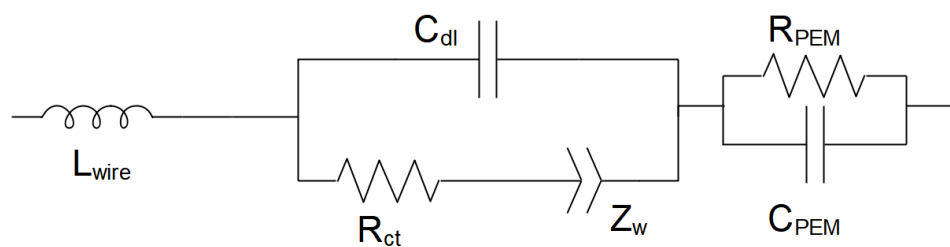
Figure 3.9: PCB 2-point probe measurement of 3M 825EW control at 80°C; (a) Nyquist Plot (b) Bode Plots; (red line) EIS data (green line) simplified circuit model fit.

The equivalent circuit model for 2-point probe measurements is shown in Figure 3.10a and describes the system diagram shown in Figure 3.10b. Since the system is symmetric and the reaction at the electrodes are the same, the equivalent circuit can be simplified because the components should have comparable values. This simplified equivalent circuit is shown in Figure 3.10c.





(b)



(c)

Figure 3.10- (a) Equivalent circuit model of 2-point Au parallel plate capacitor test cell (b) diagram of EIS measurements 2-point probe cell: (yellow) electrodes (blue) PEM (c) Simplified circuit model.

In the 2-point probe circuit model shown in Figure 3.10c, (C_{PEM}) is the capacitance of the membrane due to the 2-point parallel plate capacitor probe design, (R_{PEM}) is the resistance of proton conductivity through the membrane, (R_{ct}) is the charge transfer resistance, (C_{dl}) is the double layer capacitance and (Z_w) is the Warburg diffusion limiting element. This equivalent circuit model fits the semicircle of the EIS data and the Warburg diffusion limiting element which was used to simulate the electrodes and PEM in the test cell. The measurement was performed to determine electrolyte resistance (R_{PEM}) shown in Figure 3.10 which correlated to proton conductivity in the PEM. The intrinsic proton conductivity (σ) of the membrane can be determined using Equation 3.7 where (t) is the thickness of the PEM and (A_c) is the cross-section area of the membrane.

$$\sigma = \frac{t}{R_{PEM}A_c} \quad [3.7]$$

In Figure 3.9, the 3M 825EW control sample was tested with EIS at 80°C at approximately 5% R.H. The results were interpreted with the simplified circuit model shown in Figure 3.10c. The proton conductivity was calculated to be 2.21E-4 S/cm.

The limitations of the 2-point EIS measurements were considered to ensure the impedance of the membranes were measured and not the impedance of the parallel plate capacitor test cell. Since the 2-point test cell has a capacitor in parallel with the membrane, the ratio of these impedances will determine if the conductivity of the membrane can be measured. The capacitance of the PEM was calculated to be on the order of 60 or 15 pF for each test cell shown in Figure 3.7a and 3.7b respectively using equation 3.8.

$$C_{PEM} = \frac{k\epsilon_0 A}{d} \quad [3.8]$$

In this equation, k is the dielectric constant of the PEM, ϵ_0 is the permittivity of free space, A is the surface area of the parallel plate electrodes and d is the electrode spacing (membrane thickness) of the 2-point probe test cell. The impedance (Z) of these capacitors is a function of frequency and can be calculated using equation 3.9 for simulating the EIS impedance spectrum.

$$Z = -\frac{1}{C_{ppc}w}j \quad [3.9]$$

In this equation, C_{ppc} is the capacitance of the parallel plate capacitor, w is the applied frequency and j is a vector component not a variable. This equation shows that the impedance of a capacitor decreases at higher frequencies. The highest frequency that was measured during this research was 10^7 Hz. The impedance at this frequency for the parallel plate capacitor test cells would be 1.7E3 Ω and 6.6E3 Ω respectively. If the impedance of the PEM was above these

impedance values, the high frequency region would be dominated by the parallel plate capacitor, preventing the proton conductivity of the PEM from being measured. This conclusion was drawn from the calculated impedance current path of the equivalent circuit at high frequencies. The high frequency intercept would only be equal to R_{PEM} if the membranes are sufficiently proton conductive. Figure 3.11 shows how the capacitance of the 2-point probe parallel plate capacitor would limit the range of useful frequencies of the EIS measurement. For the proton conductivity to be accurately measured, the impedance of R_{PEM} must be below C_{PEM} which it is parallel with and significantly above C_{dl} and other impedances it is in series with.

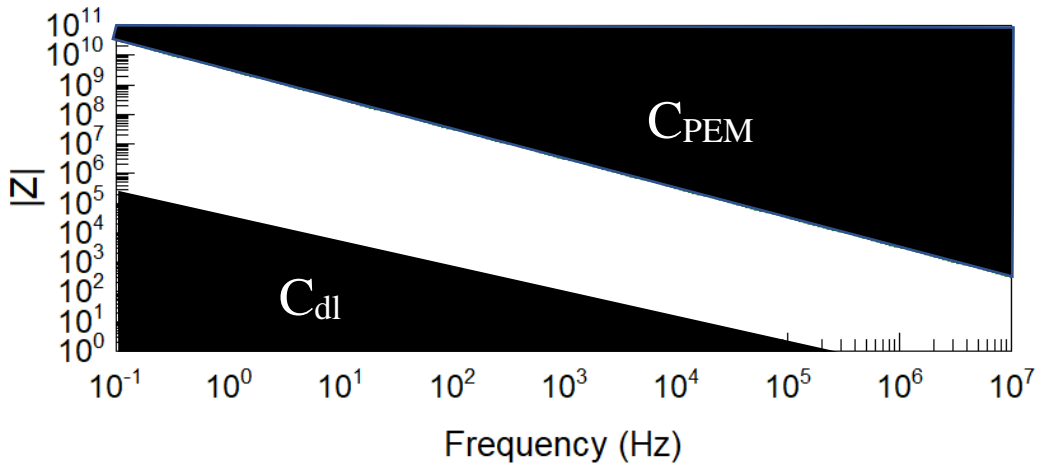


Figure 3.11: Limiting frequency range of 2-point parallel plate capacitor probe EIS measurements (black). Threshold frequency range simulated for C_{PEM} of 60pF predicted for the PCB 2-point probe and C_{dl} 5uF.

As the capacitance of the PEM increases, the black region of the plot where the membrane would be bypassed will appear at lower impedances, further limiting the frequency range that can be

measured. The parallel plate capacitance appeared in the high frequency region of the 3M 2-point probe EIS data shown in Figure 3.9 by the 90° phase shift. This demonstrates that the limitations of the test cell shown by the equivalent circuit model must be considered when evaluating EIS measurements.

3.3.6.3 4-Point Probe Analysis

The initial 4-point probe design shown in Figure 3.8a has four platinum wires with diameter (0.003 in.) parallel to each other with 1cm spacing. However, the thin platinum wires had a tendency to break after each measurement, which led to the development of a more robust PCB cell shown in Figure 3.8b. The copper wires of the PCB were plated with nickel and then platinum for electrical contact and chemical resistance. These 4-point probes were designed to replicate the setup used at 3M Company for PEM conductivity measurements. In order to calibrate the EIS test cells, measurements were made using a 3M 825EW control PEM, which had known proton conductivity values.

The 4-point probe measurements were conducted with the EIS galvanostatic mode. An AC voltage of 1μA was applied to the electrodes and the voltage response measured. Figure 3.12 shows how EIS data was collected and analyzed with the 4-point Pt wire probe using a Nyquist plot, (Figure 3.12a) and Bode plots (Figure 3.12b). The four platinum wires in the 4-point probe were spaced 1 cm apart. The EIS data was interpreted with an equivalent circuit model to evaluate proton conductivity of the membrane.

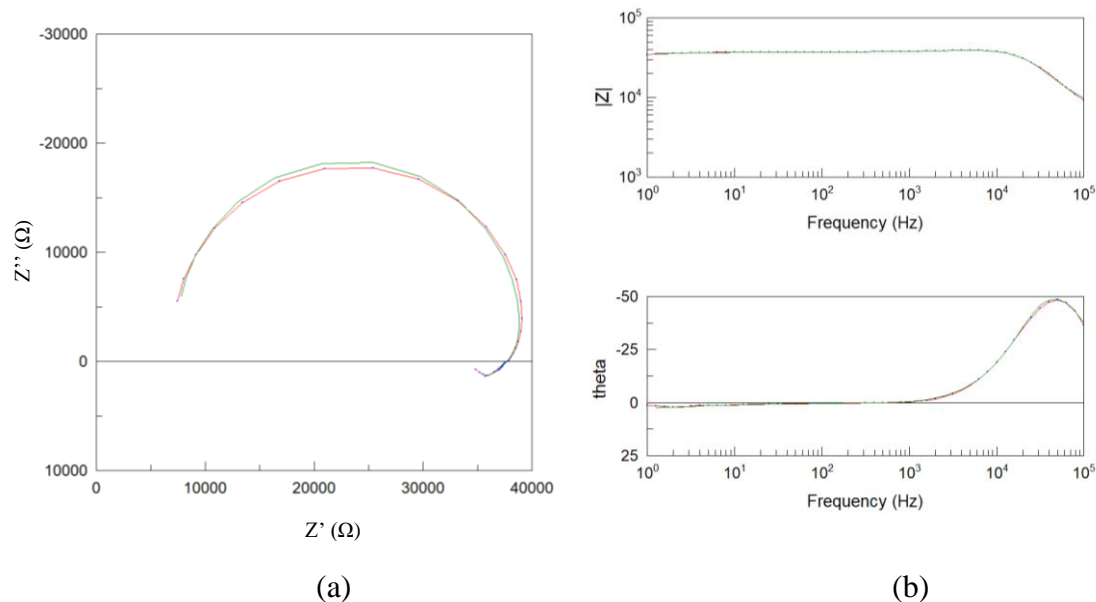
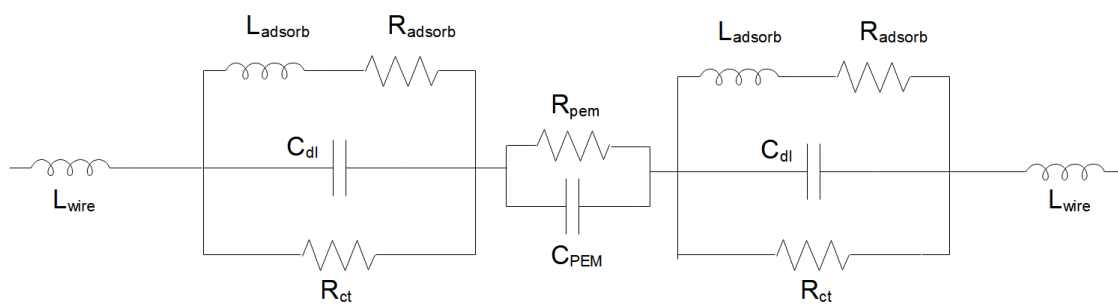


Figure 3.12: 4-point probe analysis 3M Company 825EW Control at 60°C, 20% R.H.; (a) Nyquist Plot (b) Bode Plots; (red line) EIS data (green line) simplified circuit model fit

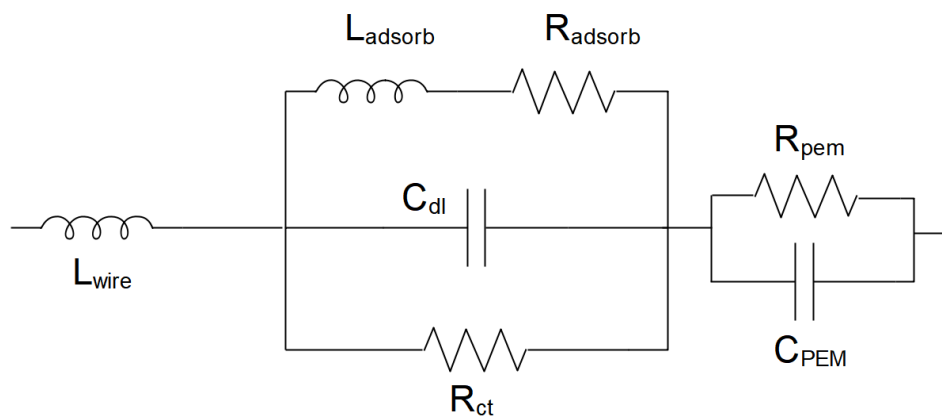
The equivalent circuit model for 4-point probe measurements is shown in Figure 3.13a and describes the system diagram shown in Figure 3.13b. Because the system is symmetric and the reaction at the electrodes are the same, the equivalent circuit can be simplified because the components should have comparable values. This simplified equivalent circuit is shown in Figure 3.13c.



(a)



(b)



(c)

Figure 3.13: (a) Equivalent circuit model of 4-point Pt wire test cell (b) Diagram of EIS measurement 4-point probe cell (c) Simplified circuit model.

For this equivalent model; (R_{PEM}) is the resistance of proton conductivity in the membrane, (C_{PEM}) is the capacitance of the membrane, (R_{ct}) the charge transfer resistance, (C_{dl}) the double layer capacitance, (L_{adsorb}) and (R_{adsorb}) components are the low frequency inductance and resistance of hydrogen adsorption for the Pt wire electrodes.

The simplified circuit model shown in Figure 3.13c was selected to represent the electrochemical system in the PEM studied with the 4-point probe. This model fits the semicircle of the EIS data which was used to simulate the electrodes and PEM in the test cell. It also simulates the low frequency inductance observed in the data due to the adsorption of hydrogen onto the Pt electrode.[119] This measurement was performed to determine electrolyte resistance (R_{PEM}) shown in Figure 3.13c which correlates to proton conductivity in the PEM. The intrinsic proton conductivity (σ) of the membrane can be determined using Equation 3.10 where (l) is the electrode spacing, (w) is the width of the membrane and (t) is the thickness of the membrane.

$$\sigma = \frac{l}{R_{PEM}wt} \quad [3.10]$$

In the example above in Figure 3.12, the 3M 825EW control sample was tested with EIS at 60°C and 20% R.H., the results were interpreted with the equivalent circuit model and the proton conductivity was calculated using Equation 3.10 to be 0.043 S/cm.

The limitations of the 4-point EIS measurements were considered to ensure the impedance of the membranes were measured. It was possible the 4-point probe test cell could have a capacitor in parallel with the membrane impedance due to the finite mobility of charge in

conductive polymers. In this case the membrane would act as a capacitor and resistor in parallel with each other as shown in the equivalent circuit model in Figure 3.13c. The charge build-up in a conductive polymer can be modeled as a capacitor in parallel with the membrane. Due to the different geometry of the membrane and decrease of cross-section of the membrane being measured, the C_{PEM} would be on the order of 0.25 pF. The ionic liquid PEMs were insulating, and the mobility of charges were confined by localized potentials of grafted heterocyclic amine ionic liquids. Other than protons, no other charge ions could freely move through the membranes. The EIS measurements only reflected the proton conductivity of the membrane and the effect of other charged ions species were not significant. [120] The low C_{PEM} capacitance would create a very high impedance where it does not affect the proton conductivity measurements and can be removed from the equivalent circuit model for 4-point probe measurements. This capacitance was also not observed in the EIS data for the 3M sample nor the ionic liquid PEM, therefore verifying no impact to the 4-point equivalent circuit model fit. Figure 3.14 shows how the 4-point probe geometry created a much large frequency window for the proton conductivity R_{PEM} to be measured compared to the 2-point probe.

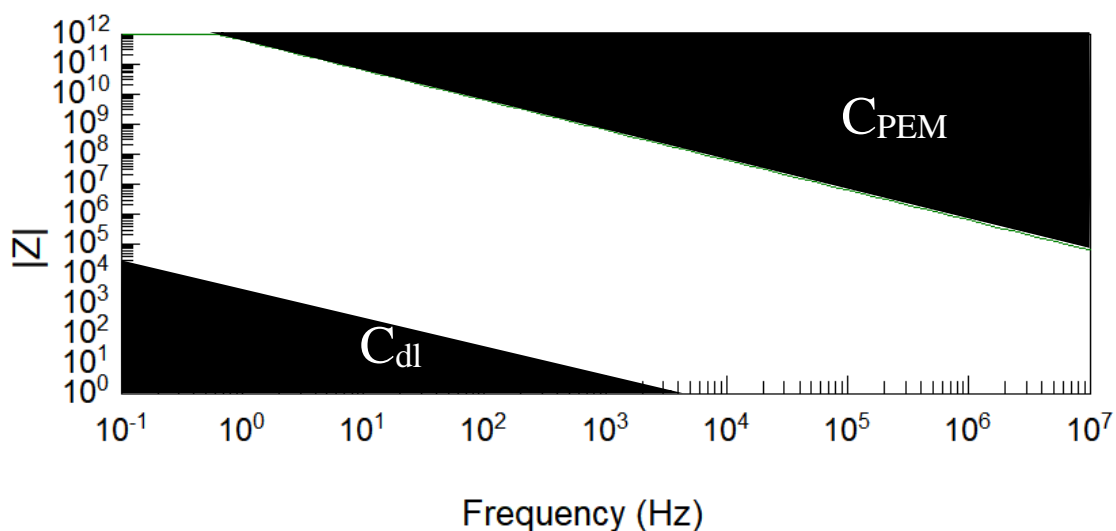


Figure 3.14: Limiting frequency range of 4-point wire probe EIS measurements (black).

Threshold frequency range simulated for C_{PEM} of 0.25 pF predicted for the 4-point probe and Cdl 0.5uF.

The EIS tests, equivalent circuit models and calculations were applied to all prepared membranes in this research as various 2-point and 4-point probe designs were evaluated. The values of the known components were calculated, and a simulation was run before a fit was performed using Scribner Z-View software to obtain the best possible fits. The calculated values of capacitance were compared to the expected values from literature to determine how the model shifted with frequency and treatment conditions.[116] EIS is a non-destructive technique and can be used to evaluate the temperature and humidity dependence of the PEMs synthesized for this project. An environmental chamber was used to measure the PEM conductivity at temperature 80°C for 20, 40, 60 and 80% R.H. Temperatures of 100, 120, 140 and 160 °C were also tested, to evaluate the grafted ionic liquid PEM under anhydrous conditions. If the membranes have an anhydrous proton conducting mechanism, they will maintain their proton conductivity as temperature increases in the absence of water.

3.4 Small Angle Neutron Scattering

Small Angle Neutron Scattering (SANS) measurements were used to investigate the internal proton conductive system of solid-state PEM. SANS measurements were conducted at NIST Center for Neutron Research (NCNR) and the instrument diagram is shown in Figure 3.10. SANS has been used in the past to study the size and distribution of proton conductive water channels of Nafion™ which were on the order of 1-3 nm in size. [121],[122],[123] With neutron scattering there is a strong contrast between fluorocarbon and hydrocarbon polymers

which should allow the extent and distribution of grafting to be determined within the PEM. SANS measurements were used to study the membrane composition: including crystal structure, grafting composition and residual ionic liquids bound within the membranes. Due to the higher resolution of neutrons with hydrogen, SANS measurements could give insight into the proton conductive mechanism within the protic ionic liquid PEM. SANS samples were prepared by folding 3 cm x 10 cm membranes into a 1cm square with 10 layers of membrane. The sample was folded to magnify the neutron scattering from the samples because the PEM were too thin for significant scattering. These samples were compressed between quartz windows by an aluminum sample holder. SANS analysis of Nafion membranes is shown in Figure 3.11, in which measurements were used to determine the microstructure within PEM samples. In particular, SANS was used to determine the ionomer peak (Gaussian Peak) which provides information on the proton conducting network channels within the PEM.

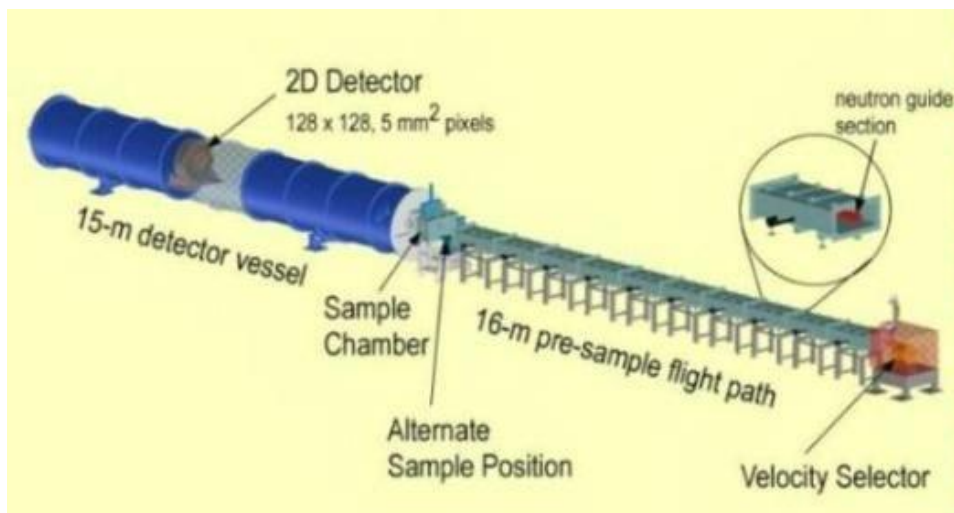


Figure 3.10-SANS beam line at NIST[124]

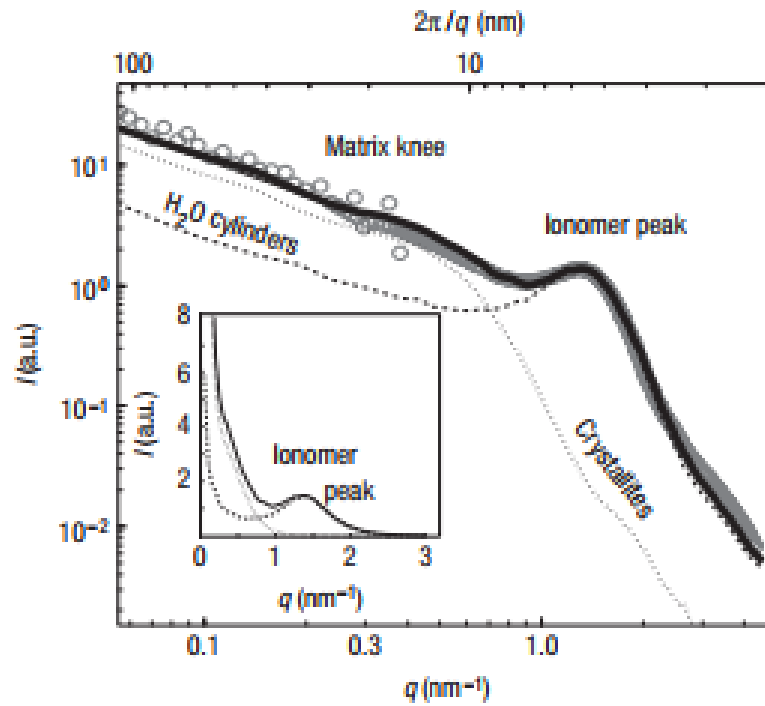


Figure 3.11-SANS measurement of Nafion Membrane showing the proton conductive water cylinder nanostructure and ionomer structure within the PEM[121]

SANS measurement will be important to understand how the structure of the anhydrous ionic liquid PEM will affect proton conductivity.

4.0 Results and Discussion

Throughout the course of this research project different radiation grafting techniques were utilized to covalently bond proton conductive ionic liquids to fluorocarbon substrates. The principle ionic liquids monomers tested were 4-vinylpyridine and 5-vinylpyrimidine, both containing a heterocyclic amine group. The heterocyclic amine group is recognized for having proton conducting capability at high temperatures. In the first phase of experiments, a direct grafting method was considered. However, there was difficulty establishing a system that would graft uniformly to the membrane due to monomer polymerization during radiation treatment. Indirect grafting was successful in achieving monomer binding to the substrate and thereby creating PEM. The fluorocarbon substrates and the grafted proton conducting groups were prepared and evaluated for free radical generation, degree of grafting, composition uniformity, structure and proton conductivity. The results and discussion are reported in this chapter.

4.1 EPR Analysis of Free Radicals in Fluorocarbon Substrates

The kinetics of free radical decay and structure of grafting sites within the fluorocarbon substrate after radiation was determined by Electron Paramagnetic Resonance (EPR) spectroscopy. The free radical, types and their relative concentrations generated in the fluorocarbon substrates, FEP, PCTFE and PVF, were measured. The type and availability of these free radical sites were important to allow for grafting ionic liquid monomers onto the fluorocarbon substrates. The time dependence for free radical decay after radiation treatment was established to assure that free radicals were present in a concentration suitable for grafting. This is important when using the indirect radiation grafting method, in order to establish a maximum hold time between radiation treatment and monomer addition.

The fluorocarbon membranes, FEP, PCTFE and PVF, were radiation treated with a 50 kGy dose at a dose rate of 1000 kGy/hr. for 3 minutes using the MIRF electron beam. The EPR samples were prepared according to procedures in section 3.3.1 within approximately 15 minutes after radiation treatment and stored at -40°C until EPR analysis. The samples were returned to room temperature immediately before EPR measurements were performed.

The EPR spectra for irradiated FEP, PCTFE and PVF membranes were acquired using a Bruker Elexsys Spectrometer at NIST. The following instrument parameters were used: microwave frequency of 9.822 GHz, microwave power of 0.6362 mW, frequency modulation of 100 kHz, modulation amplitude of 5 G, receiver gain of 50, center field at 3480 G, sweep width of 300 G, data conversion time of 40.96 ms and time constant of 20.48 ms at room temperature 25 °C. These instrument parameters affect the shape and intensity of the EPR spectrum. The same instrument settings were used through the course of the experimentation.

4.1.1 EPR Analysis of FEP

The EPR spectrum for irradiated FEP is displayed below in Figure 4.1. The data was used to determine the decay of free radicals with time. The peak in the EPR spectrum represents free radicals present within the sample.

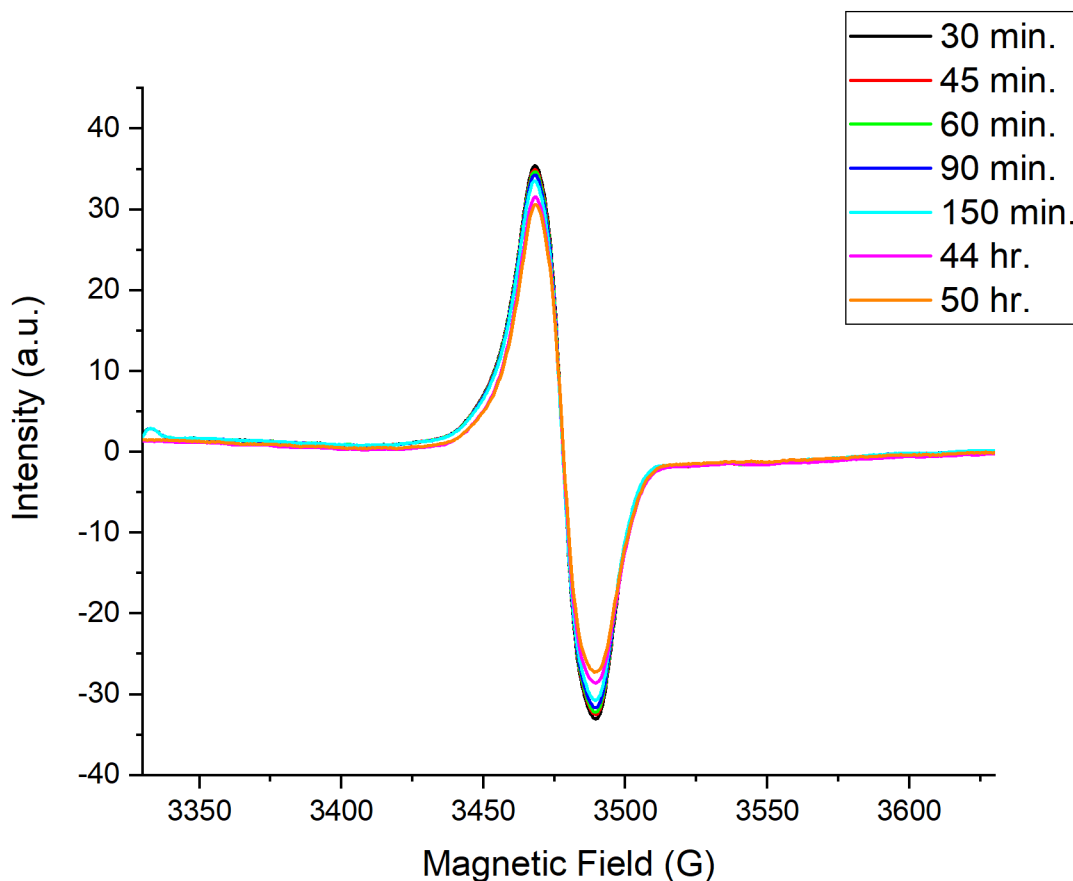


Figure 4.1-1st derivative EPR spectrum of irradiated FEP substrate treated with MIRF set at 10.5MeV electron beam, 50 kGy dose at a 1000 kGy/hr dose rate.

For FEP, a single absorption peak was observed at 3477.21G after irradiation. This peak decreased with time as the free radicals in the sample decayed. The free radical peak in this EPR spectrum corresponds to a free radical g-factor of 2.018. As a reference, the g-factor of $^*\text{CF}_3$ is 2.0031[125]. While there is a shift in the g-value due to interference in polymer chains, this still indicates that the free radicals in FEP corresponds to a perfluoronated carbon centered free radical. Also shown in Figure 4.1, no hyperfine coupling occurred even though it was expected for fluoride groups. Possible structures of free radicals produced by radiation induced scissions

of FEP samples are depicted in Figure 4.2. Structure 1 corresponds to a fluorocarbon center free radical. C-F bonds are stronger in comparison to the C-C bonds due to higher bond dissociation energy, making them less likely to break due to radiation induced scissions. The free radical structures 2 and 3 in Figure 4.2 are not expected to be present because they require a C-F bond scission. This is substantiated by the relatively low G-value of fluorine gas radiation yield when fluorocarbon polymers are irradiated [126]. Between the two C-C bond types (structure 4 and 5) in Figure 4-2, the electron withdrawing nature of the trifluoromethyl group weakens the C-CF₃ bond making it four times more likely to break after radiation treatment compared to the C-F bond. A study was conducted with radiation of perfluoromethylcyclohexane in which the radiation-chemical yield G-values were calculated. P. Gehringer et al. were able to show that it was more probable that the fluorinated methyl group bonds would break rather than the hexane ring to open.[127] This contributes to the observed greater radiation resistance of FEP over PTFE because backbone scissions are less likely. The free radical structure observed in the EPR spectra, Figure 4.1, is likely structure 1 depicted in Figure 4.2.

Free Radicals Generated by Radiation Treatment of FEP

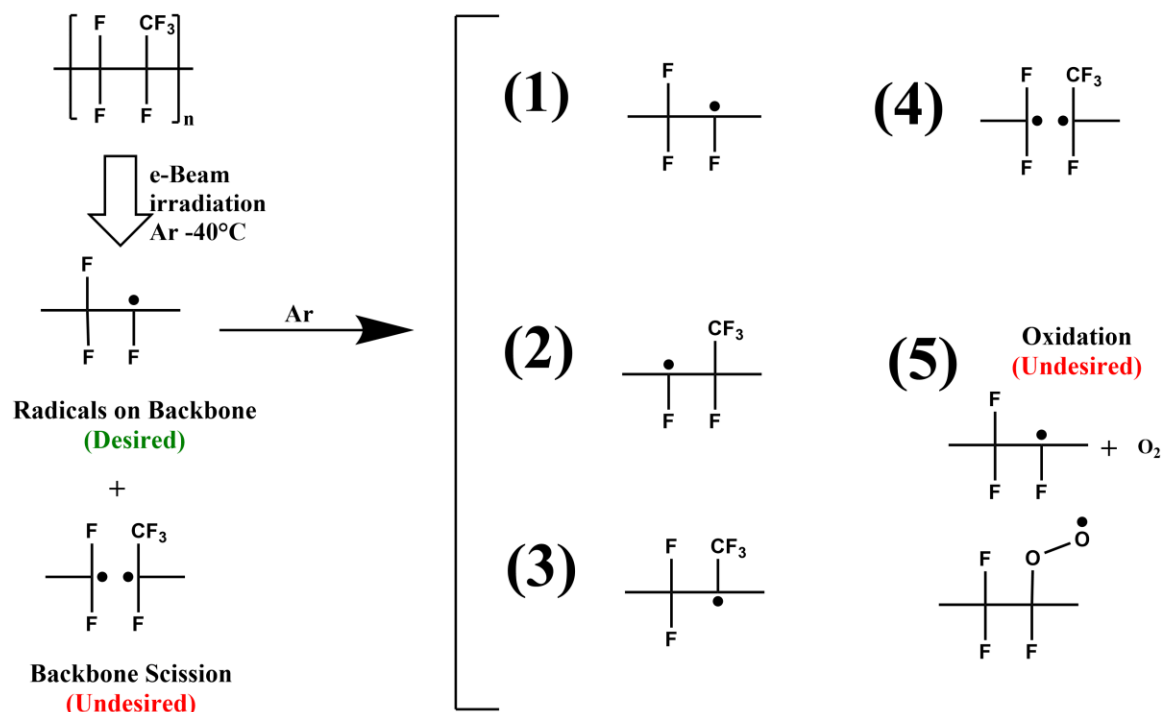


Figure 4.2- Free radicals generated by radiation treatment of FEP

The concentration of free radicals is proportional to the area under the curve of the absorption spectrum which was used to determine the decay of free radicals with time, as shown in Figure 4.3.

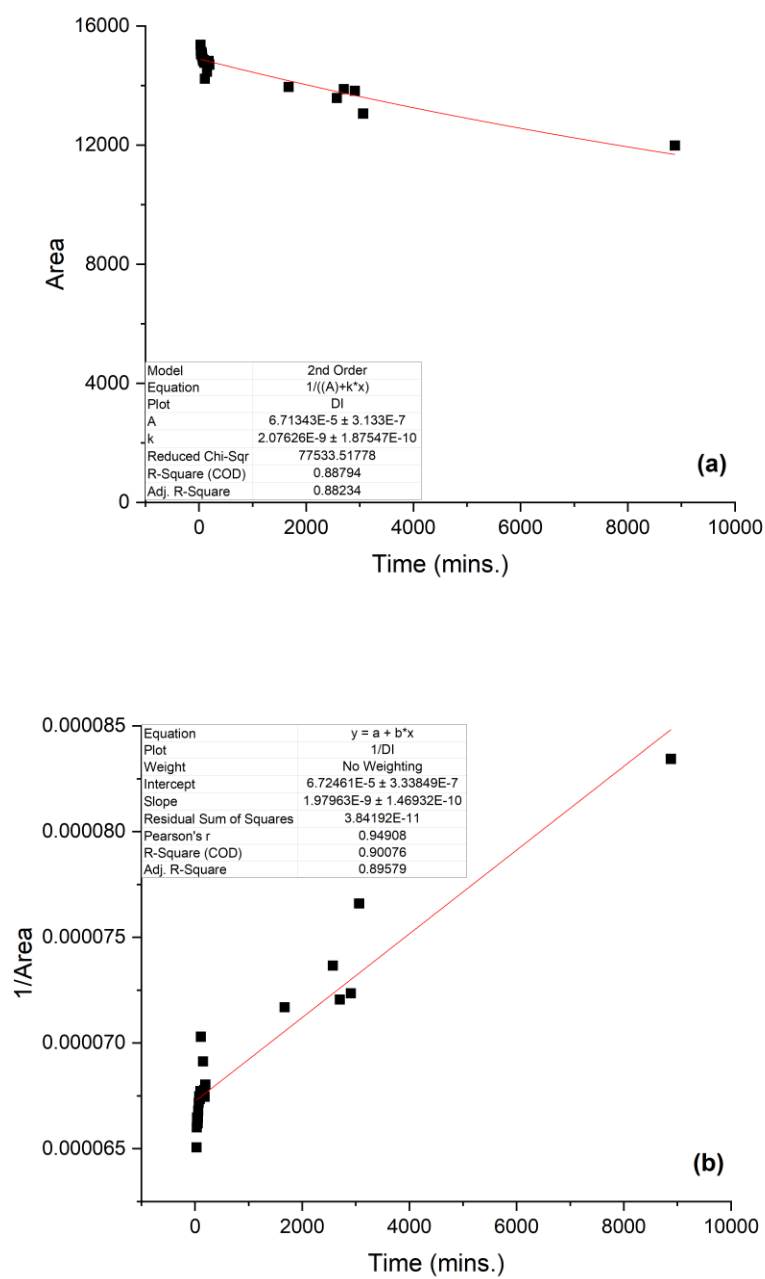


Figure 4.3-FEP free radical decay: (a) Area of EPR absorption spectrum vs. time.
 (b) Free radical decay of irradiated FEP thin films fit with a 2nd order reaction decay in red.

The decrease in free radical concentration with time for FEP films is depicted in Figure 4.3. The free radicals in FEP decayed slowly based on the data collected when compared to other polymer free radicals. Using a second order reaction model, free radical decay to 50% concentration can be extrapolated to 23.59 days at 25°C. Based on this slow decay rate, there would be sufficient free radicals available for indirect grafting to the FEP substrates after a hold time of 15 minutes post radiation treatment. This slow decay rate demonstrates how fluoride groups in fluorocarbons sterically stabilize the free radicals compared to hydrogen in hydrocarbons. In hydrocarbons, free radicals are able to move along the backbone by using neighboring hydrogen atoms. This gives the free radicals a higher mobility and faster decay rate in hydrocarbons compared to fluorocarbon based polymers.[57] The free radical decay is a second order reaction because the rate of decay changes with time. A second order fit was applied to the EPR data as shown in Figure 4.3. The best fit was a 2nd order reaction with $k = 1.980\text{E-}9$ and $A = 6.725\text{E-}5$. The fit had a $R^2 = 0.901$ as shown in Figure 4.3 which is a strong correlation. A second order reaction is expected for free radical decay because the free radical concentration will decrease through a cross-linking reaction between two free radicals. The free radicals of FEP were very stable with active sites available for grafting long after the radiation treatment.

4.1.2 EPR Analysis of PCTFE

The EPR spectra of irradiated PCTFE is displayed in Figure 4.4 and was used to calculate the free radical decay with time. In the EPR spectrum there were two different types of free radicals present; one that decreases with time and one that initially increases and was more stable.

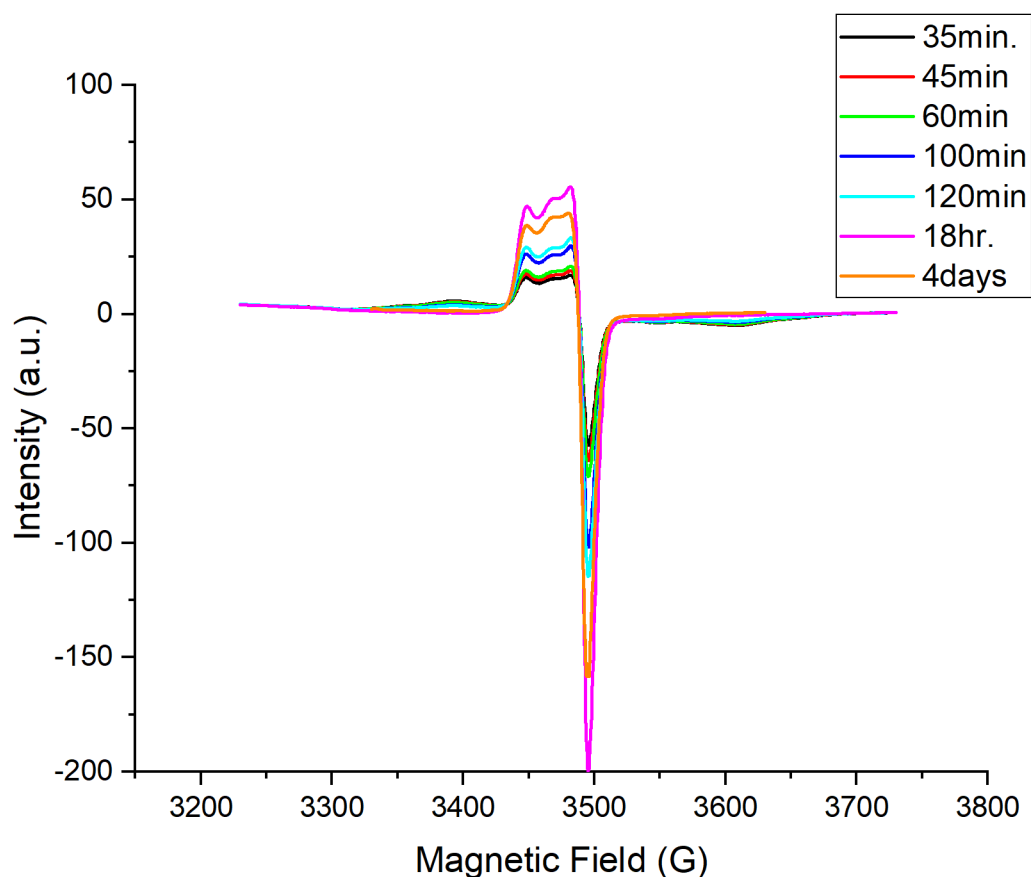


Figure 4.4-1st derivative of EPR spectrum of irradiated PCTFE substrate treated with the MIRF set at 10.5 MeV electron beam, 50 kGy Dose at a 1000 kGy/hr. dose rate.

In the absorption spectrum there are two peaks that overlap each other, representing two different free radicals. The peak heights were used to predict the decay of the free radicals because they overlapped in such a way that the peaks would be difficult to deconvolute. One peak occurred at 3488.55 G and had a g-factor of 2.011, which corresponds to structure 1 in Figure 4.5. These free radicals initially increased rapidly over the first few hours after irradiation, but then decayed gradually days after as shown in orange in Figure 4.4. The second free radical peak occurred at

3499.97G and calculates to a g-factor of 2.004 which corresponds to structure 3 in Figure 4.5.

These free radicals rapidly decreased in the sample as shown in Figure 4.4.

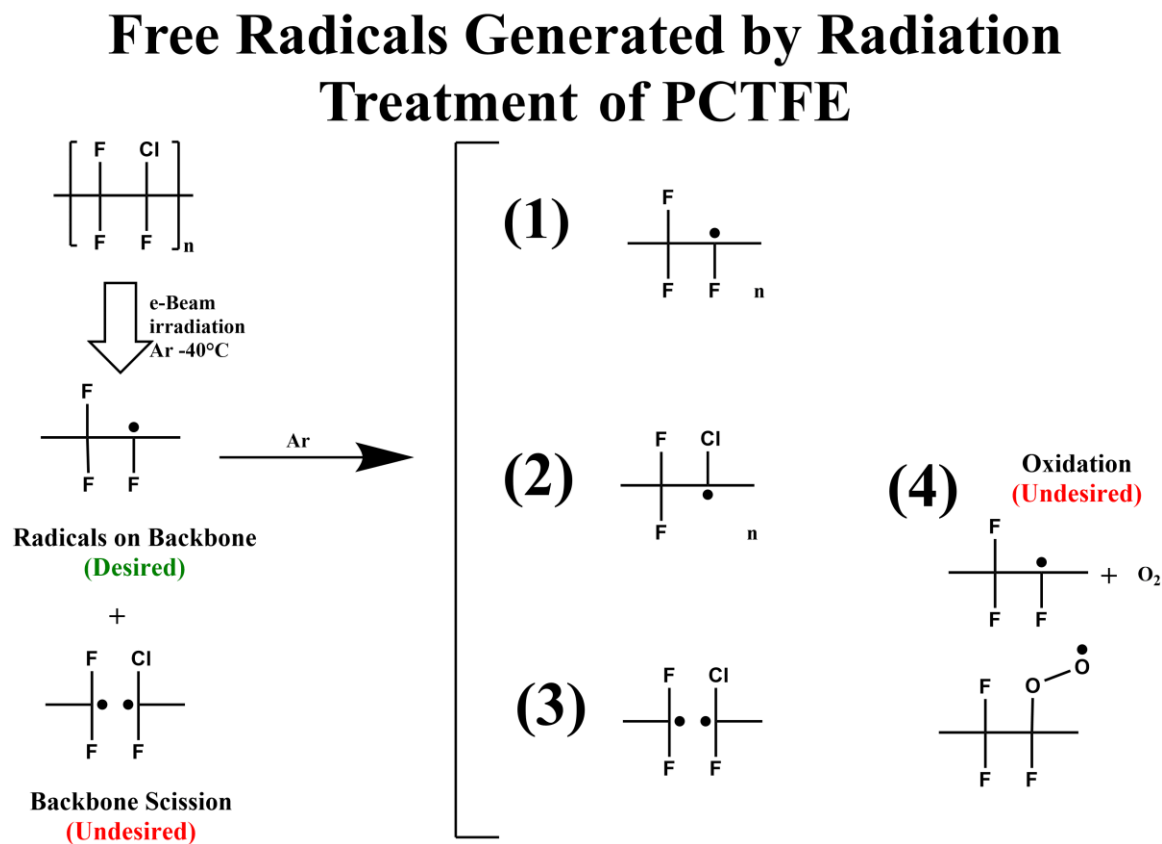


Figure 4.5 -Free radicals generated by radiation treatment of PCTFE

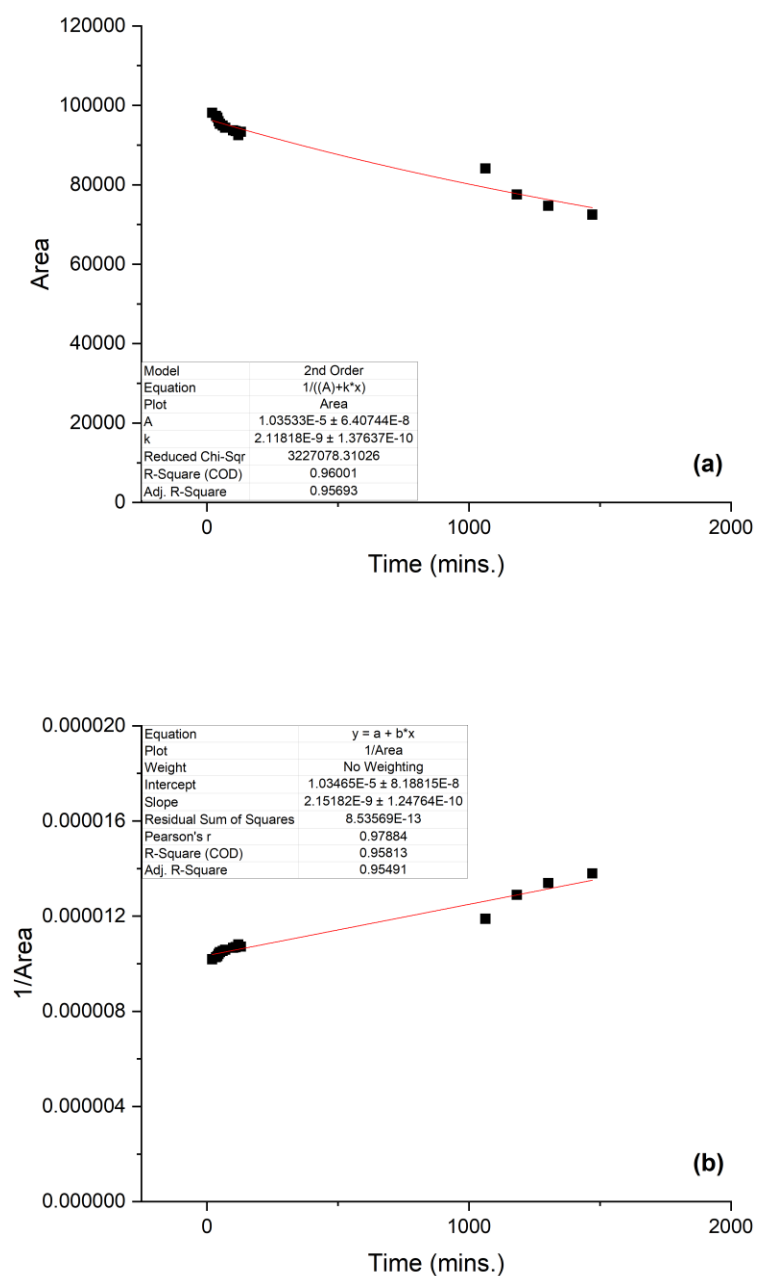


Figure 4.6- PCTFE free radical decay: (a) Area of EPR absorption spectrum vs. time.
 (b) Free radical decay of irradiated PCTFE thin films fit with a 2nd order reaction decay in red.

The best fit for the 3499.97G (Peak II) free radical decay was a zero order reaction with a linear fit of $R^2 = 0.988$ which indicated the decay was independent of free radical concentration. Since the spectrum of the EPR was broad, these peaks are likely composed of multiple types of free radicals. Most free radicals transitioned to the 3488.55G (Peak I) which would explain the increase during this time frame. The growth of Peak I was zero order with a linear fit with $R^2 = 0.988$. These two zero-order reactions indicated that there is a limiting thermal interaction that caused the free radical decay. The free radicals in PCTFE are able to transfer between polymer chains by reacting with R-Cl groups.[57] The free radical decay of Peak II corresponds with an increase in Peak I free radicals so the free radicals were not consumed and were most likely converting to a more stable form. The overall free radical decay of PCTFE is shown in Figure 4.6 where free radicals then gradually decayed. This decay was fit best by a 2nd order reaction $A = 1.035\text{E-}5$ and $k = 2.152\text{E-}9$ with a $R^2 = 0.958$. The time to 50% free radical concentration based on this decay was 80.14 hours. The free radical decay due to cross-linking interaction of free radicals, was shown by the decay being a 2nd order reaction. This means that there would be sufficient free radicals for indirect grafting 15 minutes after irradiation treatment of the PCTFE substrates.

4.1.3 EPR Analysis of PVF

The EPR spectra of irradiated PVF is displayed in Figure 4.7 and was used to determine the decay kinetics for free radicals in the PVF substrate. Figure 4.7 shows there is a single free radical that decays with time with hyperfine coupling.

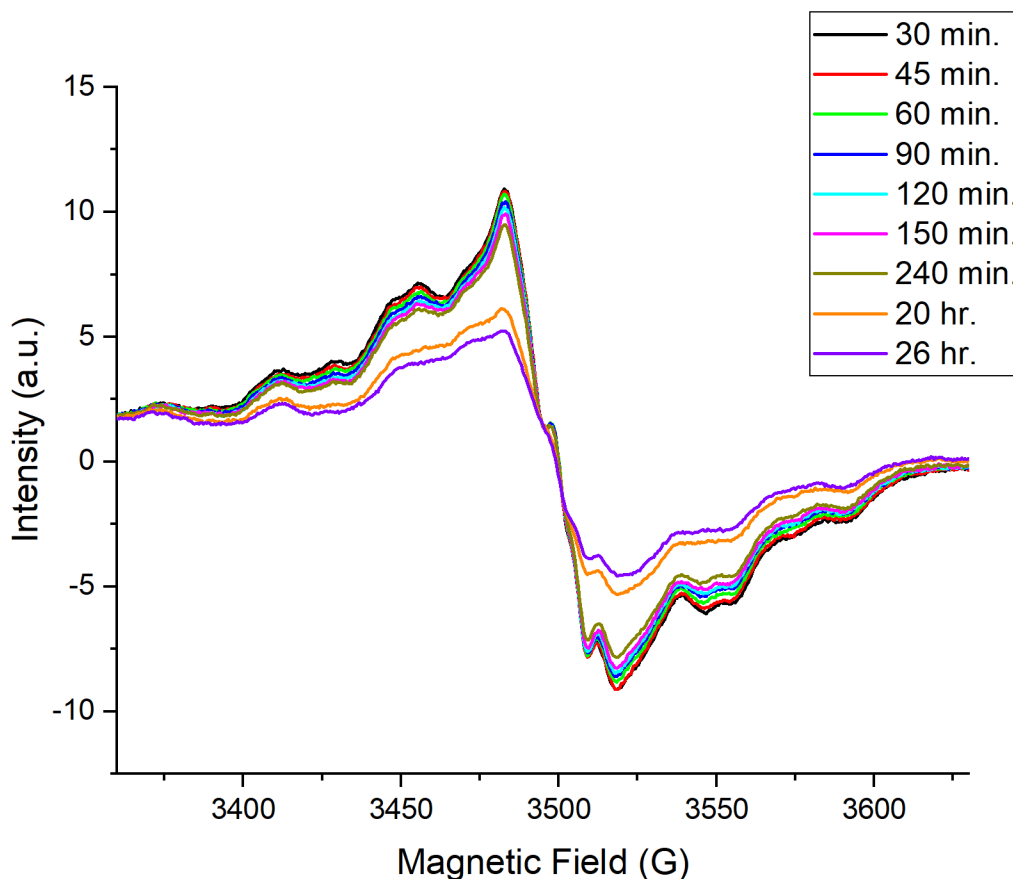


Figure 4.7- 1st derivative EPR spectrum of irradiated PVF substrate treated with the MIRF set at 10.5MeV electron beam, 50kGy dose at a 1000kGy/hr. dose rate.

The plots in Figure 4.7 show there is a single free radical peak when the magnetic field is 3499.50 G which corresponds to a g-factor of 2.0048. The free radical also has hyperfine interactions septet which are expected due to the magnetic field of hydrogen atoms in PVF. The possible free radicals generated by radiation scissions of PVF are shown in Figure 4.8. The radiation scissions will cause C-H and C-C bonds to break and form free radicals shown in structures 2, 3 and 4. The free radical shown in the EPR of Figure 4.7 likely corresponds to a free radical with structure 3 in Figure 4.8. The fluoride group is electron withdrawing which will

stabilize the free radicals on the nearby carbon atom. The hydrogen groups in PVF will also allow the free radicals a high degree of mobility along the backbone. The four hydrogen groups around structure 3 also correspond with the septet hyperfine coupling observed in the EPR spectrum.

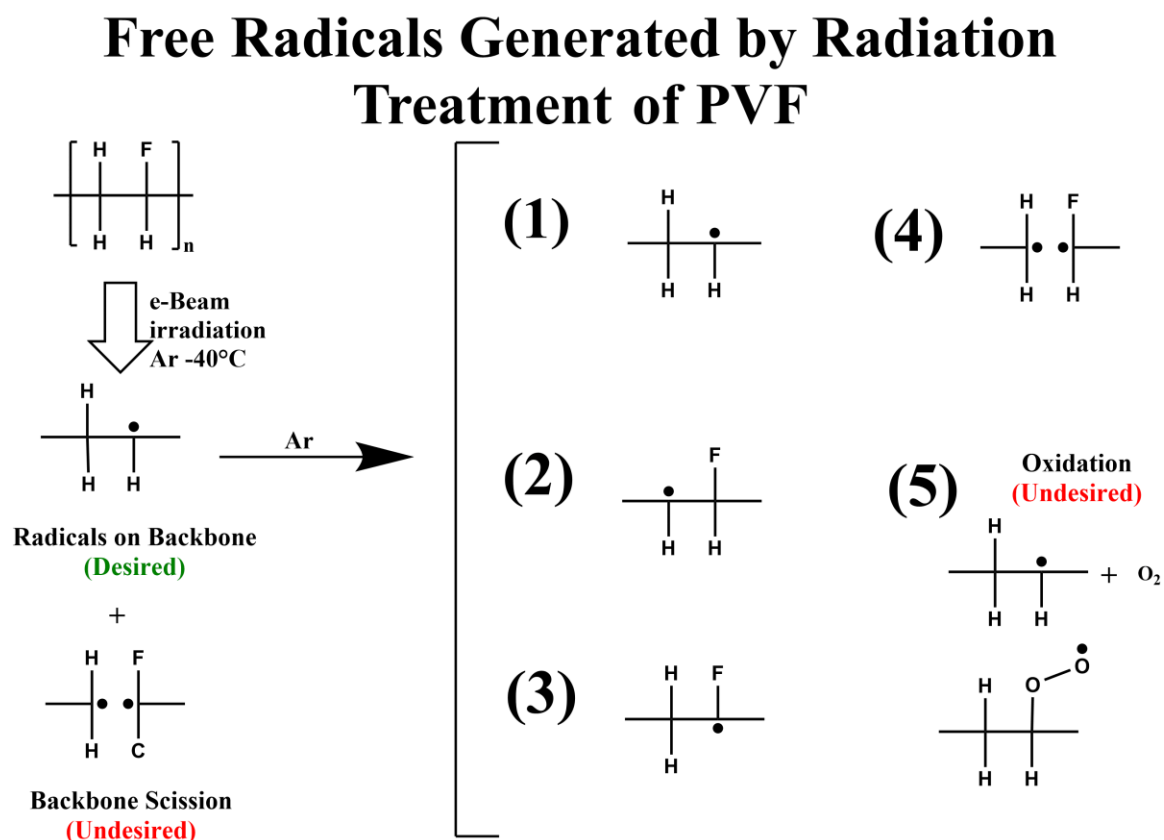


Figure 4.8-Free Radicals generated by radiation treatment of PVF

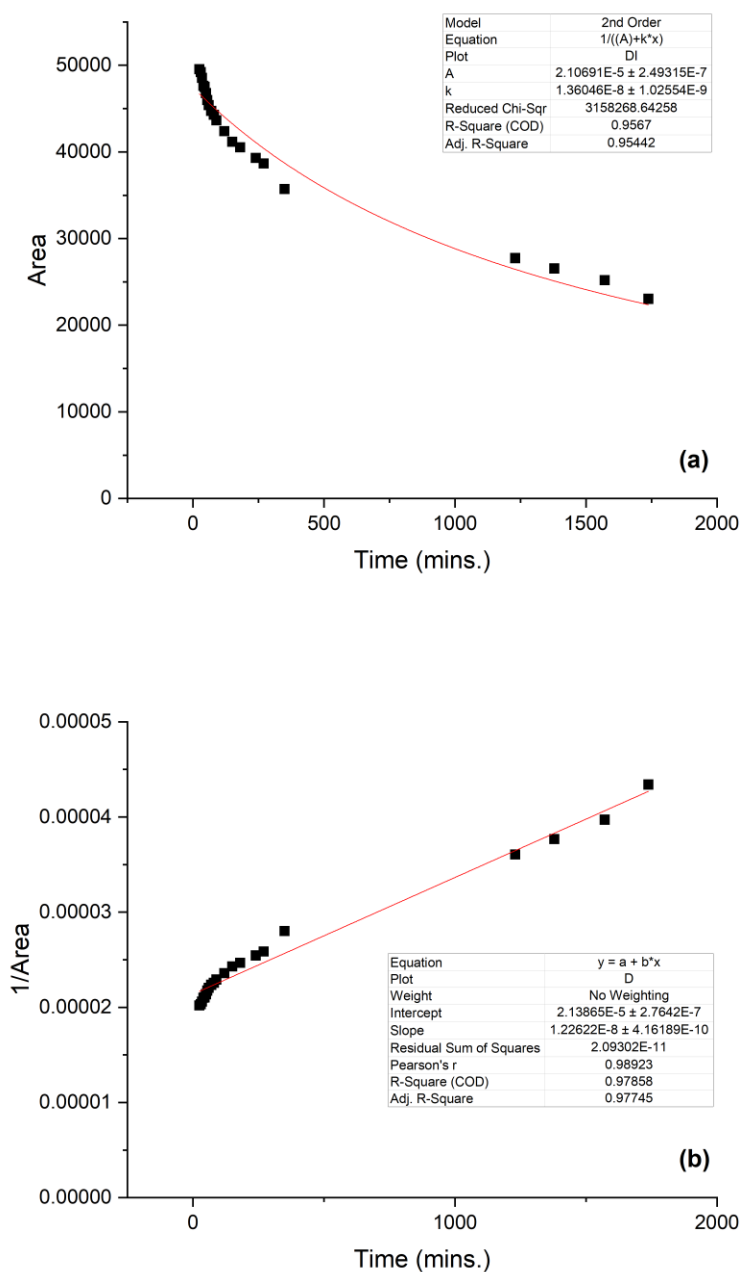


Figure 4.9- PVF free radical decay: (a) Area of EPR absorption spectrum vs. time.
 (b) Free radical decay of irradiated PVF thin films fit with a 2nd order reaction decay in red.

The decay in concentration of free radicals with time of PVF films is depicted in Figure 4.9. The plot is based on the area under the absorption spectrum versus time. The free radicals in PVF decayed with a projected time to 50% concentration of 29.07 hours. To determine the order of the reaction and insight into the mechanism of the free radical decay, 2nd order decay fit was applied as shown in Figure 4.9. This 2nd order reaction had a $R^2 = 0.979$, which is a strong fit. This 2nd order reaction decay was expected due to cross-linking reactions of free radicals that are very mobile. These free radicals decayed through interactions such as cross-linking and formation of double bonds along the back bone. The free radicals in PVF have a higher degree of mobility due to C-H bonds along the backbone and free radicals are stabilized on carbon atoms adjacent to fluoride groups. Of the three fluorocarbon substrates, free radical decay occurred fastest in PVF because of the hydrogen groups and lower glass transition temperature (T_g) of the polymer. Dry ice was used to preserve the free radicals before ionic liquid monomer addition to ensure there were enough free radicals for grafting. Even based on this faster decay rate (t_{50} –29.07 hr), there would be sufficient free radicals available for indirect grafting to the PVF substrates after a hold time of 15 minutes post radiation treatment.

4.2 Radiation Grafting Results

Through the course of this research, polymers were synthesized using beta radiation to graft proton conductive ionic liquids onto fluorocarbon substrates. There are two methods of radiation grafting direct and indirect which are discussed below.

4.2.1 Direct Radiation Grafting Synthesis

The first approach to synthesize PEM utilized a direct radiation grafting method. A diagram of the procedure is shown in Figure 4.10. Samples were prepared by cutting

fluorocarbon substrates and placing them into vials containing solutions of ionic liquid monomer. The samples were purged with Argon gas to remove oxygen from the system. The samples were then treated with radiation and placed in an oven at 80°C for 5-hours. This experimental process was a one-step synthesis method in which substrate was submerged in ionic liquid solutions in a vial and irradiated together to produce PEM. The reason this process was initially pursued, was its one step methodology allowed for quick screening of many combinations of fluorocarbon substrate, ionic liquid monomers, and radiation parameters.

The samples were evaluated by measuring degree of grafting by weight gain. Through this screening method, no samples showed significant grafting above 5% after treatment. Direct radiation grafting usually benefits from hydrogen abstraction of hydronium ions produced by radiolysis of water. This reaction causes free radicals produced in the solvent of the sample to be transferred to the substrate where they can be used as sites for grafting. This reaction was not possible with fluoropolymers because of the C-F bonds which the peroxy free radicals cannot break. Because the ionic liquids that were used were hydrocarbons, direct radiation treatment resulted in polymerization of the monomer in the samples. Once the monomers dimerize, their ability to diffuse in the membrane decreased as their steric hinderance and molecular weight increased. This resulted in significantly lower degrees of grafting and at higher doses homopolymerization occurred on the surface. The grafting in these samples were only surface level and not uniformly grafted.

Direct Radiation Grafting Procedure

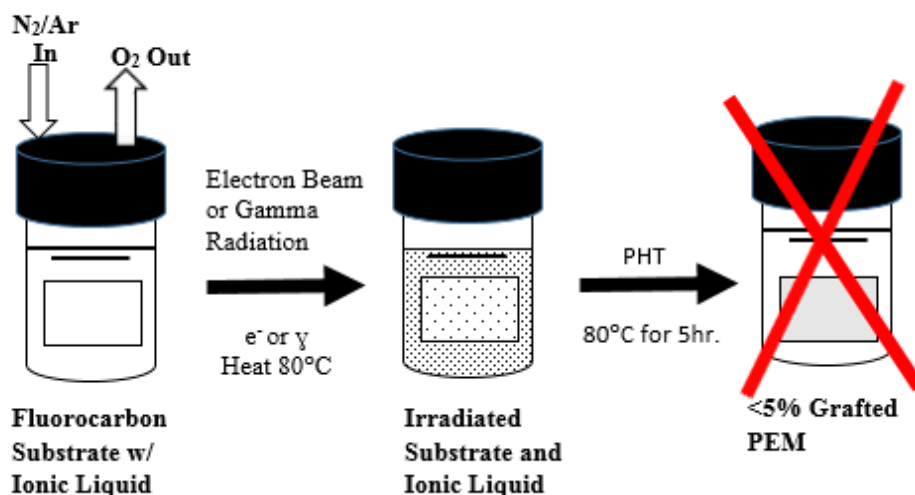


Figure 4.10: Direct Radiation Grafting Procedure-Radicals were generated in both ionic liquid monomer and substrate which caused competing reactions which prevented grafting

The failure to achieve significant grafting even though free radicals were generated can be explained by the radiation treatments producing more free radicals in the monomer solution than in the solid substrate. The free radicals generated in solution react with each other causing polymerization reactions and prevent the monomers from diffusing and grafting into the fluorocarbon films. Fluorocarbons unlike hydrocarbons do not undergo hydrogen abstraction from free radical generated in the solvent. As a result, all free radicals generated in the solvent would drive the polymerization of the monomer. Any polymerization of the monomer would sterically hinder their diffusion into the fluorocarbon substrate necessary for bulk grafting. These homopolymerization agglomerations grafted at the surface were removed by the sonication washing steps and resulted in little to no weight gain in the substrate. Additional direct radiation grafting experiments were conducted focusing on radiation parameters and sample composition to shift the reactions towards a higher degree of grafting. The parameters

investigated to improve grafting were dose, dose rate, ionic liquid monomer concentration and solvents, however no samples showed significant improvement in grafting, and the procedure of direct radiation grafting was not investigated further. In order to improve the quantity and quality of grafting in the PEM, it was decided to switch to an indirect radiation grafting method.

4.2.2 Indirect Radiation Grafting Synthesis

This research project focused on indirect grafting treatment in which the fluorocarbon substrate was first radiation treated to generate free radicals only in the substrate. This was followed by ionic liquid monomer addition and application of a post heat treatment (PHT). An overview of the indirect radiation synthesis procedure is shown in Figure 4.11.

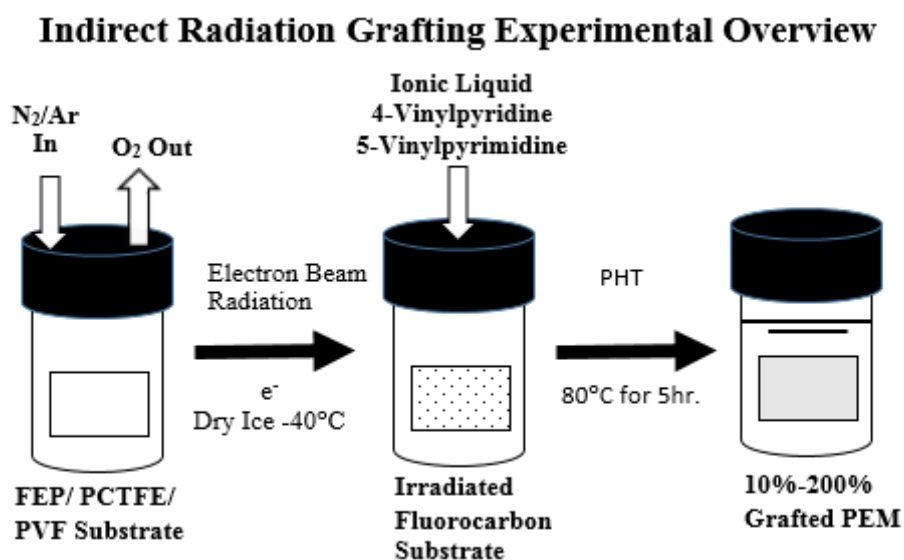


Figure 4.11: Indirect radiation grafting process

This procedure significantly reduces the amount of competing reactions and prevented the ionic liquids from polymerizing. An experiment was conducted to determine the concentration effect of ionic liquid on the degree of grafting. Table 4.1 shows the percent grafting of two

concentrations of 4-vinylpyridine added to the irradiated fluorocarbon substrates. The 100% percent ionic liquid monomer produced higher percent grafting compared to the more dilute 0.25M solutions.

Table 4.1: Indirect radiation grafting results of 4-vinyl pyridine onto fluorocarbon substrates varying ionic liquid monomer concentration

Sample # 6162016	Ionic Liquid Monomer Solution	Dose (kGy)	Dose rate (kGy/hr)	Irradiation Temperature (°C)	Post Heat Treatment (°C) (hr.)	Average Grafting (%)	STD (%)	Rep.
FEP 1-3	4-vinyl pyridine	100	100	- 45	65 and 5	16.4	3.39	3
FEP 5-8	0.25M 4- vinylpyridine with 1- butanol	100	100	- 45	65 and 5	-0.02	0.05	4
PCTFE 1-3	4-vinyl pyridine	100	100	- 45	65 and 5	39.4	10.22	3
PCTFE 5-8	0.25M 4- vinylpyridine with 1- butanol	100	100	- 45	65 and 5	0.53	3.01	4
PVF 1-3	4-vinyl pyridine	100	100	- 45	65 and 5	95.03	32.86	3
PVF 5-8	0.25M 4- vinylpyridine with 1- butanol	100	100	- 45	65 and 5	-0.11	0.24	4

4.2.3 Indirect Radiation Grafting Parameters

For the indirect grafting method, there were three important parameters tested for optimization of the radiation grafting process. The critical parameters were; dose, dose rate and PHT temperature. These parameters had a significant effect on the number and density of free radicals generated, and the amount and extent of ionic liquid grafted. Experiments were conducted to determine appropriate radiation parameters to achieve bulk grafting and homogenous films. The following parameters were evaluated:

- Doses; 12.5, 25, 50 and 100kGy
- Dose rates; 100kGy/hr (0.23Gy/pulse), 300kGy/hr (0.69Gy/pulse), 500kGy/hr (1.2Gy/pulse) and 1000kGy/hr (2.4Gy/pulse)

- Post radiation heat treatment temperatures (PHT); 65°C and 80°C for 5 hours

4.3.2.1 Grafting onto FEP

The results in Figures 4.12 and 4.13 show the optimized radiation parameters varied significantly with the fluorocarbon substrate. Figure 4.12 shows the test results for indirect radiation grafting of 4-vinylpyridine onto FEP substrates. There are two trends observed from the data; the degree of grafting was improved by increasing the PHT temperatures to 80°C and a lower dose rate of 100kGy/hr improved the percent grafting for 4-vinylpyridine onto FEP. It is important to note that the glass transition temperature of the fluorocarbon membranes was 80°C which could explain the significant change in the amount of grafting between 65°C and 80°C.

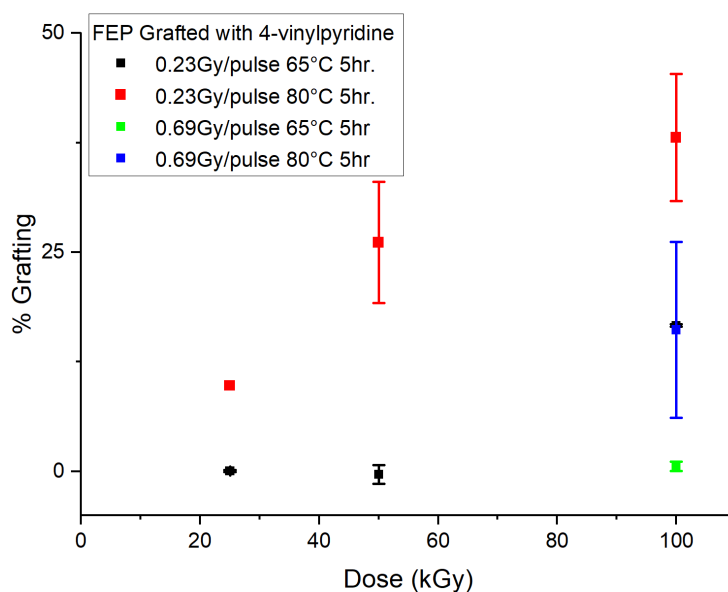


Figure 4.12: Indirect radiation grafting 4-vinylpyridine onto FEP, monomer was added 15 mins after radiation treatment PHT (n=2)

FEP being a fully fluoronated polymer, produced one free radical type after radiation treatment (Figure 4.2-1). The free radicals were stable with a free radical decay to 50% concentration of 23.59 days. The subsequent grafting results shown in Figure 4.13. indicates that after a 6 hour hold time before ionic liquid addition, significant amount of grafting was achieved. As shown, higher dose rates led to higher percent grafting for the FEP substrate.

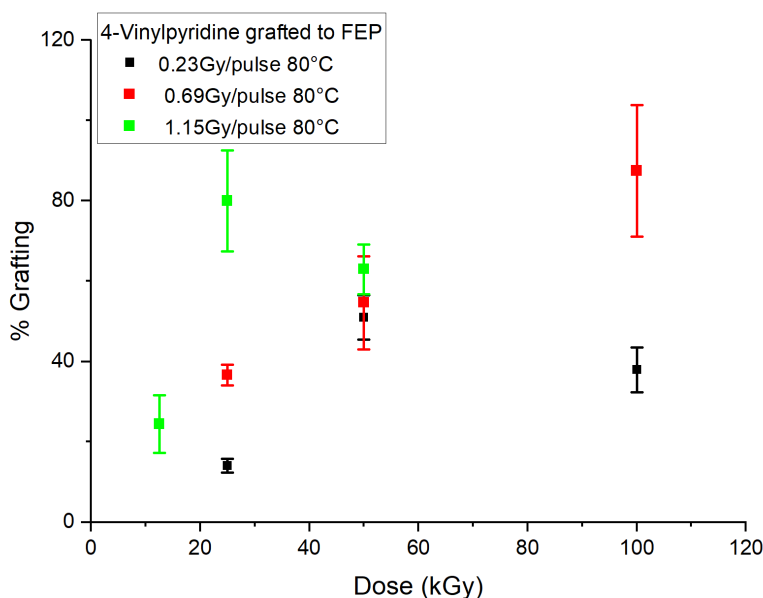


Figure 4.13 -Indirect grafting of 4-vinylpyridine onto FEP, free radicals were preserved under dry ice, monomer added after 6 hrs. (n=3)

4.3.2.2 Grafting onto PCTFE

Figure 4.14 shows the test results for indirect radiation grafting of 4-vinylpyridine onto PCTFE substrate. There were two trends in this data. The degree of grafting was improved by increasing the PHT temperature from 65°C to 80°C and a higher dose rate of 300kGy/hr improved the percent grafting.

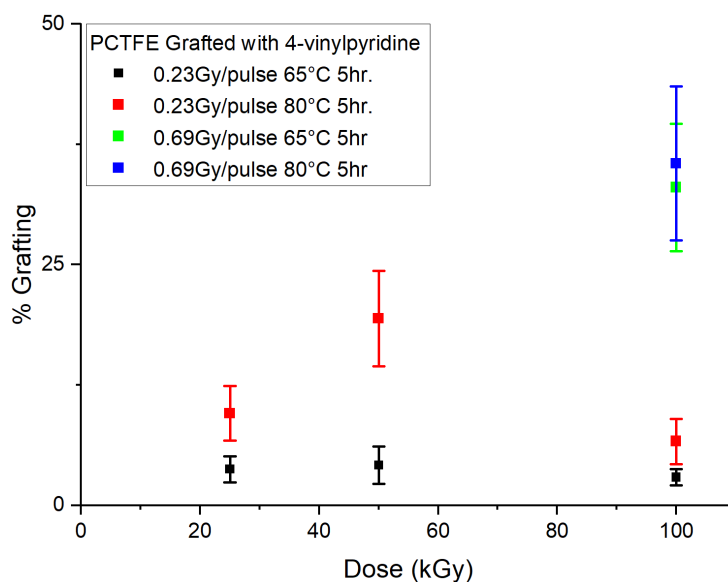


Figure 4.14: Indirect radiation grafting 4-vinylpyridine onto PCTFE (n=2)

Of the three fluorocarbon substrates samples, membrane of PCTFE became considerably more brittle after radiation grafting. This was due to the lack of crosslinking which supports the radiation resistance of the PEM to maintain its mechanical properties. PCTFE free radicals also have a free radical decay to 50% concentration of 80.14 hours due to the low rate of termination. There should have been enough time for the grafting reactions to occur. The lower degree of grafting compared to other fluorocarbon substrates was due to the PCTFE's higher % crystallinity. The grafting can only occur in the amorphous regions of the fluorocarbon substrate where the monomer can diffuse.

4.3.2.3 Grafting onto PVF

PVF is hydrocarbon based and has a lower glass transition temperature than the other fluorocarbon substrates tested making this polymer's surface more available for grafting. Figure

4.15 shows the test results for indirect radiation grafting of 4-vinylpyridine onto PVF substrates. The degree of grafting was increased by using a PHT temperature of 80°C. When the percent grafting was above 100%, there is a potential that the ionic liquid monomer has polymerized on the surface. This will prevent bulk grafting and the formation of a uniform PEM for proton conductivity.

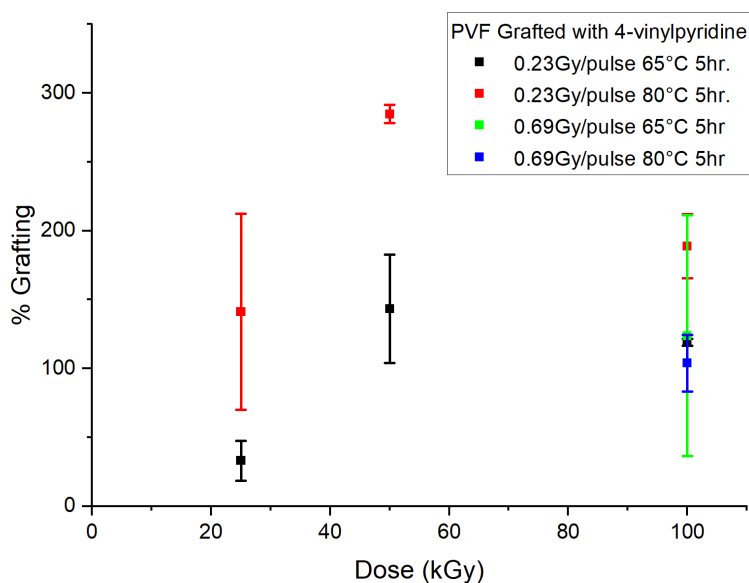


Figure 4.15: Indirect radiation grafting 4-vinylpyridine onto PVF (n=2)

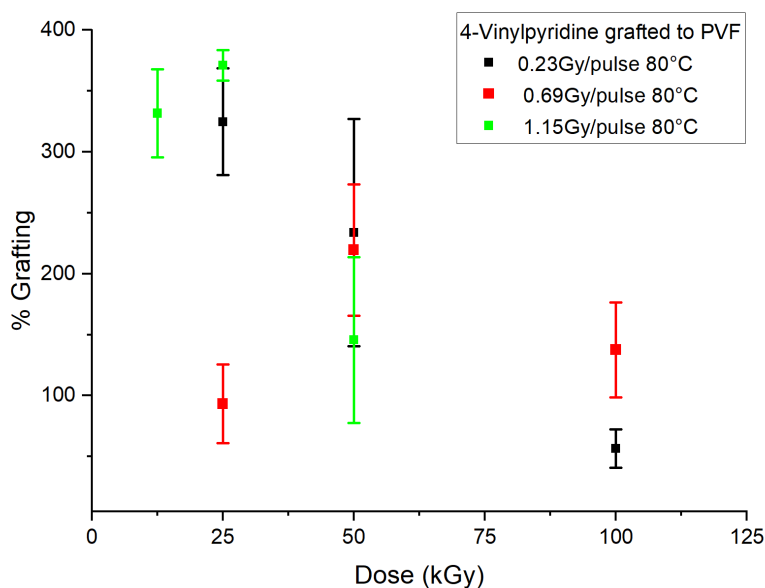


Figure 4.16- Indirect grafting of 4-vinylpyridine onto PVF, free radicals were preserved under dry ice, monomer added after 6 hrs. (n=3)

Indirect grafting of 4-vinylpyridine grafted to PVF substrate free radicals were preserved under dry ice, monomer added after 6 hrs. is shown in Figure 4.16.

To further optimize percent grafting, experiments were performed at a dose rate of 1000kGy/hr. (2.31Gy/pulse) along with a post heat treatment temperature of 80°C for 5 hrs. and doses ranging from 25kGy to 100kGy. Due to the free radical decay to 50% concentration of 29.07 hours for PVF, the higher dose rate was selected to reduce the time between the initial radiation treatment and monomer addition to preserve free radicals for grafting. However, a disadvantage of the higher dose rate was unwanted cross-linking prior to the monomer addition may occur. Both 4-vinylpyridine and 5-vinylpyrimidine were grafted to the fluorocarbon substrates (FEP, PCTFE and PVF) using the radiation conditions noted in Table 4.2 with the high dose rate of 1000kGy/hr. The percent grafting results are shown in Table 4.2.

Table 4.2: Indirect radiation grafting 4-vinylpyridine and 5-vinylpyrimidine onto fluorocarbon substrates at high dose rates

Sample # 3222017	Ionic Liquid Monomer	Dose (kGy)	Dose rate kGy/hr	Irradiation Temperature (°C)	Post Heat Treatment (°C) (hr.)	Average Grafting (%)	STD (%)	Rep.
FEP-1 (a-e)	5-vinyl pyrimidine	25	1000	-45	80 and 5	19.62	3.18	5
PCTFE-3 (a-e)	5-vinyl pyrimidine	100	1000	-45	80 and 5	11.82	2.77	5
PVF-1 (a-e)	5-vinyl pyrimidine	25	1000	-45	80 and 5	44.63	4.95	5
PVF-3 (a-e)	5-vinyl pyrimidine	100	1000	-45	80 and 5	29.45	3.49	5
PCTFE-2 (a-e)	4-vinylpyridine	50	1000	-45	80 and 5	7.70	4.95	5
PCTFE-1 (a-e)	4-vinylpyridine	100	1000	-45	80 and 5	20.23	5.64	5
FEP-3 (a-e)	4-vinylpyridine	50	1000	-45	80 and 5	18.57	4.57	5

The results show that a higher dose rate of 1000kGy/hr. still achieved an acceptable level of grafting. The percent grafting increased with radiation dose for 4-vinylpyridine grafted onto PCTFE. The percent grafting decreased with 5-vinylpyrimidine onto PVF with increasing dose. The difference in these grafting trends are due to the mobility of free radicals in the fluorocarbon substrate and the competing reactions of grafting and crosslinking that occur.

4.3 PEM Composition Analysis

4.3.1 SEM/EDS Cross-section Analysis

The following section will discuss the SEM/EDS analysis of the PEM to determine atomic composition of the samples. These measurements were conducted to understand the

grafting profile through the cross-sectional membranes. The anhydrous ionic liquid PEM were synthesized by grafting hydrocarbon based ionic liquids onto fluorocarbon substrates. A successful grafting reaction will increase the carbon to fluorine ratio in the membrane. Samples were embedded in epoxy and cross-sectioned using a Lecia microtome using the method discussed in section 3.3.3. EDS analysis was used to track the carbon to fluorine ratio through the membrane as a means to determine the relative concentrations of the grafted ionic liquid monomer. The fluoride groups have a higher electron density as compared to hydrogen, which allows the grafting concentration gradient to be observable in the SEM images. These measurements will also indicate if the membranes are homogeneously grafted and capable of proton conductivity through the membrane. PEM synthesized by radiation grafting of 4-vinylpyridine and 5-vinylpyrimidine onto FEP, PCTFE and PVF fluorocarbon substrates are discussed below.

4.3.1.1 FEP SEM/EDS Analysis

To quantify the change in the carbon to fluoride ratio, an untreated FEP control was used as a reference. The FEP substrate (FEP 100) was manufactured by DuPont. The SEM image of the FEP control is shown below in Figure 4.17. The EDS spectrum is shown in Figure 4.18 and the atomic composition analysis is provided in Table 4.3, with C-37.74%, N-0.04%, O-1.38% and F-60.83%. The initial carbon to fluorine ratio of untreated FEP substrate is 0.620. This value is higher than 0.500 which is expected based on the chemical structure of pure chains of FEP. This deviation can be caused by chemical additives, cross-linking and oxidation present within the untreated film. This carbon to fluoride ratio was used to determine the relative amount of grafting in the ionic liquid grafted FEP PEM.

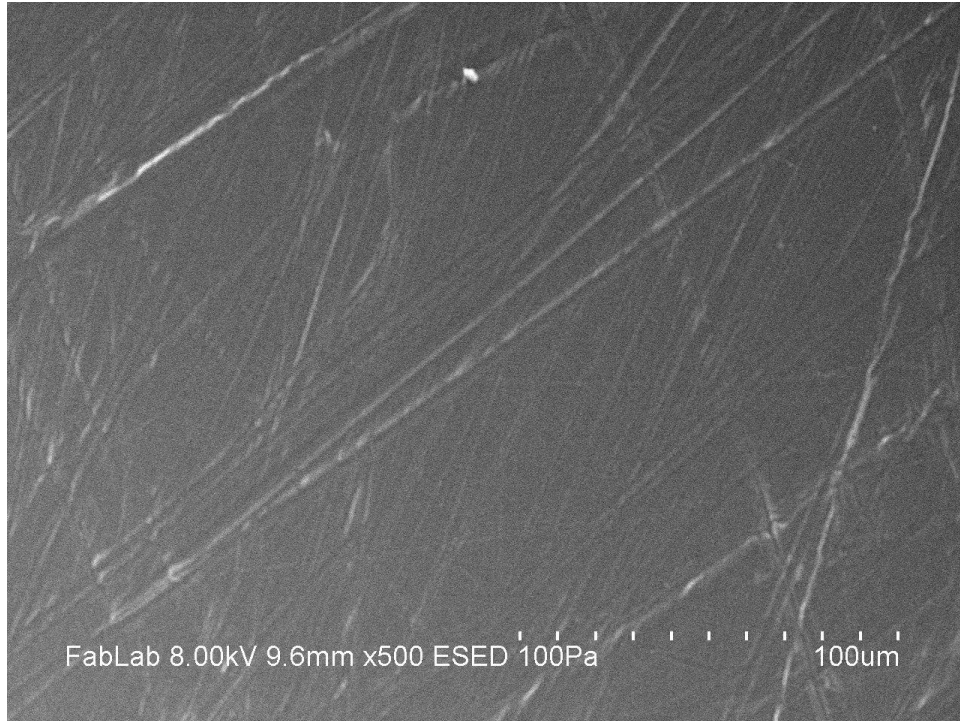


Figure 4.17- SEM Image of FEP substrate

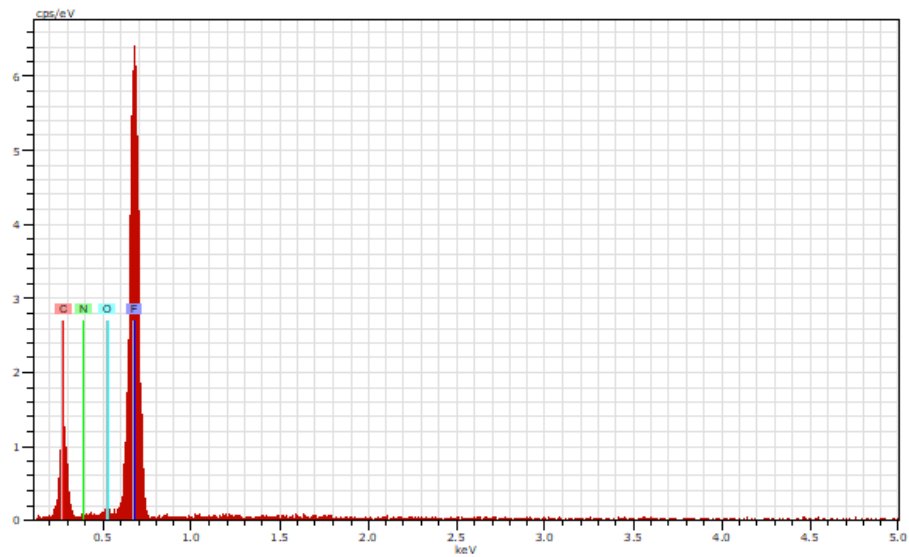


Figure 4.18- EDS of FEP substrate

Table 4.3: EDS Atomic composition analysis of FEP Substrate

Element	Norm C %wt	Atom C %at	Sigma STD
C	27.78	37.74	0.50
N	0.03	0.04	0.06
O	1.36	1.38	0.09
F	70.82	60.83	0.51

The SEM image in Figure 4.19 is the cross-section of Sample 20180910 FEP-10a. This sample was synthesized using indirect radiation grafting of 4-vinylpyridine onto FEP substrate with a 25kGy and 100kGy/hr. treatment. The sample had 15.1% grafting. The EDS spectrum in the center of the cross-section is shown in Figure 4.20 and the analysis of the spectrum shown in Table 4.4, with C-66.52%, O-14.23%, and F-17.01% atomic composition. The ratio of carbon to fluoride ratio is 3.91, which is substantially higher than the initial FEP substrate ratio of 0.620 and shows grafting through the center of the membrane.

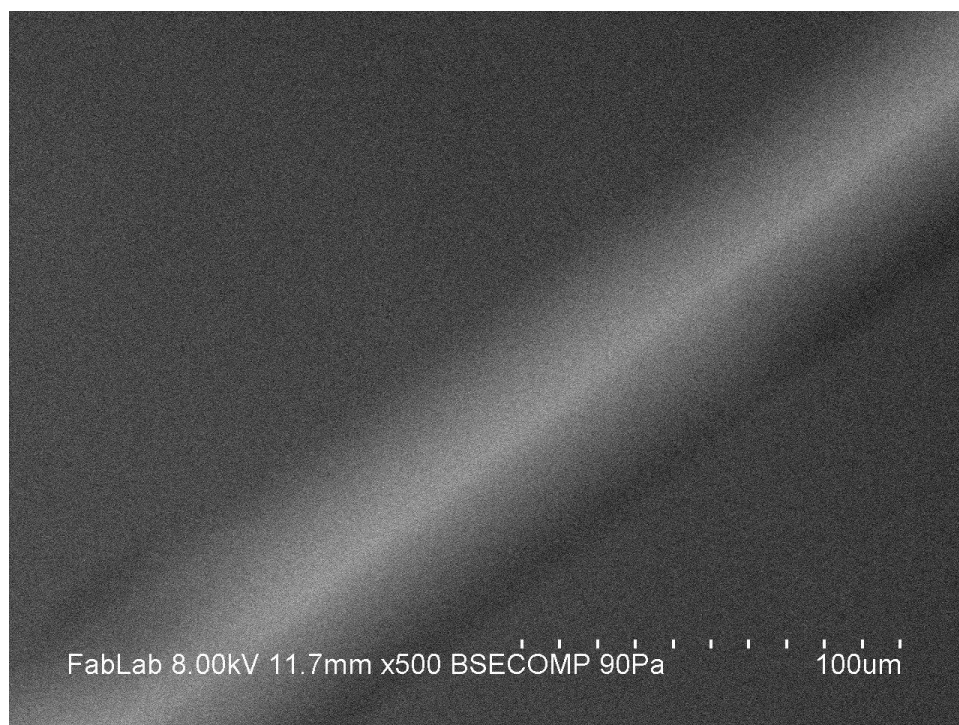


Figure 4.19-SEM image of sample 20180910 FEP-10a

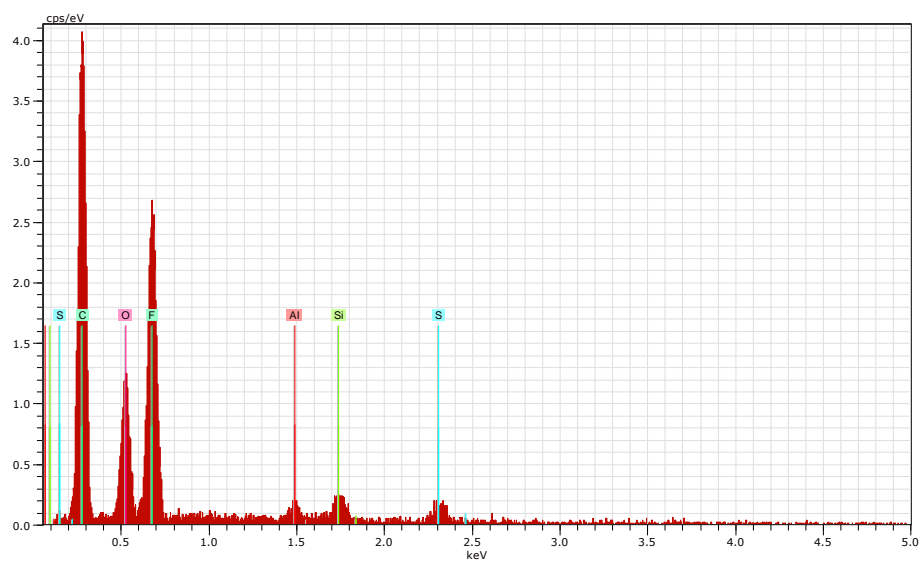
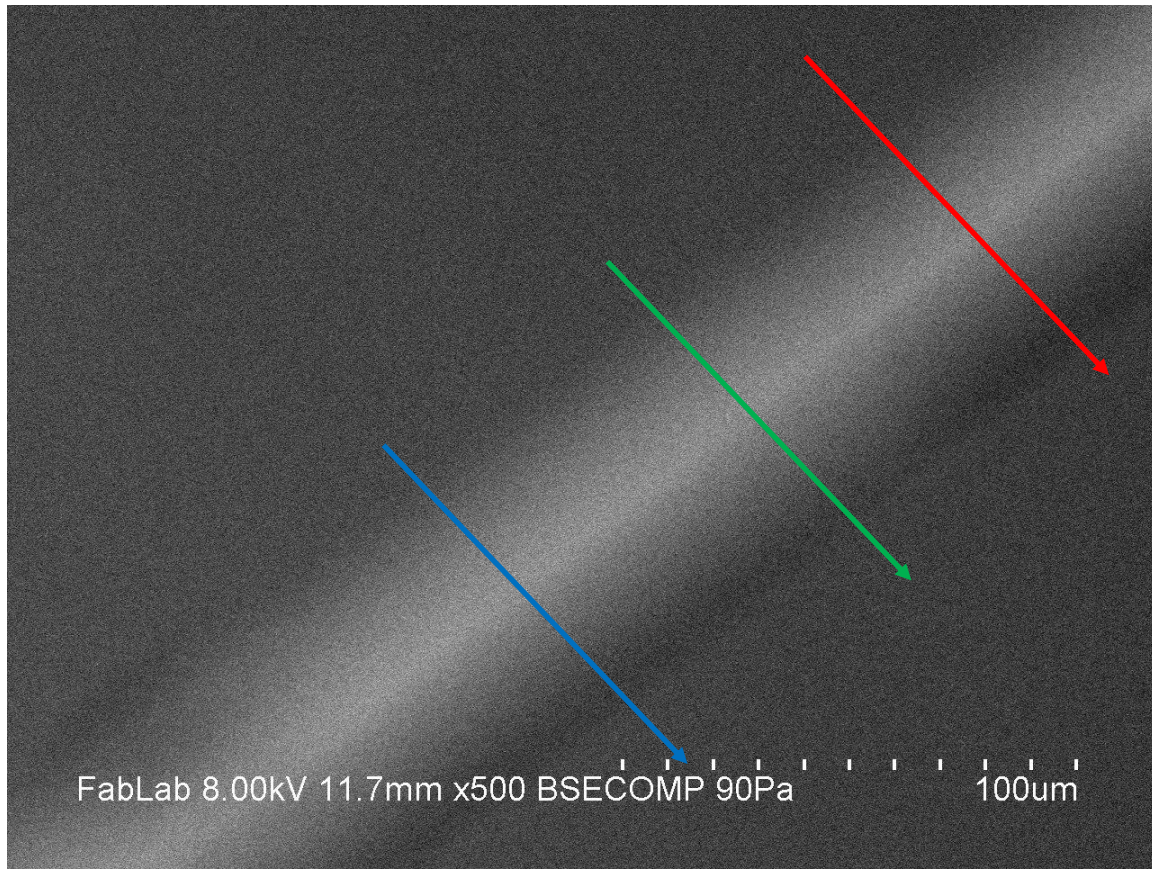


Figure 4.20-EDS of center of cross-section for sample 20180910 FEP-10a

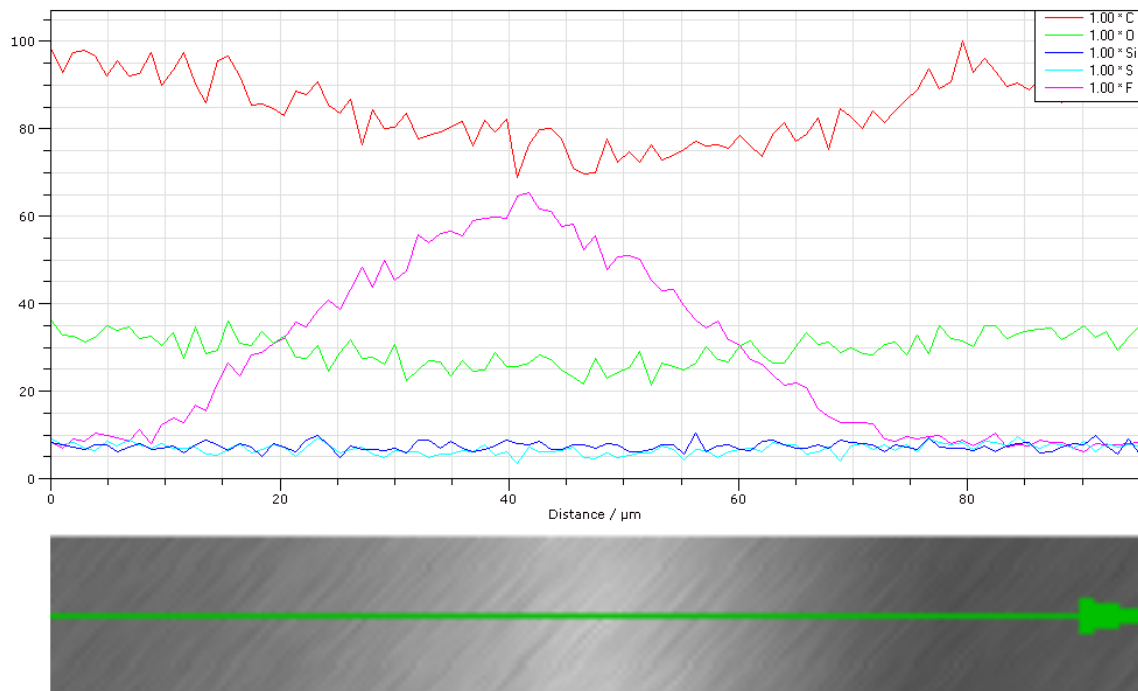
Table 4.4: EDS atomic analysis of sample 20180910 FEP-10a

Element	Norm C %wt	Atom C %at	Sigma STD
C	56.46	66.52	1.25
O	16.09	14.23	0.87
F	22.82	17.01	2.17
Al	0.64	0.34	0.01
Si	2.32	1.17	0.14
S	1.66	0.73	0.16

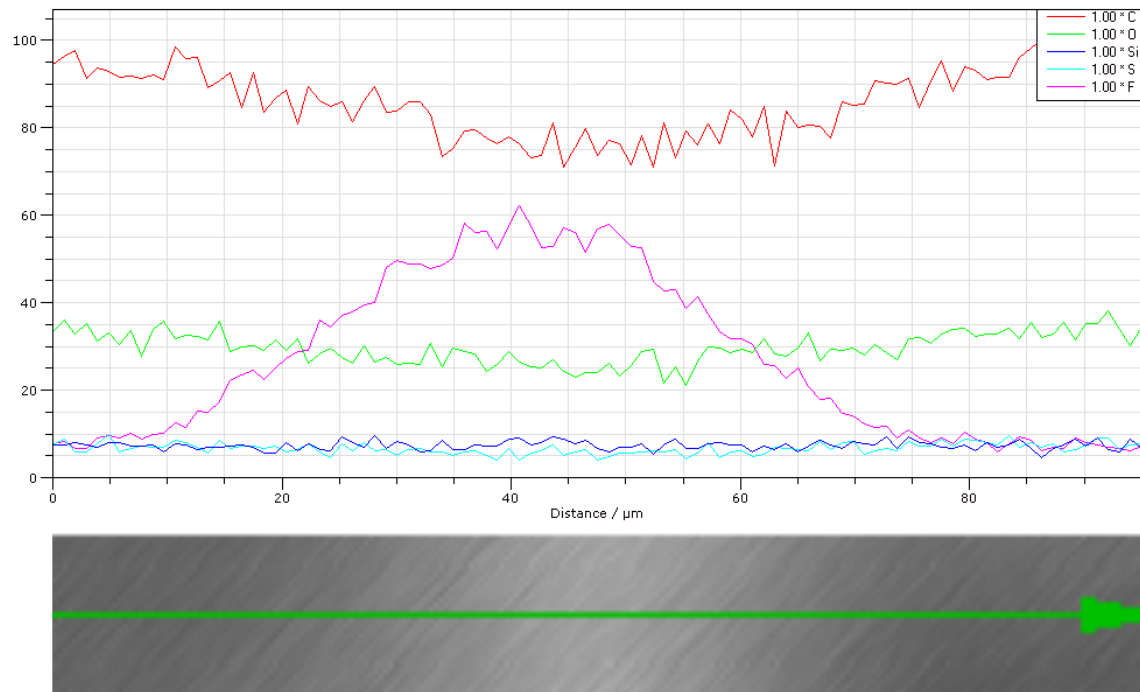
To evaluate the grafting profile through the membrane, EDS line scans were made across the cross-section of the membrane. The results of these line scans for sample 20180910 FEP-10a are shown in Figure 4.21 below. Three SEM/ EDS line scans of the sample cross-section test area are shown by red, blue or green colored arrows. The test area results show relative atomic composition across the cross-section in Figure 4.21 (b), (c) and (d). The scans show that there was a significant concentration gradient of the grafted ionic liquid from the surface to the center of the membrane. This indicates while there was grafting through the membrane, the composition was not homogeneous. This would effect the proton conductivity through this membrane.



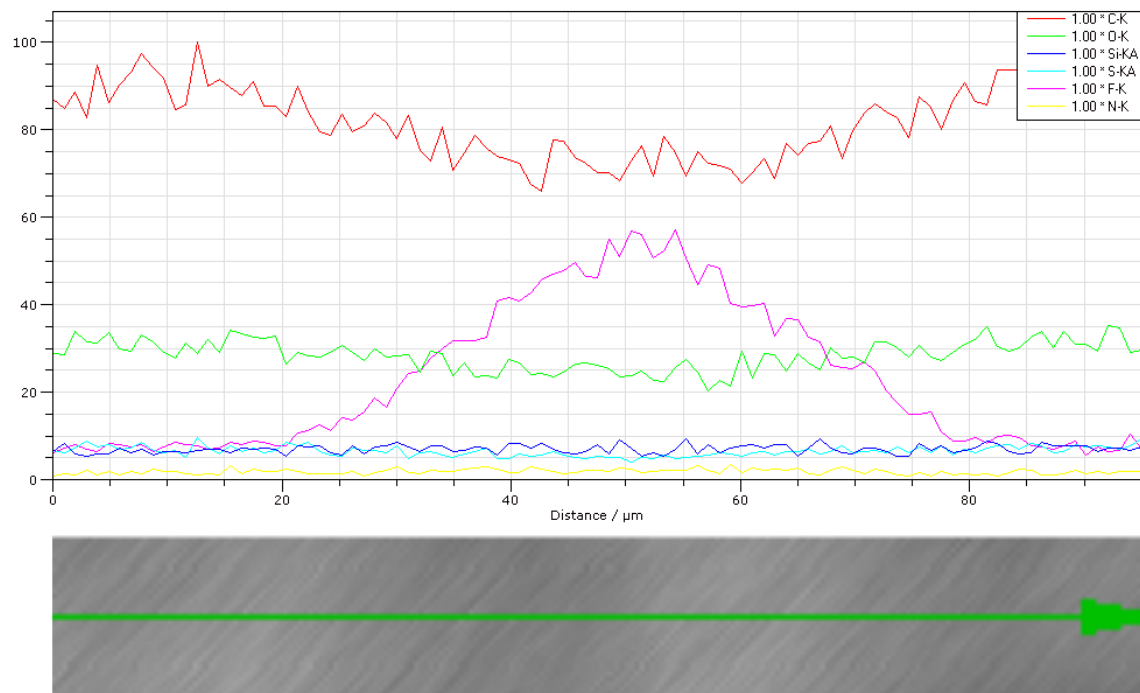
(a)



(b)



(c)



(d)

Figure 4.21- (a) Three SEM/EDS line scans across the cross-section of sample 20180910 FEP-10a and corresponding test area results for (b) red (c) green (d) blue.

Figures 4.21, b, c, d show the gradient through the membrane with a decrease in fluorine (pink) on the surfaces and increasing moving towards the center. This would indicate the grafting is not uniform.

The SEM image in Figure 4.22 is the cross-section of Sample 20180910FEP-11a. This sample was synthesized using indirect radiation grafting for 4-vinylpyridine onto FEP substrate with a 25kGy and 300kGy/hr. treatment. This sample had 38.61% grafting. The EDS spectrum of the center of cross-section is shown in Figure 4.23 and the analysis of this spectrum is shown in Table 4.5 with C-69.32% , N- 3.15%, O-10.11% and F-16.25% atomic composition. The ratio of carbon to fluoride ratio is 4.27, which is substantially higher than the initial FEP substrate ratio of 0.620 and shows grafting occurred through the center of the membrane.

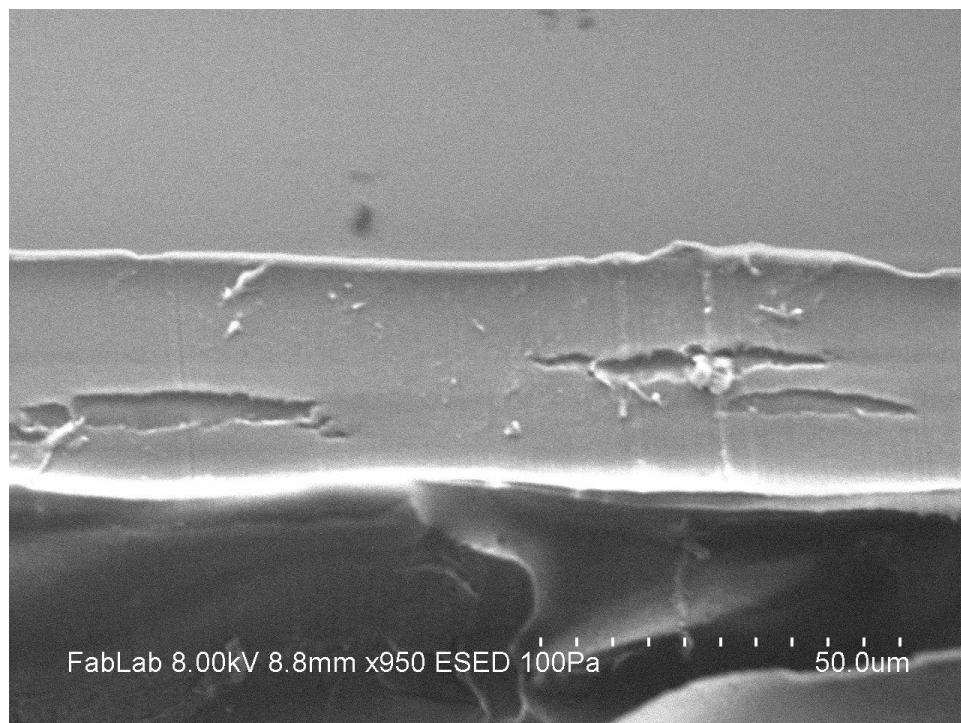


Figure 4.22-SEM image of sample 20180910FEP-11a

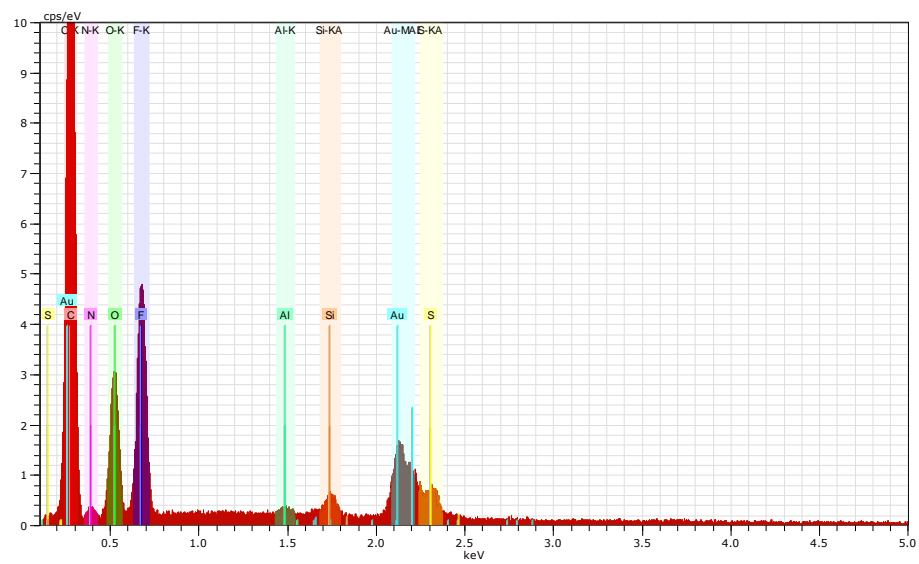


Figure 4.23-EDS from center of sample 20180910FEP-11a cross-section

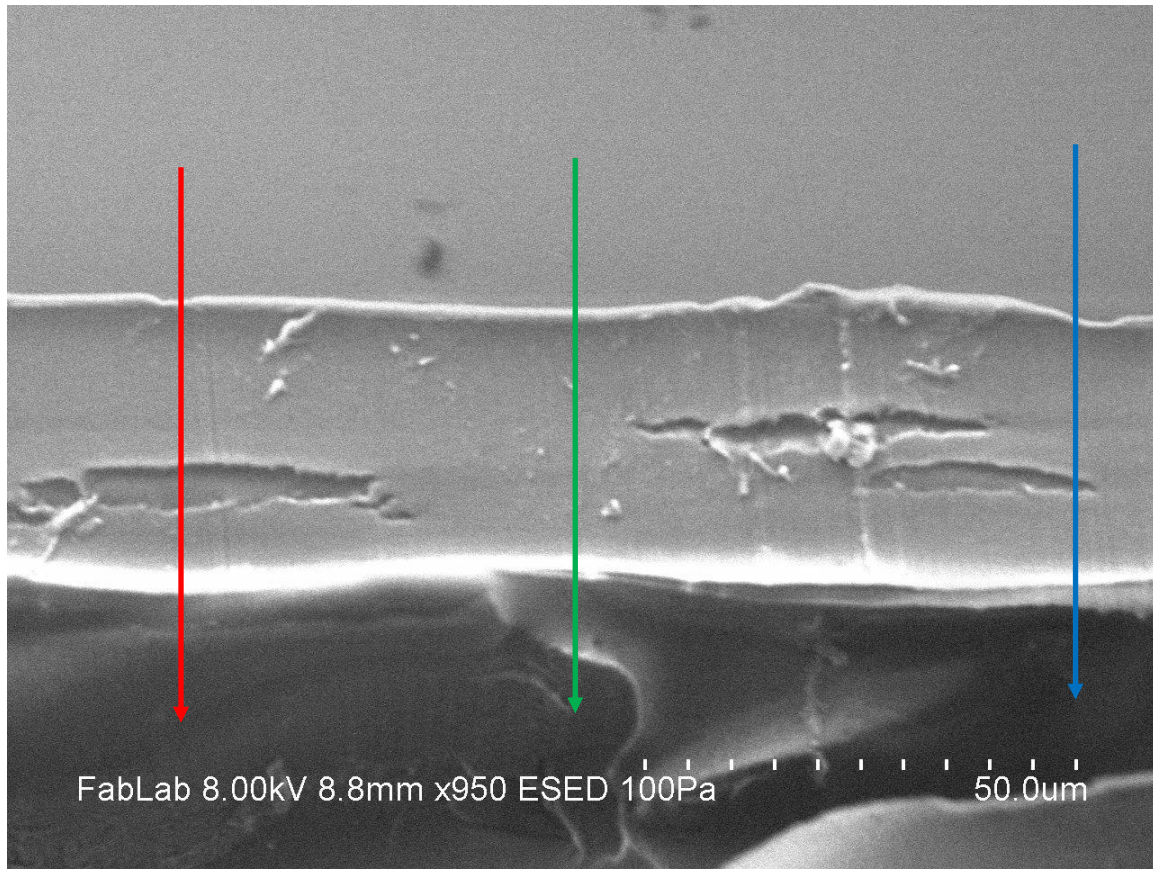
Table 4.5: EDS analysis from center of 20180910FEP-11a cross-section

Element	Norm C %wt	Atom C %at	Sigma STD
C	52.88	69.32	1.15
N	2.81	3.15	1.10
O	10.27	10.11	0.63
F	19.58	16.25	1.96
Au	14.46	1.16	0.13

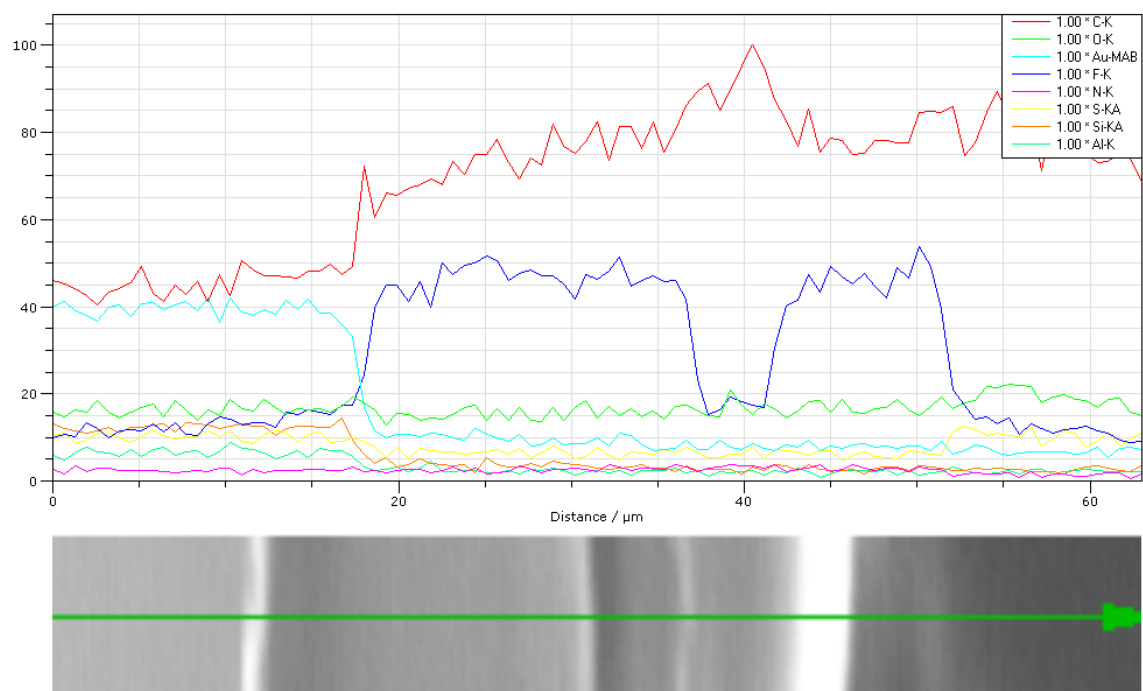
The grafting profile through the membrane was determined by EDS line scans of the cross-section. The results of these line scans for sample 20180910 FEP-11a are shown in Figure 4.24. Three SEM/ EDS line scans of the sample cross-section test area are shown by red, blue or green colored arrows. The test area results show relative atomic composition across the cross-section in Figure 4.24 (b), (c) and (d). These scans indicate that there is a significant gradient of the concentration grafted ionic liquid from the surface to the center of the membrane.

The results of the EDS line scans show the gradient through the membrane with a steady concentration of fluorine (blue). This would indicate the grafting is uniform. Some changes in the composition in the line scans occurred due to roughness of the sample surface and are unlikely from compositional changes. Comparatively the two 4-vinylpyridine FEP samples synthesized at a low and high radiation dose rates of 100 and 300kGy/hr show differences in grafting uniformity.

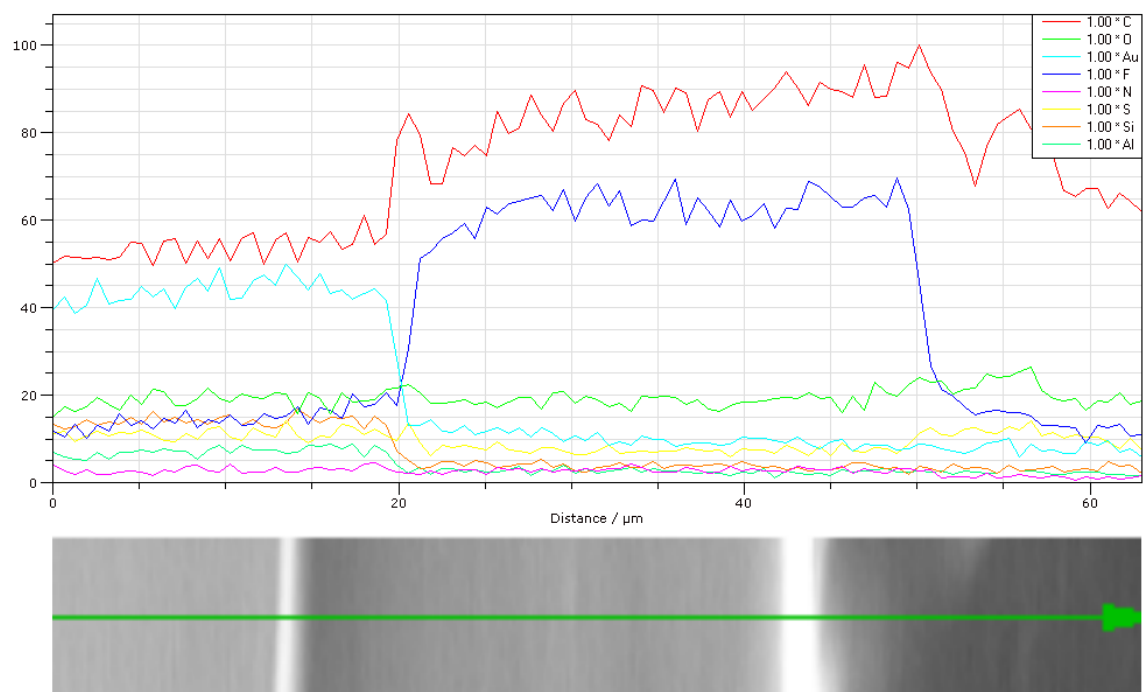
The sample prepared with the higher dose rate, resulted in more uniform atomic composition and higher concentration of grafted protic ionic liquid polymer. The generated sample would support solid state proton conductive network through the membrane which is needed for PEMFC fuel cell applications.



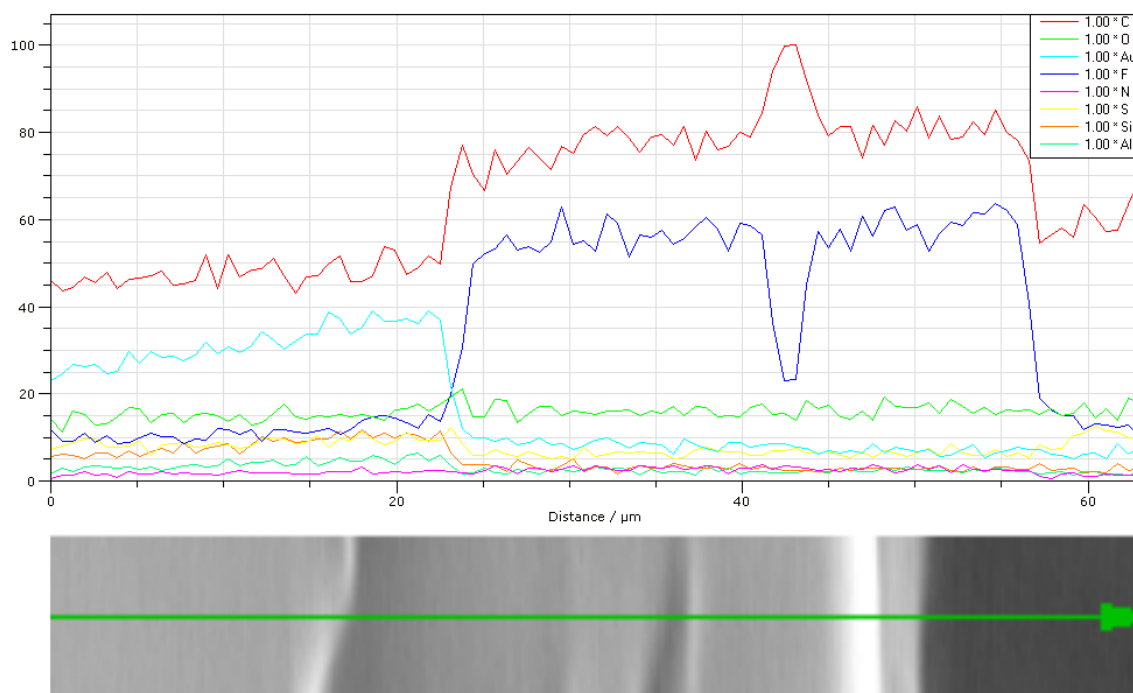
(a)



(b)



(c)



(d)

Figure 4.24- (a) Three SEM/EDS line scans across the cross-section of sample 20180910 FEP-11a and corresponding test area results for (b) red (c) green (d) blue.

4.3.1.2 PCTFE SEM/EDS Analysis

The untreated PCTFE substrate (Hydroblock) was manufactured by Honeywell. The SEM image of untreated PCTFE substrate will act as a control and is shown below in Figure 4.25. The EDS spectrum is provided in Figure 4.26, and the atomic composition analysis in Table 4.6 is C-41.08%, N-0.74%, O-0.32%, F-43.93% and Cl-13.94%. The carbon to fluorine ratio of untreated PCTFE substrate is 0.935. This ratio value is higher than 0.666 which is expected based on the chemical structure of pure chains of PCTFE. This deviation again can be caused by chemical additives, cross-linking and oxidation present within the film. The carbon to fluorine ratio will be used to determine the relative amount of grafting in the ionic liquid PCTFE PEM.

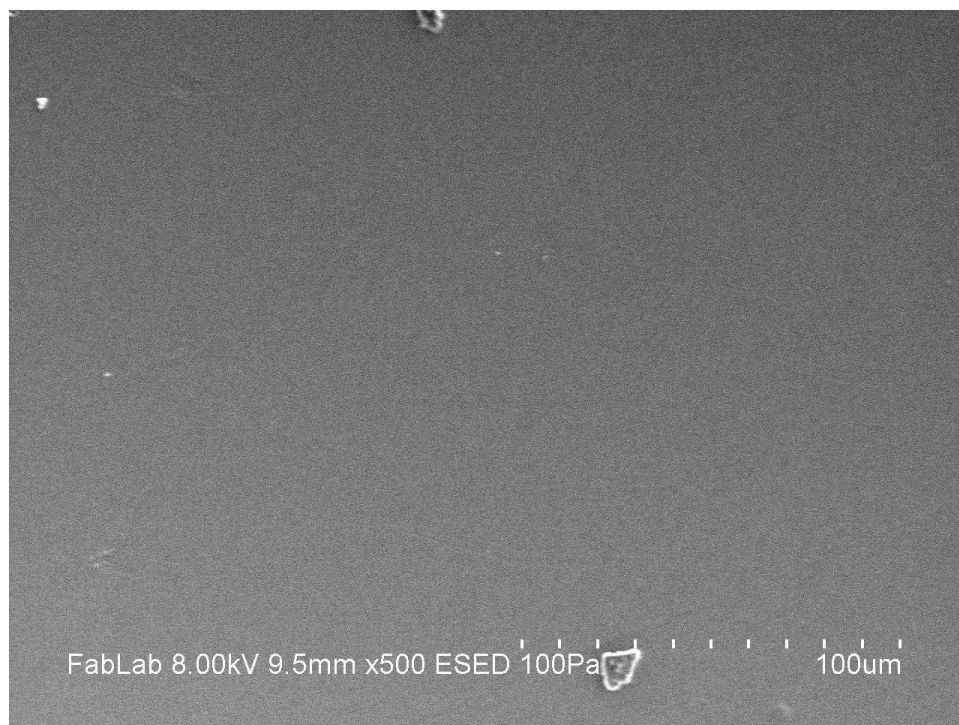


Figure 4.25-SEM Image of untreated PCTFE substrate

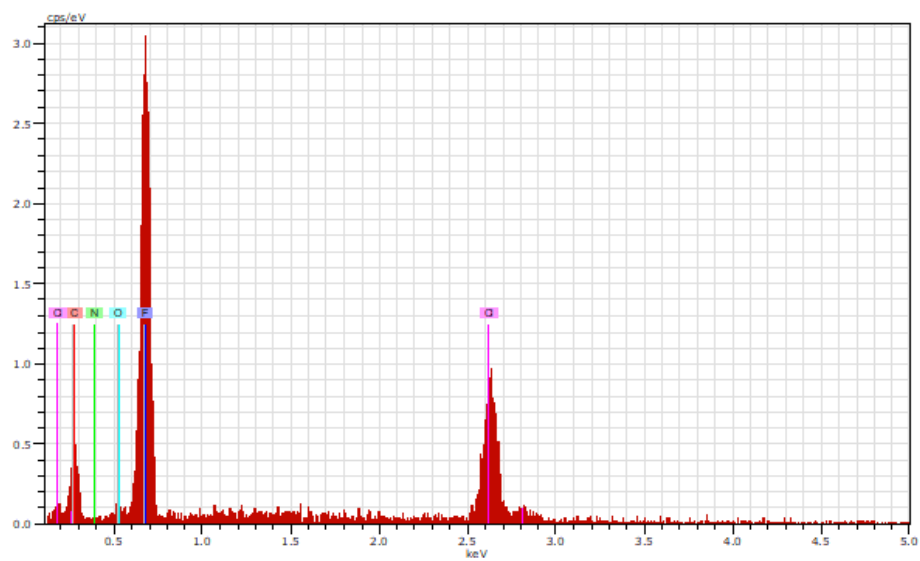


Figure 4.26-EDS of untreated PCTFE substrate

Table 4.6: EDS atomic analysis of untreated PCTFE

Element	Norm C %wt	Atom C %at	Sigma STD
C	22.54	41.08	0.88
N	0.47	0.74	0.44
O	0.23	0.32	0.28
F	38.12	43.93	0.65
Cl	22.57	13.94	0.36

The SEM image in Figure 4.27 is the cross-section for sample 8112016PCTFE-16. This sample was synthesized using indirect radiation grafting of 4-vinylpyridine onto PCTFE substrate with a 100kGy and 300kGy/hr. treatment. The sample had 41.16% grafting. The EDS spectrum of the center of cross-section is shown in Figure 4.28 and the analysis of this spectrum is shown in Table 4.7, with C-72.51%, N-2.03%, O-13.51%, F-3.28% and Cl-5.33% atomic composition. The ratio of carbon to fluoride is 22.1 which is substantially higher than the initial PCTFE substrate 0.935 and indicates grafting occurred through the center of the membrane.

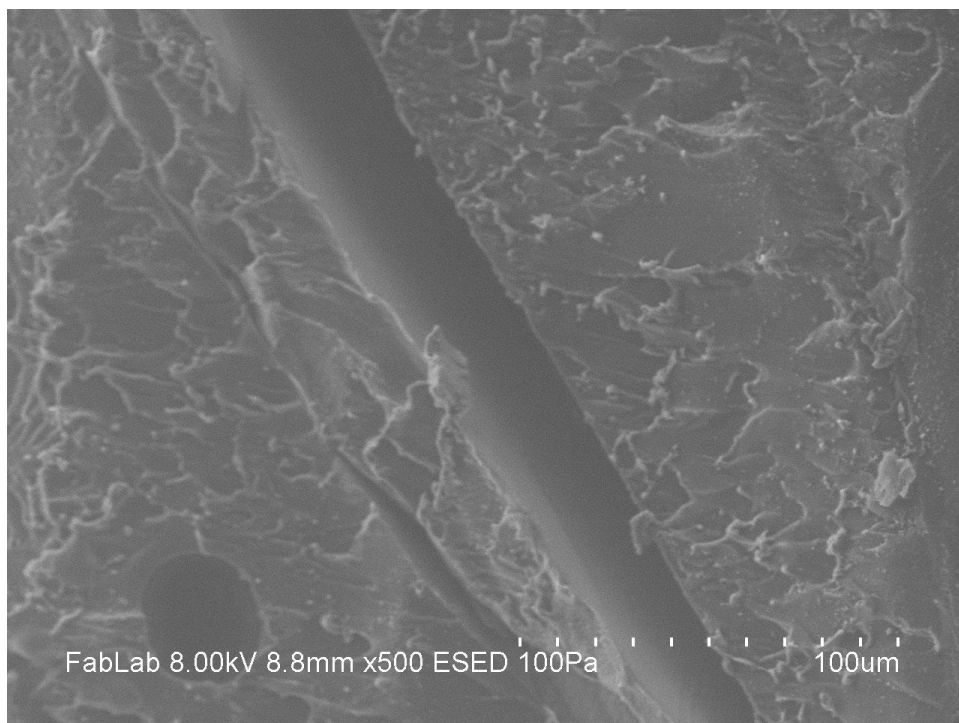


Figure 4.27- SEM image of Sample 8112016PCTFE-16

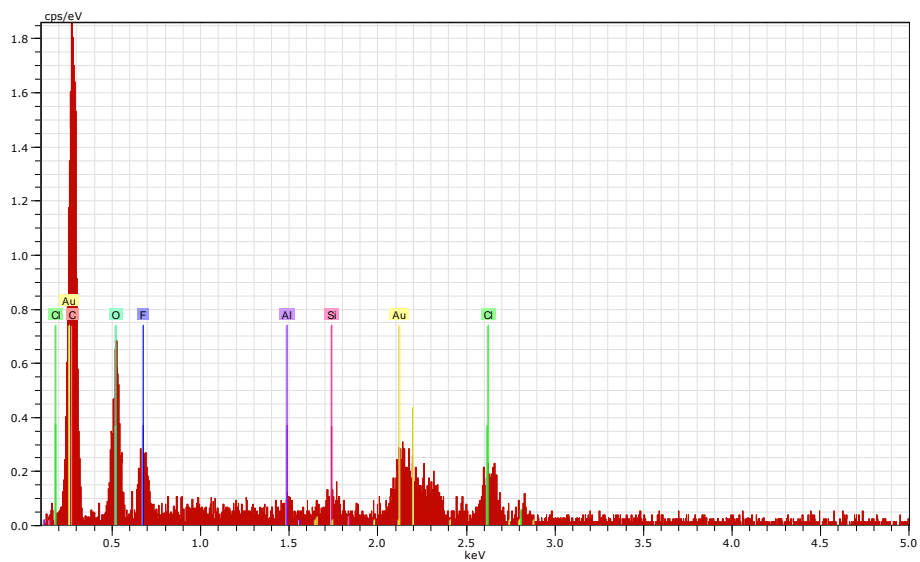
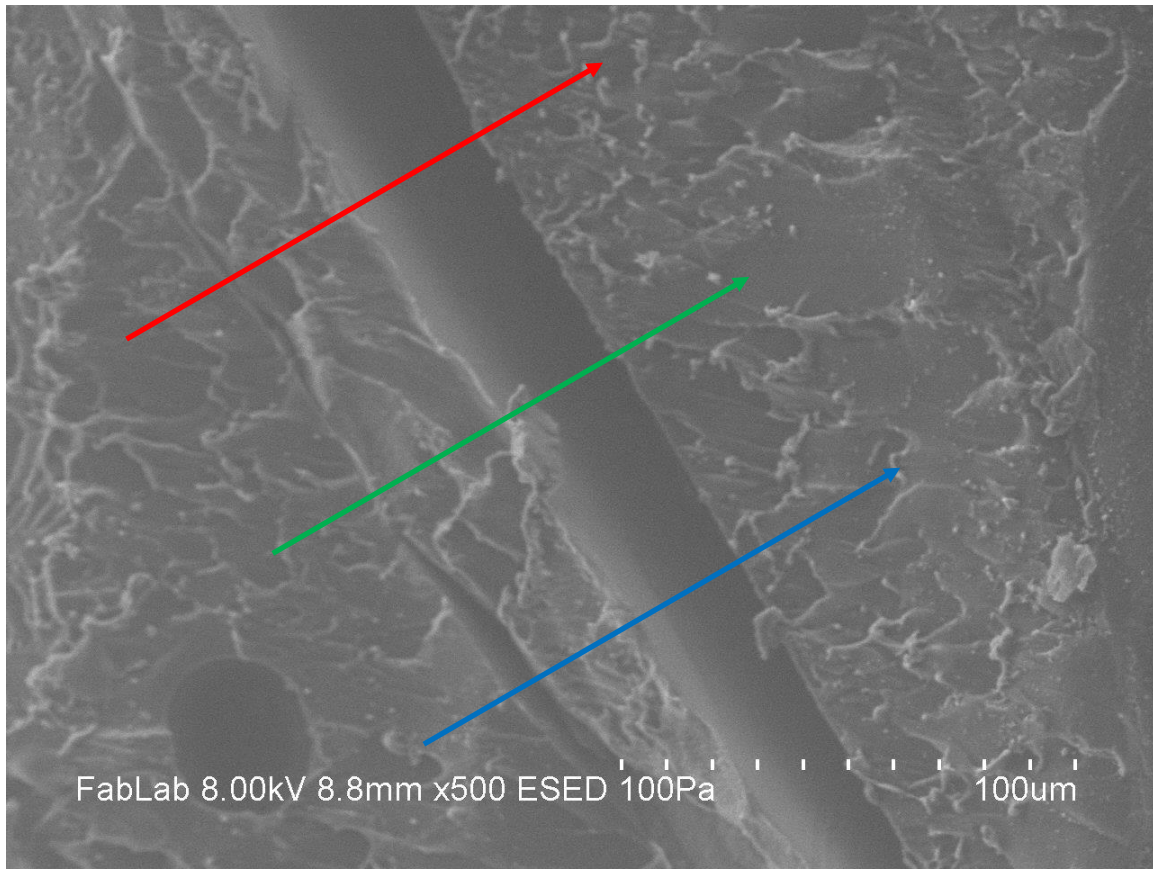


Figure 4.28- EDS of Sample 8112016PCTFE-16

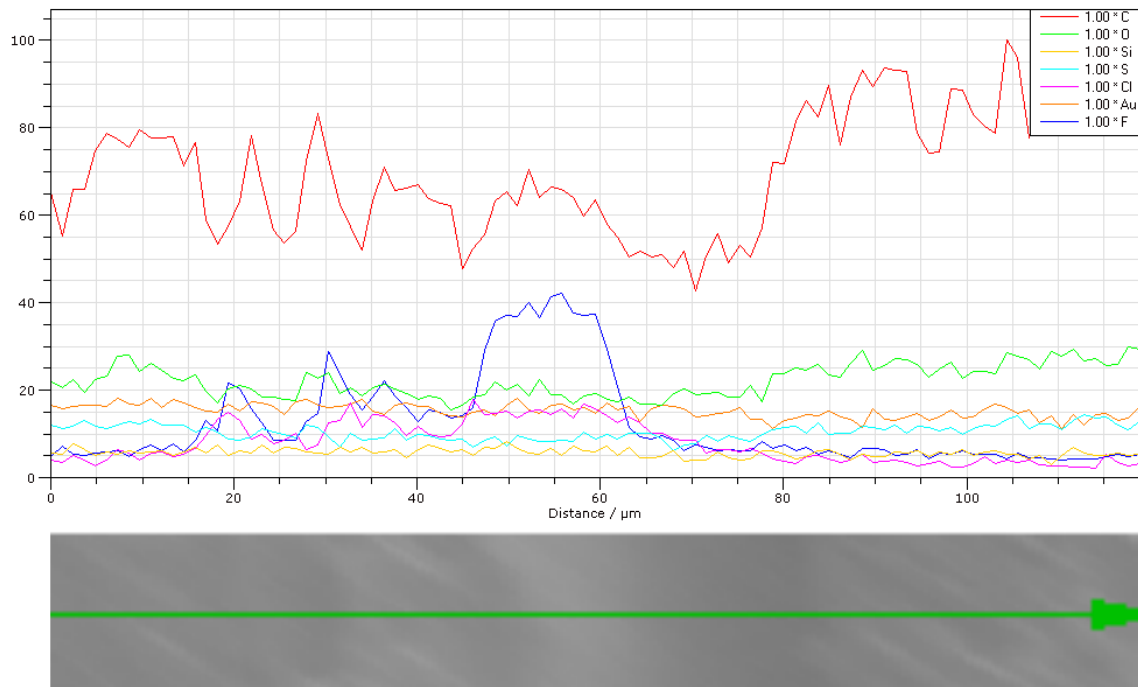
Table 4.7: EDS analysis of atomic composition of Sample 8112016PCTFE-16

Element	Norm C %wt	Atom C %at	Sigma STD
C	48.93	72.51	1.54
N	1.62	2.03	0.14
O	12.14	13.51	0.40
F	3.49	3.28	0.30
Cl	8.00	5.33	2.27
Au/Si/Al/S	25.82	3.34	2.04

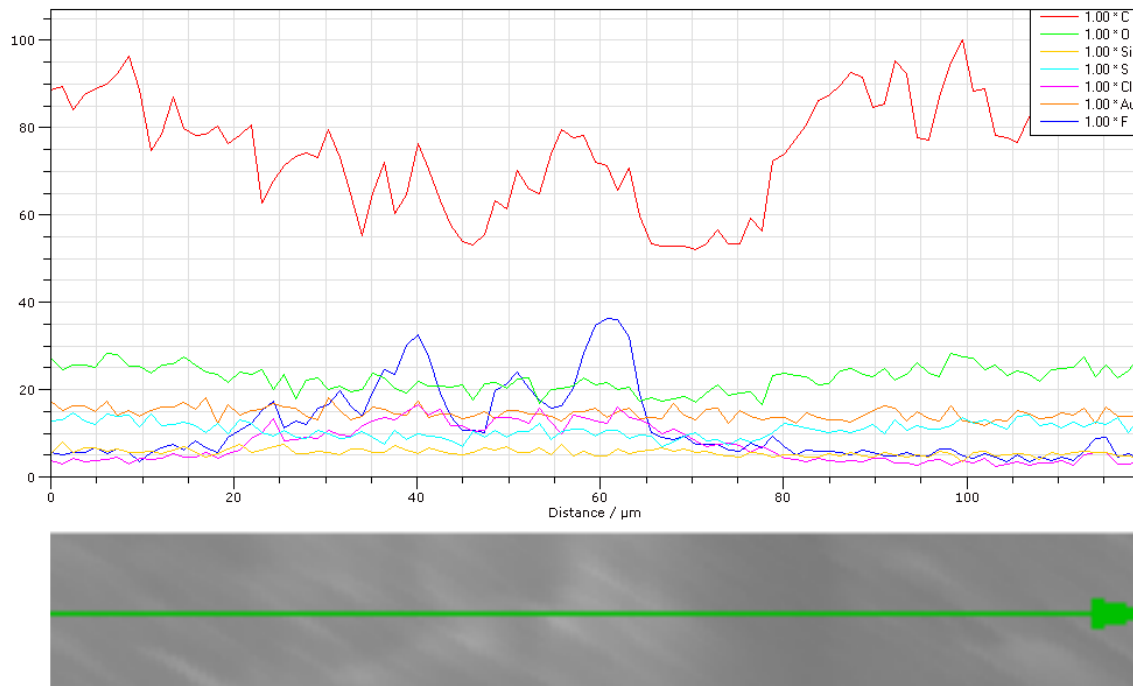
The grafting profile through the membrane, EDS line scans were tested across the membrane's cross-section. The results of these line scans for Sample 8112016PCTFE-16 are shown in Figure 4.29. Three SEM/ EDS line scans of the sample cross-section test area are shown by red, blue or green colored arrows. The test area results show relative atomic composition across the cross-section in Figure 4.29 (b), (c) and (d). These scans show that there is significant change in the concentration of grafted ionic liquid from the surface to the center of the membrane. However, the results of the EDS line scans show there was significant grafting through the center of the membrane. The sharp changes in composition (fluorine-blue line) coincide with a significant difference in electron density in the sample which indicates that the membrane is not uniformly grafted. These observations of sharp changes in composition does not support a homogenous proton conductive membrane for PEMFC applications.



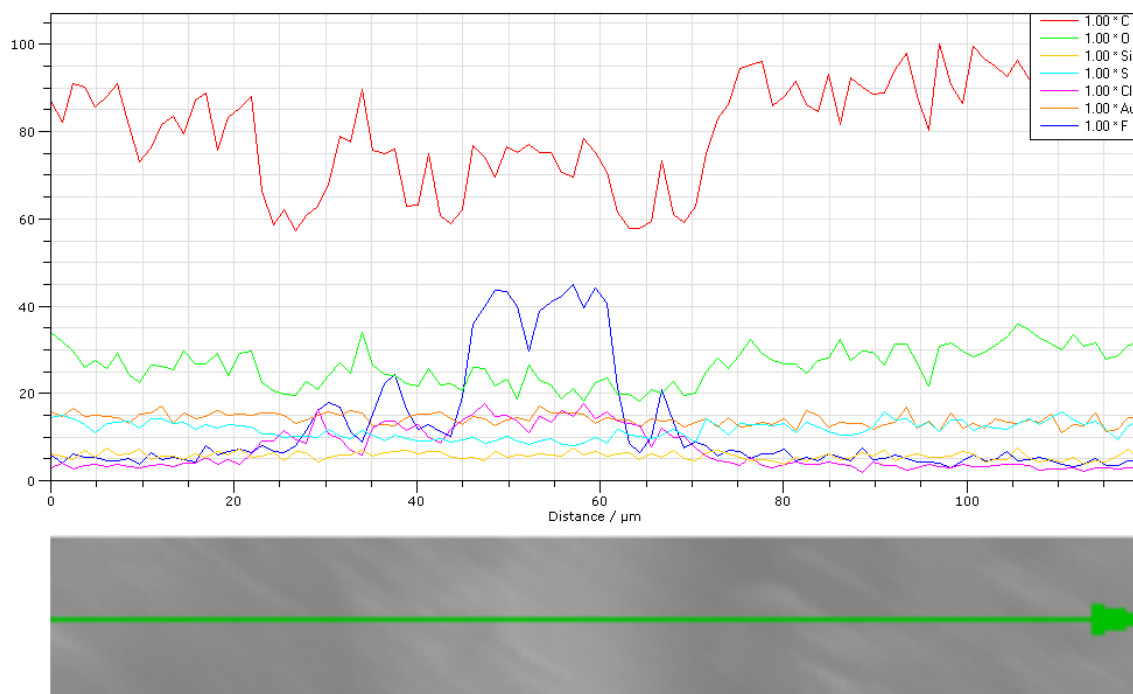
(a)



(b)



(c)



(d)

Figure 4.29- (a) Three SEM/EDS line scans across the cross-section of sample 8112016PCTFE-16 and corresponding test area results for (b) red (c) green (d) blue.

SEM image in Figure 4.30 is the cross-section of Sample 3222017PCTFE-3c. This sample was synthesized using indirect radiation grafting of 5-vinylpyrimidine onto PCTFE substrate with a 100kGy and 1000kGy/hr. treatment. The sample had 15.77% grafting. The EDS spectrum of the cross-section is shown in Figure 4.31 and the analysis of this spectrum is shown in Table 4.8, with C-72.10%, N-2.99%, O-13.44%, F-7.72% and Cl-2.17% atomic composition. The carbon to fluorine ratio is 9.34 and is higher than the untreated PCTFE substrate at 0.935. This shows grafting occurred through the center of the membrane.

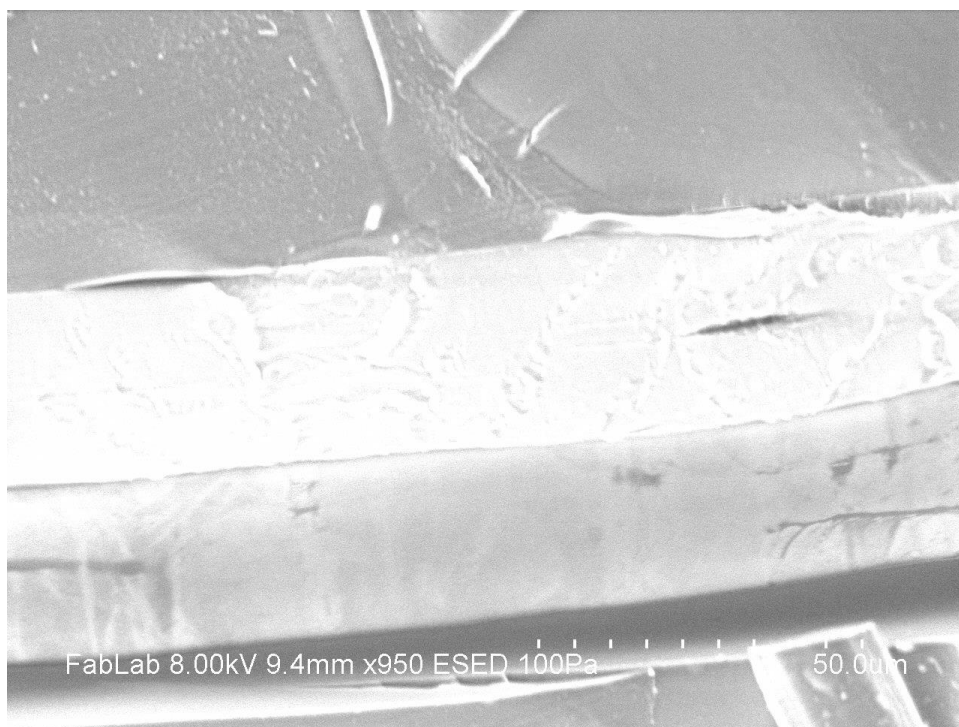


Figure 4.30-SEM Cross-section of Sample 3222017PCTFE-3c

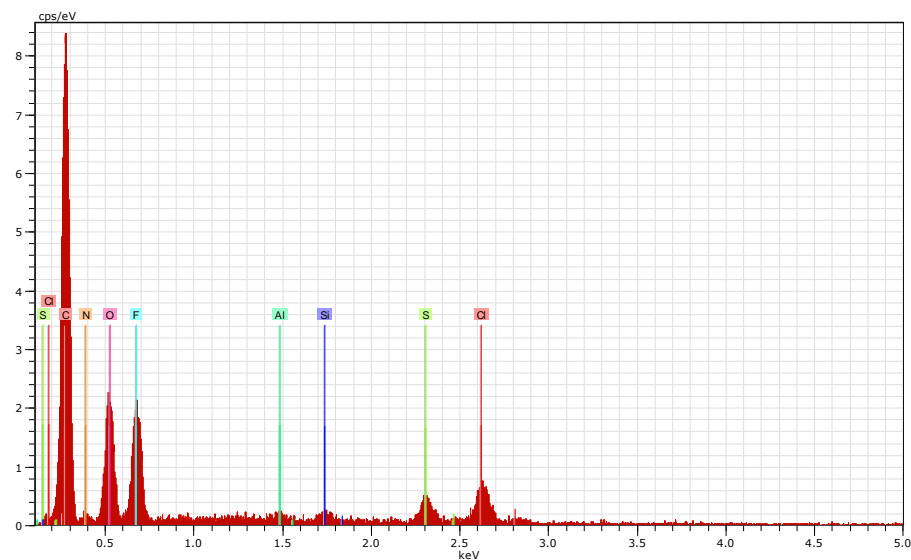


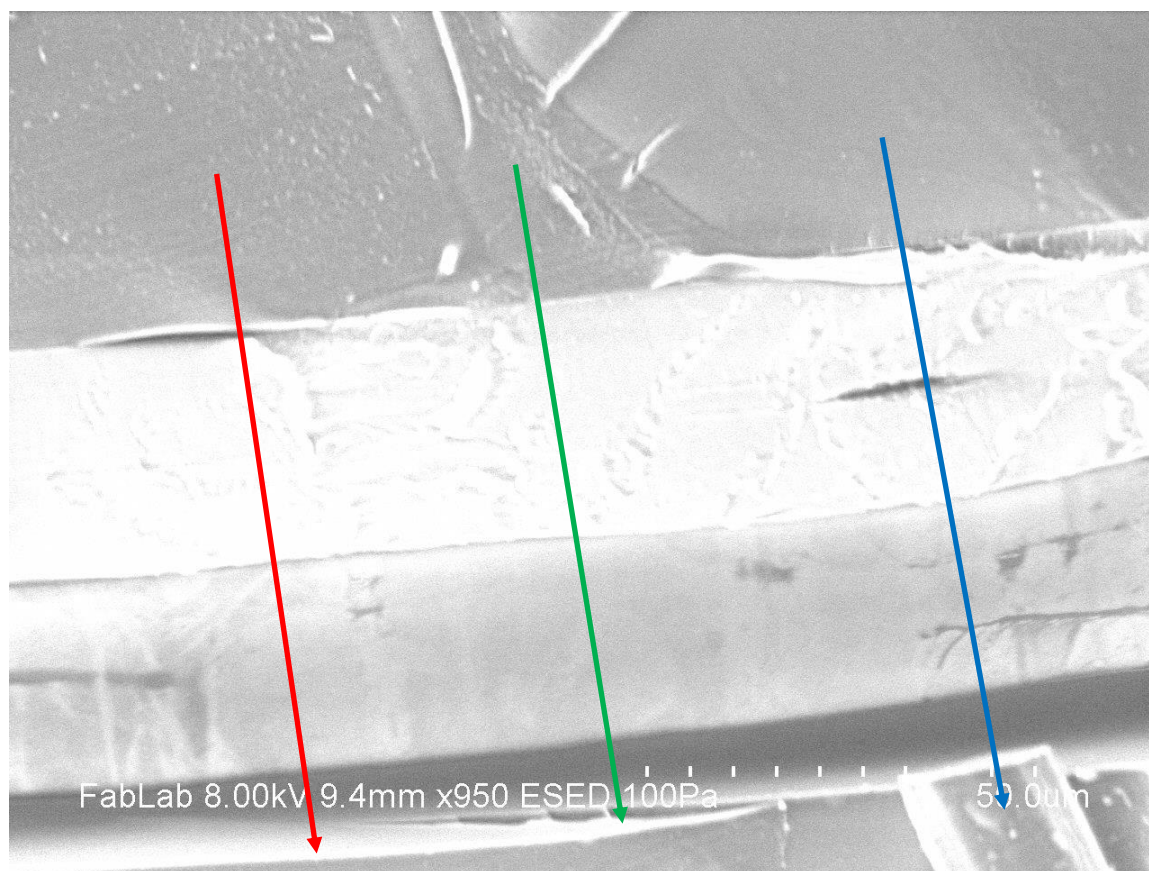
Figure 4.31-EDS of Sample 3222017PCTFE-3c

Table 4.8: EDS analysis of Sample 3222017PCTFE-3c atomic composition

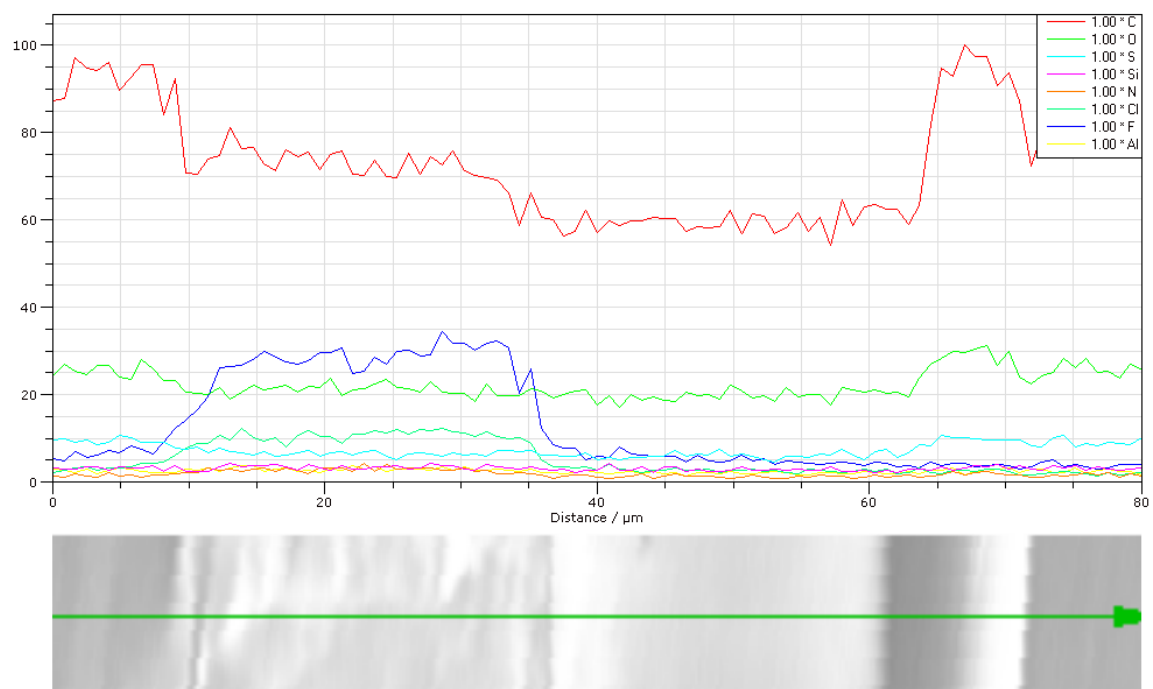
Element	Norm C %wt	Atom C %at	Sigma STD
C	62.08	72.10	0.62
N	3.00	2.99	0.41
O	14.76	13.44	0.15
F	9.53	7.72	0.40
Al	0.21	0.13	0.03
Si	0.68	0.40	0.04
S	1.97	1.06	0.04
Cl	5.52	2.17	0.09

To understand the grafting profile through the membrane, EDS line scans were tested across the membrane's cross-section. The results of these line scans for Sample 3222017PCTFE-3c are shown in Figure 4.32. Three SEM/ EDS line scans of the sample cross-section test area are shown by red, blue or green colored arrows. The test area results show

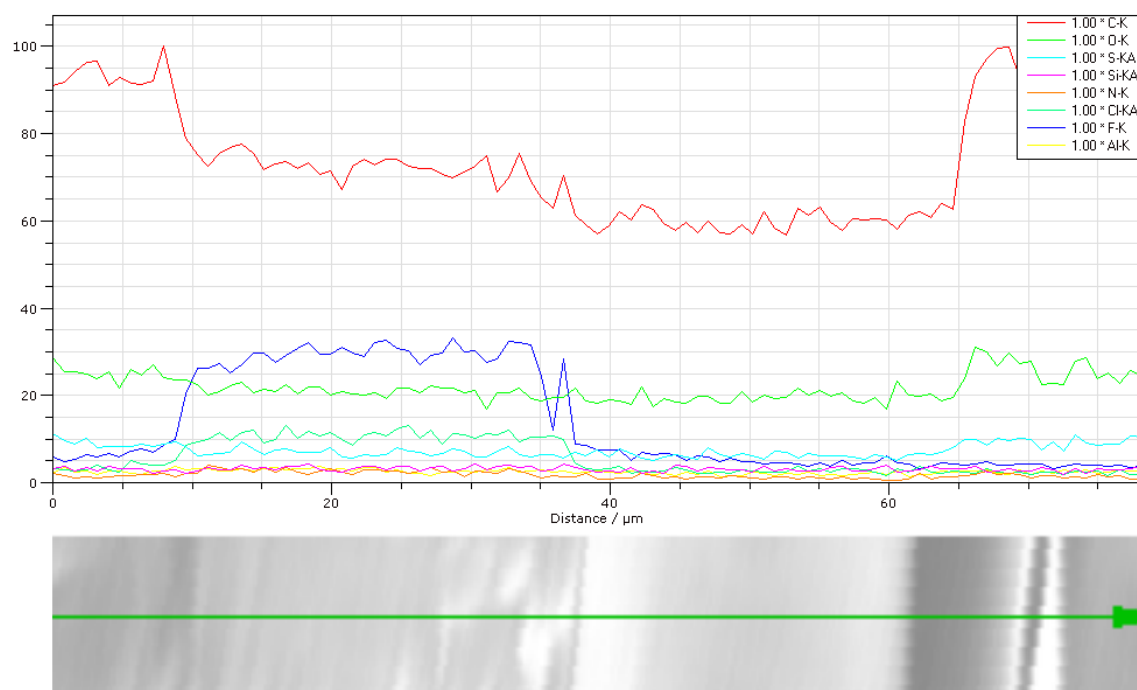
relative atomic composition across the cross-section in Figure 4.32 (b), (c) and (d). The scans indicate the membrane has a uniform concentration of grafted ionic liquid from the surface to the center of the membrane. There are no sharp changes in atomic composition in the membrane compared to the edges of the membrane (fluorine-blue line). These observations support a homogeneous proton conductive membrane for PEMFC applications. In comparing these two PCTFE PEMs, the higher dose rate produced more uniform membranes.



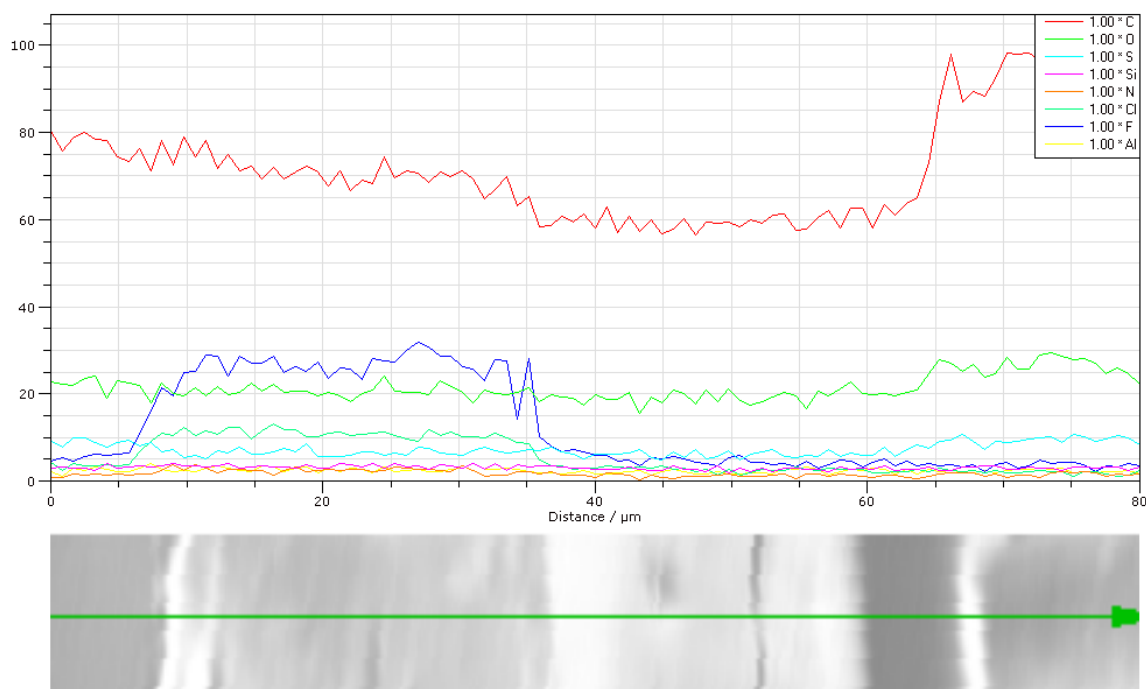
(a)



(b)



(c)



(d)

Figure 4.32- (a) Three SEM/EDS line scans of Sample 3222017PCTFE-3c cross-section and corresponding test area results for (b) red (c) green (d) blue.

4.3.1.3 PVF SEM/EDS Analysis

To quantify the change in carbon to fluorine ratio, a base line scan of the untreated PVF film was used as a reference. The PVF substrate was manufactured by DuPont under the trade name Tedlar. The SEM image of the FEP substrate is shown below in Figure 4.33. The EDS spectrum is shown in Figure 4.34 and the atomic composition analysis presented in Table 4.9, with atomic composition; C-78.73%, N-0.06%, O-0.67% and F-20.54%. The initial carbon to fluorine ratio of untreated PVF substrate is 3.83. This value is higher than 2.00 which is expected based on the chemical structure of pure PVF. The ratio difference can be caused by chemical additives, cross-linking and oxidation present within the film. The carbon to fluoride

ratio will be used to determine the relative amount of grafting in the ionic liquid grafted PVF PEMs.

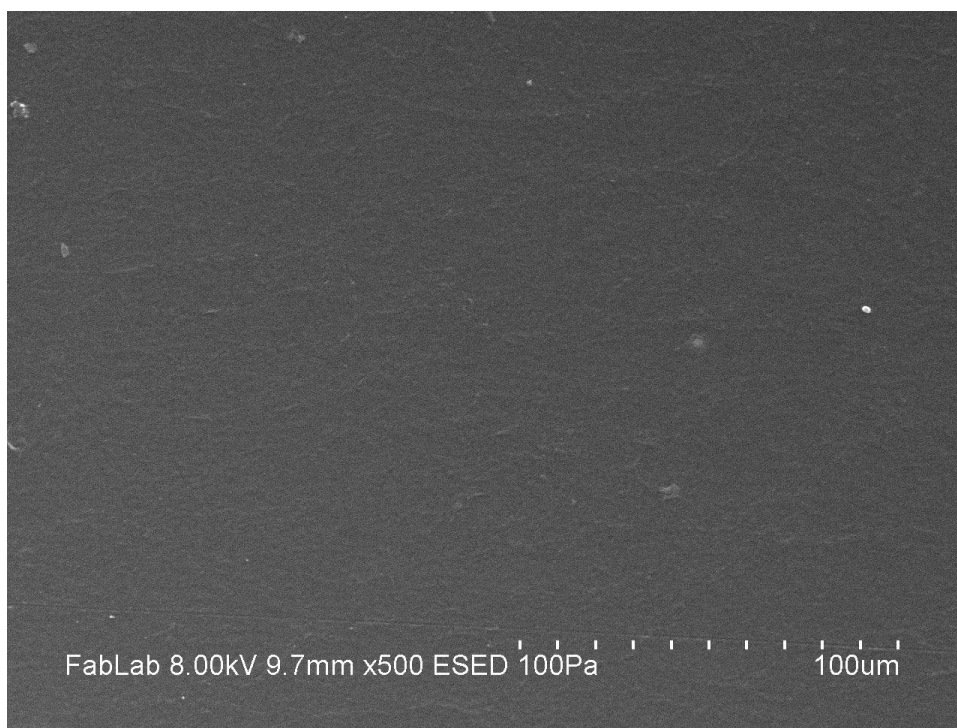


Figure 4.33- SEM image of PVF substrate

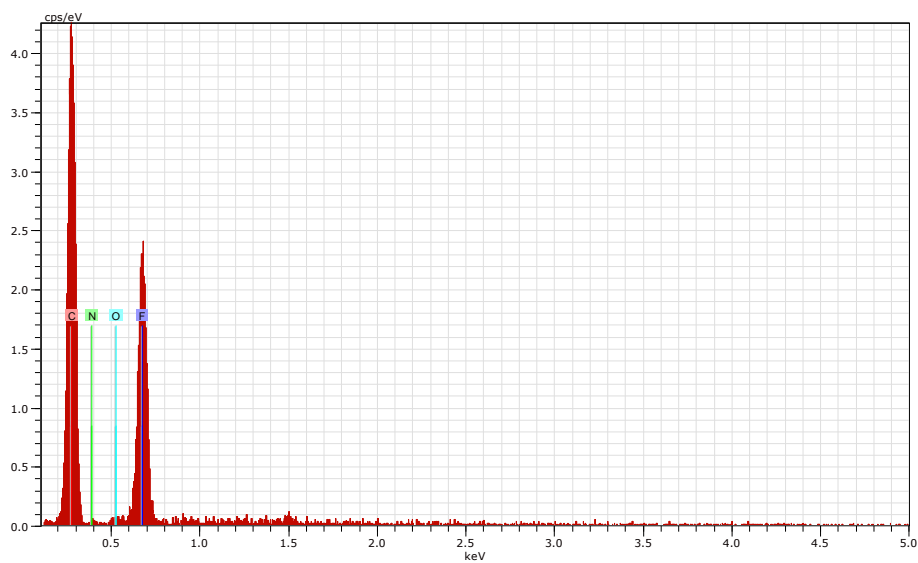


Figure 4.34-EDS PVF substrate

Table 4.9: EDS analysis of untreated PVF atomic composition

Element	Norm C %wt	Atom C %at	Sigma STD
C	70.19	78.73	0.30
N	0.06	0.06	0.14
O	0.79	0.67	0.16
F	28.95	20.54	0.30

The SEM image in Figure 4.35 is the cross-section of Sample 20180910PVF-10b. The sample was prepared using indirect radiation grafting of 4-vinylpyridine onto PVF substrate with a 25kGy and 100kGy/hr. treatment. The sample had 318% grafting. The EDS spectrum of the cross-section is shown in Figure 4.36 and the analysis of this spectrum is presented in Table 4.10, with C-81.26%, N-5.14%, O-10.83%, and F-1.78% atomic composition. The carbon to fluorine ratio is 45.7 which is substantially higher than the untreated PVF substrate (3.83) and shows grafting occurred through the center of the membrane.



Figure 4.35- SEM of Sample 20180910PVF-10b cross-section

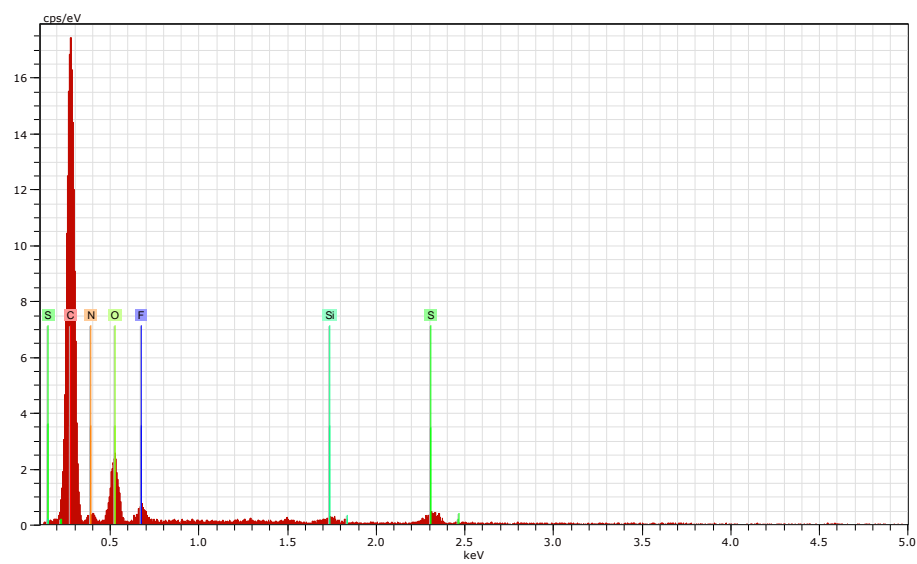
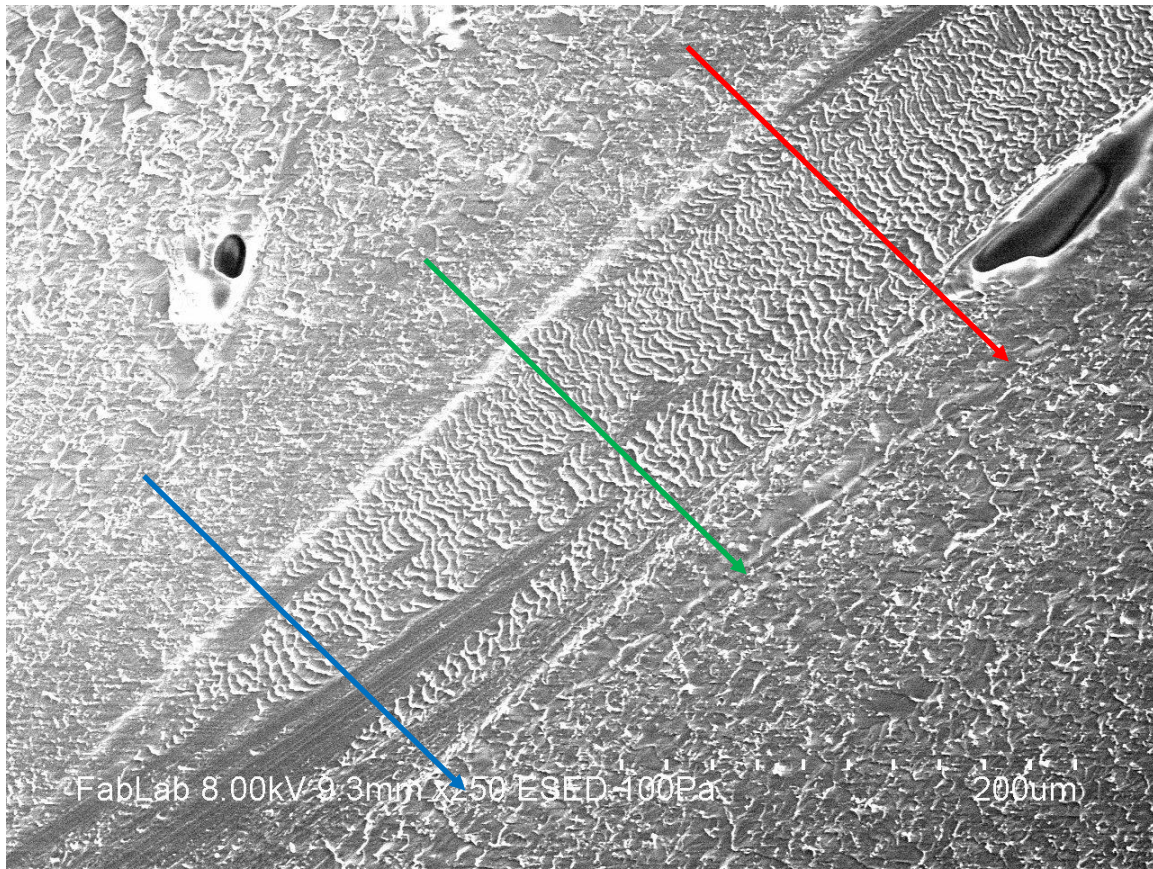


Figure 4.36-EDS of Sample 20180910PVF-10b cross-section

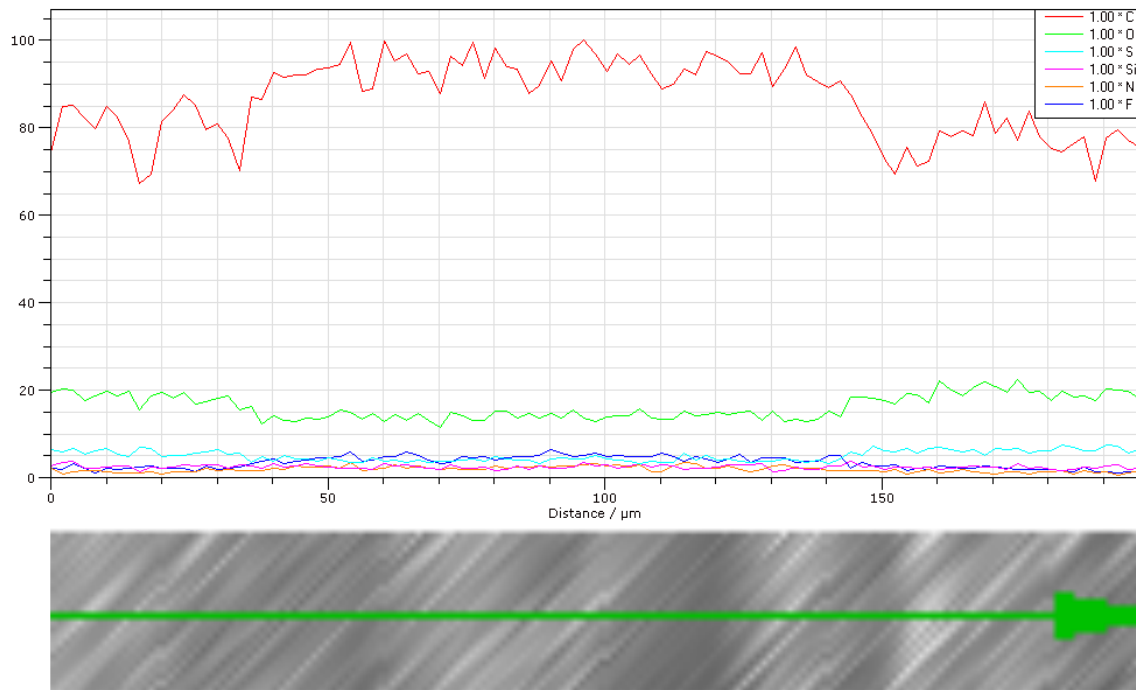
Table 4.10: EDS analysis of Sample 20180910PVF-10b atomic composition

Element	Norm C %wt	Atom C %at	Sigma STD
C	75.90	81.26	0.11
N	5.60	5.14	0.14
O	13.47	10.83	0.08
F	2.63	1.78	0.18
Si	0.70	0.32	0.04
S	1.71	0.69	0.05

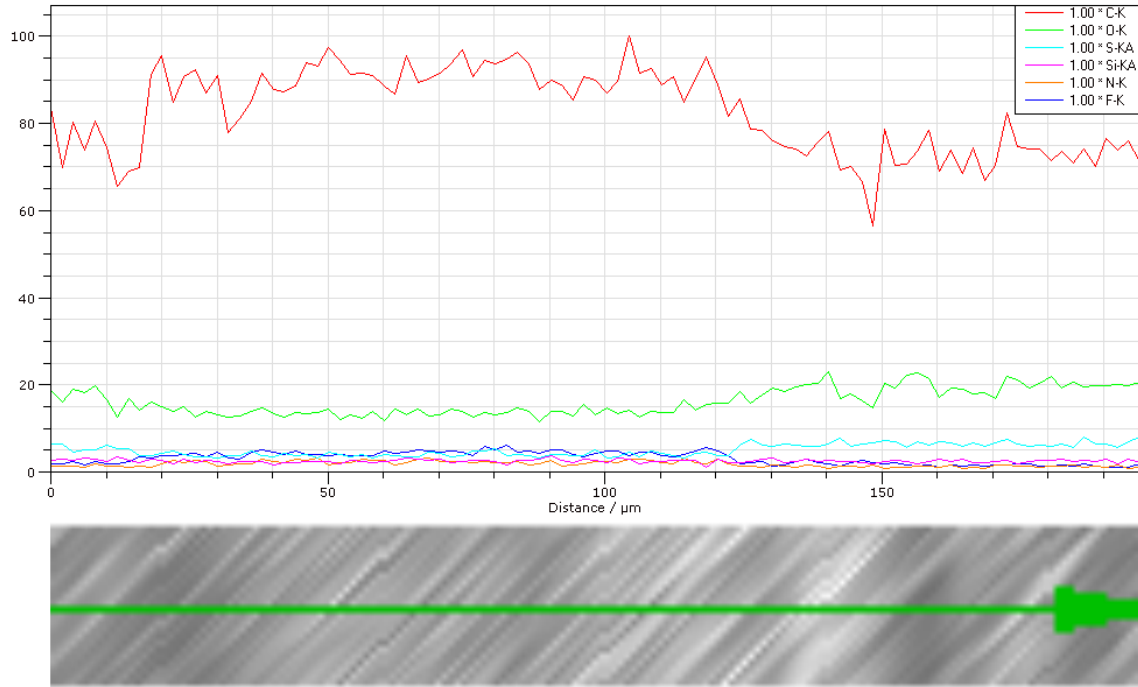
To understand the grafting uniformity of PEM Sample 20180910PVF-10b, EDS line scans were measured along the cross-section. These line scans are depicted in Figure 4.37. Three SEM/ EDS line scans of the sample cross-section test area are shown by red, blue or green colored arrows. The test area results show relative atomic composition across the cross-section in Figure 4.37 (b), (c) and (d). The line scans show that the atomic composition in the membranes is uniform. However, at the surface there is a very gradual gradient of increasing monomer concentration. This result is expected for a sample that has 318% grafting and is 120 μm thick. The membrane thickness prior to grafting was 25 μm . The surface of the sample is composed of polymerized ionic liquid from excessive polymerization reactions. The center of the membrane is uniform with a high amount of grafting. The membrane would support a proton conductive systems but it is not homogeneous (fluorine-blue). There will be significant differences in proton conductivity measurements between the surface and through the membrane.



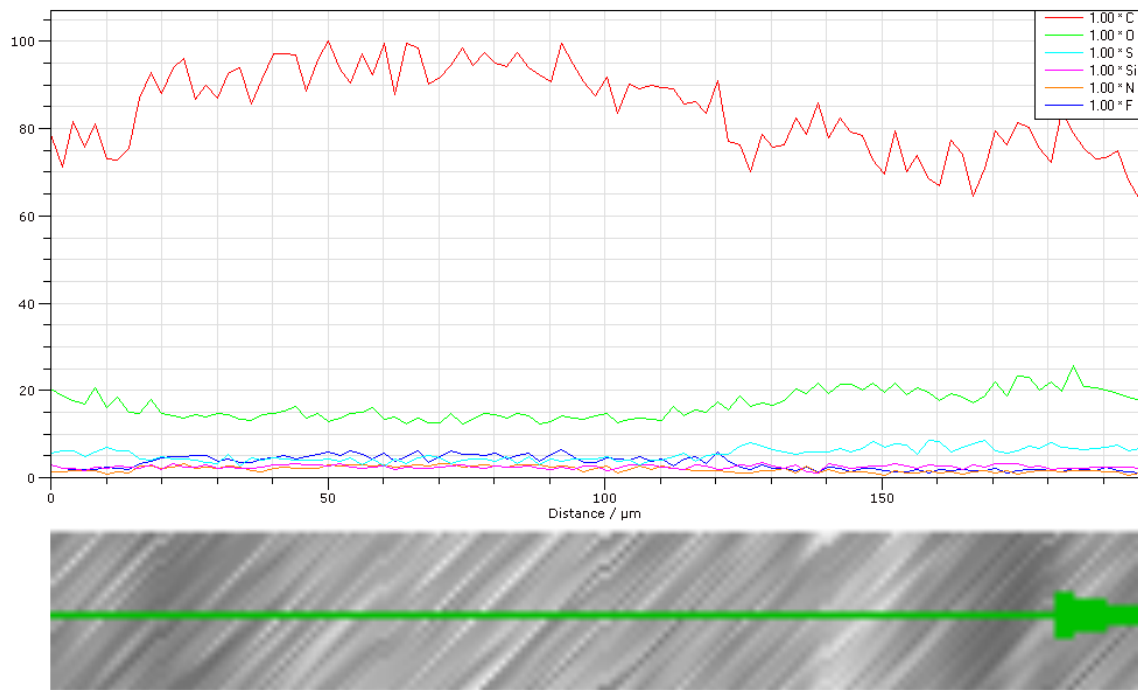
(a)



(b)



(c)



(d)

Figure 4.37-(a) Three SEM/EDS line scans of Sample 20180910PVF-10b cross-section and corresponding test area results for (b) red (c) green (d) blue.

The SEM image in Figure 4.38 is the cross-section of Sample 3222017PVF-1a. This sample was prepared using indirect radiation grafting of 5-vinylpyrimidine onto PVF substrate with a 25kGy and 1000kGy/hr. treatment. The sample had 50.56% grafting. The EDS spectrum of the cross-section is shown in Figure 4.39 and the analysis of the spectrum is shown in Table 4.11, with C-80.43%, N-5.28%, O-9.45%, and F-2.72% atomic composition. The carbon to fluorine ratio is 29.6 which is higher than the untreated PVF substrate with a carbon to fluorine ratio of 3.83. This shows grafting occurred through the center of the membrane.

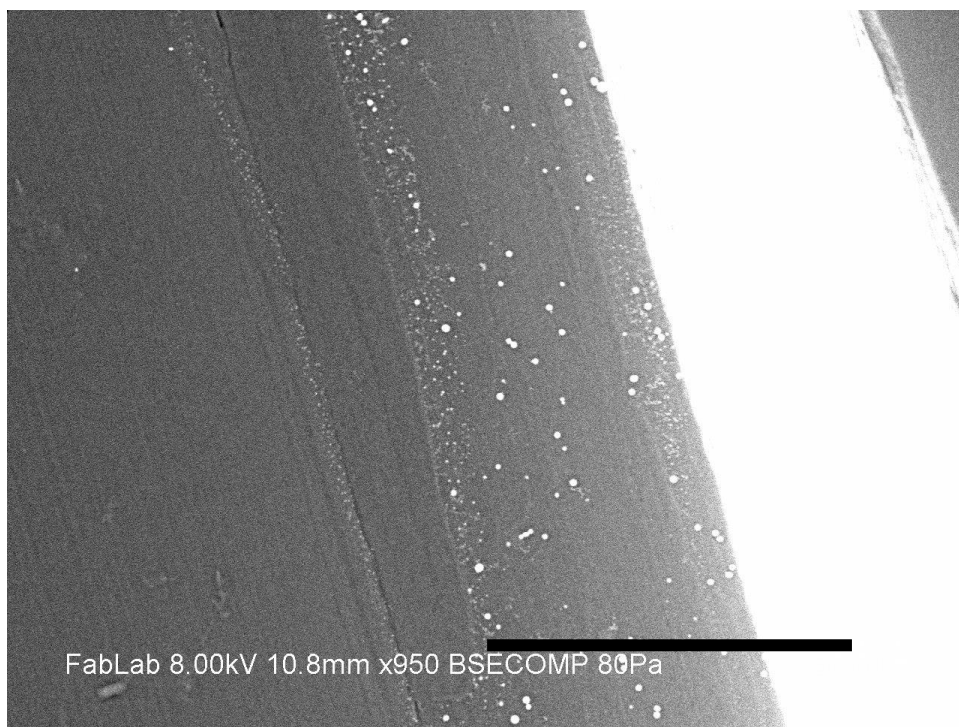


Figure 4.38-SEM cross-section of 3222017PVF-1a (black bar is 50um)

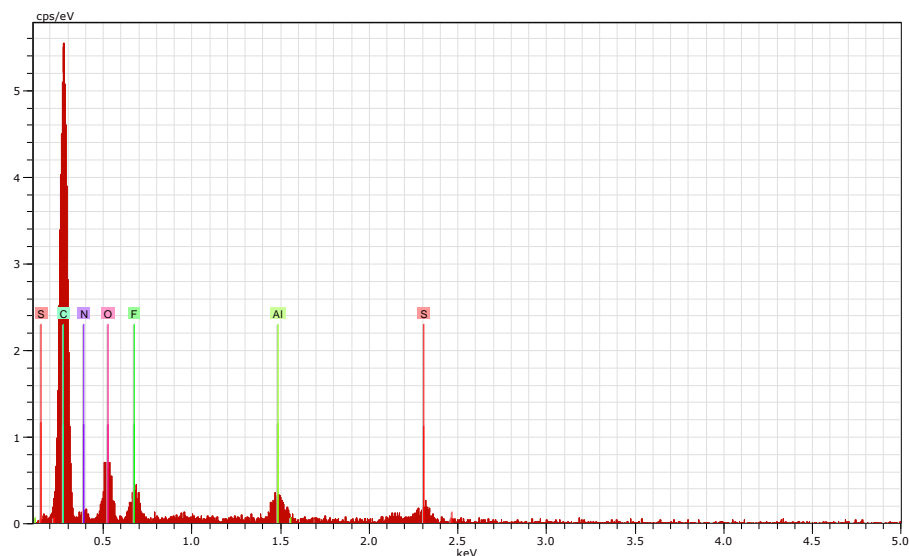


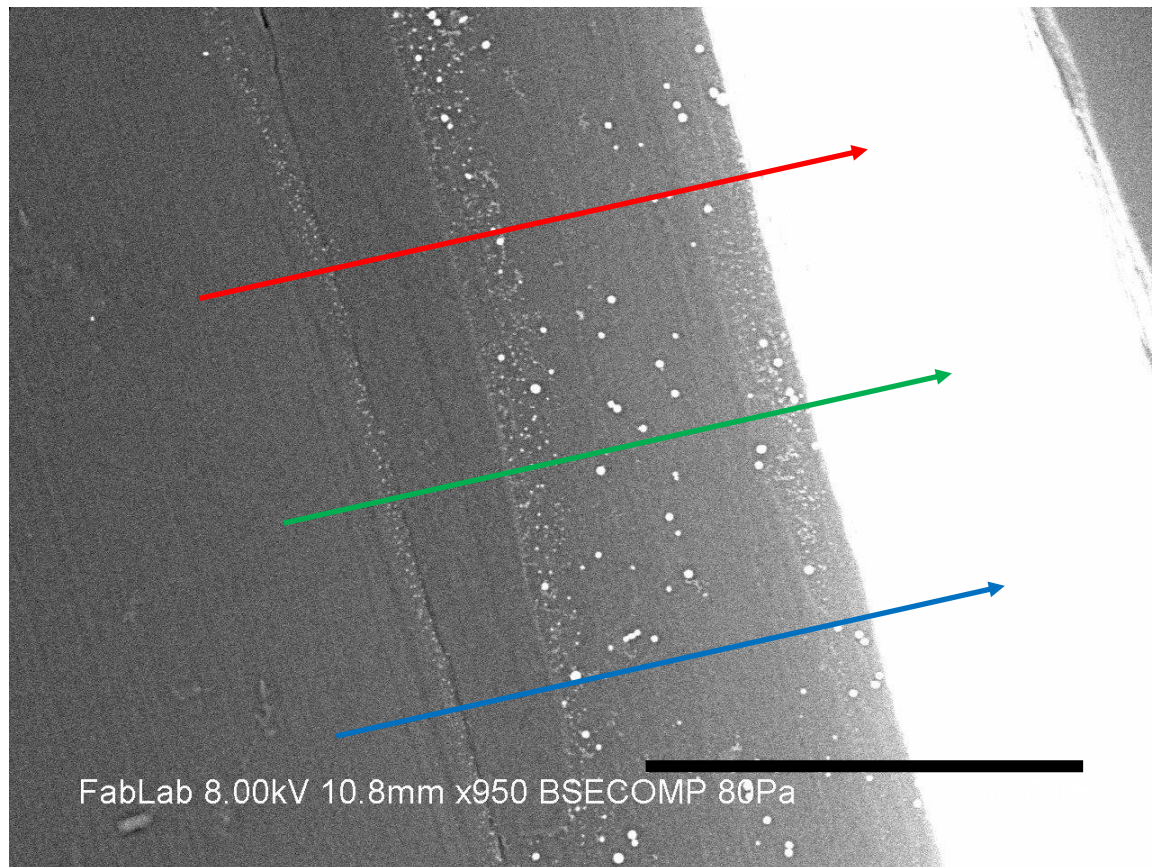
Figure 4.39-EDS of sample 3222017PVF-1a

Table 4.11: EDS analysis of sample 3222017PVF-1a atomic composition

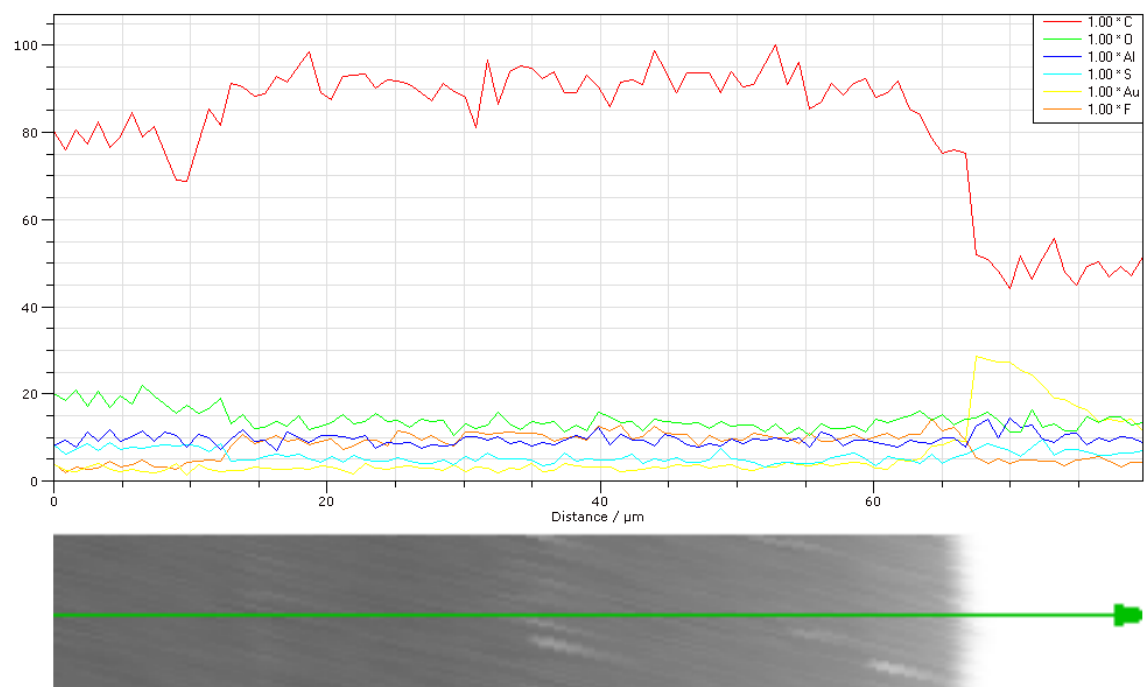
Element	Norm C %wt	Atom C %at	Sigma STD
C	74.06	80.43	0.62
N	5.67	5.28	0.24
O	11.59	9.45	0.58
F	3.96	2.72	0.20
Al	2.64	1.28	0.21
S	2.09	0.85	0.13

Figure 4.40 shows the results of SEM/EDS line scans conducted on sample 3222017PVF-1a to determine grafting distribution through the PEM. Three SEM/ EDS line scans of the sample cross-section test area are shown by red, blue or green colored arrows. The test area results show relative atomic composition across the cross-section in Figure 4.40 (b), (c) and (d). The membrane was observed to be uniform with a constant carbon to fluorine ratio

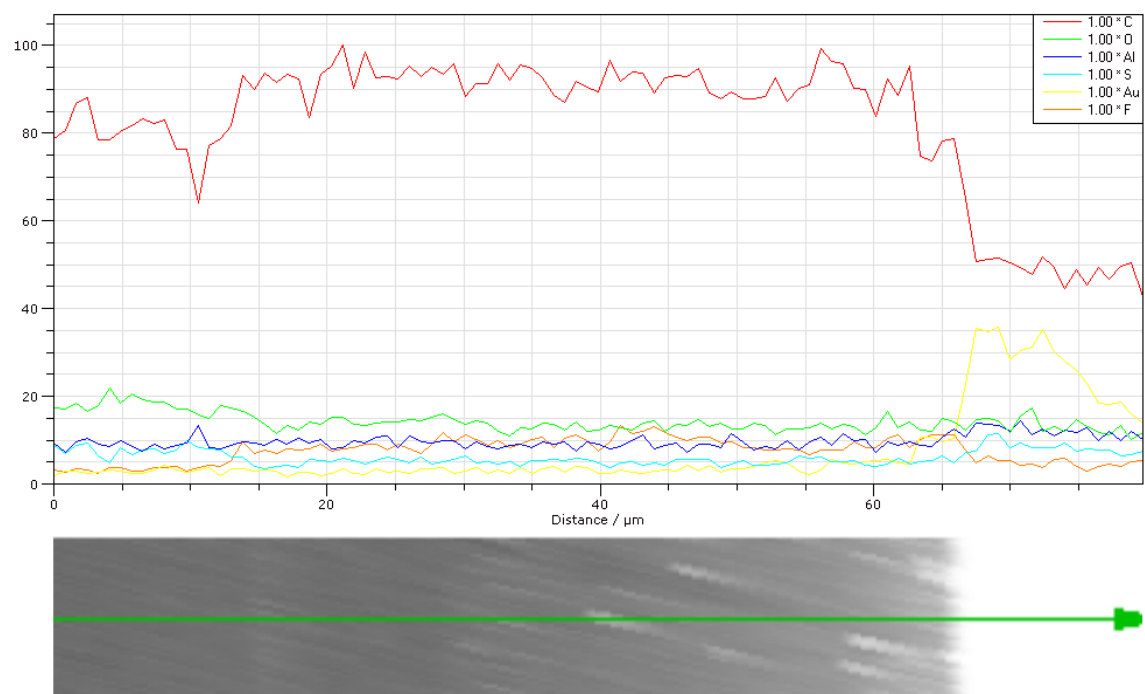
(fluorine-pink line). This observation supports that the membrane has a homogeneous composition and is capable of conducting protons through the membrane.



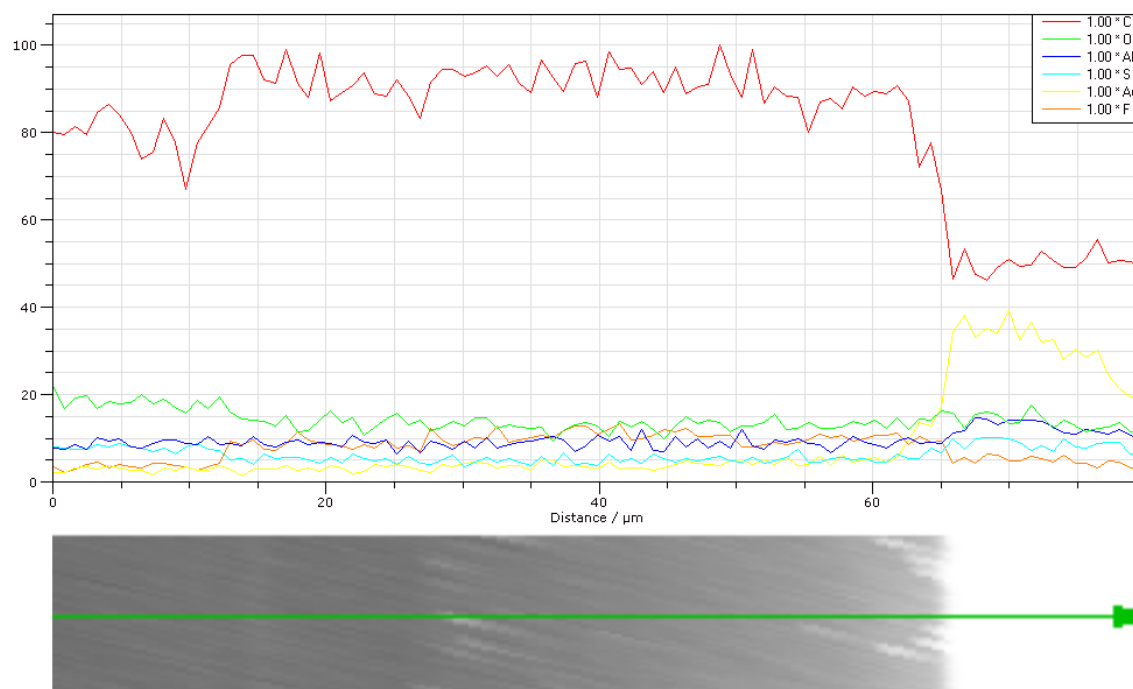
(a)



(b)



(c)



(d)

Figure 4.40- (a) Three SEM/EDS line scans of sample 3222017PVF-1a cross-section and corresponding test area results for (b) red (c) green (d) blue.

SEM/EDS was a suitable method to evaluate the extent of grafting in PEM. Despite poor contrast between carbon and nitrogen in EDS, the extent of grafting was determined by comparing the carbon/fluorine ratio. The observed changes in this ratio are due to both defluorination of FEP, PCTFE, and PVF during radiation treatment and subsequent ionic liquid grafting of 4-vinylpyridine and 5-vinylpyrimidine. EDS data provides atomic compositions and not chemical or structural information for the grafted membranes. It was further observed that the higher the dose rate, the more uniform the grafted sample for the data presented. In order to identify the chemical structure of the anhydrous protic ionic liquid PEM, FTIR measurements were conducted as per Section 4.3.3.

4.3.2 Ramman Spectroscopy

In order to determine the structure of the grafted PEM, Ramman spectroscopy was utilized to characterize phonon modes of the grafted monomer. However, it is documented that heterocyclic amine ionic liquids being researched are photofluorescent.[128] This photofluorescence confounds the Raman data by decreasing resolution and masking the signal from the sample. As such, Ramman spectroscopy could not be pursued for this project to understand the grafting structure and morphology of the grafted ionic liquids.

4.3.3 FTIR/ATR Measurements

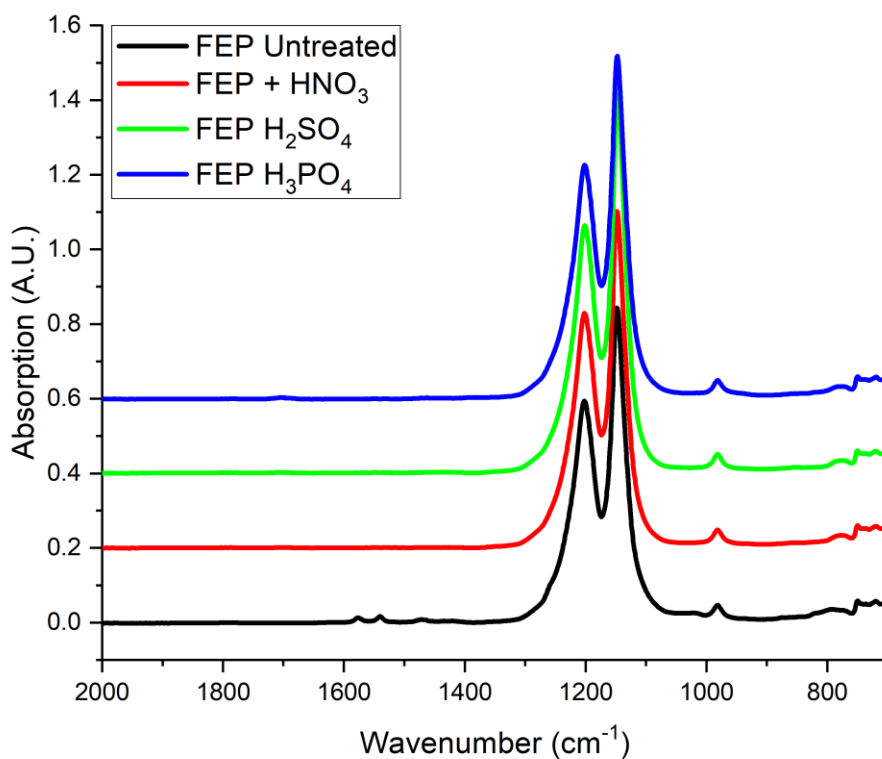
Fourier transform infrared microscopy (FTIR) measurements were performed to identify chemical changes within the synthesized PEM by comparing the FTIR- ATR spectrum before and after radiation grafting treatments. It was also used to understand the acid treatment used to dope the PEM with hydrogen for proton conductivity measurements. FTIR utilizes the energy absorption of bond resonance vibration modes in the infrared region to identify the chemical composition of samples. This technique was used to confirm that ionic liquid grafted to the membrane.

The FTIR/ATR absorption spectrum can identify important peaks for fluorocarbon polymers and the grafted ionic liquids. The following peaks of the FTIR spectrum are important to characterize the PEM grafting being studied[129]:

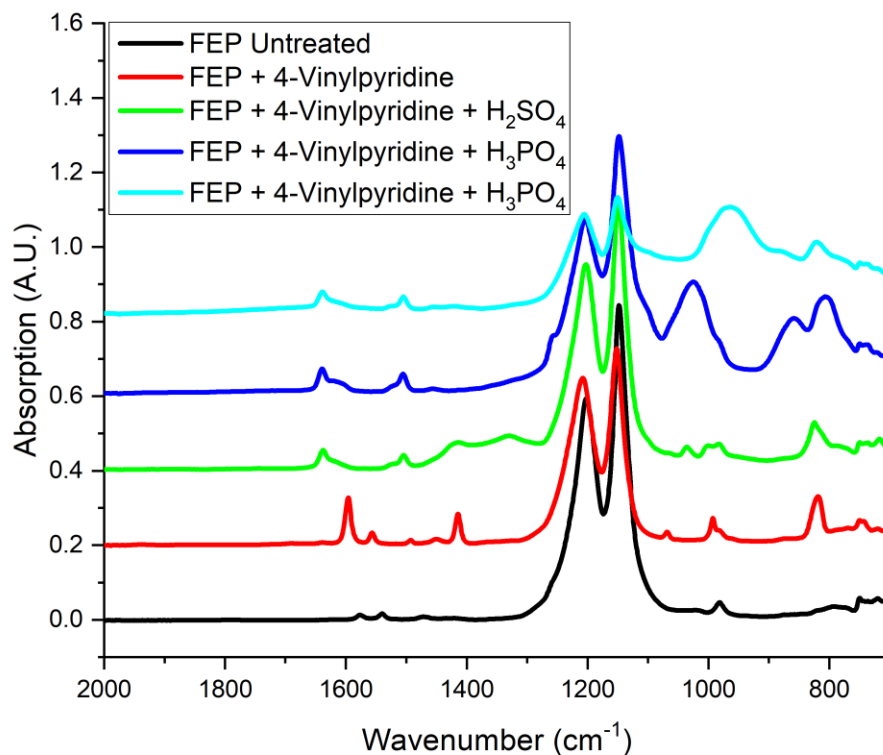
- Broad peak at 2365 cm^{-1} indicates CF_2 backbone for fluorocarbon polymers
- Strong peak between 1000 to 1400 cm^{-1} represents the C-F stretching vibration of the fluorocarbon

- Band at 1882 cm^{-1} is assigned to carbonyl stretching vibration and indicates unwanted oxidation
- Two medium peaks at 1414 cm^{-1} and 1595 cm^{-1} which indicate C-C/C-N bond for 4-vinylpyridine indicating grafting occurred[130]

After radiation grafting, the FTIR spectrum shows two medium peaks for 4-vinylpyridine at 1414 cm^{-1} and 1595 cm^{-1} respectively for C-C/C-N bonds, which indicates grafting of the protic ionic liquid as shown below in Figure 4.41.[130] There are also no major peaks at 1882 which indicates the free radicals did not oxidize.



(a)



(b)

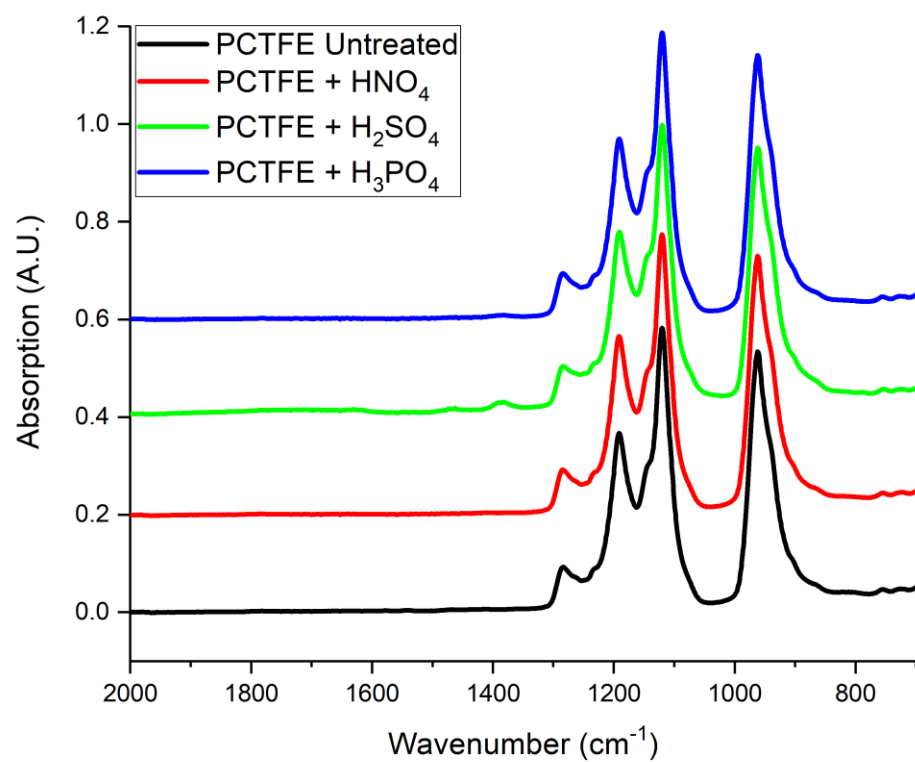
Figure 4.41: FTIR analysis of (a) FEP substrates acid treated (b) Sample 8122016FEP-9 PEM synthesized with 4-vinylpyridine and acid treatments for proton conductivity measurements.

The FTIR ATR measurements were conducted to understand how the acid treatments would affect the membranes which was part of the preparations for the EIS measurements. These measurements were conducted for FEP, PVF and PCTFE substrates. Figure 4.41 shows impact of acid treatments of nitric acid, sulfuric acid and phosphoric acid to the PEM which are required to add protons prior to conductivity measurements. Figure 4.41a shows the acid treatment with 5% concentration nitric acid (red), sulfuric acid (green) and phosphoric acid (blue) of FEP substrate. There was no significant chemical change in the FTIR spectrum due to

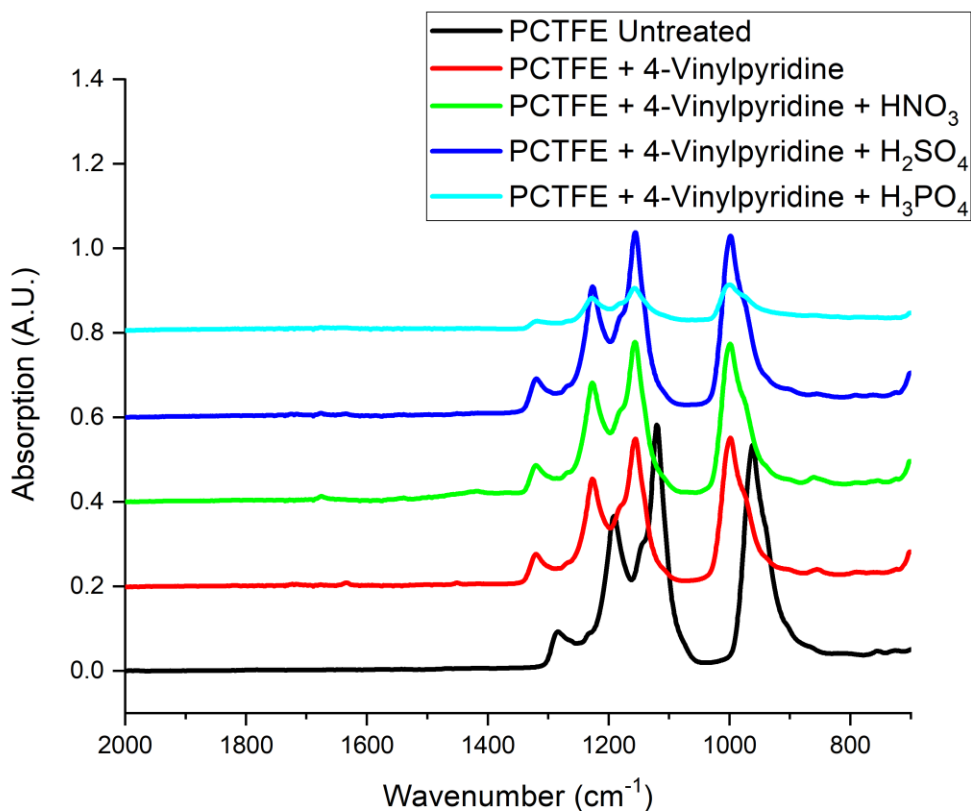
the acid treatment of the FEP substrate. This observation can be attributed to the high chemical resistance of FEP and shows that the acid treatments will only cause protonation of the ionic liquid groups. Figure 4.41b shows the FTIR Spectrum of FEP substrate (black), grafted 4-vinylpyridine on FEP PEM (red), 5% nitric acid treated FEP PEM (green), 5% sulfuric acid treated FEP PEM (blue) and 5% phosphoric acid treated FEP PEM (aqua). These acid treatments in Figure 4.41b caused the 4-vinylpyridine peaks to shift to the left which indicates the protonation of the pyridine group.[130] Additional peaks also appear on the FTIR analysis after acid treatments as follows:

- Nitric acid N-O 1330cm^{-1} and 1525cm^{-1}
- Sulfuric Acid O=S 880cm^{-1} and O=S=O 1258cm^{-1}
- Phosphoric Acid P-O 962cm^{-1}

These bond groups are present due to the conjugate acid remaining in the membrane after protonation of the ionic liquid. These results show that the acid treatment used to dope the membranes with protons for EIS measurements will only protonate the FEP ionic liquid PEM membranes and will not chemically react with untreated membranes.



(a)

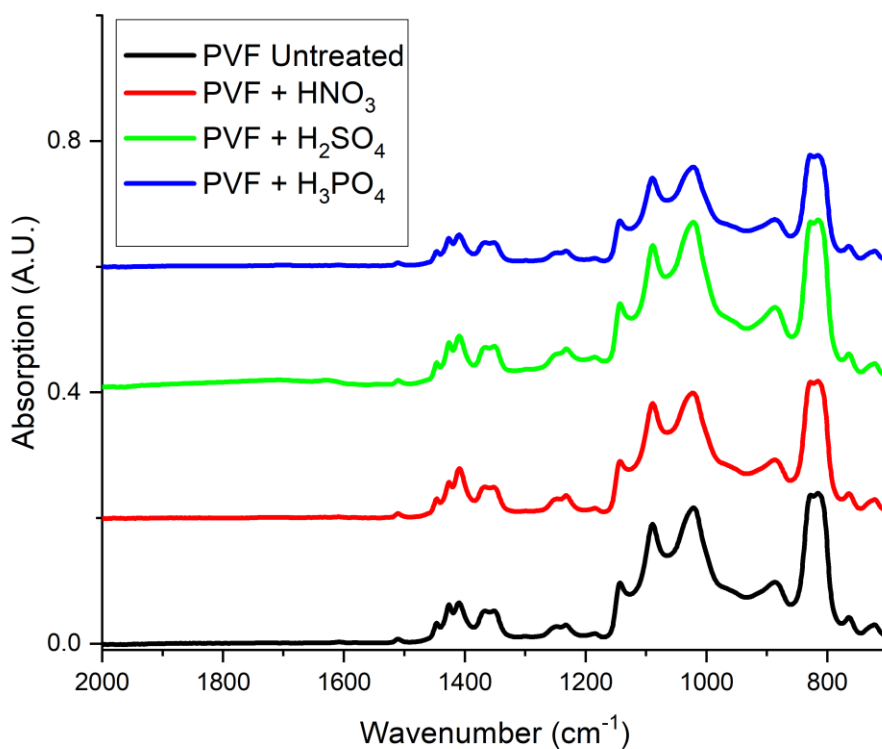


(b)

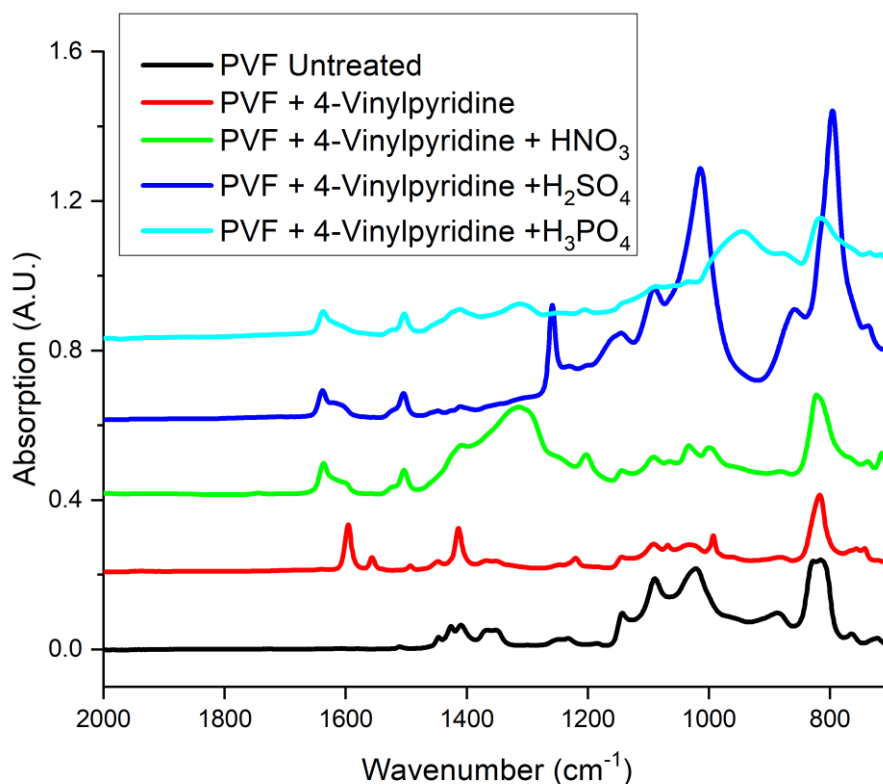
Figure 4.42: FTIR analysis of (a) PCTFE substrates acid treated (b) Sample 8112016PCTFE-9 PEM synthesized with 4-vinylpyridine and acid treatments for proton conductivity measurements.

Figure 4.42 shows impact of acid treatments of nitric acid, sulfuric acid and phosphoric acid to PCTFE PEM which are required to add protons prior to conductivity measurements. Figure 4.42a shows the acid treatment with 5% concentration nitric acid (red), sulfuric acid (green) and phosphoric acid (blue) of PCTFE substrate. There was no significant chemical change in the FTIR spectrum due to the acid treatment of the PCTFE substrate. This observation can be attributed to the high chemical resistance of PCTFE and shows that the acid treatments

will only cause protonation of the ionic liquid groups. Figure 4.42b shows the FTIR spectrum of PCTFE substrate (black), grafted 4-vinylpyridine on PCTFE PEM (red), 5% nitric acid treated PCTFE PEM (green), 5% sulfuric acid treated PCTFE PEM (blue) and 5% phosphoric acid treated PCTFE PEM (aqua). These acid treatments in Figure 4.42b caused the 4-vinylpyridine peaks to shift to the left which indicates the protonation of the pyridine group.[130] Additional peaks also appear on the FTIR analysis after acid treatments and are due to the conjugate acids. These results show that the acid treatment used to dope the membranes with protons for EIS measurements will only protonate the PCTFE ionic liquid PEM membranes and will not chemically react with the membranes.



(a)



(b)

Figure 4.43: FTIR analysis of (a) PVF substrates acid treated (b) Sample 8122016PVF-9 PEM synthesized with 4-vinylpyridine and acid treatments for proton conductivity measurements.

Figure 4.43 shows impact of acid treatments of nitric acid, sulfuric acid and phosphoric acid to the PEM which are required to add protons prior to conductivity measurements. Figure 4.43a shows the acid treatment with 5% concentration nitric acid (red), sulfuric acid (green) and phosphoric acid (blue) of PVF substrate. There was no significant chemical change in the FTIR spectrum due to the acid treatment of the PVF substrate. This observation can be attributed to the high chemical resistance of PVF and shows that the acid treatments will only cause protonation of the ionic liquid groups. Figure 4.43b shows the FTIR Spectrum of PVF substrate

(black), grafted 4-vinylpyridine on PVF PEM (red), 5% nitric acid treated PVF PEM (green), 5% sulfuric acid treated PVF PEM (blue) and 5% phosphoric acid treated PVF PEM (aqua). These acid treatments in Figure 4.43b caused the 4-vinylpyridine peaks to shift to the left which indicates the protonation of the pyridine group.[130] Additional peaks also appear on the FTIR analysis after acid treatments are due to the conjugate acids from the acid treatment. These results show that the acid treatment used to dope the membranes with protons for EIS measurements will only protonate the PVF ionic liquid PEM membranes and will not chemically react with the membranes.

4.4 Proton Conductivity of PEM

Electrochemical impedance spectroscopy (EIS) was used to determine proton conductivity of radiation grafted PEM. The measurements were collected using a potentiostat on the membrane and current and voltage data was recorded as a function of frequency. PEMs were pre-treated with 5% acid solution by volume for proton doping and rinsed with deionized water to remove residual acid from the membrane surface before conductivity testing. Before EIS measurements were collected, the samples were equilibrated in a chamber at select temperature and humidity conditions. Proton conductivity of ionic liquid PEMs were evaluated using two probe types which were described in section 3.3.6. One type was a 2-point parallel plate capacitor probe which measured conductivity through the PEM. The second type was a 4-point probe which used parallel wires to study the proton conductivity across the surface of the PEMs. Different iterations of these probes were used as more accurate test methods were developed. The dimensions of the sample and the test cell affected the accuracy of the EIS measurement. It is important that the impedance and capacitance measured was within the limits of the instrument

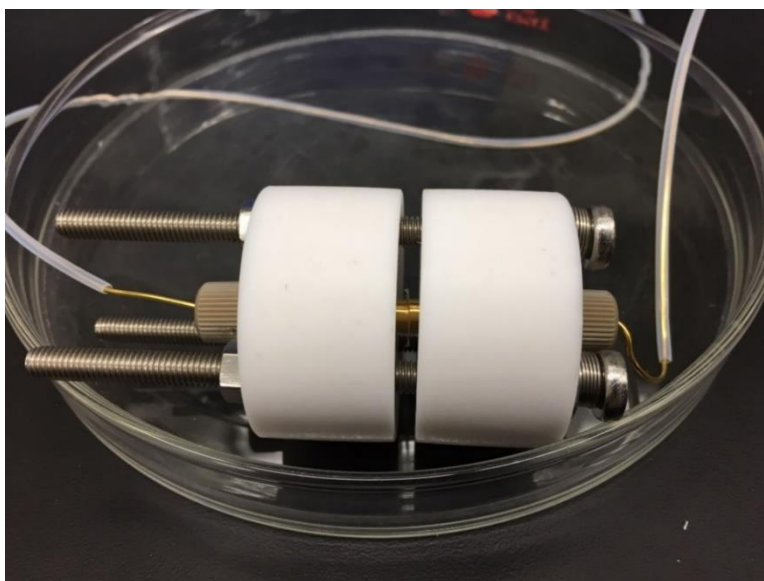
during the measurement. Conductivity data was collected using Scribner ZPlot® and analyzed using ZView® software. Data from the samples were fit using the simplified circuit models that were established in section 3.3.6 for the 2-point and 4-point test cells. Nyquist plots of the collected EIS data can be found in Appendix A.

4.4.1 Two Point Parallel Plate Capacitor Probe EIS Analysis

Initially, the 2-point probe cell was developed to measure conductivity through the membranes. Two test cells were built to measure the proton conductivity of the PEM and their designs are shown in Figure 4.44. The first design was a high temperature PCB parallel plate test probe with gold plated copper electrodes shown in Figure 4.44a. The second design was a Teflon parallel plate test probe with gold electrodes shown in Figure 4.44b. The second cell design was used to address concerns that the gold plating was not a sufficient barrier to prevent oxidation which could affect conductivity measurements. Gold was selected as the electrode material to prevent the acid treated membranes from reacting with the electrode. The parallel plate capacitor test probe was designed to create an electric field when voltage was applied, to establish a potential for diffusion of protons in the PEM. By taking impedance measurement at different frequencies, the reactance of the membranes could be accessed. Due to the high mobility of protons in the PEM compared to other charged species generated from the acid treatment, only the proton conductivity of the PEM was measurable at the high frequency range of the EIS measurements.



(a)



(b)

Figure 4.44- 2-point Probe Parallel Plate Capacitor Test Cells: (a) PCB test cell gold plated electrode (b) Teflon conductivity test cell with gold electrodes

An example of the EIS spectrums of samples using 2-Point Probe Parallel Plate Electrode Test Cells is shown below in Figure 4.45 for sample 81212016PVF-12 grafted with 4-

vinylpyrimidine. The simplified circuit model shown in Figure 3.10c was used to analyze this data. The R_{PEM} was determined to be 20.12 Ω . The proton conductivity of this ionic liquid PEM was calculated as 1.14E-2 S/cm.

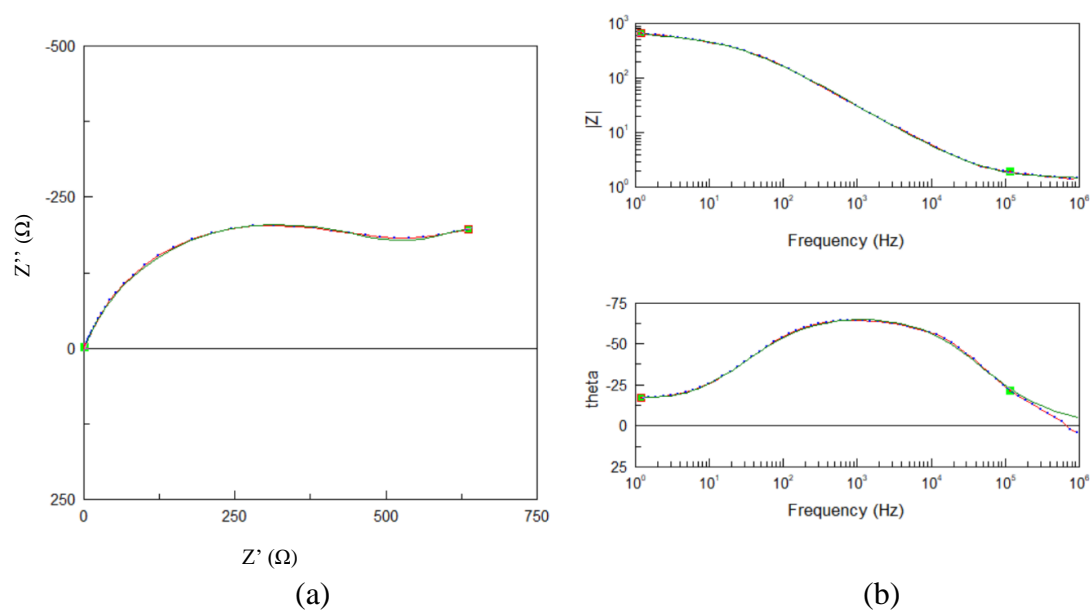


Figure 4.45: 2-Point Probe analysis: (a) Nyquist Plot (b) Bode plot, (red line) EIS data for 81212016PVF-12 at 120°C, (green line) simplified circuit model fit of the equivalent circuit model that is shown in Figure 3.10c

The results of EIS proton conductivity measurements of 4-vinylpyridine PEMs conducted with the PCB 2-point Parallel Plate Electrode Test Cell are shown in Figure 4.46.

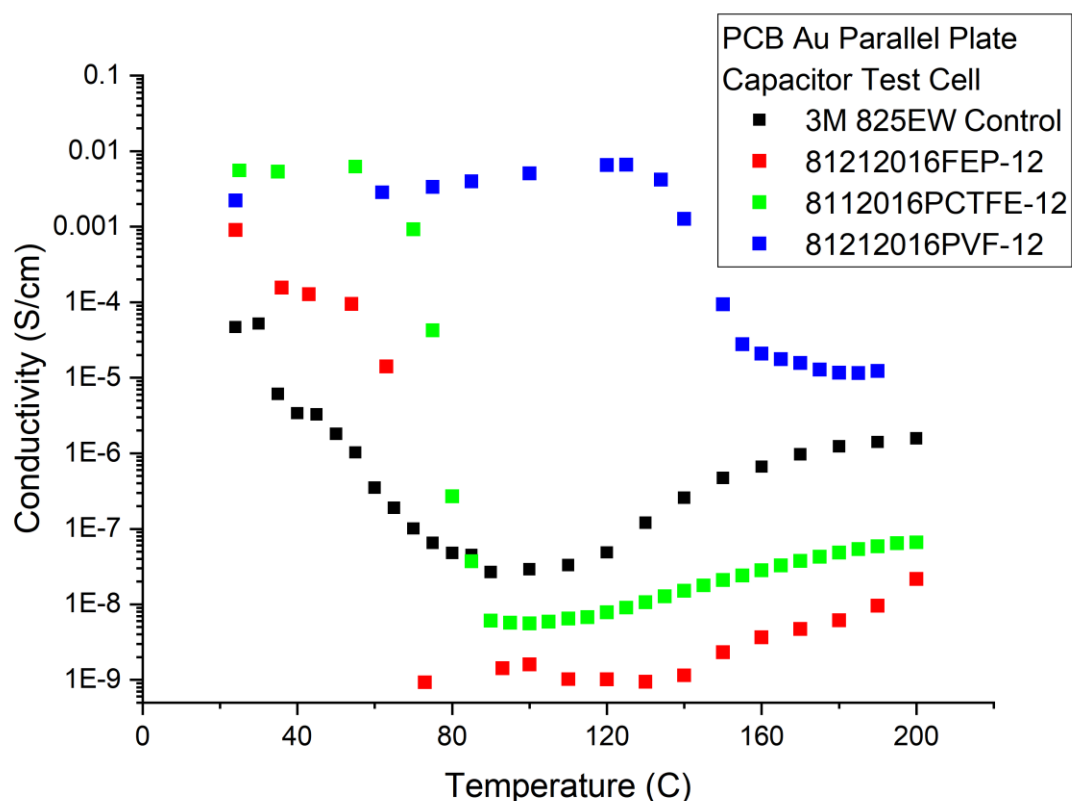


Figure 4.46-EIS proton conductivity vs. temperature PCB 2-Point Parallel Plate Capacitor Test Cell: (black) 3M 825EW Control, 4-vinylpyridine PEM: (red) 81212016FEP-12, (green) 8112016PCTFE-12, (blue) 81212016PVF-12; samples were acid treated with 5% HNO_3 , $n = 1$

The PCB 2-point probe test cell was used to determine the conductivity of PEM grafted with 4-vinylpyridine onto the three fluorocarbon substrates (red) 81212016FEP-12 with 21.2% grafting, (green) 8112016PCTFE-12 with 22.8% grafting, (blue) 81212016PVF-12 with 280% grafting. The highest conductivity at 120°C was the PVF PEM with a proton conductivity of 6.5×10^{-3} S/cm. The conductivity of this ionic liquid PEM was significantly higher than the 3M control when humidity was not applied. These results can be explained by the impact of increased temperature on the 3M control, which is representative of a PEM that relies on water for proton

conductivity. At 100°C the relative humidity was 5% and for temperatures above 120°C the relative humidity was 0.1%. At these conditions the membranes were completely dehydrated. Therefore, the high proton conductivity of the ionic liquid PEM demonstrates they are proton conductive without relying on water as a medium. Whereas, 3M membranes dehydrated, which caused a rapid decrease in proton conductivity with increasing temperatures. The conductivity of PVF PEM with 4-vinylpyridine, peaked around 120°C. This was due to the weakening of N-H bonds through thermal induced scissions allowing higher proton conductivity. This is supported by a study conducted by D. W. Lim et al who showed amine polymers at 120°C exhibit proton conductivity.[131] This was also collaborated by FTIR measurements conducted M.S. Miran et al. which showed chemical shifts and broadening of the N-H bond peak in heterocyclic amine ionic liquids with increasing temperature.[92] They also investigated the interrelationship between pKa and the coordination in ionic liquids. The glass transition temperature of the grafted polyvinylpyridine groups tested in this research is in the range of 100°C to 140°C which explains the fluctuation in proton conductivity in the ionic liquid PEM. The PEMs made with FEP and PCTFE had rapidly decreasing proton conductivity with increasing temperature. This occurred because the proton conductive channels collapsed as the membranes dehydrated. A stable proton conductive network was not established in these PEM and they could not be used for high temperature anhydrous applications.

The reason that the proton conductivity decreases with increasing temperature above 120°C is due to the proton conductive ionic liquid channels being affected by the conformation of the PEM. A stable ionic liquid network is required for charge transfer and proton hopping to occur. Thermal induced lattice vibration hinders proton conductivity across the membrane by causing charge to scatter due to Brownian motions within the grafted ionic liquid polymer.

After the EIS results described in Figure 4.46, the 2-point probe test cell was redesigned to address two issues. First, was the replacement of Au-plated electrodes with solid gold electrodes to eliminate possible corrosion. Second, compression springs were mounted on the cell to maintain contact between the membrane and electrode. As the temperature increased during EIS measurements, PEMs dehydrate causing them to pull away from the surface of the electrodes, effecting the measurements. Also, the electrode in the PCB test cell was flush with the surface of the cell making it difficult to maintain good contact for EIS measurement.

With these two changes, PEM samples grafted with 4-vinylpyridine were tested using EIS with a gold(Au) 2-Point Parallel Plate Capacitor Test Cell. The conductivity results are shown in Figure A-1. As temperature increased, the membranes dehydrated which caused their conductivity to drop by two orders of magnitude. As the temperature increased, proton conductivity rapidly decreased specifically for 3M 825EW control membranes due to membrane dehydration. The same conductivity trend can be seen across the three fluorocarbon substrates grafted with 4-vinylpyridine. The proton conductivity dropped by two orders of magnitude as the membranes dehydrated at 100°C but then plateaued at higher temperatures showing thermal stability. The sample 9102018FEP-13 shown in red was synthesized with 50kGy dose and 100kGy/hr. dose rate with 51.0% grafting. The sample 8112016PCTFE-16 shown in green was treated with 100kGy 300kGy/hr. 41.2% grafting. The PEM 9102018PVF-13 shown in blue was treated with 50kGy Dose and 100kGy/hr. dose rate with 234% grafting. The proton conductivity of PEM synthesized with 4-vinylpyridine were humidity dependent. Even though they showed high thermal stability their low proton conductivity made them not optimal for anhydrous fuel cell operation.

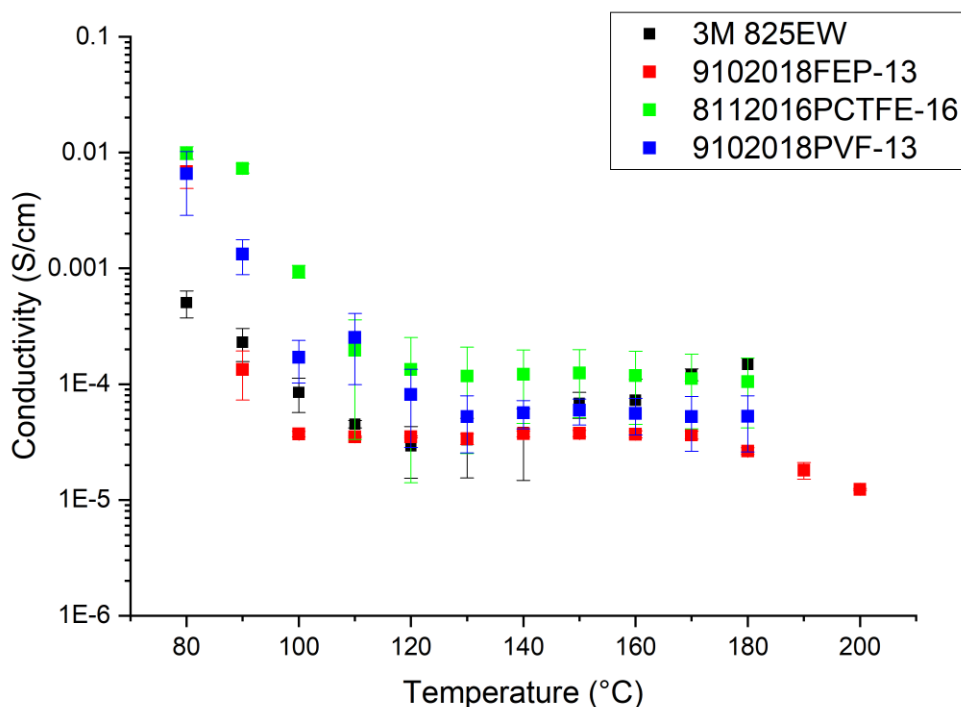


Figure B.25: EIS proton conductivity vs. temperature Au 2-Point Parallel Plate Capacitor Test Cell: (black) 3M 825EW Control, 4-vinylpyridine PEM: (red) 9102018FEP-13, (green) 8112016PCTFE-16, (blue), 9102018PVF-13; samples were acid treated with 5% HNO_3 , $n = 3$

Additionally, select samples of 5-vinylpyrimidine ionic liquid grafted to FEP, PVF and PCTFE proton conductivity were tested and the results are shown in Table 4.12. The sample that showed the highest proton conductivity, $1.8\text{E-}2 \text{ S/cm}$ at 120°C , was sample 9122018FEP-2Na. This PEM had 15.4% 5-0vinylpyrimidine grafted onto a FEP substrate. The temperature dependence on proton conductivity of the PEM is depicted in Figure 4.47. There is a similar trend seen with the PCB 2-point probe test cell where the conductivity peaks around 120°C then decreased. This was due to increasing temperature destabilizing the structure of ionic liquid channels used for proton conductivity in PEM. The proton conductivity of 5-vinylpyrimidine PEM was more stable with temperature than 4-vinylpyridine PEM. This was due to the higher

degree of coordination for ionic liquid groups in the 5-vinylpyrimidine PEM. In comparison, the proton conductivity of PEM grafted with 5-vinylpyrimidine samples were significantly lower than 4-vinylpyridine PVF sample. 5-vinylpyrimidine was expected to have higher proton conductivity because of the lower pKa which makes it more acidic. In addition, 5-vinylpyrimidine also has two cyclic amine groups available for proton conductivity which increases the probability for proton transfer interactions between ionic liquid polymer groups. However, the 2-point probe proton conductivity results presented did not support these expected chemical and physical advantages.

It was difficult to measure membranes with high proton conductivity with the 2-point probe designs shown in Figure 4.44, because of the low thickness of the PEMs. This made the proton conductivity of the membrane difficult to model from the EIS measurement. Companies that manufacture PEM use a 4-point surface probe measurement to ensure the proper distance between electrodes can be adapted to measure a larger range of proton conductivities. The following section covers the results and discussion of 4-point probe surface EIS measurements conducted as a part of this research.

Table 4.12: Conductivity Results of 2-point Au Parallel Plate Cell

Sample	IL Monomer	% grafting	Acid Treatment	Temp. (°C)	Conductivity (S/cm)	STD
9122018FEP-2Na	5-vinylpyrimidine	15.4	5%HNO3	80	7.1E-06	2.1E-06
9122018FEP-2Na	5-vinylpyrimidine	15.4	5%HNO3	100	1.2E-05	2.0E-06
9122018FEP-2Na	5-vinylpyrimidine	15.4	5%HNO3	120	5.9E-05	3.2E-06
9122018FEP-2Na	5-vinylpyrimidine	15.4	5%HNO3	140	2.0E-05	3.7E-07
9122018FEP-2Na	5-vinylpyrimidine	15.4	5%H2SO4	120	1.8E-02	3.0E-03
9122018FEP-2Na	5-vinylpyrimidine	15.4	5%H2SO4	140	9.9E-05	1.0E-05
9122018FEP-2Na	5-vinylpyrimidine	15.4	5%H2SO4	160	2.9E-06	1.1E-07
9122018FEP-2Na	5-vinylpyrimidine	15.4	5%H3PO4	120	9.0E-05	1.4E-05
3222017FEP-1b	5-vinylpyrimidine	22.7	5%H2SO4	120	6.2E-04	1.2E-04
3222017PVF-1a	5-vinylpyrimidine	50.6	5%HNO3	120	8.3E-04	1.5E-04
3222017PVF-1a	5-vinylpyrimidine	50.6	5%H2SO4	80	3.6E-04	3.4E-05
3222017PVF-1a	5-vinylpyrimidine	50.6	5%H2SO4	100	6.9E-04	1.4E-05
3222017PVF-1a	5-vinylpyrimidine	50.6	5%H2SO4	120	5.6E-04	5.7E-05
3222017PVF-1a	5-vinylpyrimidine	50.6	5%H2SO4	140	1.9E-04	3.4E-05
3222017PVF-1a	5-vinylpyrimidine	50.6	5%H3PO4	120	1.5E-04	1.6E-05
3222017PVF-3d	5-vinylpyrimidine	30.7	5%HNO3	120	1.8E-05	3.3E-06
3222017PCTFE-3c	5-vinylpyrimidine	15.8	5%HNO3	120	1.0E-05	1.4E-06

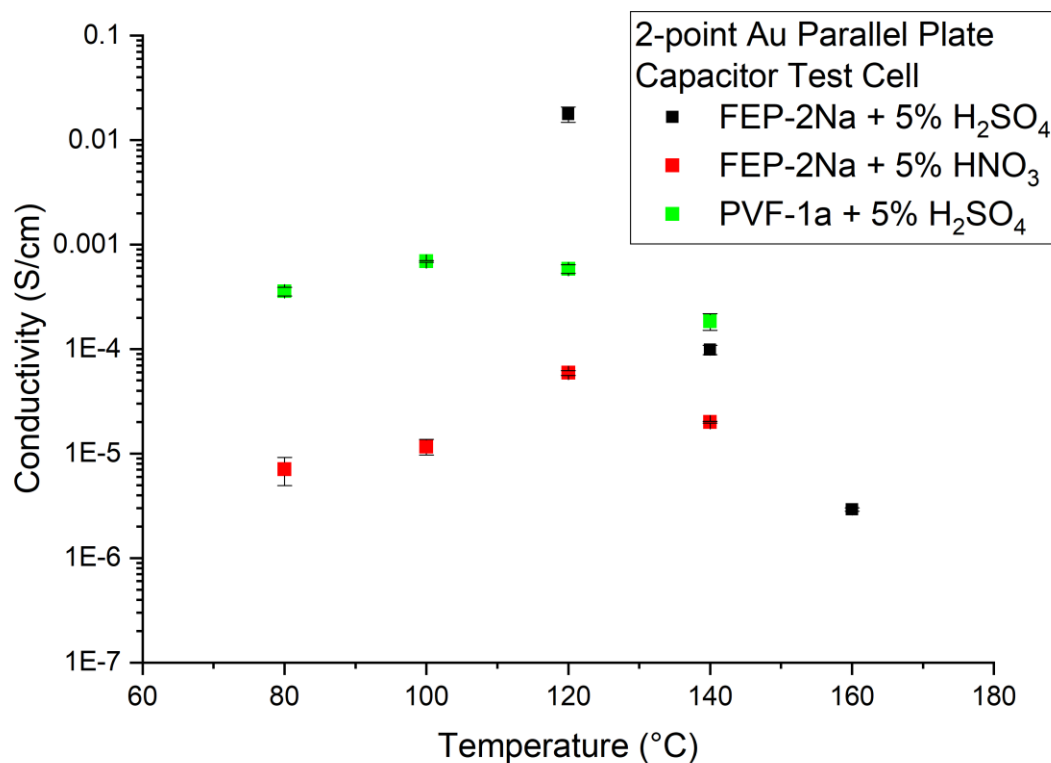


Figure 4.47-EIS proton conductivity vs. temperature 2-Point Au Parallel Plate Capacitor Test Cell: 5-vinylpyrimidine (black) Sample 9122018FEP-2Na treated with 5% H₂SO₄ (red) Sample 9122018FEP-2Na treated with 5% HNO₃ (green) Sample 3222017PVF-1a treated with 5% H₂SO₄, n = 3

4.4.2 Four Point Probe EIS Analysis

The 4-point probe used parallel wires to study the proton conductivity across the surface of the PEMs. The probe set-up had to be refined to accurately measure conductivity. For this reason, the 4-point probe was used for surface measurements of PEM because placement of the wires can cover a wider impedance test range. 4-point surface probe measurements were conducted with the 3M Company industrial standard test methodology.

Initially PEMs prepared with indirect radiation grafted 4-vinylpyridine and 5-vinylpyrimidine were analyzed for 4-point EIS at the 3M Company (Michigan) to measure proton conductivity. The results of these samples are shown in Figure 4.48 and Figure 4.49. The conductivity of the ionic liquid PEM samples using 4-vinylpyridine at 80°C was below the conductivity measured for the 3M control (3M 825EW). The PEM grafted with 4-vinylpyridine showed a strong humidity dependence as shown in Figure 4.48. These PEM rely on water as part of their conductivity mechanism at a temperature of 80°C.

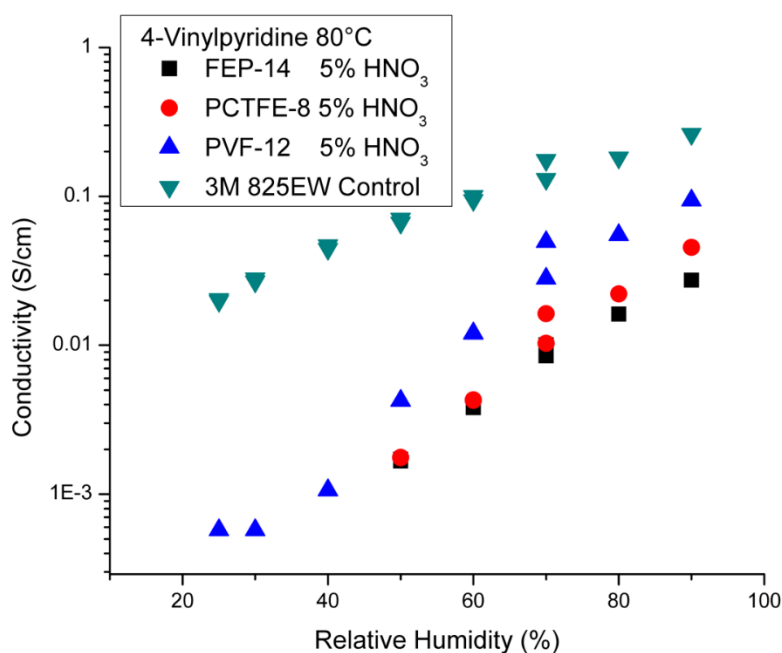


Figure 4.48: Conductivity data of 4-vinylpyridine grafted onto fluorocarbon films:

(black) FEP-14: 60.17% grafting, (red) PCTFE-8: 37.7% grafting, (blue) PVF-12: 280% grafting, (green) 3M 825EW standard control

The conductivity measurements of PEMs synthesized with 5-vinylpyrimidine onto PVF were treated with different acids and tested for conductivity at the 3M Company. These results are shown in Figure 4.49. The results indicate that proton conductivity in these PEM were in general

humidity independent at 80°C. This was most likely due to the symmetry of 5-vinylpyrimidine groups after acid treatment. After acid treatment only one nitrogen is protonated, allowing pyrimidine groups to form a solid-state network for proton conductivity.

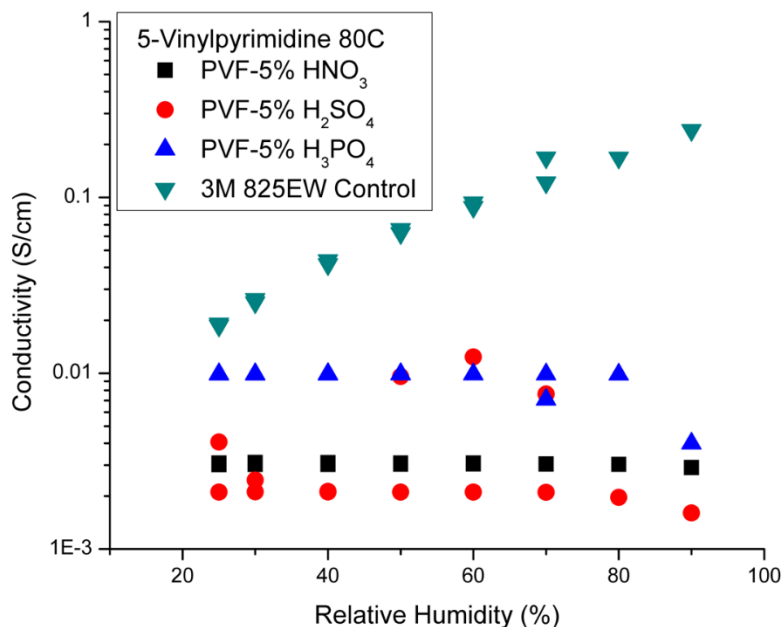
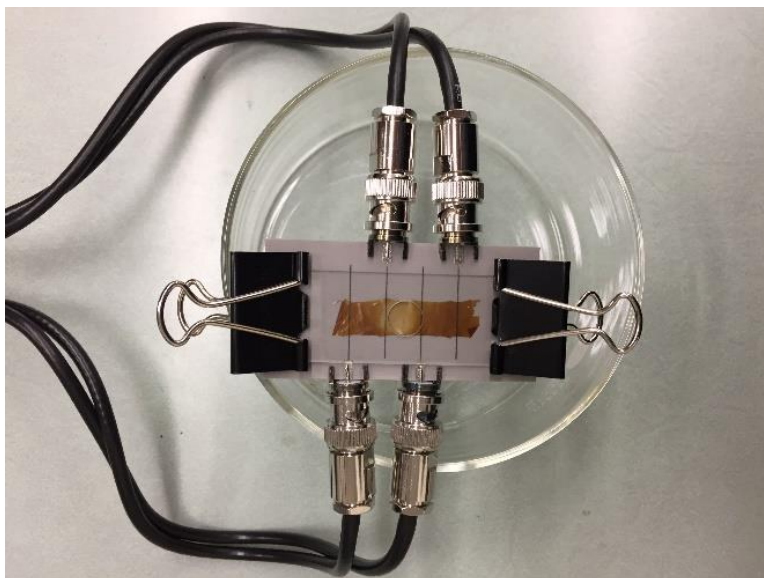


Figure 4.49: 5-vinylpyrimidine 50.5% grafting on PVF-1d and acid treated: (black) 5% nitric acid, (red) 5% sulfuric acid, (blue) 5% phosphoric acid, (green) 3M 825EW standard control

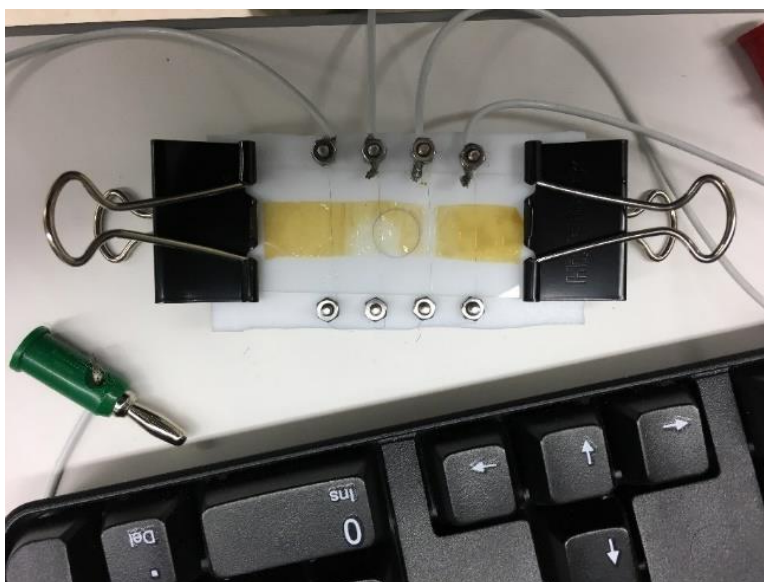
Additional conductivity data was collected at a temperature range between 80-120°C and relative humidity between 0.1 - 80% to give insight into the mechanism of proton transport. The design of the 4-point probe test cell utilized for this project was based on the experimental set-up used by 3M.

Two 4-point probe test cells designs were constructed at the University of Maryland as a part of this research project. The designs are shown in Figure 4.50. Figure 4.50a is a PCB 4-point probe test cell with Pt plated electrodes. Figure 4.50b is a 4-point probe with Platinum (Pt)

wire electrodes. The accuracy of measurement for the 4-point probe cell was dependent on the even spacing of the wire electrodes with the membrane.



(a)



(b)

Figure 4.50: 4-point probe EIS test cells (a) PCB 4-point probe Cell Cu/Ni/Pt plated (b) 4- point probe platinum wires

The PCB 4-point probe test cells were designed to have low tolerances so that the spacing of the electrodes would be more reproducible than the Pt wire 4-point probe test cell. However, this 4-point probe setup failed due to the plated electrode. EIS data using the PCB 4-point probe cell showed a combination of inductance and capacitance of the sample, which caused the spiral loop appearing in the Nyquist Plot. The inductance that appears in the EIS measurement, results in the negative phase shift across the frequency sweep as depicted in the Bode plot. This inductance was caused by the corrosion of the Pt plated electrodes. It was observed after these measurements, that green copper oxide was generated on the Pt plated electrodes. The Cu/Ni/Pt plating failed to act as a protective coating to prevent corrosion of the underlying Cu. The acidic conditions of the acid treated membrane caused this corrosion. The inductance caused by the corrosion, confounded the EIS data and prevented the evaluation of proton conductivity of the PEM with this PCB test cell. The design of this test cell was modified by replacing the Pt plated electrodes with pure Pt electrodes.

Figure 4.51 shows an example of a measurement conducted with a 4-point Pt wire probe cell. The sample depicted in this data is PVF-1e which was grafted with 5 -vinylpyrimidine at 120°C and 0.1% relative humidity. There was no low frequency inductance observed in the ionic liquid PEM measurements. The resistance of the R_{PEM} of this membrane was 11940 Ω and the proton conductivity of this PEM was determined to be 2.23E-2 S/cm according to equation 3.10.

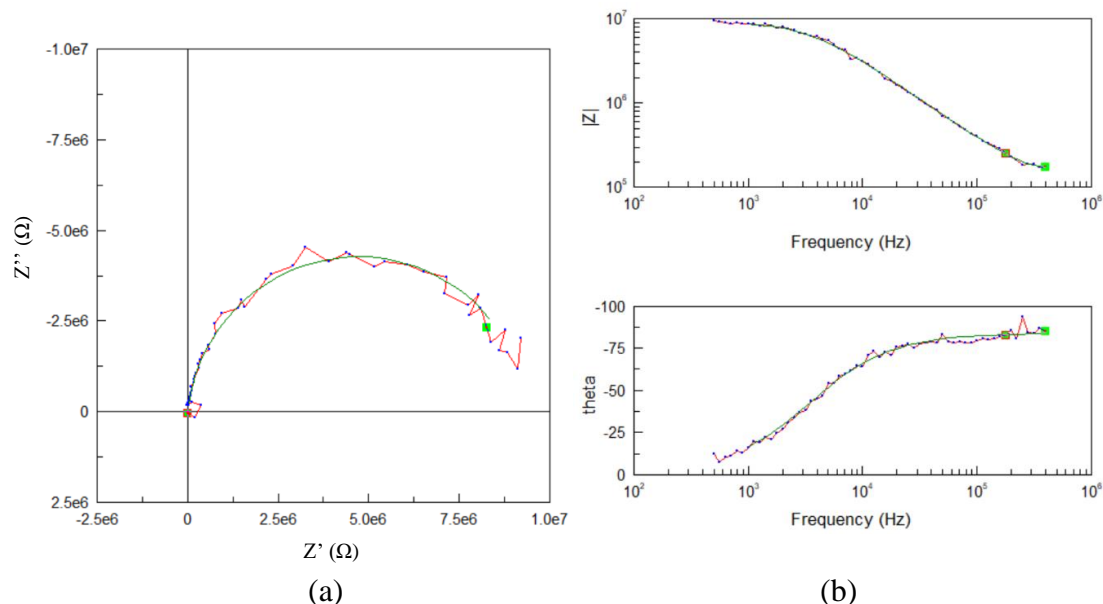


Figure 4.51: 2 Point Probe analysis: (a) Nyquist Plot; (red line) EIS data for PVF-1e at 120°C and 0.1% RH, (green line) Randles equivalent circuit model fit (b) Bode plot; the equivalent circuit model that was used is shown in Figure 3.13c

EIS data collected using the 4-point probe Pt wire test cell in Figure 4.50b is shown in Table 4.13. The proton conductivity data of the PEM grafted with 5-vinylpyrimidine is shown in Figure 4.52 and Figure 4.53. Figure 4.52 shows the relationship between proton conductivity and relative humidity. The 3M control demonstrated increased proton conductivity with increasing humidity. The proton conductivity of PEM grafted with 5-vinylpyridine and FEP shown in (red) did not change significantly with increasing humidity. Sample 3222017FEP-1b had 22.7% grafting of 5-vinylpyridine. The proton conductivity of PEM grafted with 5-vinylpyridine and PCTFE (green) increased between 40 and 60% relative humidity. The PCTFE-3c sample had 15.8% grafting of 5-vinylpyrimidine. The water uptake of PEM due to high humidity conditions, caused their proton channels to swell, effecting their proton conductivity. The proton conductivity of PEM grafted with 5-vinylpyridine and PVF (blue) did

not change significantly with relative humidity. Sample 3222017PVF-1e had 43.1% grafting.

The ionic liquid PEMs are designed to operate under anhydrous conditions and the proton conductivity should not change significantly with relative humidity.

Table 4.13: EIS conductivity Data 4-Point Surface probe Pt Wire

Sample	IL Monomer	% grafting	Acid Treatment	Temp. (C)	R.H.	Conductivity (S/cm)	STD
3M 825EW Control	N/A	N/A	N/A	80	20%	8.1E-03	1.2E-04
3M 825EW Control	N/A	N/A	N/A	80	40%	3.4E-02	1.1E-04
3M 825EW Control	N/A	N/A	N/A	80	60%	7.6E-02	5.9E-04
3M 825EW Control	N/A	N/A	N/A	80	80%	1.5E-01	1.2E-03
3M 825EW Control	N/A	N/A	N/A	100	0%	9.8E-05	4.9E-06
3M 825EW Control	N/A	N/A	N/A	120	0%	3.1E-05	2.9E-07
3222017FEP-3c	4-vinyl pyridine	23.2	5%HNO3	80	20%	1.1E-02	2.8E-03
3222017FEP-3c	4-vinyl pyridine	23.2	5%HNO3	80	40%	1.4E-02	1.8E-03
3222017FEP-3c	4-vinyl pyridine	23.2	5%HNO3	80	60%	3.1E-03	9.3E-05
3222017FEP-3c	4-vinyl pyridine	23.2	5%HNO3	80	80%	1.3E-02	1.1E-04
3222017FEP-3c	4-vinyl pyridine	23.2	5%HNO3	100	0%	1.6E-02	6.6E-03
3222017FEP-3c	4-vinyl pyridine	23.2	5%HNO3	120	0%	1.8E-02	4.6E-03
3222017FEP-1b	5-vinyl pyrimidine	22.7	5%HNO3	80	20%	1.9E-03	3.0E-04
3222017FEP-1b	5-vinyl pyrimidine	22.7	5%HNO3	80	40%	1.6E-03	4.3E-05
3222017FEP-1b	5-vinyl pyrimidine	22.7	5%HNO3	80	60%	1.5E-03	9.2E-05
3222017FEP-1b	5-vinyl pyrimidine	22.7	5%HNO3	80	80%	1.7E-03	1.1E-04
3222017FEP-1b	5-vinyl pyrimidine	22.7	5%HNO3	100	0%	1.7E-03	3.7E-05
3222017FEP-1b	5-vinyl pyrimidine	22.7	5%HNO3	120	0%	1.6E-03	1.7E-05
3222017PCTFE-3c	5-vinyl pyrimidine	15.8	5%HNO3	80	20%	2.1E-03	1.4E-04
3222017PCTFE-3c	5-vinyl pyrimidine	15.8	5%HNO3	80	40%	2.1E-03	8.5E-05
3222017PCTFE-3c	5-vinyl pyrimidine	15.8	5%HNO3	80	60%	1.6E-02	4.9E-03
3222017PCTFE-3c	5-vinyl pyrimidine	15.8	5%HNO3	80	80%	1.7E-02	2.1E-03
3222017PCTFE-3c	5-vinyl pyrimidine	15.8	5%HNO3	100	0%	1.9E-03	1.2E-04
3222017PCTFE-3c	5-vinyl pyrimidine	15.8	5%HNO3	120	0%	2.0E-03	1.2E-04

Table 4.13: EIS conductivity Data 4-Point Surface probe Pt Wire Continued

Sample	IL Monomer	% grafting	Acid Treatment	Temp. (C)	R.H.	Conductivity (S/cm)	STD
3222017PVF-1e	5-vinyl pyrimidine	43.1	5% HNO ₃	80	20%	2.0E-02	2.1E-03
3222017PVF-1e	5-vinyl pyrimidine	43.1	5% HNO ₃	80	40%	9.0E-03	2.1E-03
3222017PVF-1e	5-vinyl Pyrimidine	43.1	5% HNO ₃	80	60%	1.2E-02	3.0E-03
3222017PVF-1e	5-vinyl pyrimidine	43.1	5% HNO ₃	80	80%	6.8E-03	1.6E-04
3222017PVF-1e	5-vinyl pyrimidine	43.1	5% HNO ₃	100	0%	1.6E-02	1.9E-03
3222017PVF-1e	5-vinyl pyrimidine	43.1	5% HNO ₃	120	0%	3.1E-02	4.0E-03
3222017PVF-3d	5-vinyl pyrimidine	30.7	5% HNO ₃	80	20%	1.8E-03	5.9E-05
3222017PVF-3d	5-vinyl pyrimidine	30.7	5% HNO ₃	80	40%	1.6E-03	1.4E-04
3222017PVF-3d	5-vinyl pyrimidine	30.7	5% HNO ₃	80	60%	1.7E-02	3.3E-03
3222017PVF-3d	5-vinyl pyrimidine	30.7	5% HNO ₃	80	80%	1.6E-02	8.7E-04
3222017PVF-3d	5-vinyl pyrimidine	30.7	5% HNO ₃	100	0%	1.7E-03	3.5E-05
3222017PVF-3d	5-vinyl pyrimidine	30.7	5% HNO ₃	120	0%	1.8E-03	6.2E-05

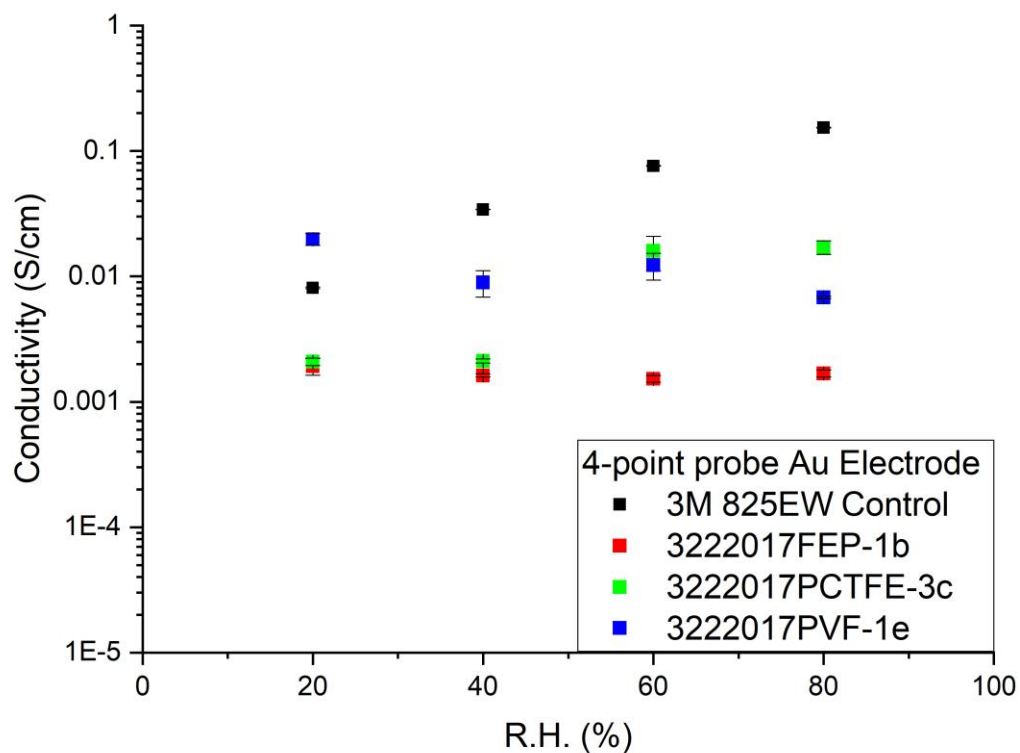


Figure 4.52: EIS Proton conductivity as a function of relative humidity at 80°C treated with 5% HNO₃: (black) 3M 825EW Control; PEM were grafted with 5-vinylpyrimidine: (red) 3222017FEP-1b, (green) 322017PCTFE-3c, (blue) 3222017PVF-1e, n = 3

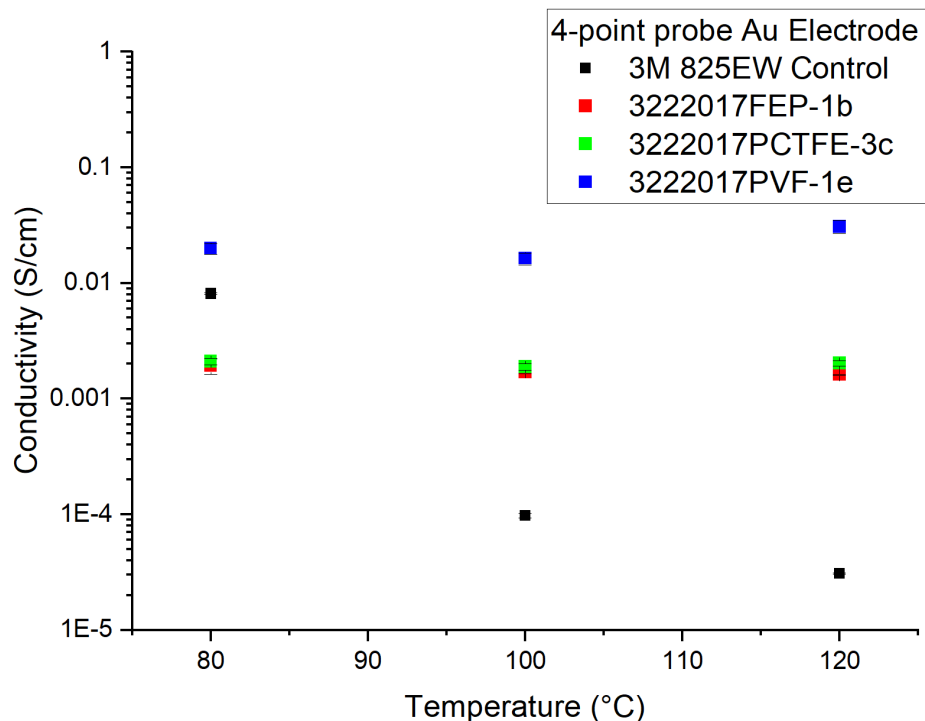


Figure 4.53 - EIS proton conductivity as a function of temperature without humidity control treated with 5% HNO₃: (black) 3M 825EW Control; PEM grafted with 5-vinylpyrimidine: (red) 3222017FEP-1b, (green) 322017PCTFE-3c, (blue) 3222017PVF-1e, n = 3

The 3M 825EW Control (black) represents a traditional fuel cell membrane that uses water channels for proton conductivity. Without a humidity support system, the proton conductivity of the 3M membrane decreased as it approached 100°C as shown in Figure 4.53. Whereas, the anhydrous ionic liquid PEM containing 5-vinylpyrimidine maintained their proton

conductivity with increasing temperature. Of the 3 ionic liquid PEM samples, 3222017PVF-1e (blue) had a higher overall proton conductivity and had higher grafting (43.1%) which contributed to this higher performance. These results show that PEM synthesized from 5-vinylpyrimidine can operate in anhydrous conditions and the ionic liquids even when grafted can act as medium for proton conductivity.

4.4.3 Distribution of Relaxation Time (DRT) and Equivalent Circuit Model Analysis of EIS Data

When developing new materials for electrical applications, it is important to evaluate the electrochemical impedance spectroscopy equivalent circuit model to separate charge kinetics within the system. The EIS data output is affected by the geometry of the test cell and multiple equivalent circuit models could be used to fit the same data. It is important to further substantiate the electrochemical reactions that are present to select the appropriate equivalent circuit model. Relaxation time can be used to differentiate chemical reactions only if they have significantly different reaction rates within a system. Distribution of relaxation time (DRT) analysis was used by Y. Hung et al., to evaluate new cathode materials for solid oxide fuel cells. Through their DRT analysis, it was possible to distinguish between ion transport peak at 10^{-4} - 10^{-3} sec, surface chemical peak at 10^{-3} -0.1sec, and gas diffusion reaction peak at 0.1 to 1sec from the EIS spectrum.[132] Y. Hung et al. was able to identify these relaxation times by varying fuel cell operating conditions.[132] The relaxation times are characteristic of electrochemical reactions at the electrodes and within the fuel cell membrane. The reaction's relaxation time is the amount of time it takes for the chemical reaction to occur. Within a fuel cell system these

relaxation times are modeled as time constants of resistors and capacitors parallel in the EIS spectrum and DRT analysis.

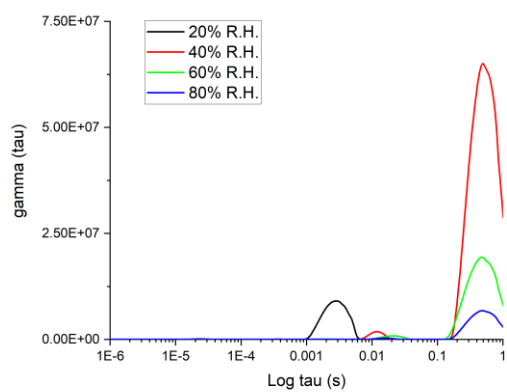
Electrochemical reactions can be convoluted in the Nyquist plots of the EIS spectrum if they have similar relaxation times. DRT analysis allows for the separation of electrochemical reactions by their relaxation time constants within an EIS spectrum by applying an algorithm to evaluate the first and second derivative of both the real and imaginary components.[133] These real and imaginary electrochemical components make up the equivalent circuit used to model the EIS data. The DRT analysis uses a statistical certainty factor to distinguish different time constants from the EIS data. The selection of the certainty factor is important to evaluate the reactions in the system. For polymer electrolyte membrane fuel cells, peaks in the DRT analysis represent mobility of protons in the membrane and their reactions at the electrodes. The DRT analysis was performed on the EIS data from radiation synthesized PEMs using the software DRTTools designed by T.H. Wan et al. run with Matlab.[134] During DRT analysis a certainty factor of 10^{-3} was used to analysis both the real and imaginary EIS data. These results were used to determine the electrochemical relaxation times present in the EIS data. The time constants in the equivalent circuit model used to fit the EIS data were comparable to the relaxation times determined in DRT analysis. A summary of the DRT analysis of a synthesized ionic liquid membrane and 3M control is described in the following section.

For high temperature PEMFCs, the DRT analysis shows three distinct regions within the EIS spectrum. High frequency peaks >100 Hz are attributed to electrode phenomena and membrane resistance. Peaks representing charge kinetics are between 10-100Hz and low frequency mass transport is attributed to peaks between 1-10Hz.[135] The region of interest of the DRT spectrum which is associated with the relaxation time of proton conductivity through

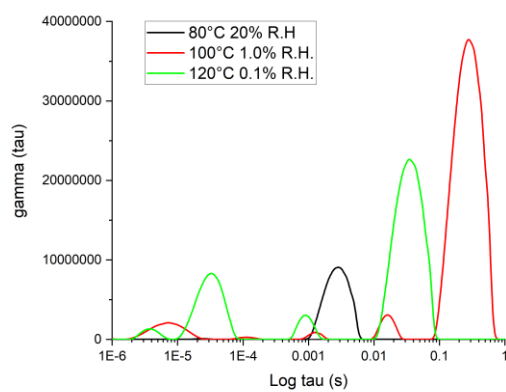
the PEMs occurs between 0.0001s to 0.01s (10-0.1kHz) in Nafion membranes.[136],[137] M. Heinzmann et al. showed that humidity had a significant impact on the proton conductivity and relaxation time in Nafion membranes. This relaxation peak range correlates to proton transport in water nanochannels of Nafion membranes under different humidity conditions. The N-H hydrogen bond channels in heterocyclic amine ionic liquid PEM are expected to behave similarly to the hydrogen bond system found within the Nafion membranes. DRT analysis was used to separate the real and imaginary circuit model components and electrochemical reactions through their relaxation times. Shifts in the DRT plot signify changes in reaction kinetics and the proton conductive mechanisms of the membrane. It was possible to distinguish between electrode reactions and membrane reactions to determine the proton conductivity of the membrane. For this thesis, PEM were prepared for EIS measurements by treating with 5% acid, followed by a DI water rinse and dried. The membranes were equilibrated under variable temperature and humidity for 30 minutes before EIS testing using a Pt 4-point probe test cell. Evaluating the EIS data, DRT peak shifts were observed under changing temperature and humidity conditions. Since the membranes were acid treated, all the electrochemical reactions measured with EIS are related to the proton transport in the membrane and reactions of protons with the electrode.

Figure 4.54 shows the DRT analysis results for the 3M 825EW control under variable temperature and humidity. The number of peaks in the DRT spectrum supports the electrochemical model that was used to analyze the EIS data. Figure 4.54(a) shows, as relative humidity decreases at 80°C, there is an increased of the peak at 0.5s (2 Hz) due to low frequency mass transport of protons at the electrode. Under these conditions, water is the primary method for proton conductivity and charge transport.[26] Once the membrane drops to 20% R.H. at 80 °C, the mechanism for conductivity changes as seen by the emergence of a second DRT peak

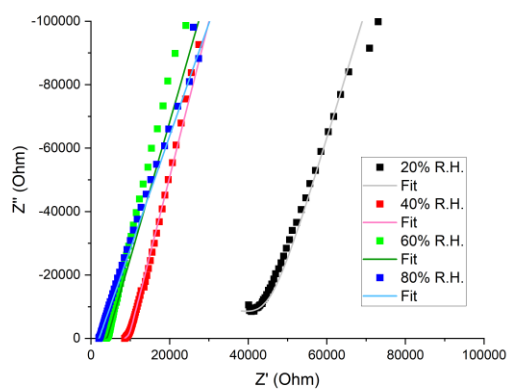
0.002 s (500 Hz, black). This frequency range correlates to the hydrogen bond relaxation time within the nanochannels used for proton conductivity and this peak shift was observed in literature for Nafion. [136],[138] Figure 4.54(b) shows a shift in DRT peaks observed at 100 °C in which the membranes continue to dehydrate, changing the medium for proton conductivity from water to functional groups in the membranes. This shift in DRT peak location was also observed in DRT analysis of Nafion membranes tested under dry hydrogen conditions by M. A. Travassos et al.[139] These results are expected since PEMs are not homogenous between their hydrophobic and hydrophilic polymer structure. PEM that rely on water for proton conductivity usually show strong humidity dependencies since hydration allows the proton conductive nanochannels in the amorphous region to function.[136] The 3M 825EW control membranes show 4 orders of magnitude decrease in proton conductivity due to the decrease in humidity and dehydration. As the temperature increased above 100°C, there are two additional peaks in the DRT at the 0.01s (100Hz) to 1s (1Hz) region. These peaks likely represent the hydrogen bond network becoming more mobile with increased lattice vibrations at this temperature. This results in improved localized mobility of protons and limited diffusion to the electrodes.[138] The 3M sample's change in relaxation time with humidity is an example of a shift in proton conductive mechanisms in the membrane. Figure 4.55 shows the equivalent circuit model components resistors (R_{PEM} , R_{CT}) and constant phase elements (CPE_{PEM} , CPE_{DL}) of 3M 825EW control under temperature and humidity conditions. The relaxation time range for PEM membranes is similar to the response time determined by R_{PEM} and CPE_{PEM} due to proton conductivity in the membrane. R_{PEM} was then used to determine the proton conductivity of the membranes.



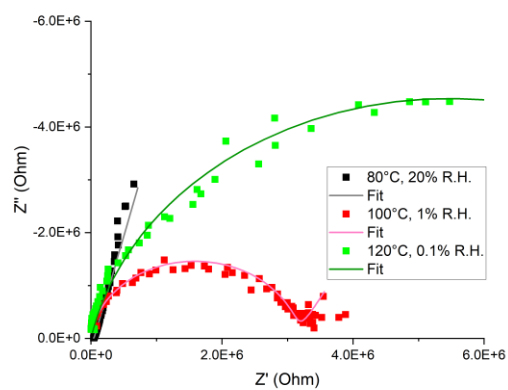
(a)



(b)

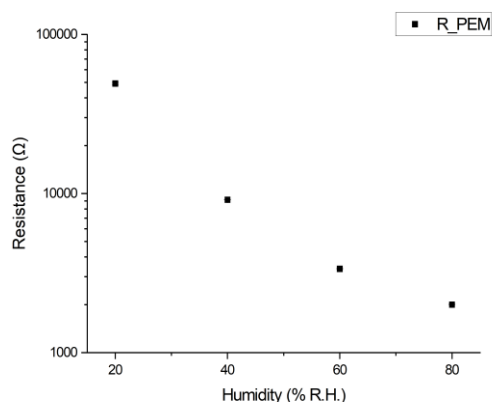


(c)

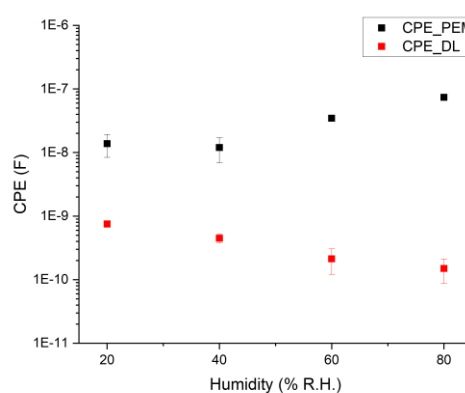


(d)

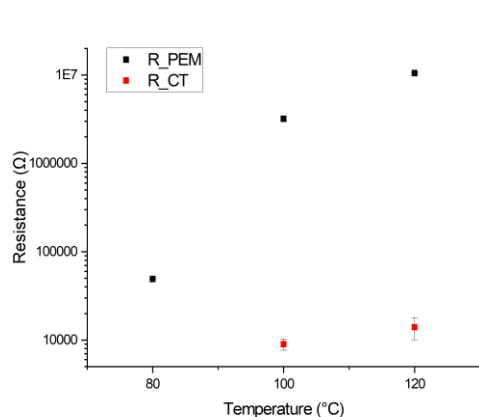
Figure 4.54- Analysis of Pt 4-point probe EIS data 3M825EW Control (a) DRT analysis at 80C 20%,40%,60% and 80% relative (b) DRT analysis of temperature. Nyquist Plot of EIS data (c) function of humidity (d) function of temperature



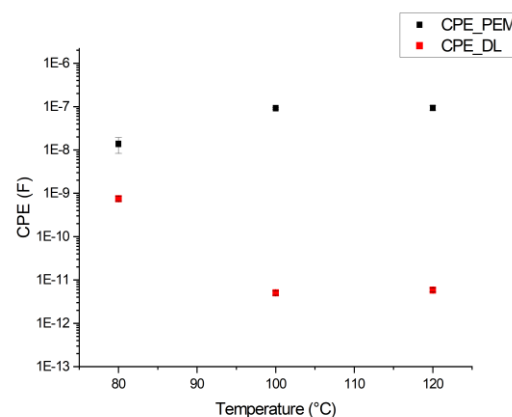
(a)



(b)



(c)



(d)

Figure 4.55- Evaluation of equivalent circuit fit elements for 3M 825EW Control; function of humidity: (a) resistors (b) constant phase elements and function of temperature: (c) resistors (d) constant phase elements

Ionic liquid PEMs synthesized with 5-vinylpyrimidine and PVF demonstrated proton conductivity under high temperature, anhydrous conditions. The DRT analysis of EIS spectrum for this sample (PVF-1e) is shown in Figure 4.56. The DRT peaks of interest for the membrane conductivity is between ~0.0001-0.01s (10-0.1kHz). In Figure 4.56(a) the DRT peak locations did not change significantly with humidity which showed that the electrochemical reactions present stayed the same. As temperature increased, Figure 4.56(b), there was a right shift in the

DRT proton conductivity peak to longer relaxation times. This is opposite of what was observed with the 3M 825EW control. For this sample, it was observed that as temperature increased and humidity decreased, the relaxation time increased. This shift could indicate a new proton conductive mechanism transitioning in a similar manner to what was observed with 3M 825EW control and Nafion. This indicates that the relaxation time peaks between (0.0001-0.01s) (10-0.1kHz) may correspond to the conductivity between hydrogen bonded ionic liquid functional groups in the PEM. The DRT analysis shows that the EIS data is convoluted with peaks overlapping between real and imaginary electrochemical components where proton conductivity was extracted. However, the magnitude of the proton conductivity can still be determined through the EIS measurements and distinguished from the electrochemical electrode reactions through the equivalent circuit model. The relaxation time is modeled in the equivalent circuit model by the time constants of the resistors and capacitors in parallel. Equation 1 shows how the time constant τ for a resistor with resistance $R(\Omega)$ and a capacitor with capacitance $C(F)$ in parallel.

$$\tau(sec) = R * C \quad (1)$$

Figure 4.57 shows plots of the equivalent circuit resistance and capacitance values determined by the fits of the EIS data plotted as a function of humidity and temperature. The time constants of the resistances and capacitances in parallel from Figure 4.57 should match the relaxation times identified by the DRT analysis Figure 4.56. The relaxation time of the membrane can be used to separate the electrochemical reactions and identify which reactions are due to proton conductivity through the membrane. The relaxation times determined from R_{PEM} and CPE_{PEM} fall within the range of literature values associated with proton hopping in PEM nanochannels for proton conductivity through the membrane, 0.0001s to 0.01s (10-0.1kHz). The

impedance from this resistor in the electrochemical model can then be used to determine the proton conductivity of the membrane as plotted in Figure 4.47.

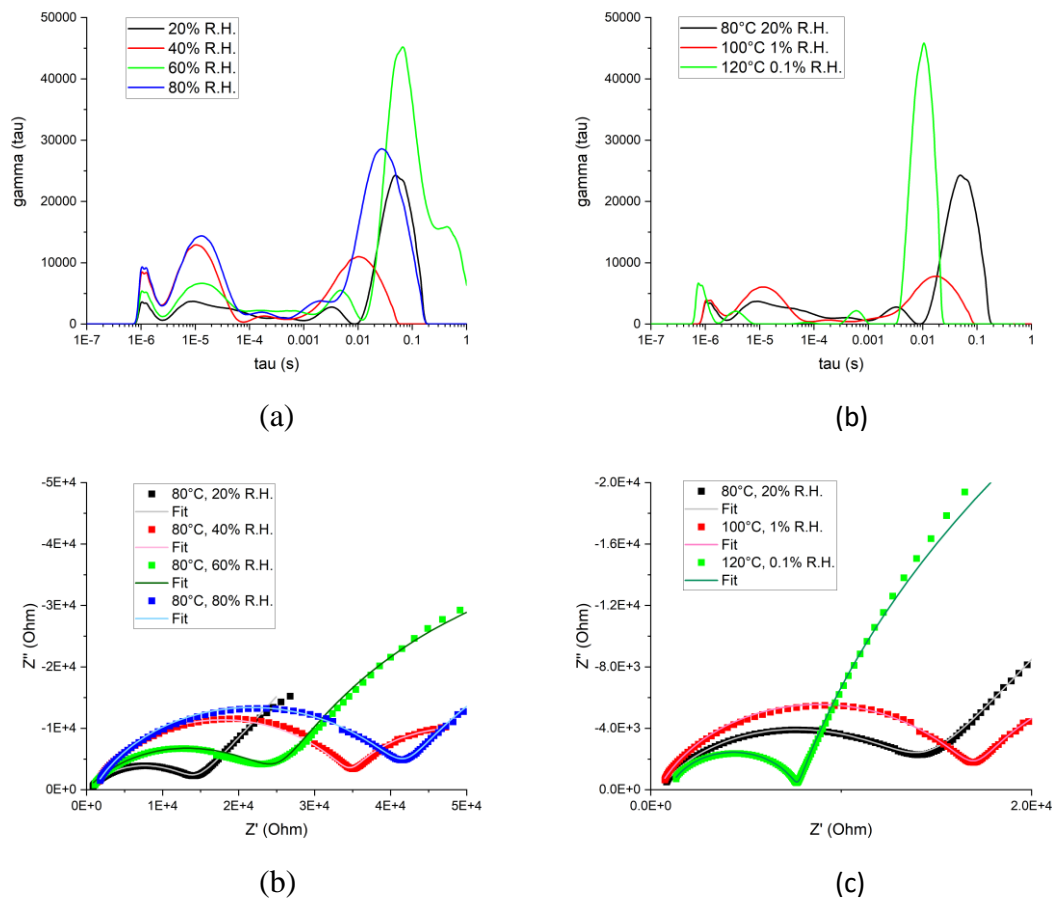


Figure 4.56-Analysis of Pt 4-point probe EIS data 322017PVF-1a ionic liquid PEM (a) DRT analysis at 80C 20%,40%,60% and 80% relative (b) DRT analysis of temperature. Nyquist Plot of EIS data (c) function of humidity (d) function of temperature

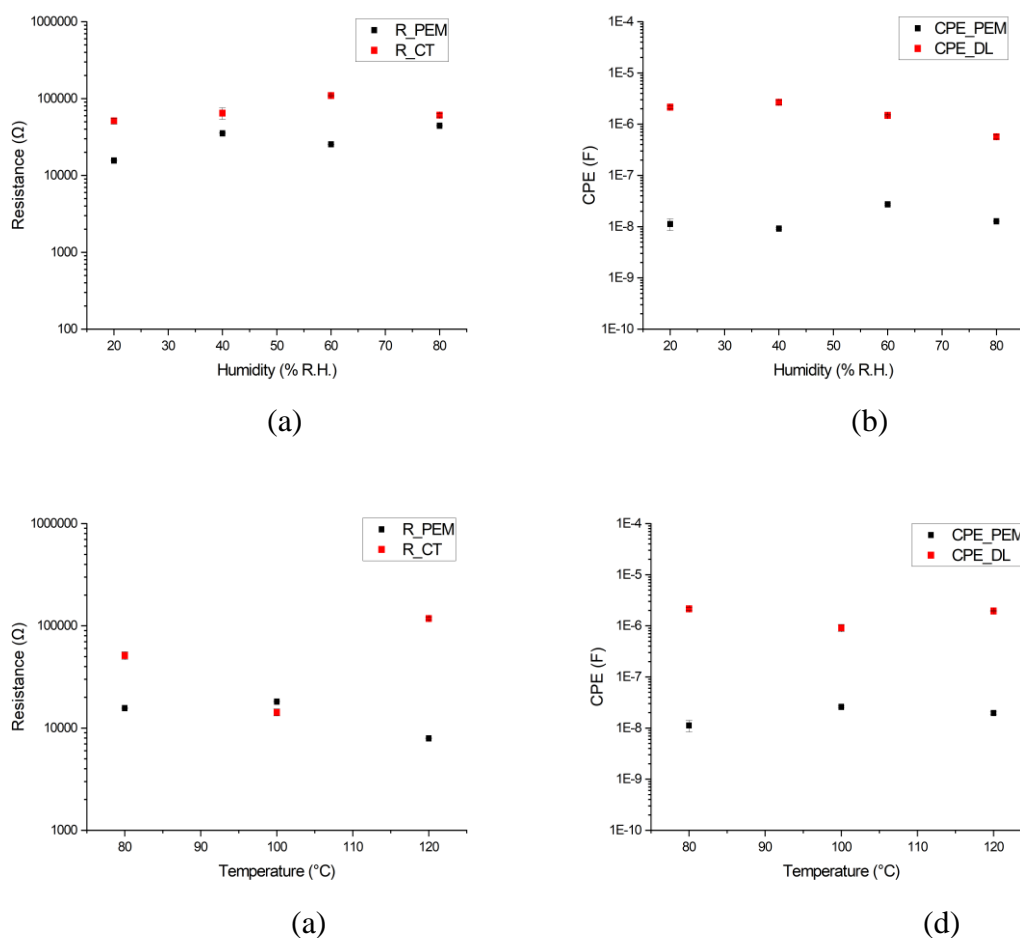


Figure 4.47- Evaluation of equivalent circuit fit elements for 322017PVF-1a; function of humidity: (a) resistors (b) constant phase elements and temperature: (c) resistors (d) constant phase elements

From the DRT analysis the relaxation time measured in the membrane matched literature values for proton conductivity in the membrane. The DRT analysis is a statistical test and shows that there is a 99.9% certainty that there is electrochemical reaction within this range. The resistance values R_{PEM} was then used to determine by the equivalent circuit fit of the EIS data and the proton conductivity using equation 3.10. The smooth transitions of the equivalent

circuit model fit values show in Figures 4.45 and 4.47 that the same equivalent circuit model of resistors and capacitors in parallel can be used to represent the system across the experimental temperature and humidity range. This test was used to validate the EIS analysis and the equivalent circuit model that was used during this research.

4.5 SANS Measurements

Small angle neutron scattering (SANS) measurements is useful in determining the microstructure of complex polymer systems. This technique is sensitive to low Z atomic numbers and can provide good contrast in polymer systems. SANS measurements were conducted in order to determine the microstructure of the grafted proton conductive ionic liquids and fluorocarbon substrate. It was also conducted to determine if the microstructure present would support a proton conductive mechanism. The amount of scattering between fluoride atoms and hydrogen is significant to provide good contrast between the fluorocarbon substrate and grafted monomer. Figure 4.58 shows the SANS measurements of PVF grafted with 50.5% 5-vinylpyrimidine: (gray) untreated PVF film, (yellow) radiation grafted PVF with 5-vinylpyrimidine, (blue) DI water treated radiation grafted PVF with 5-vinylpyrimidine and (red) 5% nitric acid treated radiation grafted PVF with 5-vinylpyrimidine. This data was fit using power law and Gaussian model. This model identified proton conductive ionomer clusters in PEM. The power law defines the order of scatter and the gaussian model describes the spacing of the scattering feature. The gaussian peak was only observed after monomer was grafted to the membrane indicating that it is due to the grafted 5-vinylpyrimidine ionic liquid. The Gaussian peak in the data was centered at 0.035 \AA^{-1} which corresponds to a repeated spacing of 18nm. The spacing for the proton channels in Nafion is on the order of 3 to 5nm.

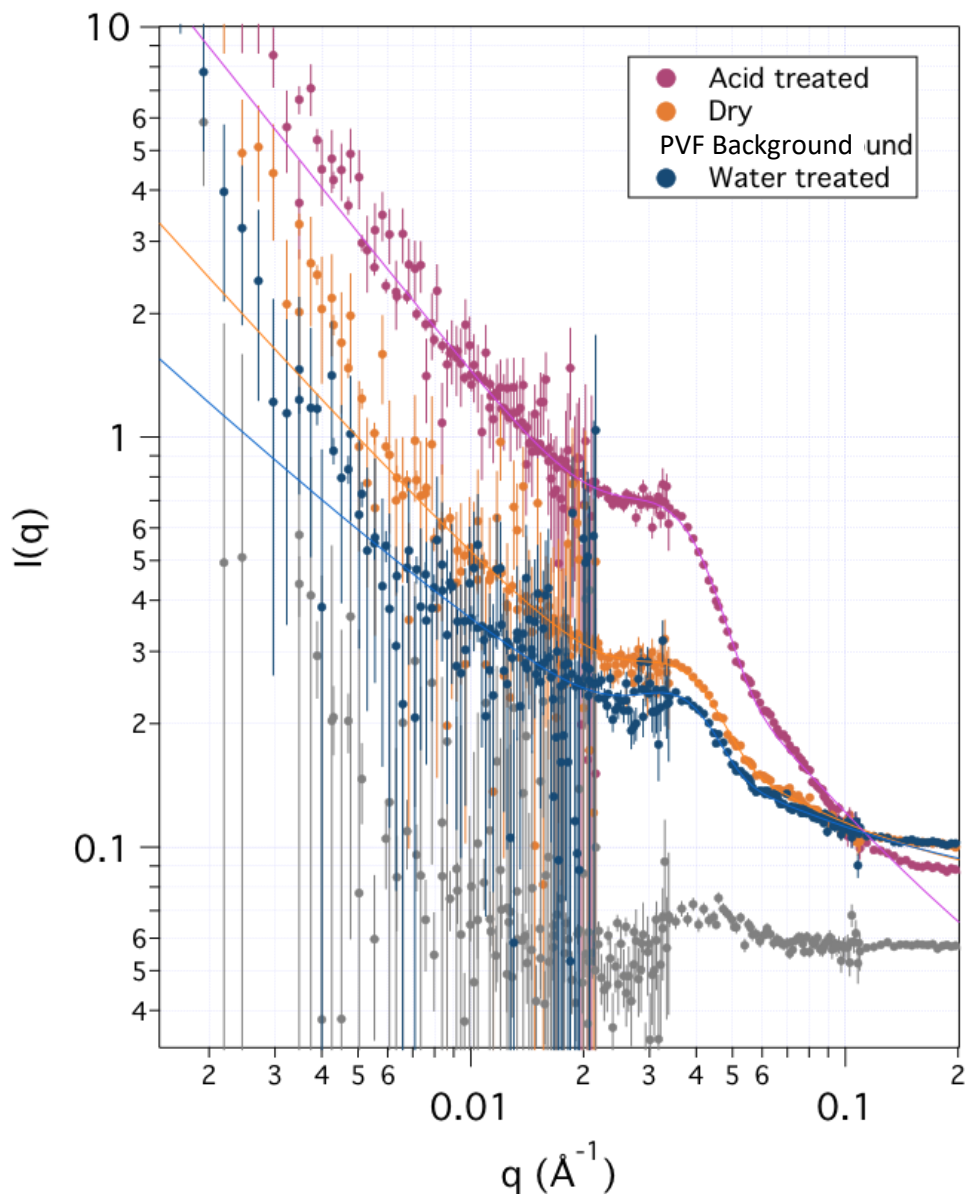


Figure 4.58-SANS measurement of PVF grafted with 50.5% 5-vinylpyrimidine: (gray) untreated PVF film (Yellow) radiation grafted PVF with 5-vinylpyrimidine (blue) wet radiation grafted PVF with 5-vinylpyrimidine (red) 5% nitric acid treated radiation grafted PVF with 5-vinylpyrimidine DI water treated

The results from the SANS measurements show that the membranes are not homogenous at the nanoscale and that there is a repeating ionic liquid cluster that can be used to conduct protons. If the distance between these structures can be decreased, a higher proton conductive ionic liquid membrane will be produced.

5.0 Conclusion and Future Plan

5.1 Conclusions

The focus of this thesis was to design, synthesize and analyze solid-state PEM that incorporate protic ionic liquids and to assess them for high temperature fuel cell applications. PEM were successfully synthesized combining the material properties of protic heterocyclic amine ionic liquids with fluorocarbon-polymeric substrates. The resulting PEM exhibited stable proton conductivity at high temperatures, above 100°C. As stated in the Section 1, the performance of traditional PEMFC are limited to temperatures below 100°C, because of their reliance on water for proton conductivity.

5.1.1 PEM design

The proton transport of heterocyclic amine ionic liquids were established as a good substitute for water to achieve higher operation temperatures. During this research, PEM membranes were synthesized with 4-vinylpyridine or 5-vinylpyrimidine; heterocyclic amine protic ionic liquid monomers by radiation grafting onto FEP, PVF or PCTFE; fluorocarbon substrates. The combination of the symmetrical structures of 4-vinylpyridine and 5-vinylpyrimidine and their respective dissociation constants (pKa) of 5.62 and 1.82, gave them favorable characteristics for proton transport.

5.1.2 PEM Synthesis

In this work it was concluded that indirect grafting is required to impede the homopolymerization reaction. The vinyl group of the ionic liquids undergo rapid polymerization when irradiated. To prevent this reaction, an indirect radiation grafting method was used so that

free radicals were only produced in the substrate. This allowed the vinyl group of the ionic liquid monomers to be covalently grafted into the amorphous regions of the fluorocarbon substrates. This process is demonstrated in Figure 5.1, which shows an overview of the indirect radiation grafting procedure and conditions which were used to successfully manufacture PEM for this research. It is evident through this research that in order to achieve bulk grafting that the ionic liquid needs to be a good solvent to the substrate for diffusion to occur. Experiments demonstrated that 100% ionic liquid monomer was required to drive the grafting front through the membrane to achieve uniform grafting.

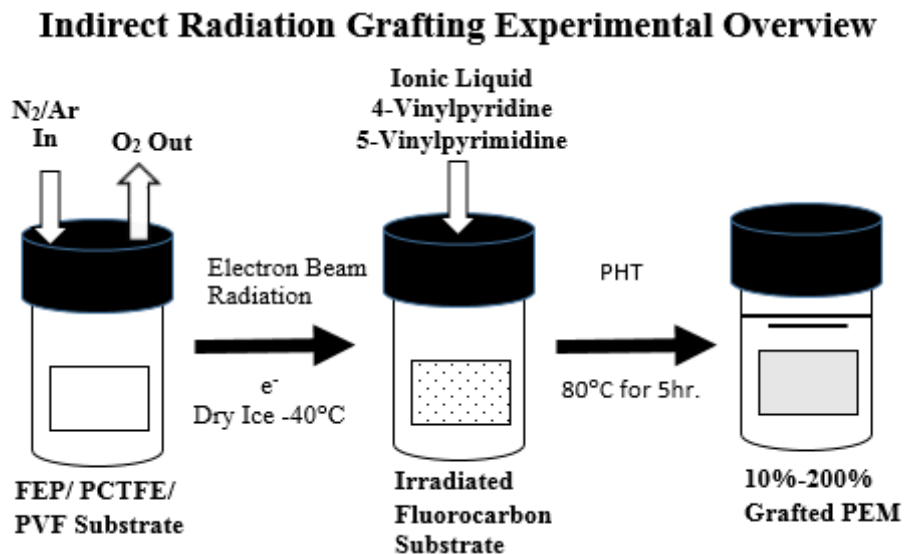

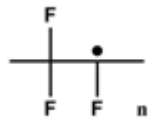
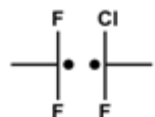



Figure 5.1: Indirect radiation grafting process

Radiation grafting experiments were conducted on FEP, PVF and PCTFE to select the optimal conditions for free radical generation and grafting of 4-vinylpyridine and 5-vinylpyrimidine. EPR measurements were taken of the free radicals and their relative concentrations generated in the fluorocarbon substrates, FEP, PCTFE and PVF. The type and availability of these free radical sites were important to allow for grafting of 4-vinylpyridine and

5-vinylpyrimidine on to the fluorocarbon substrates and for setting the optimized radiation parameters. The time dependence for free radical decay after radiation treatment was established to assure that free radicals were present in a concentration suitable for grafting. The free radical decrease in the fluorocarbon substrate decayed through cross-linking interactions and displayed second order reactions kinetics. Table 5.1 shows the dominant free radical structure after radiation for each substrate and the calculated time to 50% concentration. It was found that the time to 50% concentration of free radicals generated in the fluoropolymers followed their degree of fluorination $\text{FEP} > \text{PCTFE} > \text{PVF}$. This shows that fluoride groups help prevent radicals from decaying by immobilizing them along the polymer backbone.

Table 5.1: Comparison of Substrate-Dominant free radical structure after radiation treatment and decay rate.

Substrate	Dominant Free radical structure	Time to 50% Concentration
FEP		23.59 days
PCTFE	 	80.14 hours
PVF		29.07 hours

The degree of grafting measurements were used to evaluate the most favorable process parameters for radiation treatment. No grafting occurred in the fluorocarbon membranes unless the post heat treatment temperature was above their glass transition temperatures. This was a requirement for the ionic liquid to diffuse into the substrate. The greater the temperature applied in the post heat treatment, the greater the diffusion of the ionic liquid into the substrate and the suppression of the propagation (polymerization) reaction of the ionic liquid monomer. However, the degree of grafting measurements used to optimize the PEM synthesis did not provide information on the extent or uniformity of grafting which is essential for the functionality of proton conductive films. Consequently, uniformity of grafting of the generated PEMs was

further determined by cross-section measurements using SEM/EDS. It was determined that higher dose rates produced significantly more uniform membranes. These higher dose rates also increase the concentration of free radicals, increasing the probability of cross-linking. The post radiation process included a dry ice condition (-40 °C) to ensure the free radicals generated were preserved for grafting when the monomer was added. Together, the percent grafting experiments and the EPR results established the radiation parameters required for ionic liquid addition to the fluoro carbon membrane.

Results from the cross-section measurements using FTIR microscopy and SEM/EDS showed uniformity of grafting of 4-vinylpyridine and 5-vinylpyrimidine within PEMs constructed with FEP, PVF and PCTFE. The SEM/EDS measurements determine atomic composition of the samples in the cross-section. A successful grafting reaction increased the carbon to fluorine ratio in the membrane compared to the untreated membranes. Table 5.2 presents the ratio of carbon to fluorine based on assessment of the cross-section of the grafted PEM as compared to untreated fluorocarbon substrates. For all samples, the carbon to fluorine ratio increased indicating grafting of ionic liquids towards the center of the PEM. The carbon/fluorine rate trends followed the % grafting of the samples. However, while the grafted ionic liquid gradient front reached the center of the PEM, in some cases there was still lamination of polymerized ionic liquids on the surface of the polymer.

Table 5.2: Summary of SEM/EDS measurements

Sample #/ degree of grafting	Ionic liquid monomer	Dose (kGy)	Dose rate kGy/hr	Carbon/Fluorine ratio sample /untreated polymer
20180910 FEP-10a/ 15.1%	4-vinyl pyridine	25	100	3.91/ 0.620
20180910FEP -11a/ 38.61%	4-vinyl pyridine	25	300	4.27/ 0.620
8112016PCTF E-16/41.16%	4-vinyl pyridine	100	300	22.1 / 0.935
3222017PCTF E-3c/15.77%	5-vinyl pyrimidine	100	1000	9.34/ 0.935
20180910PVF -10b/318%	4-vinyl pyridine	25	100	45.7 / 3.83
3222017PVF- 1a / 50.56%	5-vinyl pyrimidine	25	1000	29.6/ 3.83

FTIR measurements were performed to identify chemical changes within the synthesized PEM by comparing the FTIR - ATR spectrum before and after radiation grafting treatments. These measurements were conducted for FEP, PVF and PCTFE substrates. The FTIR analysis of PEM showed chemically that the ionic liquid monomers grafted to the three fluorocarbon substrates. Acid treatments were used to add protons to the membranes for proton conductivity measurements. The FTIR data demonstrated that the acid treatments used during conductivity measurements only protonated the ionic liquid functional amine groups and did not react with the PEMs.

5.1.3 PEM Performance

Proton conductivity was measured by EIS with fabricated 2-point and 4-point probe cells for synthesized ionic liquid PEM. The temperature and humidity effects on proton conductivity were evaluated and was a key measure of the research goals. Electrochemical impedance spectroscopy (EIS) was used to determine proton conductivity of radiation grafted PEM. The results showed 3M Company Control PEM was superior to the PEM synthesized for this project under their conditions of normal operation (80°C/ 80% RH). The control membrane utilized water transport as the proton conductive medium. At temperatures above 100°C, the control membrane dehydrate while the ionic liquid PEMs had higher proton conductivity under anhydrous conditions. This trend was observed for all three fluorocarbon substrates (FEP, PVF and PCTFE) in combination with the two grafted ionic liquid monomers (4-vinylpyridine and 5-vinylpyrimidine). Some of the protic ionic liquid PEM had proton conductivities above 10^{-3} S/cm under anhydrous conditions at 120°C. These high proton conductivities were achieved by proton transport between the grafted protic cyclic amine ionic liquid groups in the membrane. For proton transport between two neighboring groups to occur, the N-H bond needs to undergo a thermal induced scission. The temperature required for the protic amine ionic liquid to become proton conductive is related to their pK_a and activation energy. This explains the increase in proton conductivity when temperature is increased up to 120°C. Above 120°C, some fabricated PEMs demonstrated a decrease in proton conductivity due to a collapse of the proton conductive pathways. The 4-point probe EIS data showed that the protic ionic liquids that were studied support proton conductivity at high temperature and anhydrous conditions. The 2-point probe EIS data showed that proton conductive network of ionic liquids was grafted into the PEM supported proton hopping through the membrane. The degree and density of grafting also

affected the proton conductivity of the PEM. If the degree of grafting was too low, the functional groups would be too far apart, increasing the activation energy for proton transport. If degree of grafting was too high, then the functional groups would be immobilized preventing proton exchange between neighboring groups.

The density of the grafted ionic liquid also affected the proton conductivity through the membrane. To understand the nanostructure of the ionic liquid PEM and the proton conductive mechanism, SANS measurements were used to determine the nanostructure of radiation grafted PVF with 5-vinylpyrimidine PEM. The results from the SANS measurements show that the membrane is not homogenous at the nanoscale and that there is a repeating ionic liquid cluster structure of 18 nm that can conduct protons. This structure is expected because the ionic liquids can only graft into the amorphous regions of the substrate. Since the size for the proton channels in Nafion is on the order of 3 to 5 nm, a modification to decrease the distance in the synthesized ionic liquid PEM should further improve conductivity. The combination of EIS and SANS measurements demonstrate a new mechanism for proton transport was produced for PEMFC applications.

5.2 Contributions to Science

This research establishes the science and methods for producing PEM with novel ionic liquid monomers for radiation grafting to fluorocarbon substrates for high temperature fuel cell applications. Heterocyclic amine ionic liquids PEM have been identified and characterized for their proton conductivity at high temperatures. This research expands the number of solid-state systems known for proton conductivity under anhydrous conditions, allowing for future development of PEMFC that have better efficiency and performance. The results of this research have demonstrated that even when ionic liquids are grafted and polymerized, they can exhibit proton hopping mechanism between amine groups. By expanding the number of polymer systems known to conduct protons under anhydrous, high temperature conditions and developing new radiation fabrication methods for PEM, this research has improved the viability of PEMFC technology.

Ionic liquids have been incorporated into Nafion and fluorocarbon membranes to improve the proton conductivity, but radiation induced grafting of ionic liquids to fluoropolymers has not been thoroughly investigated. This research demonstrated, radiation grafting of protic ionic liquids; 4-vinylpyridine and 5-vinylpyrimidine with FEP, PCTFE and PVF substrates to produce viable PEM. This synthesis incorporated a network of protic ionic liquids into the fluorocarbon substrates and new mechanisms of proton transport were produced for PEMFC applications. These membranes have stable proton conductivity and are suitable for high temperature, low relative humidity conditions.

The impact of this research is that performance of PEMFC can be improved by increasing their operation temperature above 120°C, but their current design is limited by reliance on water for proton conductivity. By designing PEMs that incorporate radiation grafted protic ionic

liquids, proton transport can be supported for high temperature and anhydrous PEMFC applications. Prepared PEM were assessed how their chemical structure and properties affected their proton conductivity. Trends found in this research will help the development of future anhydrous PEM with higher conductivity and durability for high operating temperatures.

5.3 Future Work

The focus of future work should include improvements to design, synthesis and analysis of solid-state PEM that incorporate protic ionic liquids. For design, alternative protic ionic liquids could be studied to understand the relationship between chemical properties such as pKa and effect on proton conductivity. Figure 5.2 shows the chemical structure of select heterocyclic amine ionic liquids studied (4-vinylpyridine and 5-vinylpyrimidine) and other potential heterocyclic amines that could graft to fluorocarbon polymers. Through studying additional protic heterocyclic amine ionic liquids, better proton hopping mechanisms could be demonstrated resulting in higher proton conductivity.

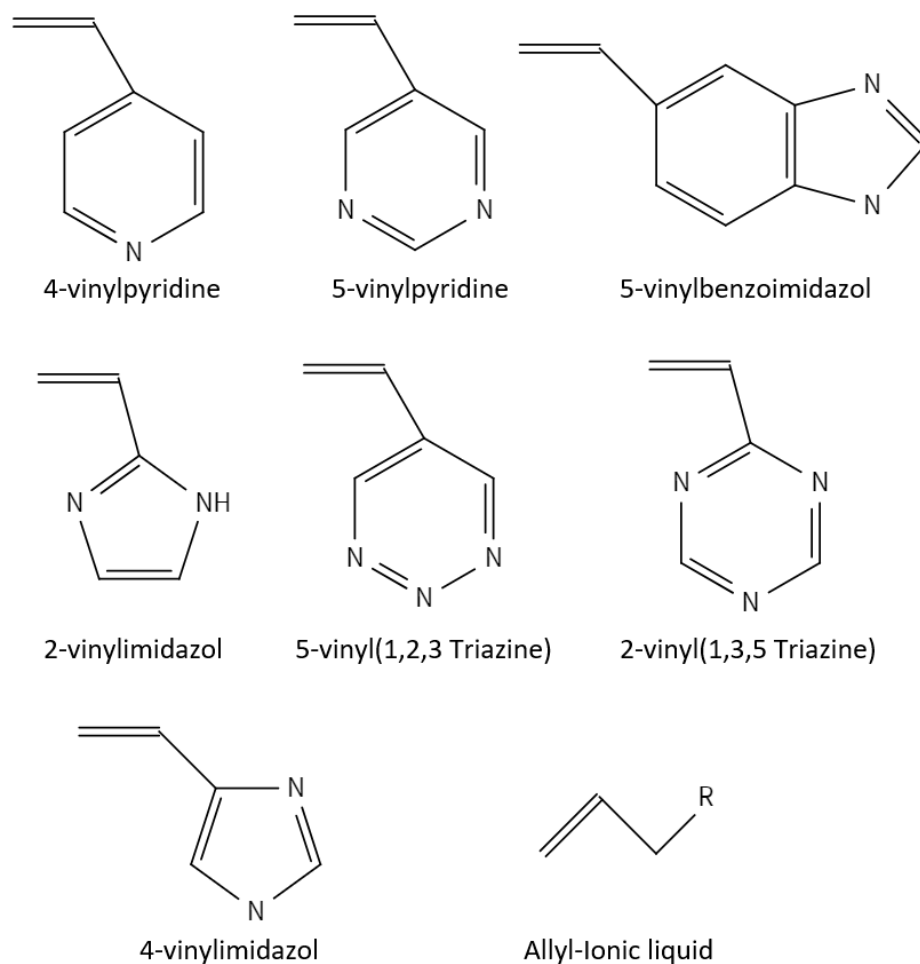


Figure 5.2: Chemical Structure of heterocyclic amine ionic liquids that can be used for PEMFC applications

Additional design improvements should focus on the nanostructure and uniformity of radiation grafted PEM to improve conductivity. This can be accomplished by radiation grafting the ionic liquids to fluorocarbon microparticles and sintering them together into a PEM. This synthesis method would allow finite control of the proton conductive channel size and distribution in the membrane. The smaller the channel size the closer the ionic liquids are packed and the higher the proton conductivity. The nanostructure and size of the channels of the

PEM can be determined using SANS. The proton conductivity of the PEM can be measured using EIS.

To improve the synthesis of radiation grafting ionic liquid PEM, further optimization of radiation parameters could be made such as testing doses above 100 kGy and dose rates above 1000 kGy/hr. The number of free radicals is proportional to the applied radiation dose. Increasing the dose above 100 kGy should allow for a higher density of grafting as long as cross-linking is controlled. Previous experiments showed improved uniformity of grafting with higher dose rates. Increasing the dose rate would find the critical point in which radiation induced cross-linking within the polymer substrate becomes the dominate reaction. The use of pulse radiolysis could be evaluated to determine the reaction rate constants for the ionic liquid radiation grafted PEM. In addition to using degree of grafting, inductively coupled plasma mass spectrometry (ICP-MS) can be used to determine the atomic composition of the membrane and by extension the density of grafted monomer.

For synthesis, 100% liquid monomer was used for the post heat treatment grafting reaction. Future work should evaluate different methods and conditions for applying the monomer to the irradiated substrate to minimize the amount of monomer required. Applying the monomer directly to the surface of the substrate, rather than submersion may improve the grafting reaction while avoiding surface polymerization and percent grafting greater than 100%.

Related to analysis, further testing of ionic liquid PEM can be performed using a hydrogen fuel cell. In this thesis, membranes were doped with protons through acid treatment. During the EIS measurements, there was a concern that the counter ions from the acid treatment might affect the proton conductivity measurements. This was corrected by selecting acids that have a lower charge to mass ratio than hydrogen. Therefore, the EIS measurement was used to

identify PEM candidates that would be further tested in a hydrogen fuel cell. Also, the long-term efficiency and reliability of the PEM can be determined during hydrogen fuel cell testing. In conclusion, there are multiple new investigation paths opened by this research.

Appendix A: EIS Proton Conductivity Measurements and Equivalent Circuit Modeling

Abstract

The following appendix details how electrochemical impedance measurements of PEM membranes were analyzed to determine their proton conductivity. All the samples tested were fit with the general model shown in Figure A.0 which represents all the electrochemical reactions within PEM and EIS test cell. The models that were used to fit the EIS data were subsets of this model which were affected by the proton conductivity of the membrane under different temperature and humidity conditions and the geometry of the test cell. It was observed that the equivalent circuit model changes due to the membrane testing conditions which causes the significant components of the proton conductivity and the time constants to shift. The components that had high impedances and were in parallel were removed from the models. It was observed, as the temperature rises from 25°C to 100°C the membrane which were loaded wet dehydrates, which significantly impacted the proton conductivity of the membrane. At this temperature range the proton conductive mechanism is forced to shift from a diffusive mechanism to proton hopping between ionic liquid groups. At approximately 120°C is the glass transition temperature of the grafted ionic liquid groups which is why there is a significant change in the EIS data. At higher temperatures, above 150°C, the substrates of the PEM approached their melting point causing a decrease in proton conductivity. For other membranes the proton conductivity increases through thermal activation if the structure is stable. The EIS results were also affected by the geometry of the test cell which was changed across the three test cells affecting both the impedance of the membranes, the interfacial capacitance and the charge

transfer resistance. This can be observed, in the difference in the extrinsic modeled impedance values between the 2-point probe and 4-point probe EIS spectroscopy measurements.

The following section is the EIS data presented as Nyquist plots and how it was analyzed through the course of this thesis. It is broken into 3 subsections sections A, B and C for the 3 test cells that were used in the course of the project PCB 2-point probe, Au 2-point probe and Pt 4-point probe respectively. The EIS data sets were plotted together to show how the data change with parameters of temperature and humidity. For select samples the fit and subsequent conductivity calculation are shown with the EIS data. From this data plots of conductivity were generated and used in the thesis which are shown at the end of each section.

The equivalent circuit model represents the electrochemical system that occur in the PEM during EIS testing. The equivalent circuit model for 2-point probe measurements is shown in Figure A.0 below.

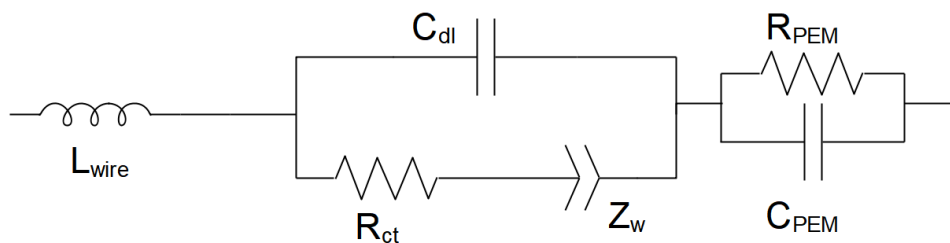


Figure A.0- Equivalent circuit model of 2-point Au parallel plate capacitor test cell

These models were used to fit the EIS data and extract the resistance of the PEM membrane.

From resistance of the PEM membrane, the conductivity of the membrane can be determined.

The following section shows the analysis of the EIS data: Fitting the equivalent circuit model and calculation of proton conductivity of the PEM.

The results of the EIS analysis showed that the membranes composed of 5-vinylpyridine had a higher degree of humidity dependence affecting the proton conductivity. Whereas, the membranes composed of 4-vinylpyrimidine demonstrated proton hopping under anhydrous conditions. The membrane substrate also impacted the thermal stability of the membrane and its behavior under EIS testing. The more amorphous the substrate the higher the proton conductivity but the lower the thermal stability. The amount of crosslinking, degree and density of grafting also significantly impacts the proton conductivity which will need to be further studied on how these inter-relate. Finding these trends will help further improve the proton conductivity and stability of ionic liquid PEM.

PCB 2-Point Probe Analysis: 3M 825EW Control

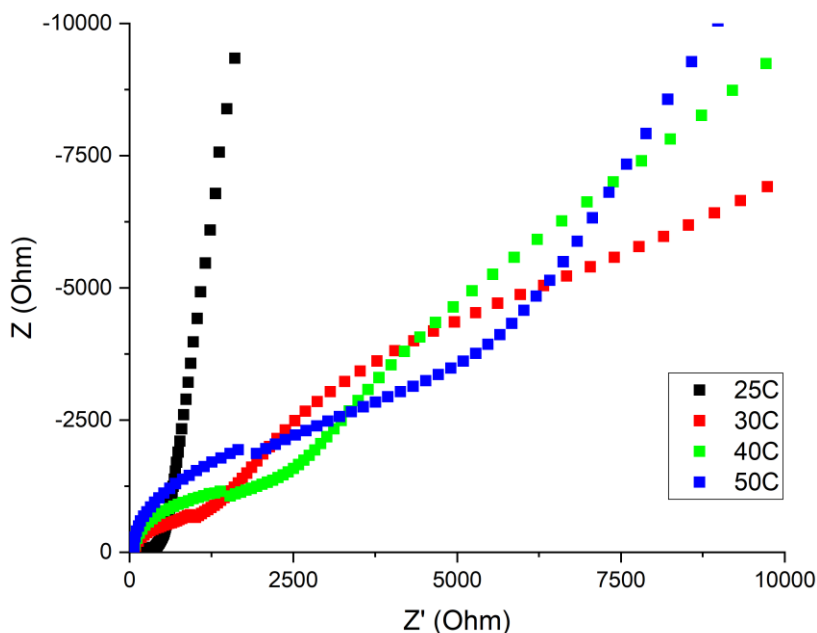


Figure A.1-Nyquist Plot of EIS 2-point probe analysis of sample 3M 825EW Control acid treated with 5% HNO₃ variable temperature 25C, 30C, 40C, 50C

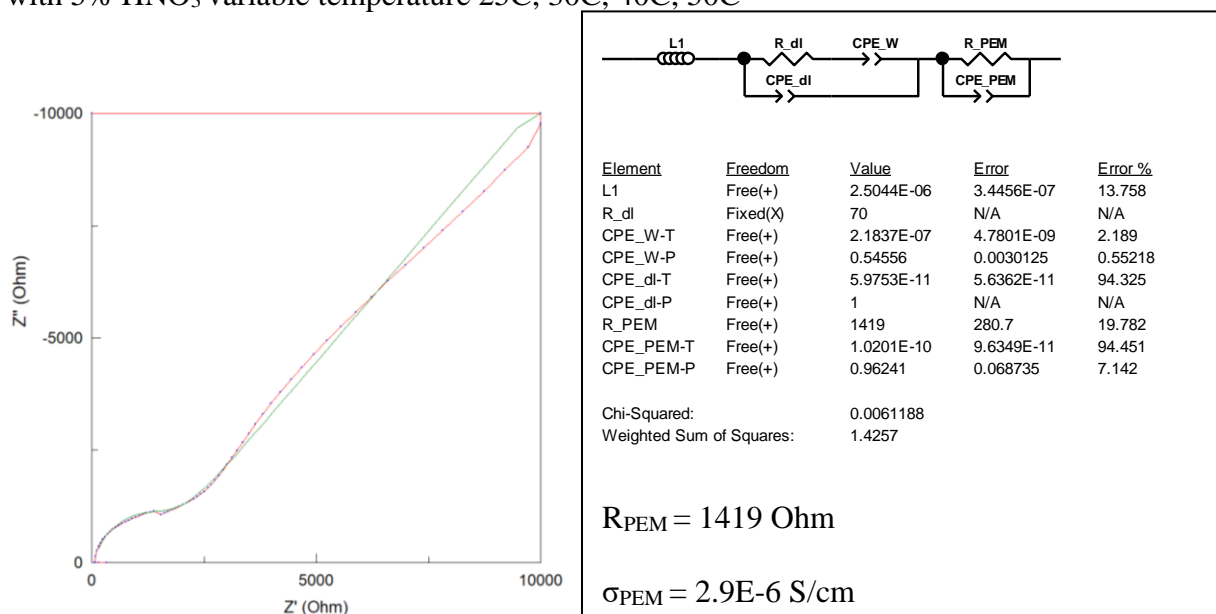


Figure A.2- EIS 2-point probe analysis of sample 3M 825EW Control acid treated with 5% HNO₃ at 40C fit with an equivalent circuit model (left) Nyquist Plot (right) equivalent circuit model fit

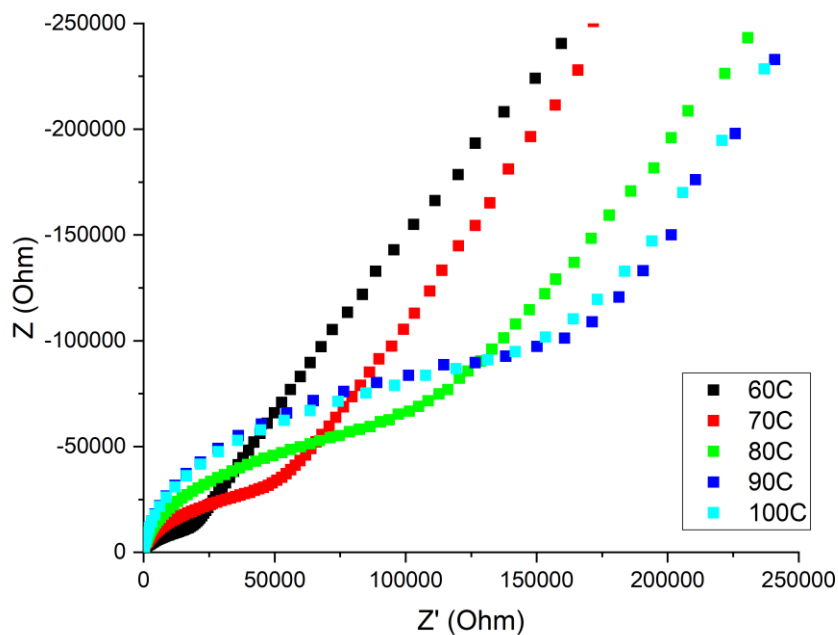


Figure A.3-Nyquist Plot of EIS 2-point probe analysis of sample 3M 825EW Control acid treated with 5% HNO₃ variable temperature 60C, 70C, 80C, 90C, 100C

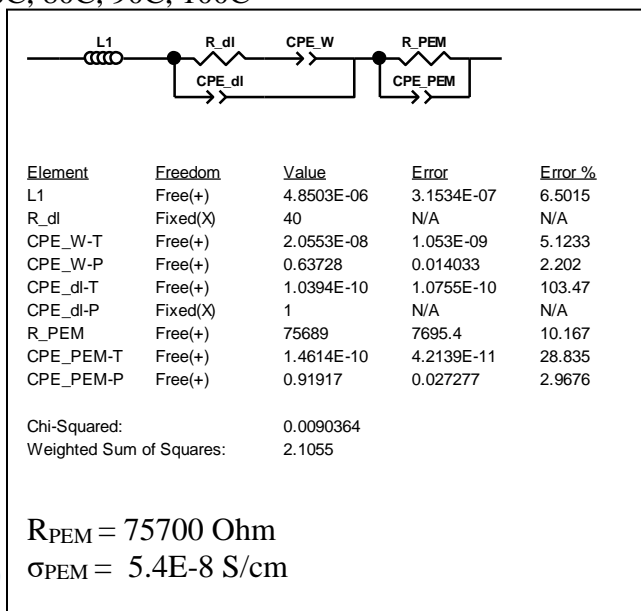
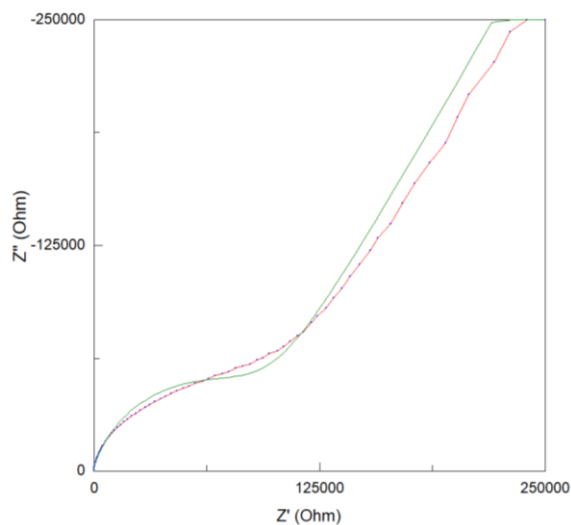


Figure A.4- EIS 2-point probe analysis of sample 3M 825EW Control acid treated with 5% HNO₃ at 80C fit with an equivalent circuit model (left) Nyquist Plot (right) equivalent circuit model fit

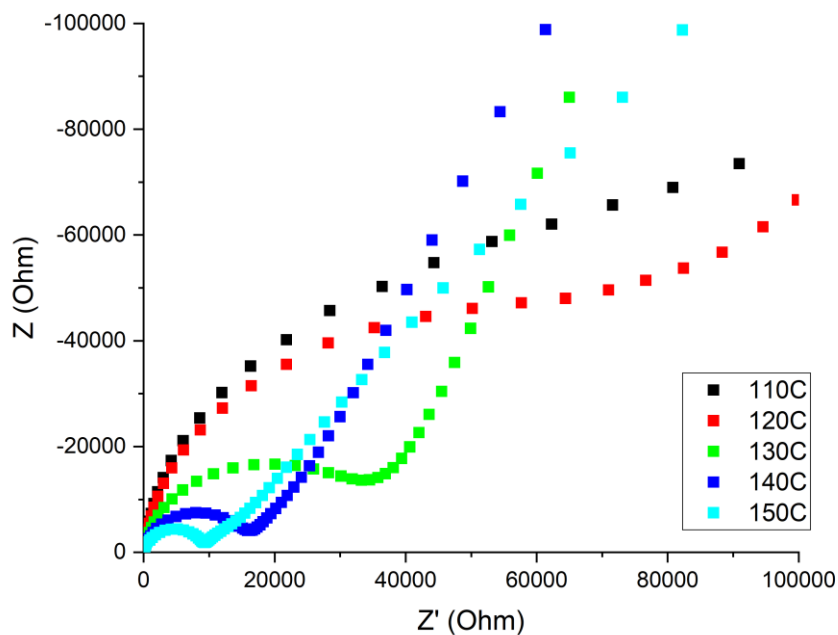


Figure A.5-Nyquist Plot of EIS 2-point probe analysis of sample 3M 825EW Control acid treated with 5% HNO₃ variable temperature 110C, 120C, 130C, 140C, 150C

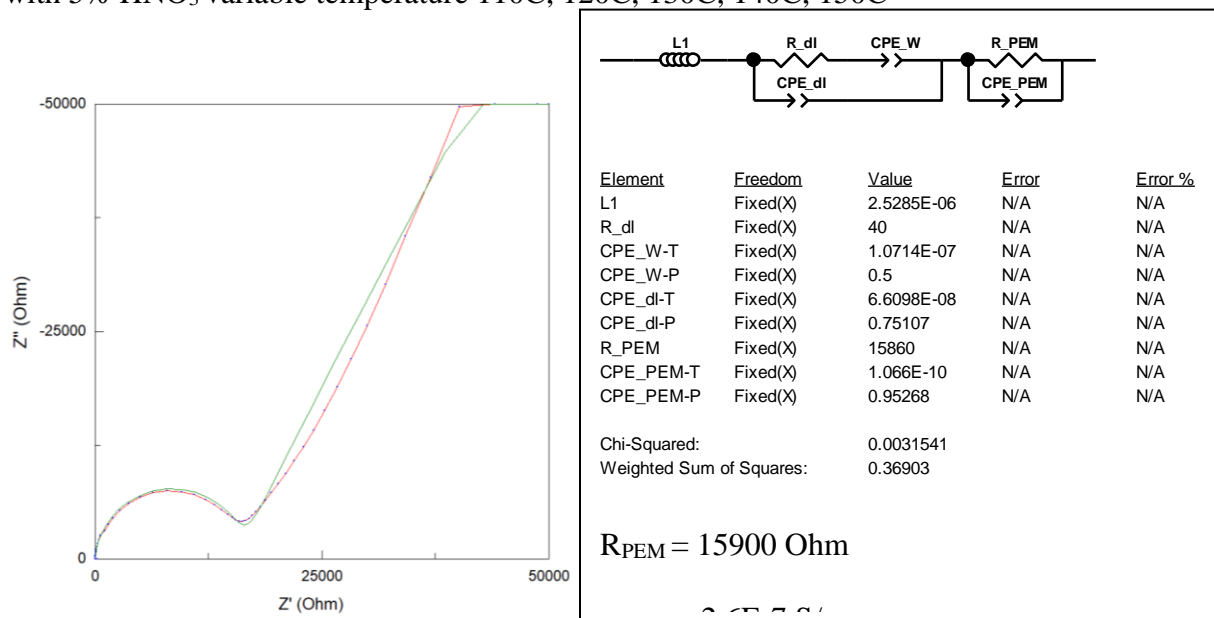


Figure A.6- EIS 2-point probe analysis of sample 3M 825EW Control acid treated with 5% HNO₃ at 140C fit with an equivalent circuit model (left) Nyquist Plot (right) equivalent circuit model fit

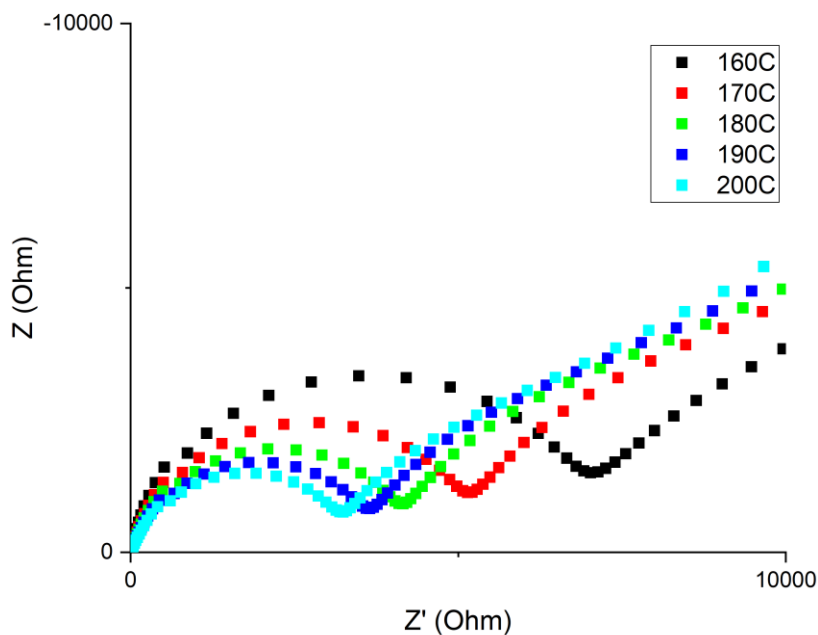


Figure A.7-Nyquist Plot of EIS 2-point probe analysis of sample 3M 825EW Control acid treated with 5% HNO₃ variable temperature 160C, 170C, 180C, 190C, 200C

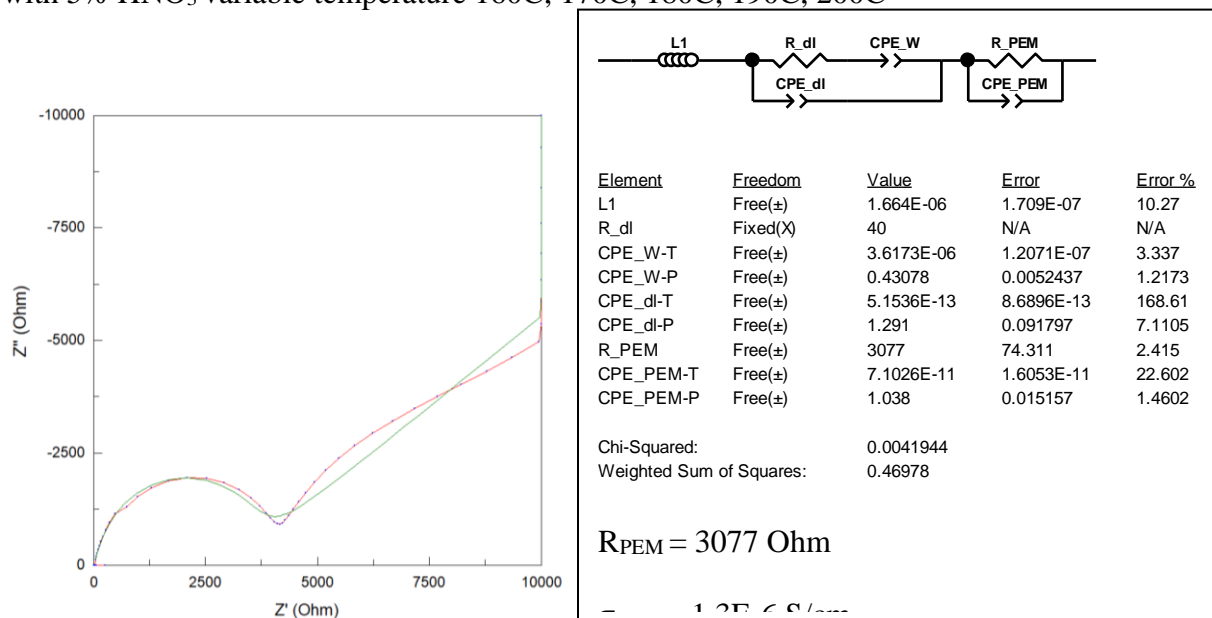


Figure A.8- EIS 2-point probe analysis of sample 3M 825EW Control acid treated with 5% HNO₃ at 180C fit with an equivalent circuit model (left) Nyquist Plot (right) equivalent circuit model fit

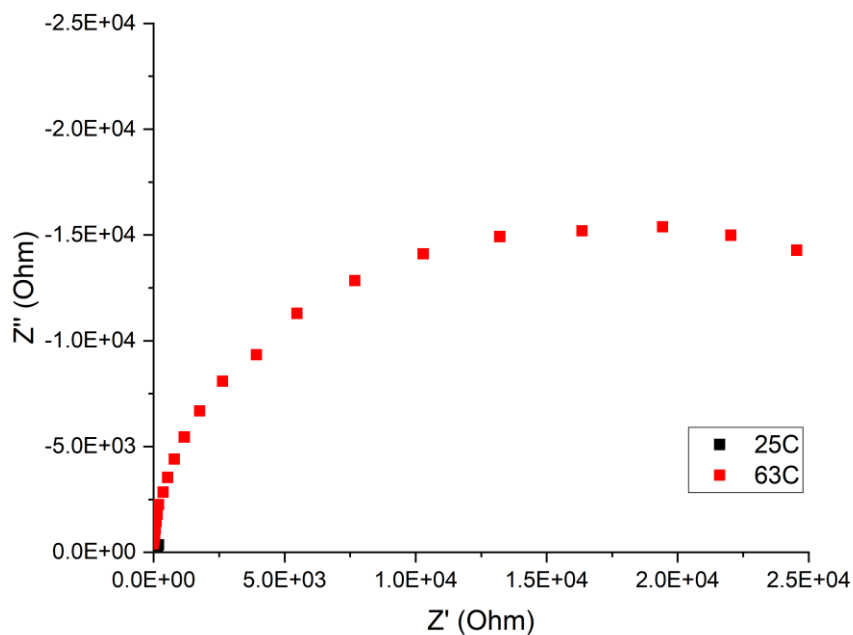


Figure A.9-Nyquist Plot of EIS 2-point probe analysis of sample 8122016FEP-12 grafted with 5-vinylpyridine and acid treated with 5% HNO_3 variable temperature 25C, 63C

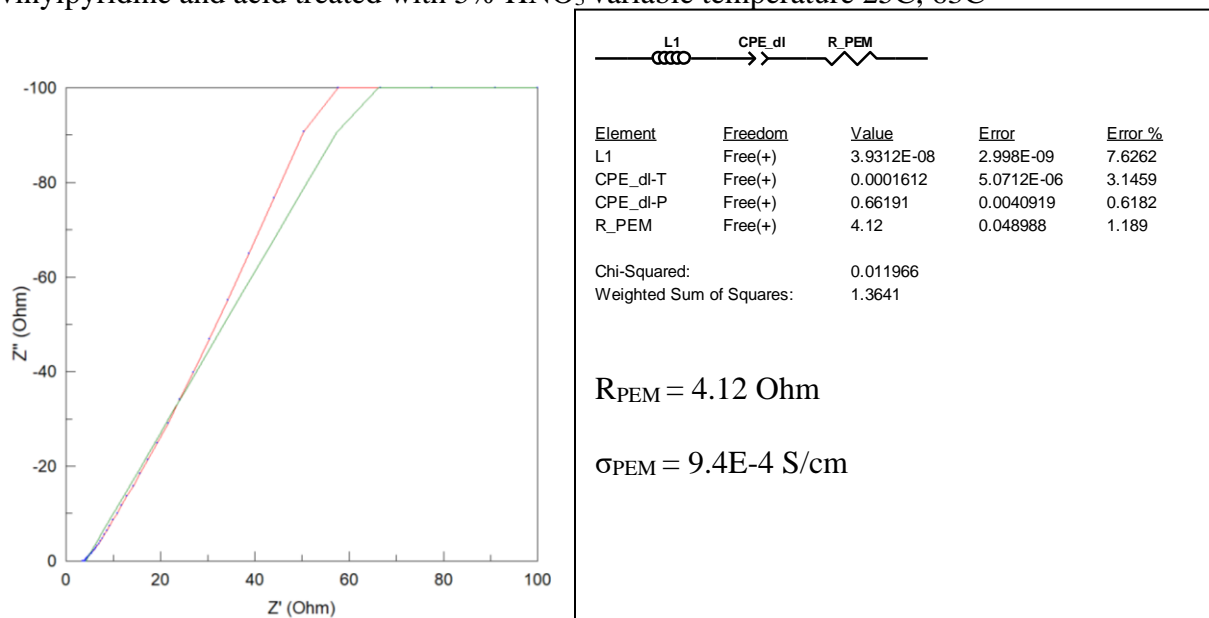


Figure A.10- EIS 2-point probe analysis of sample 8122016FEP-12 grafted with 5-vinylpyridine and acid treated with 5% HNO_3 at 25C fit with an equivalent circuit model (left) Nyquist Plot (right) equivalent circuit model fit

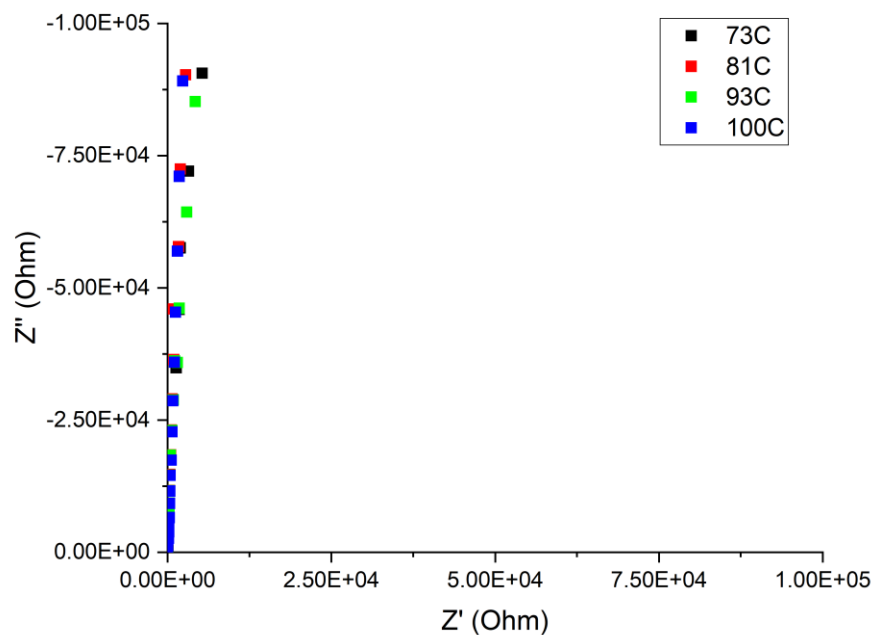


Figure A.11-Nyquist Plot of EIS 2-point probe analysis of sample 8122016FEP-12 grafted with 5-vinylpyridine and acid treated with 5% HNO_3 variable temperature 73C, 81C, 93C, 100C

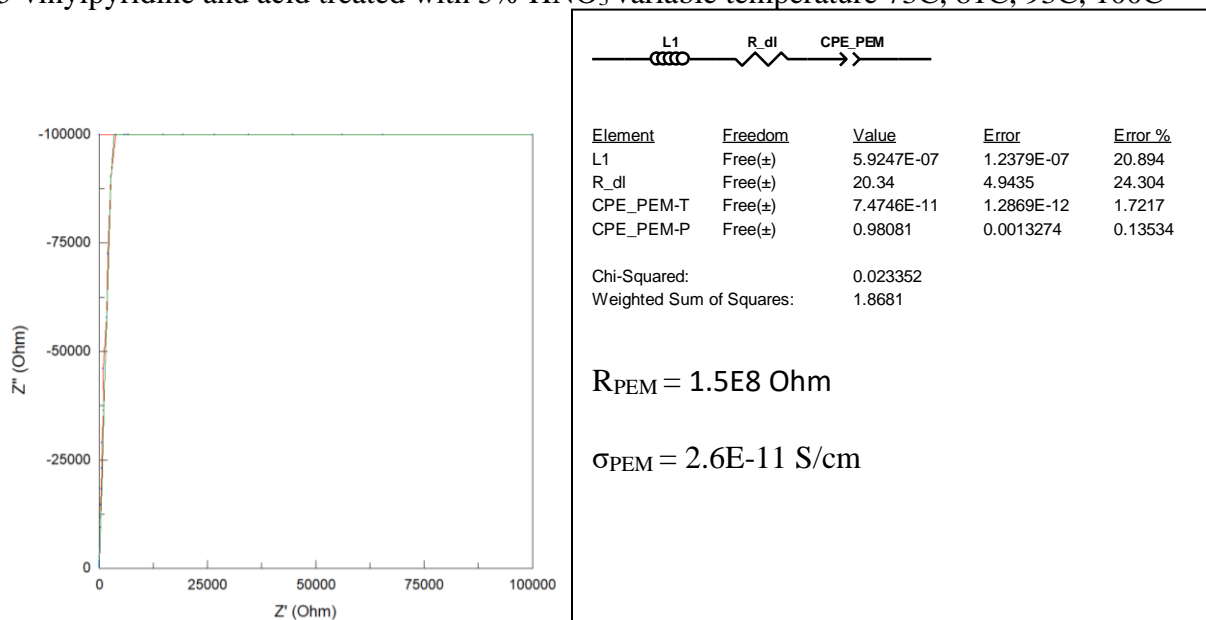


Figure A.12- EIS 2-point probe analysis of sample 8122016FEP-12 grafted with 5-vinylpyridine and acid treated with 5% HNO_3 at 81C fit with an equivalent circuit model (left) Nyquist Plot (right) equivalent circuit model fit

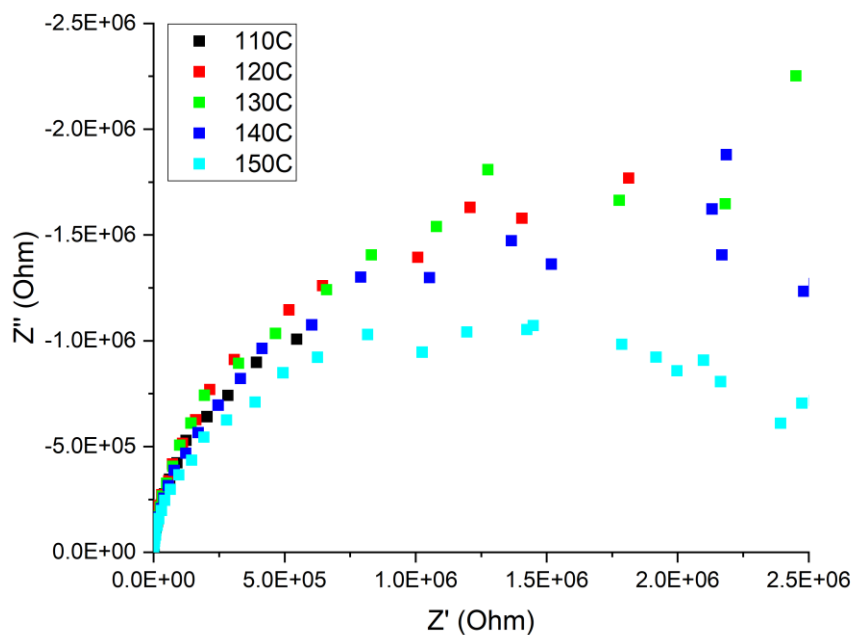


Figure A.13-Nyquist Plot of EIS 2-point probe analysis of sample 8122016FEP-12 grafted with 5-vinylpyridine and acid treated with 5% HNO_3 variable temperature 110C, 120C, 130C, 140C, 150C

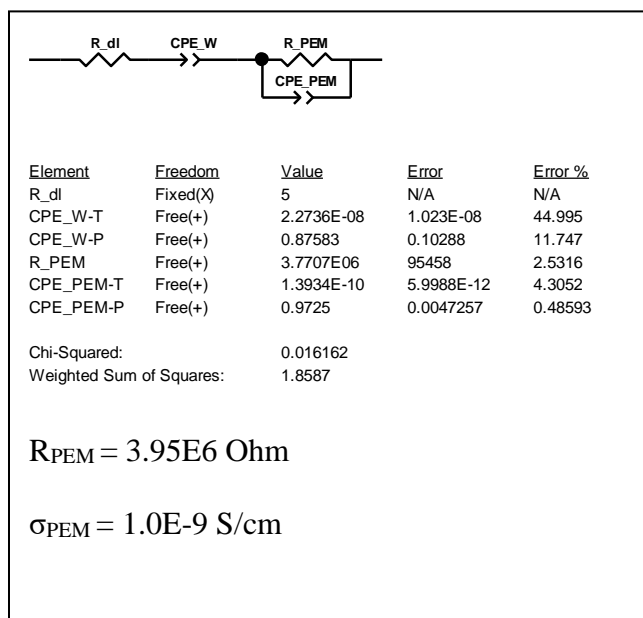
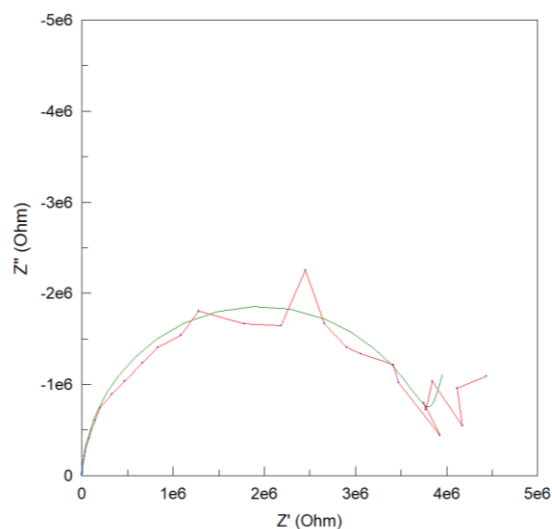


Figure A.14- EIS 2-point probe analysis of sample 8122016FEP-12 grafted with 5-vinylpyridine and acid treated with 5% HNO_3 at 130C fit with an equivalent circuit model (left) Nyquist Plot (right) equivalent circuit model fit

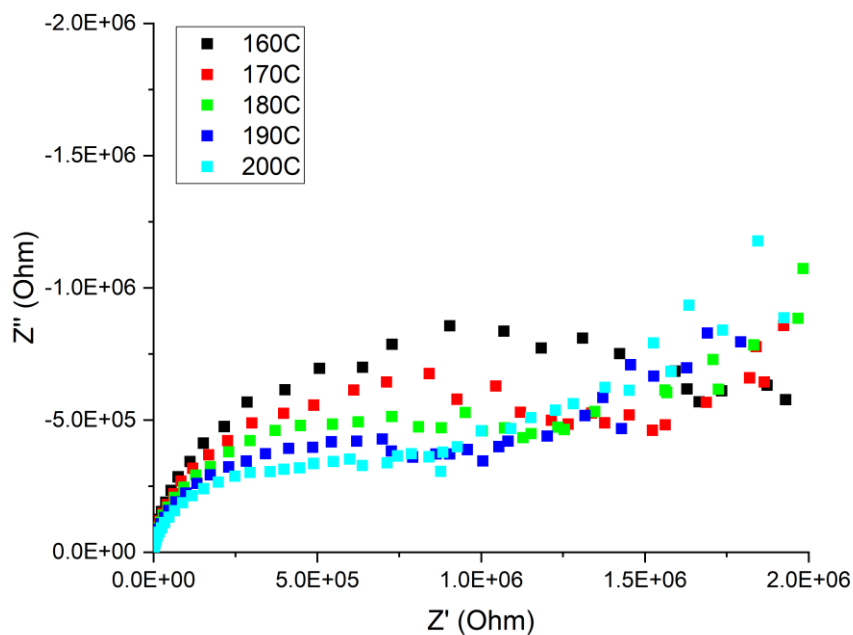


Figure A.15-Nyquist Plot of EIS 2-point probe analysis of sample 8122016FEP-12 grafted with 5-vinylpyridine and acid treated with 5% HNO_3 variable temperature 160C, 170C, 180C, 190C, 200C

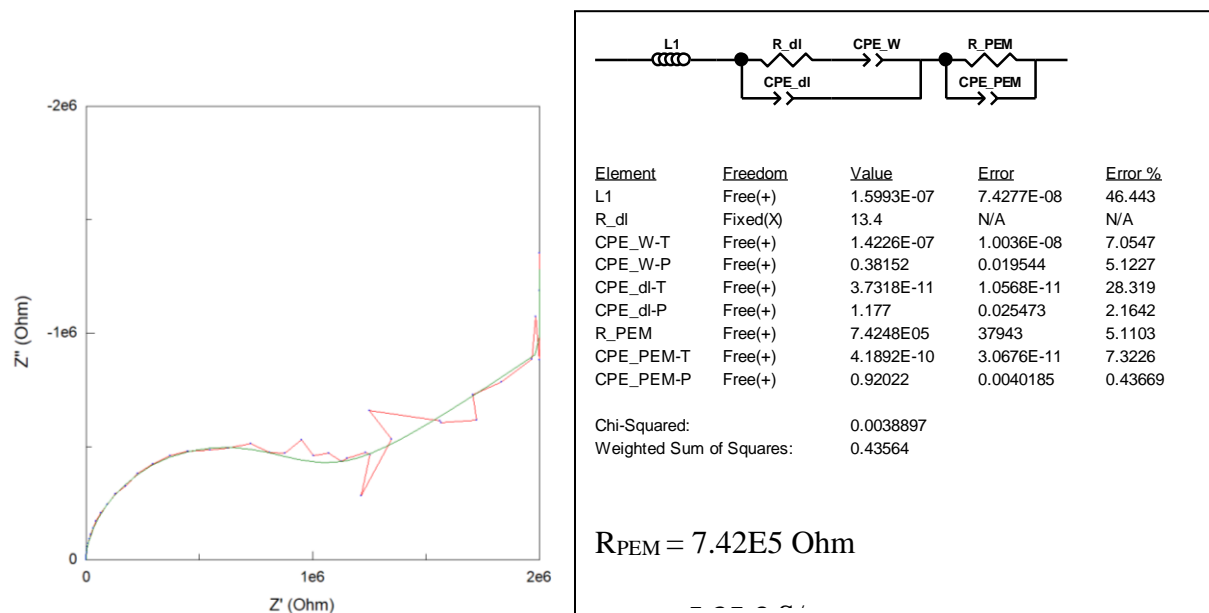


Figure A.16- EIS 2-point probe analysis of sample 8122016FEP-12 grafted with 5-vinylpyridine and acid treated with 5% HNO_3 at 180C fit with an equivalent circuit model (left) Nyquist Plot (right) equivalent circuit model fit

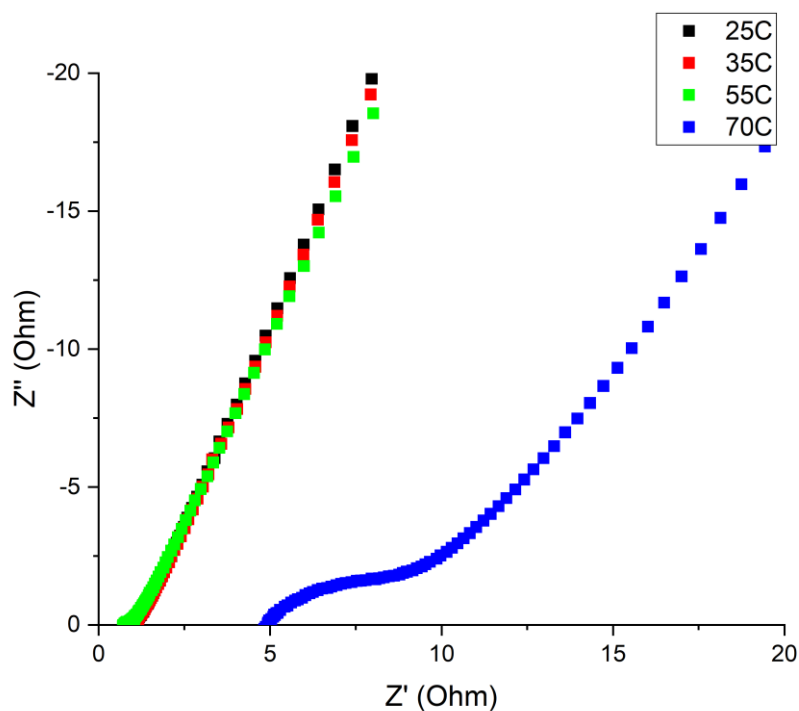


Figure A.17-Nyquist Plot of EIS 2-point probe analysis of sample 8112016PCTFE-12 grafted with 5-vinylpyridine and acid treated with 5% HNO_3 variable temperature 25C 35C 55C 70C

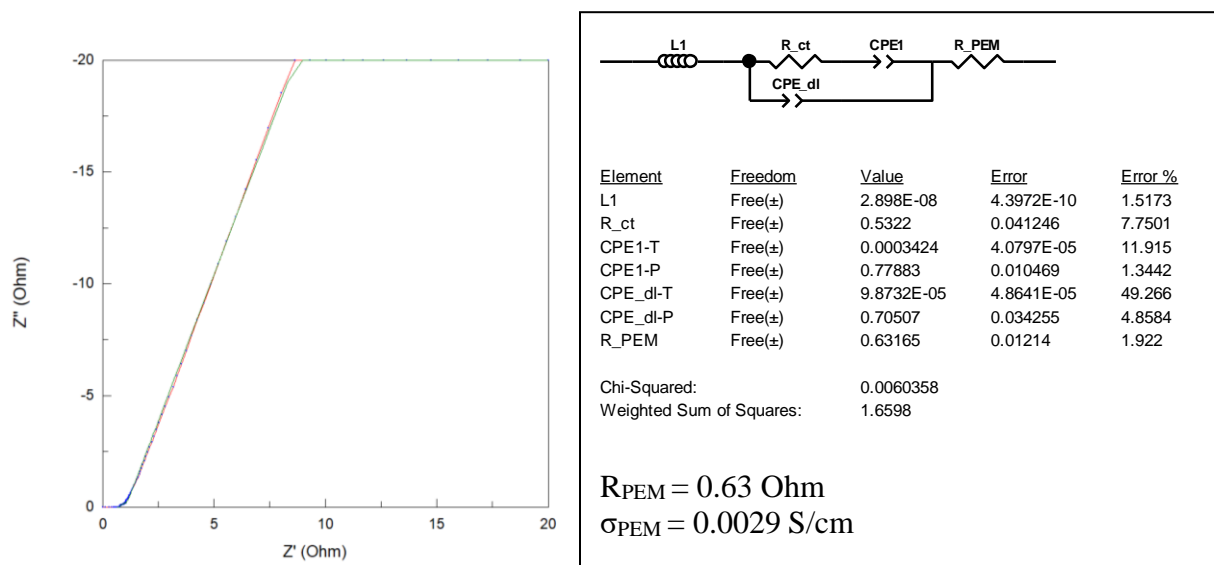


Figure A.18- EIS 2-point probe analysis of sample 8112016PCTFE-12 grafted with 5-vinylpyridine and acid treated with 5% HNO_3 at 55C fit with an equivalent circuit model (left) Nyquist Plot (right) equivalent circuit model fit

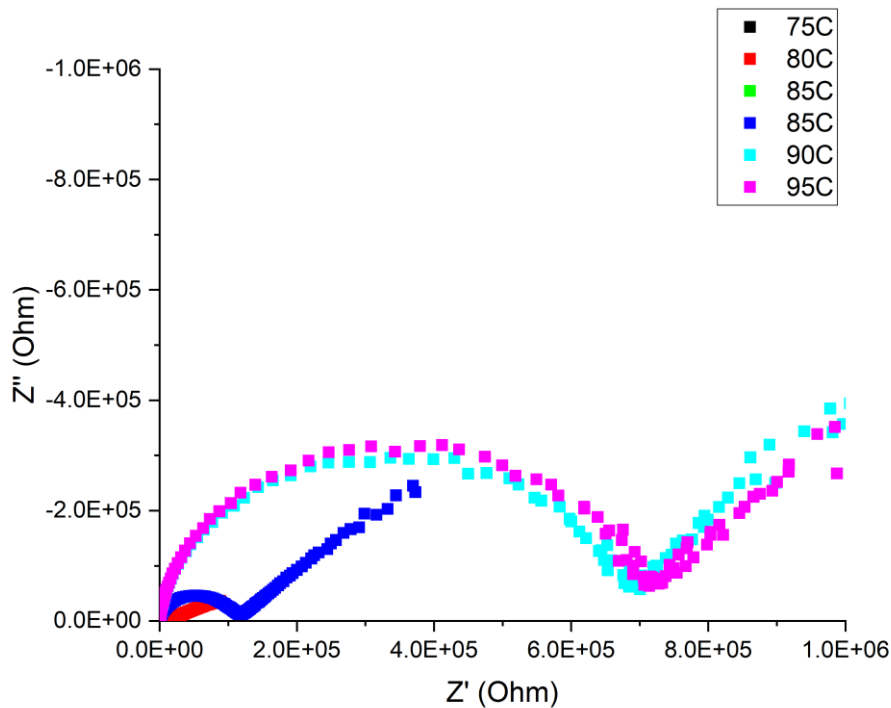
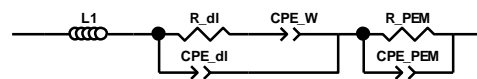
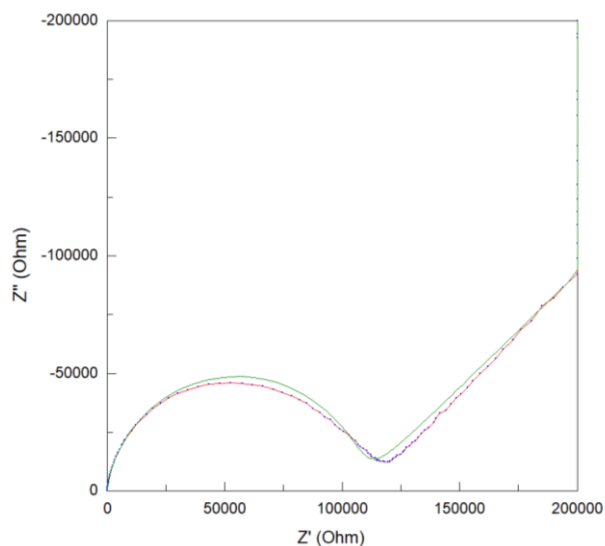


Figure A.19-Nyquist Plot of EIS 2-point probe analysis of sample 8112016PCTFE-12 grafted with 5-vinylpyridine and acid treated with 5% HNO_3 variable temperature 75C, 80C, 85C, 90C, 95C



Element	Freedom	Value	Error	Error %
L1	Free(±)	2.533E-07	8.8128E-08	34.792
R_dl	Fixed(X)	18	N/A	N/A
CPE_W-T	Free(±)	1.1775E-06	1.1378E-08	0.96628
CPE_W-P	Free(±)	0.49201	0.0029079	0.59102
CPE_dl-T	Free(±)	3.5236E-12	3.5157E-12	99.776
CPE_dl-P	Free(±)	1.344	0.065745	4.8917
R_PEM	Free(±)	1.0507E05	401.8	0.38241
CPE_PEM-T	Free(±)	1.5787E-10	3.8766E-12	2.4556
CPE_PEM-P	Free(±)	0.92731	0.0017972	0.19381

Chi-Squared: 0.0013078
Weighted Sum of Squares: 0.35833

$$R_{PEM} = 1.05E5 \text{ Ohm}$$

$$\sigma_{PEM} = 3.51E-8 \text{ S/cm}$$

Figure A.20- EIS 2-point probe analysis of sample 8112016PCTFE-12 grafted with 5-vinylpyridine and acid treated with 5% HNO_3 at 85C fit with an equivalent circuit model (left) Nyquist Plot (right) equivalent circuit model fit

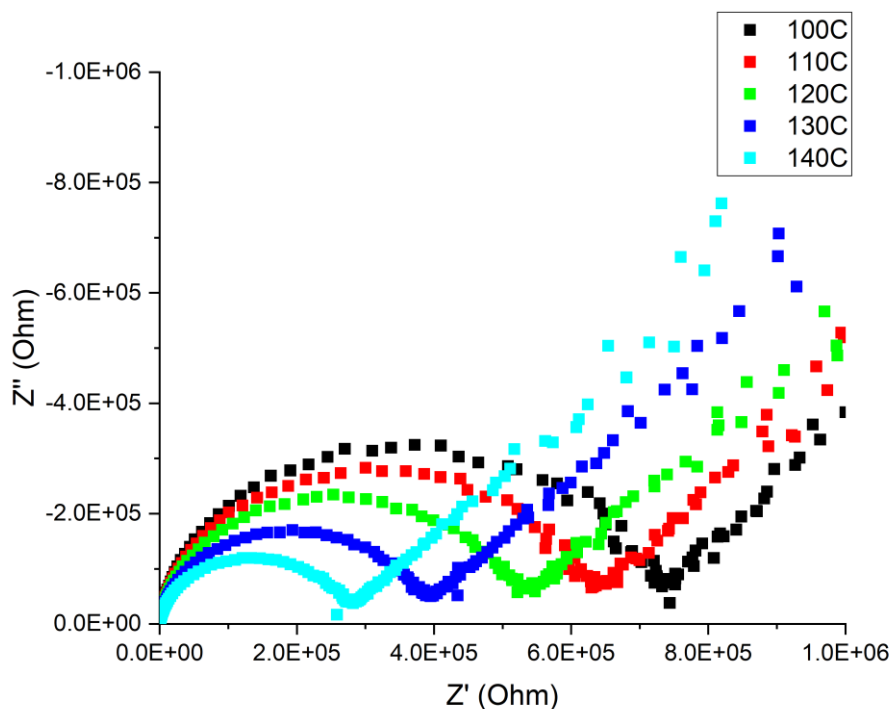


Figure A.21-Nyquist Plot of EIS 2-point probe analysis of sample 8112016PCTFE-12 grafted with 5-vinylpyridine and acid treated with 5% HNO_3 variable temperature 100C, 110C, 120C, 130C, 140C

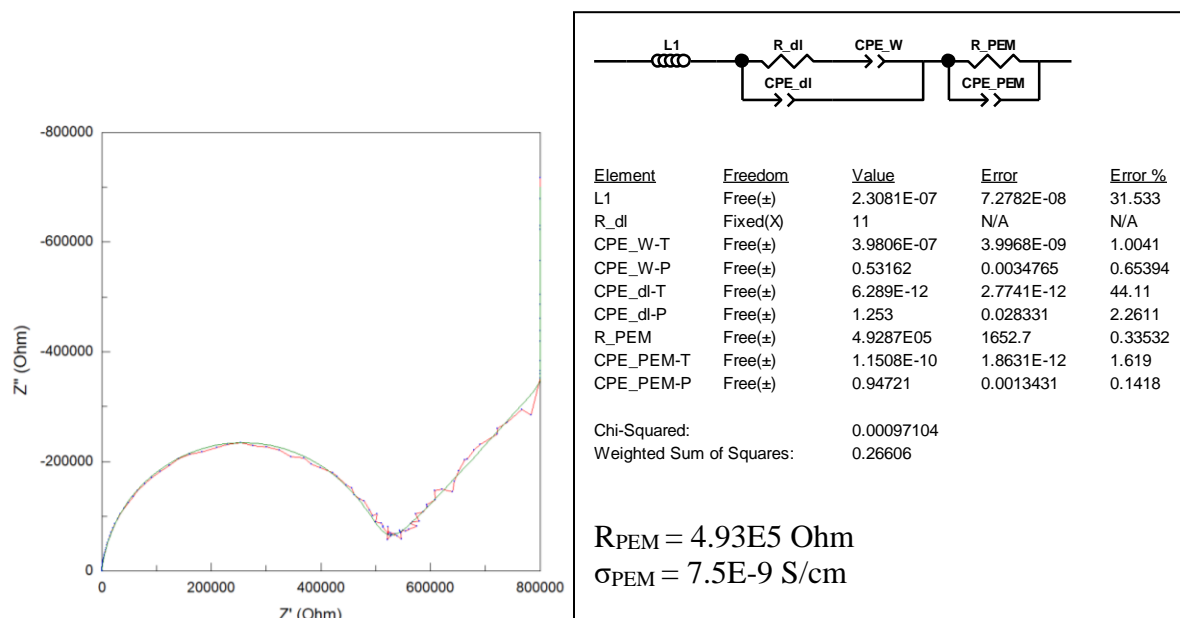


Figure A.22- EIS 2-point probe analysis of sample 8112016PCTFE-12 grafted with 5-vinylpyridine and acid treated with 5% HNO_3 at 120C fit with an equivalent circuit model (left) Nyquist Plot (right) equivalent circuit model fit

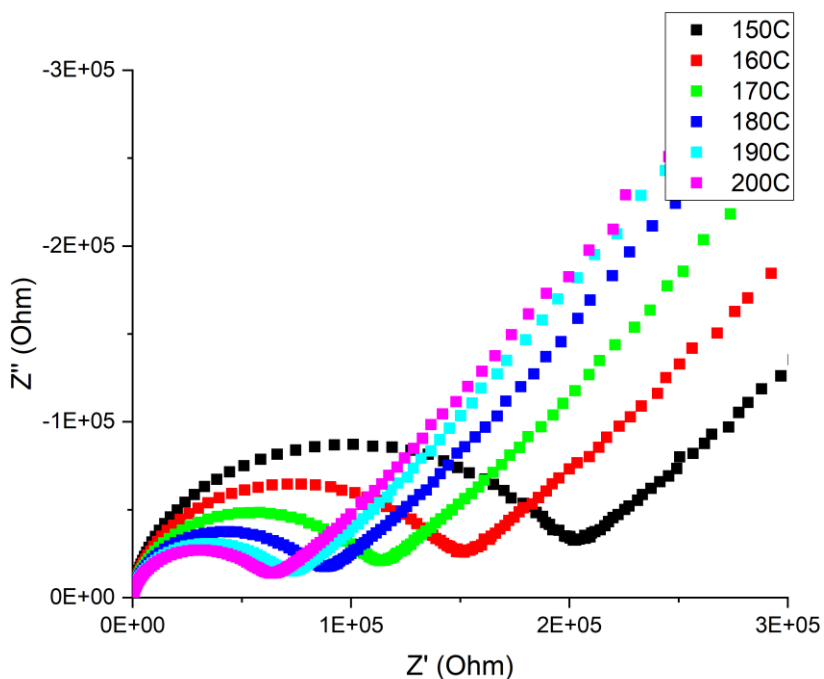


Figure A.23-Nyquist Plot of EIS 2-point probe analysis of sample 8112016PCTFE-12 grafted with 5-vinylpyridine and acid treated with 5% HNO_3 variable temperature 150C, 160C, 170C, 180C, 190C, 200C.

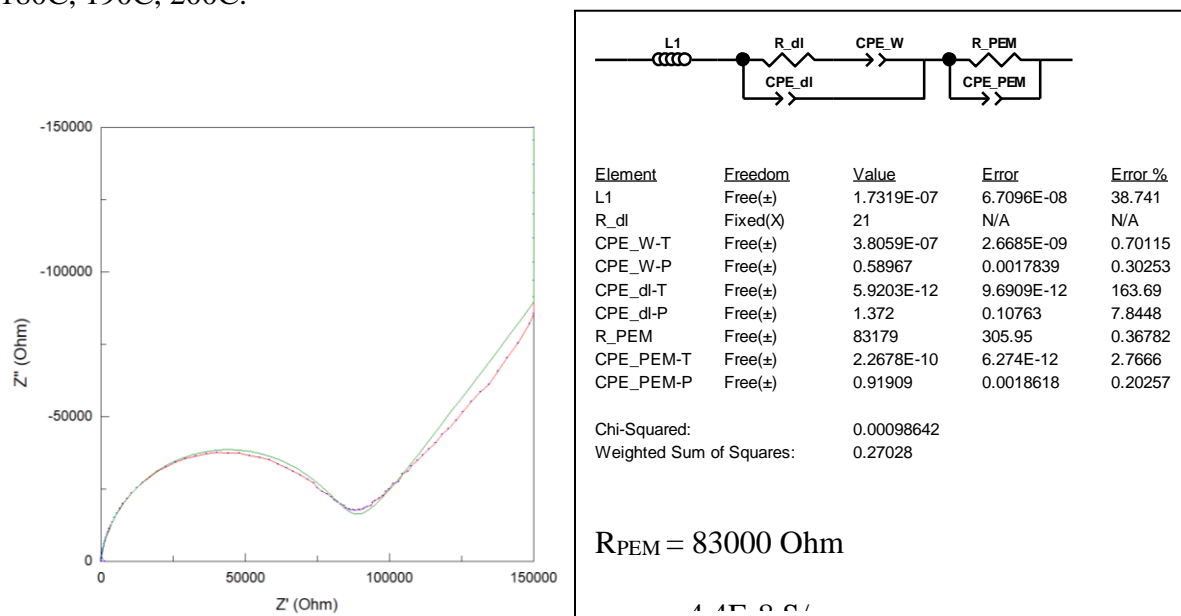


Figure A.24- EIS 2-point probe analysis of sample 8112016PCTFE-12 grafted with 5-vinylpyridine and acid treated with 5% HNO_3 at 180C fit with an equivalent circuit model (left) Nyquist Plot (right) equivalent circuit model fit

8122016PVF-12

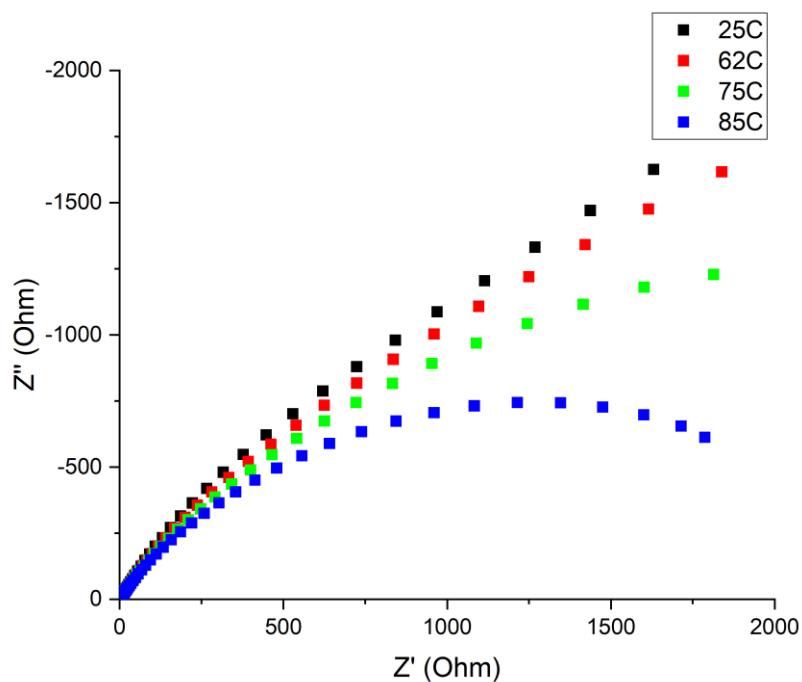


Figure A.25-Nyquist Plot of EIS 2-point probe analysis of sample 8122016PVF-12 grafted with 5-vinylpyridine and acid treated with 5% HNO₃ variable temperature 25C, 62C, 75C, 85C

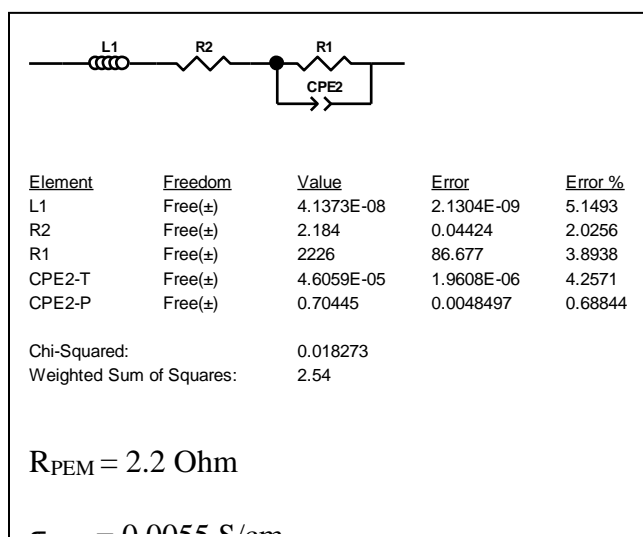
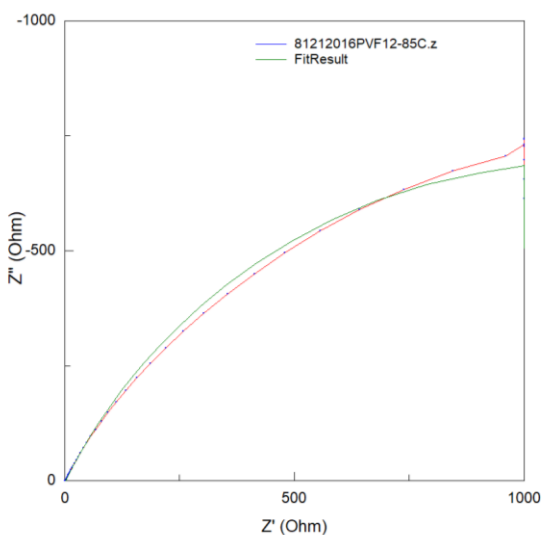


Figure A.26- EIS 2-point probe analysis of sample 81212016PVF-12 grafted with 5-vinylpyridine and acid treated with 5% HNO₃ at 85C fit with and equivalent circuit model (left) Nyquist Plot (right) equivalent circuit model fit

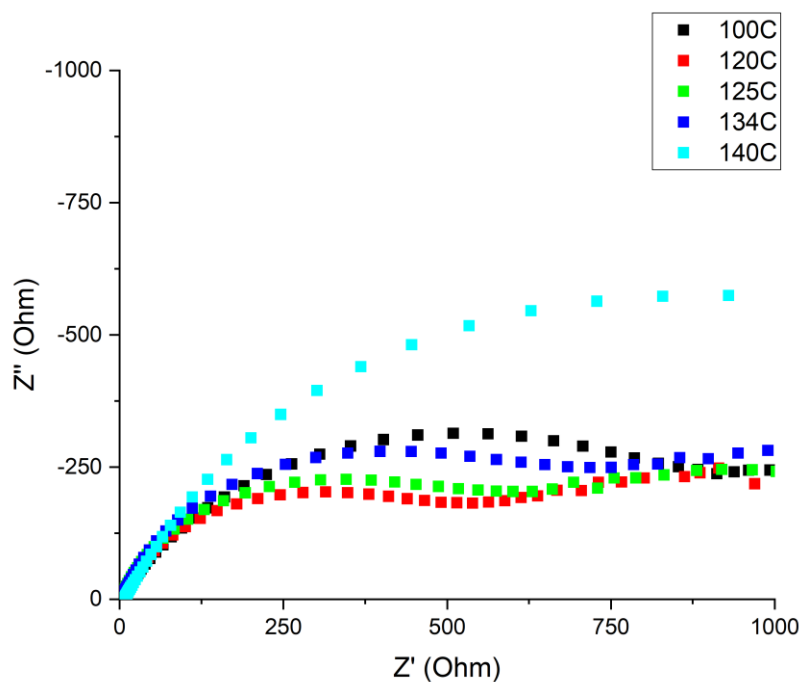


Figure A.27-Nyquist Plot of EIS 2-point probe analysis of sample 81212016PVF-12 grafted with 5-vinylpyridine and acid treated with 5% HNO₃ variable temperature 100C, 120C, 125C, 134C, 140C

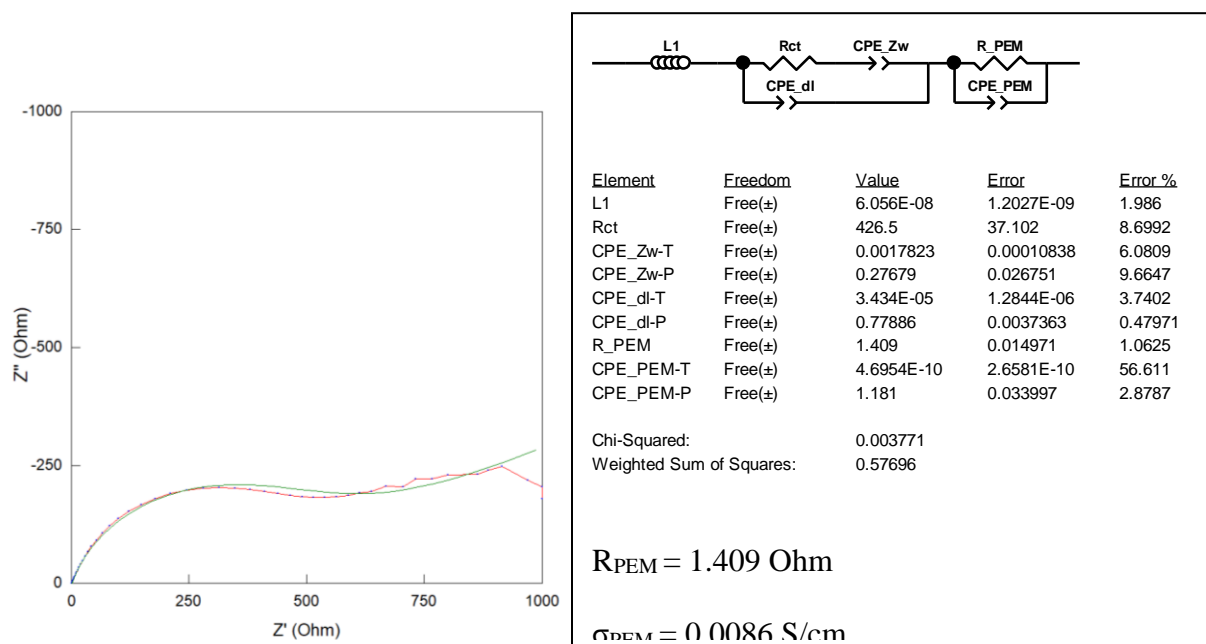


Figure A.28- EIS 2-point probe analysis of sample 81212016PVF-12 grafted with 5-vinylpyridine and acid treated with 5% HNO₃ at 120C fit with an equivalent circuit model (left) Nyquist Plot (right) equivalent circuit model fit

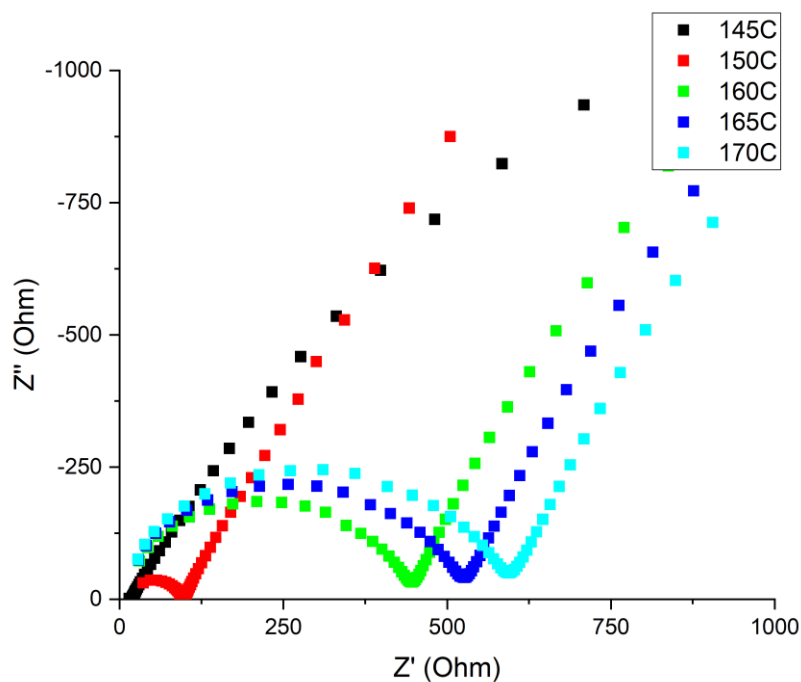


Figure A.29-Nyquist Plot of EIS 2-point probe analysis of sample 81212016PVF-12 grafted with 5-vinylpyridine and acid treated with 5% HNO₃ variable temperature 145C, 150C, 160C, 165C, 170C

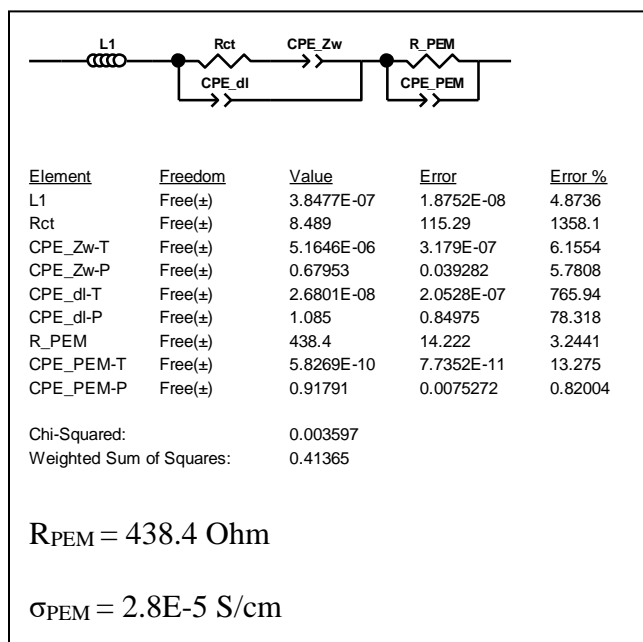
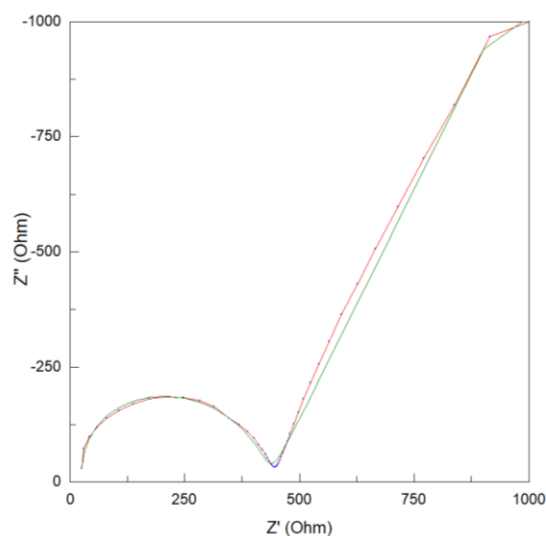


Figure A.30- EIS 2-point probe analysis of sample 81212016PVF-12 grafted with 5-vinylpyridine and acid treated with 5% HNO₃ at 160C fit with an equivalent circuit model (left) Nyquist Plot (right) equivalent circuit model fit

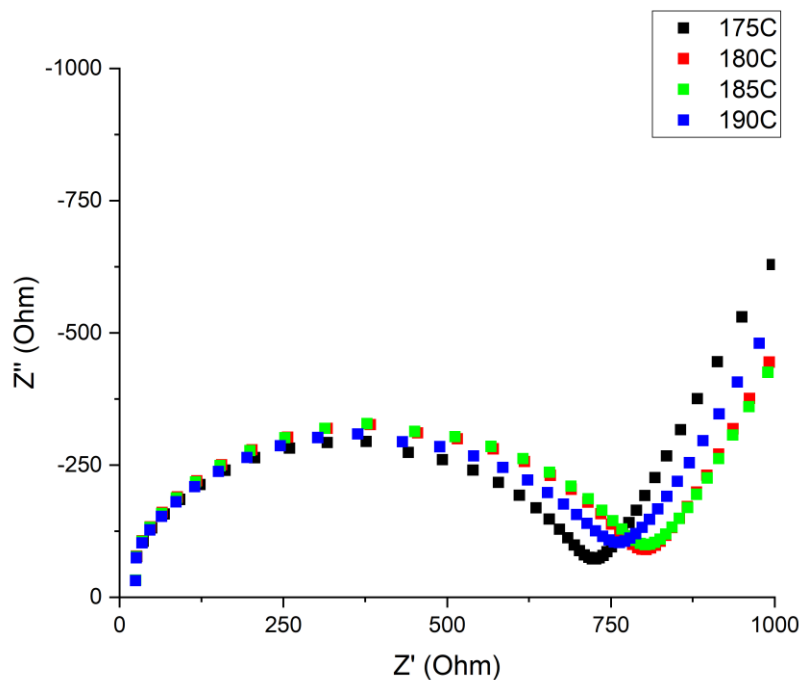
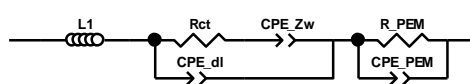
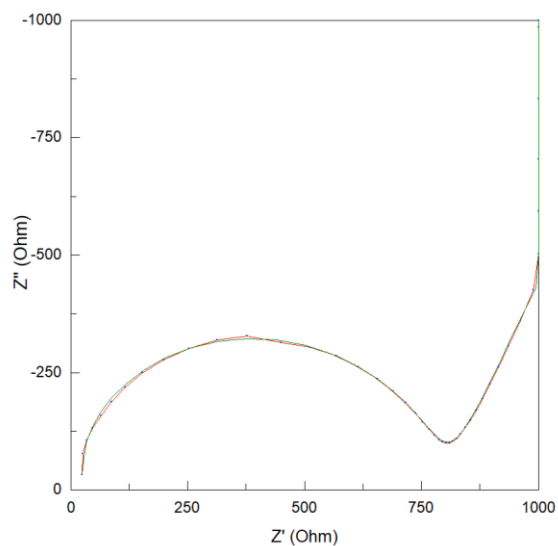


Figure A.31-Nyquist Plot of EIS 2-point probe analysis of sample 81212016PVF-12 grafted with 5-vinylpyridine and acid treated with 5% HNO₃ variable temperature 175C, 180C, 185C, 190C



Element	Freedom	Value	Error	Error %
L1	Free(±)	9.8858E-07	3.5097E-08	3.5502
Rct	Free(±)	24.6	1.5355	6.2419
CPE_Zw-T	Free(±)	1.0675E-06	6.8726E-08	6.438
CPE_Zw-P	Free(±)	0.77464	0.0070252	0.9069
CPE_dl-T	Free(±)	2.4693E-06	1.7544E-07	7.1048
CPE_dl-P	Free(±)	0.5166	0.0052962	1.0252
R_PEM	Free(±)	831.2	4.431	0.53308
CPE_PEM-T	Free(±)	2.4794E-09	1.9974E-10	8.056
CPE_PEM-P	Free(±)	0.82768	0.0051587	0.62327

Chi-Squared: 0.00061456
Weighted Sum of Squares: 0.070675

$$R_{PEM} = 831.2 \text{ Ohm}$$

$$\sigma_{PEM} = 1.5E-5 \text{ S/cm}$$

Figure A.32- EIS 2-point probe analysis of sample 81212016PVF-12 grafted with 5-vinylpyridine and acid treated with 5% HNO₃ at 185C fit with an equivalent circuit model (left) Nyquist Plot (right) equivalent circuit model fit

PCB 2-Point Probe Summary

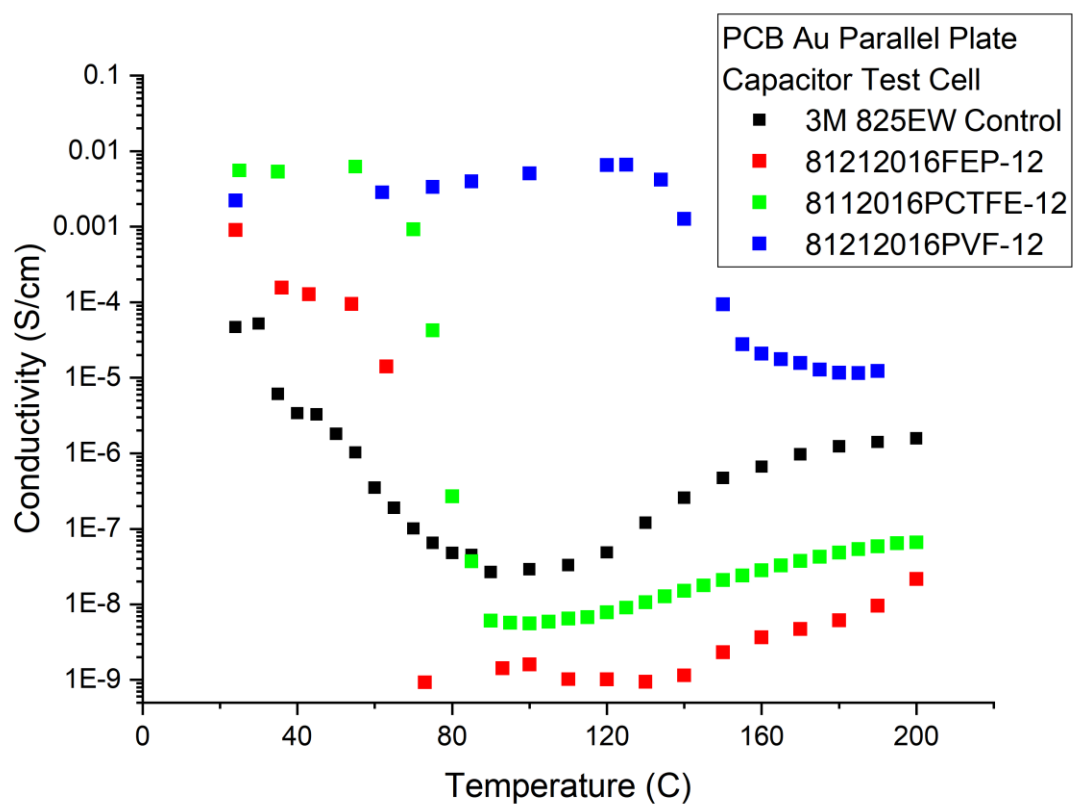


Figure A.34-EIS proton conductivity vs. temperature PCB 2-Point Parallel Plate Capacitor Test Cell: (black) 3M 825EW Control, 4-vinylpyridine PEM: (red) 81212016FEP-12, (green) 8112016PCTFE-12, (blue) 81212016PVF-12; samples were acid treated with 5% HNO_3 , $n = 1$

Au 2-Point Probe Analysis
3M 825EW Control

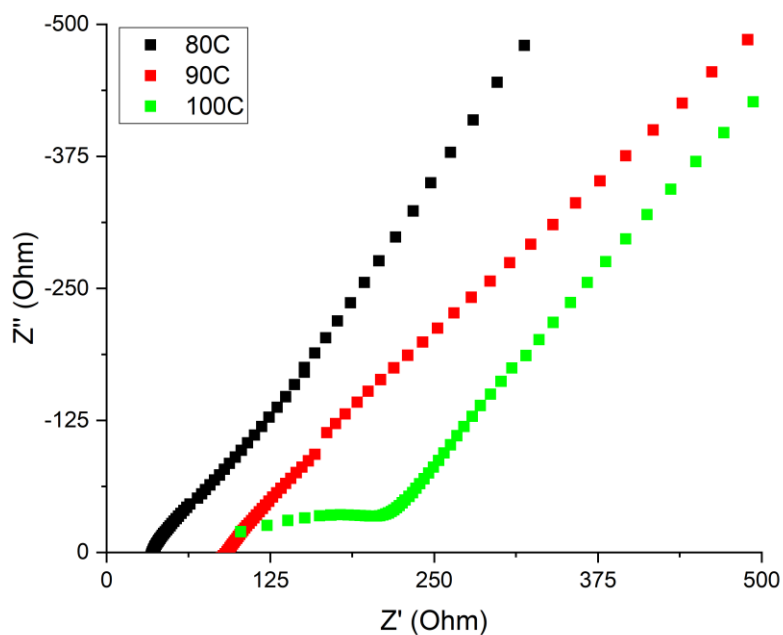


Figure B.1-Nyquist Plot of EIS 2-point probe analysis of sample 3M 825EW Control acid treated with 5% HNO₃ variable temperature 80C, 90C, 100C

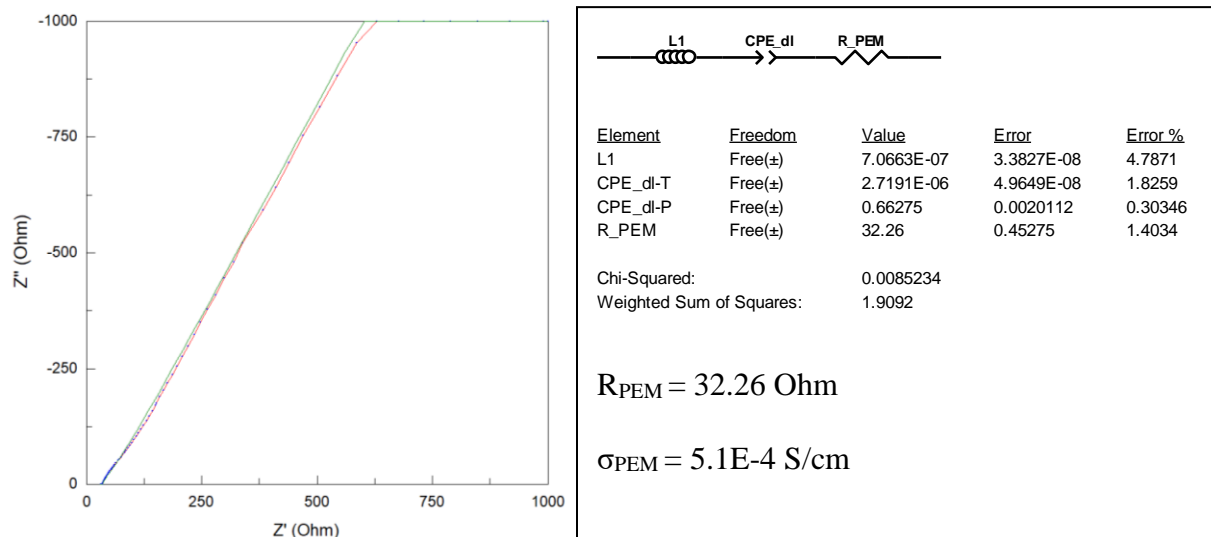


Figure B.2- EIS Au 2-point probe analysis of sample 3M 825EW Control acid treated with 5% HNO₃ at 80C fit with an equivalent circuit model (left) Nyquist Plot (right) equivalent circuit model fit

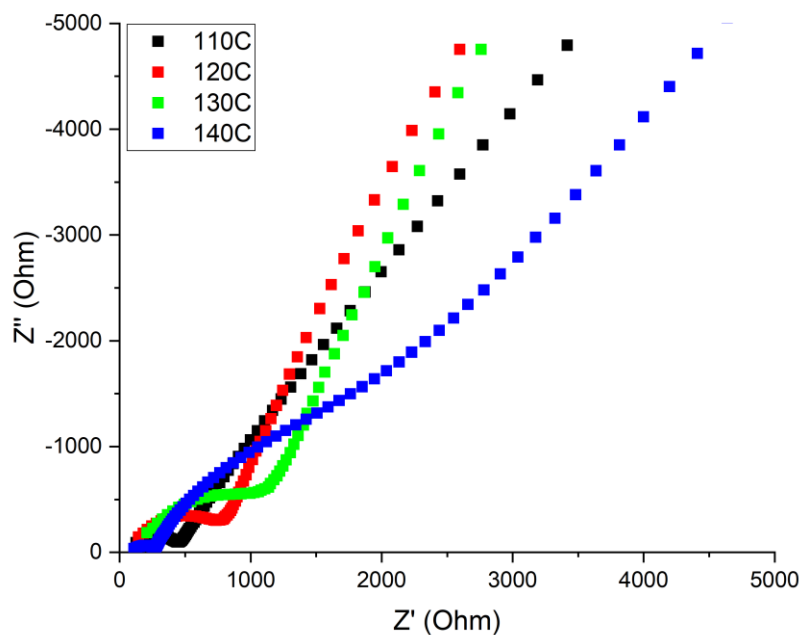


Figure B.3-Nyquist Plot of EIS Au 2-point probe analysis of sample 3M 825EW Control acid treated with 5% HNO₃ variable temperature 110C, 120C, 130C, 140C

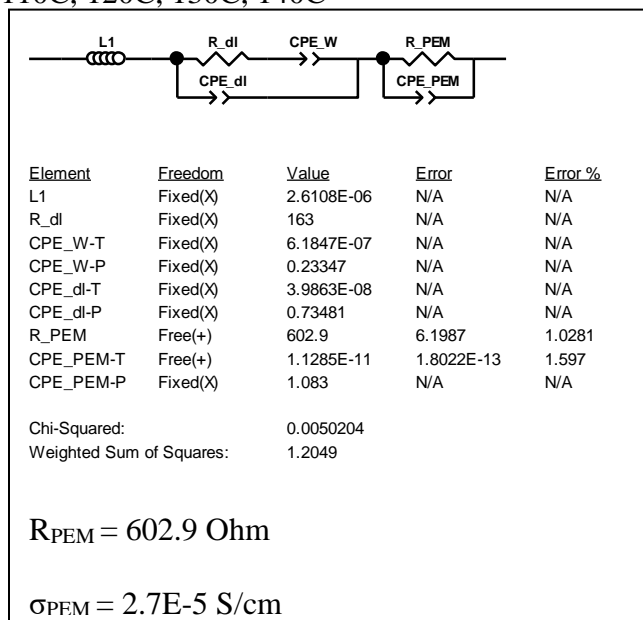
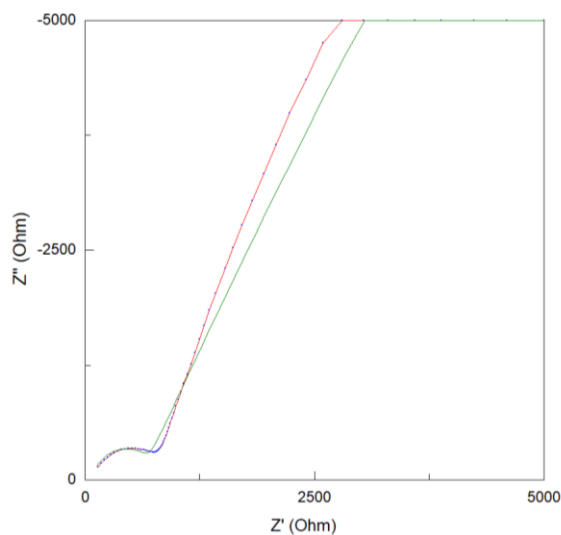


Figure B.4- EIS Au 2-point probe analysis of sample 3M 825EW Control acid treated with 5% HNO₃ at 120C fit with an equivalent circuit model (left) Nyquist Plot (right) equivalent circuit model fit

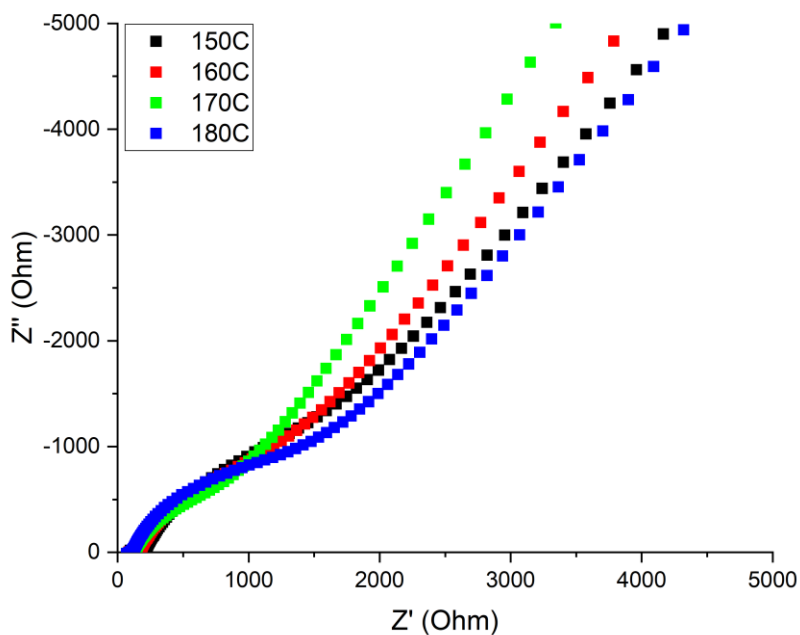


Figure B.5-Nyquist Plot of EIS Au 2-point probe analysis of sample 3M 825EW Control acid treated with 5% HNO₃ variable temperature 150C, 160C, 170C, 180C

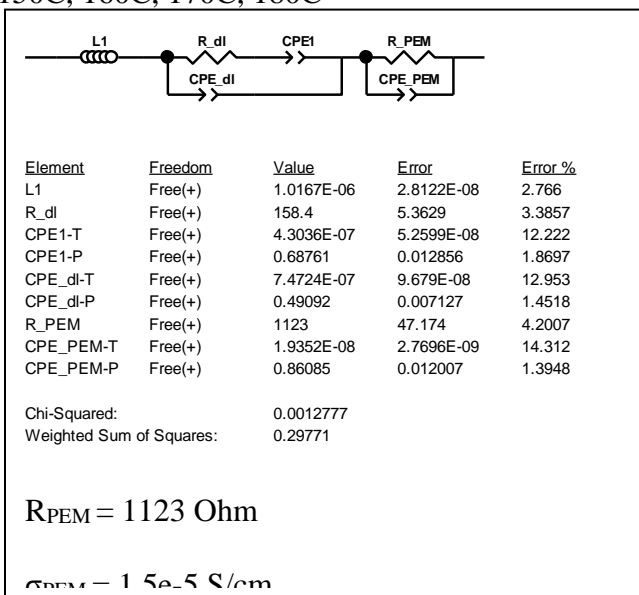
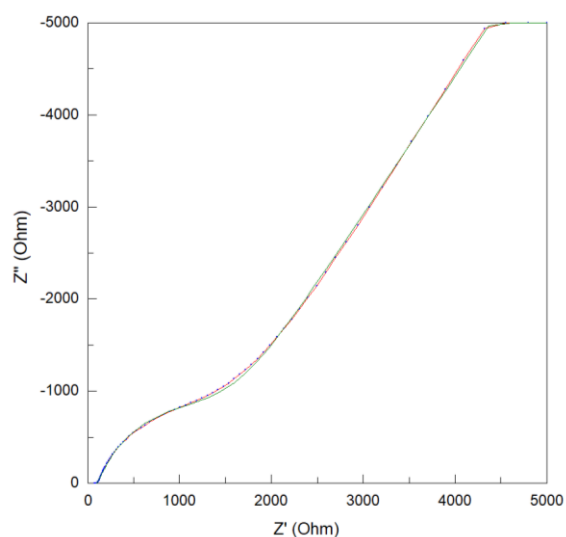


Figure B.6- EIS Au 2-point probe analysis of sample 3M 825EW Control acid treated with 5% HNO₃ at 180C fit with an equivalent circuit model (left) Nyquist Plot (right) equivalent circuit model fit

9102018FEP-13

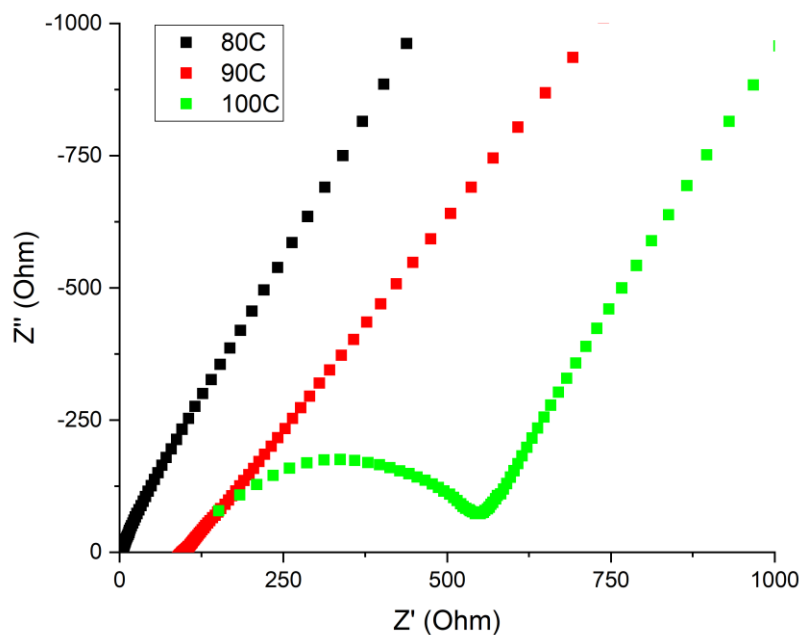
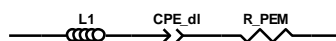
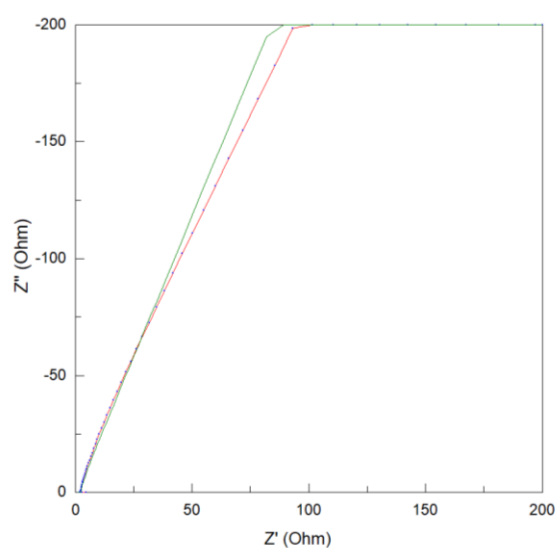


Figure B.7-Nyquist Plot of EIS Au 2-point probe analysis of sample 9102018FEP-13 grafted with 5-vinylpyridine and acid treated with 5% HNO_3 variable temperature 80C, 90C, 100C



Element	Freedom	Value	Error	Error %
L1	Free(+)	9.3299E-07	1.1915E-08	1.2771
CPE_dl-T	Free(+)	3.0979E-06	6.5255E-08	2.1064
CPE_dl-P	Free(+)	0.74957	0.0020763	0.277
R_PEM	Free(+)	0.83204	0.064181	7.7137

Chi-Squared: 0.016255
Weighted Sum of Squares: 3.7711

$$R_{\text{PEM}} = 0.83 \text{ Ohm}$$

$$\sigma_{\text{PEM}} = 0.023 \text{ S/cm}$$

Figure B.8- EIS Au 2-point probe analysis of sample 9102018FEP-13 grafted with 5-vinylpyridine and acid treated with 5% HNO_3 at 90C fit with an equivalent circuit model (left) Nyquist Plot (right) equivalent circuit model fit

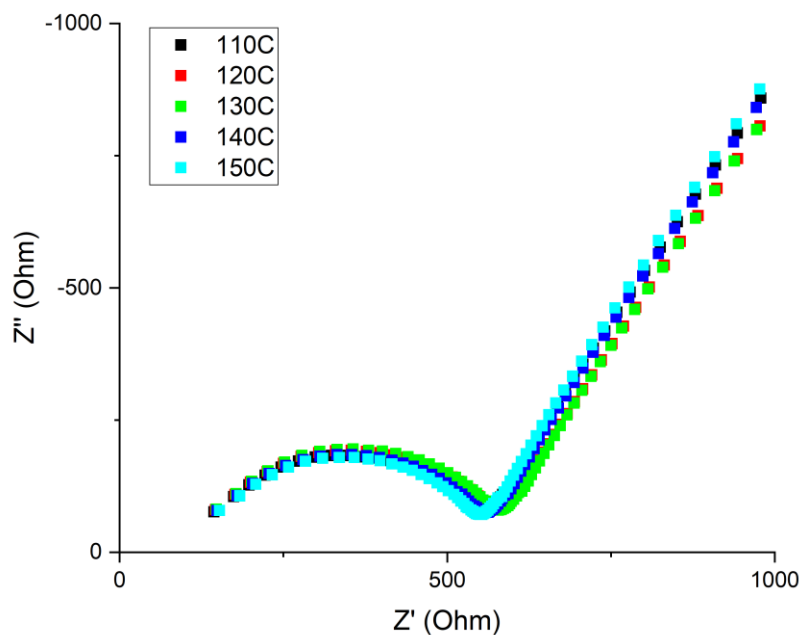


Figure B.9-Nyquist Plot of EIS Au 2-point probe analysis of sample 9102018FEP-13 grafted with 5-vinylpyridine and acid treated with 5% HNO_3 variable temperature 110C, 120C, 130C, 140C, 150C

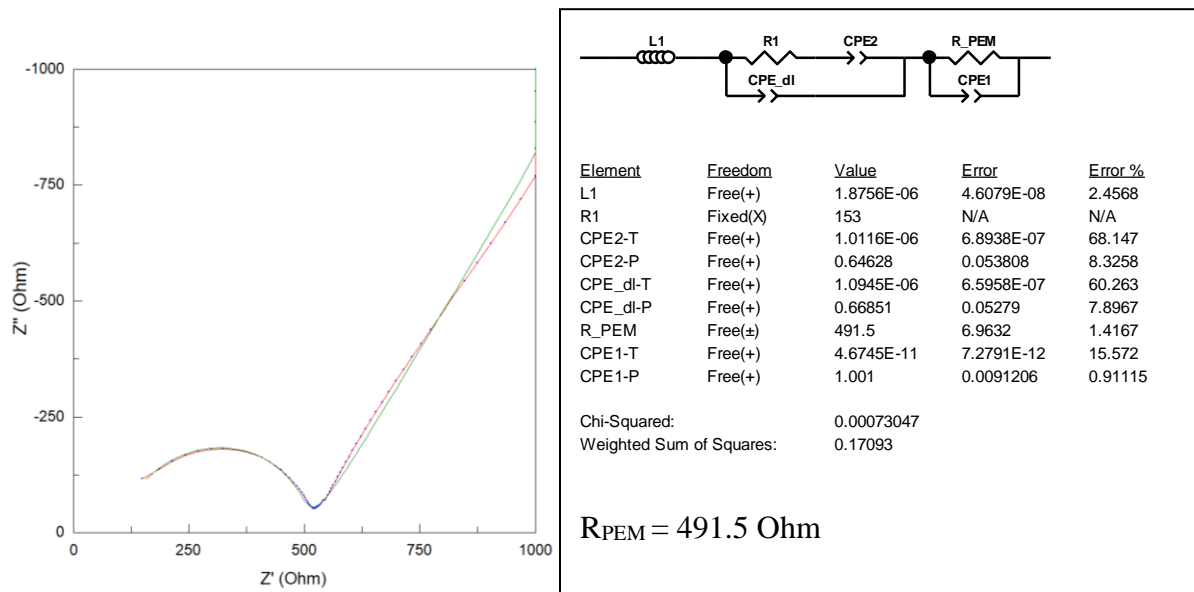


Figure B.10- EIS Au 2-point probe analysis of sample 9102018FEP-13 grafted with 5-vinylpyridine and acid treated with 5% HNO_3 at 130C fit with an equivalent circuit model (left) Nyquist Plot (right) equivalent circuit model fit

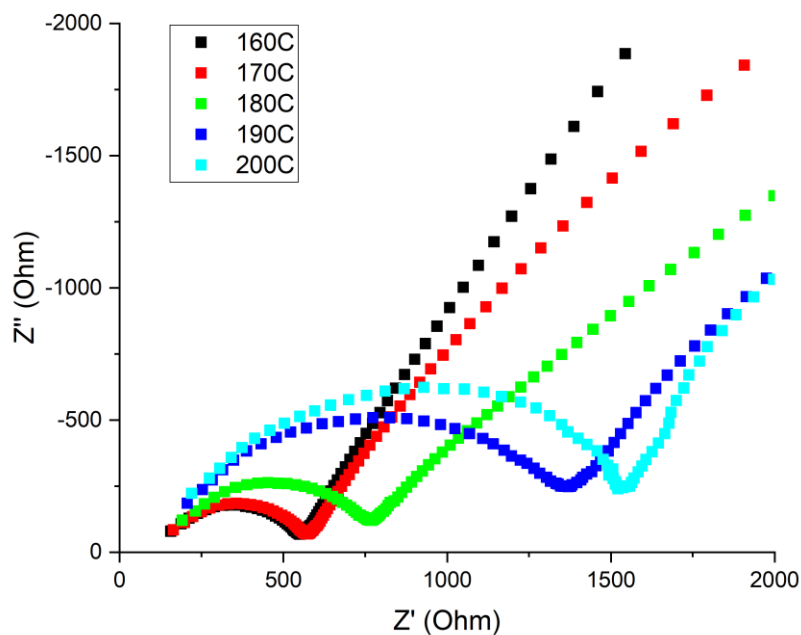


Figure B.11-Nyquist Plot of EIS Au 2-point probe analysis of sample 9102018FEP-13 grafted with 5-vinylpyridine and acid treated with 5% HNO_3 variable temperature 160C, 170C, 180C, 190C, 200C

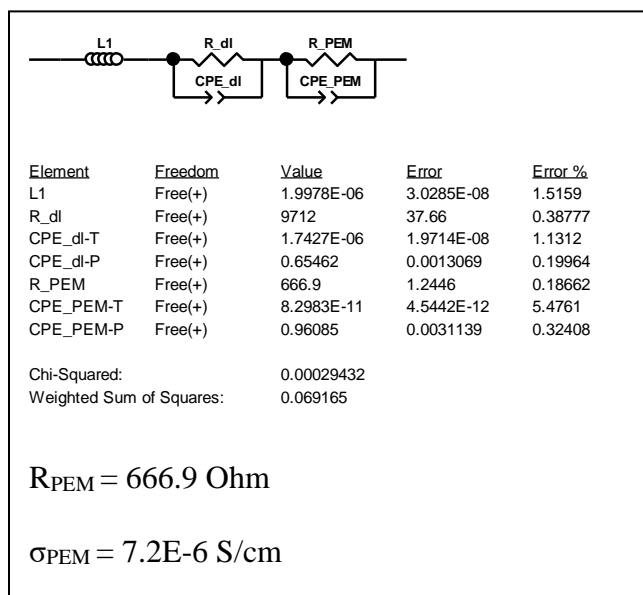
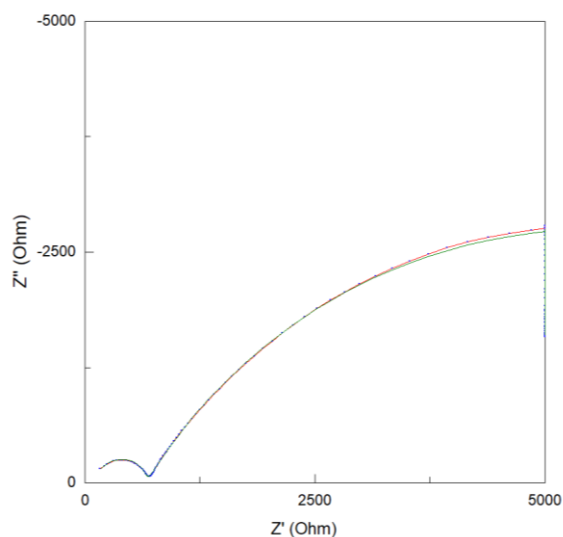


Figure B.12- EIS Au 2-point probe analysis of sample 9102018FEP-13 grafted with 5-vinylpyridine and acid treated with 5% HNO_3 at 180C fit with an equivalent circuit model (left) Nyquist Plot (right) equivalent circuit model fit

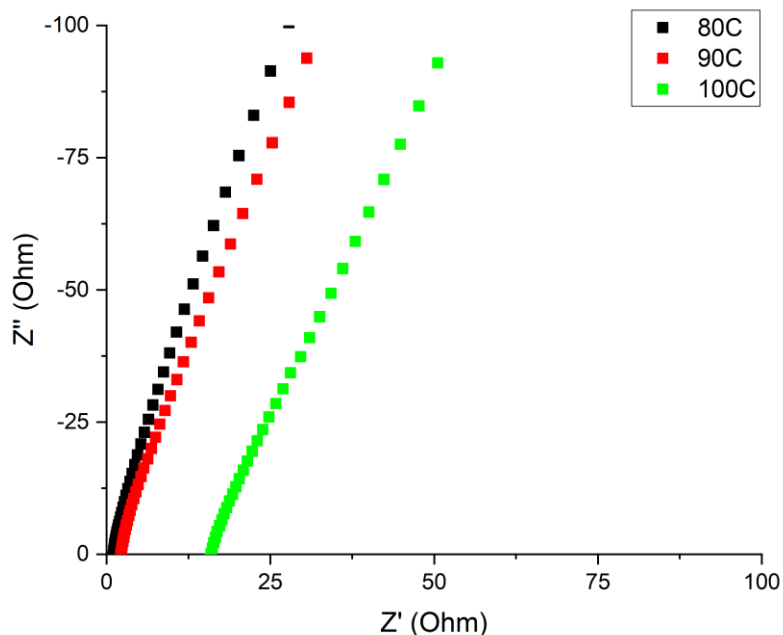


Figure B.13-Nyquist Plot of EIS Au 2-point probe analysis of sample 8112016PCTFE-16 grafted with 5-vinylpyridine and acid treated with 5% HNO_3 variable temperature 80C, 90C, 100C

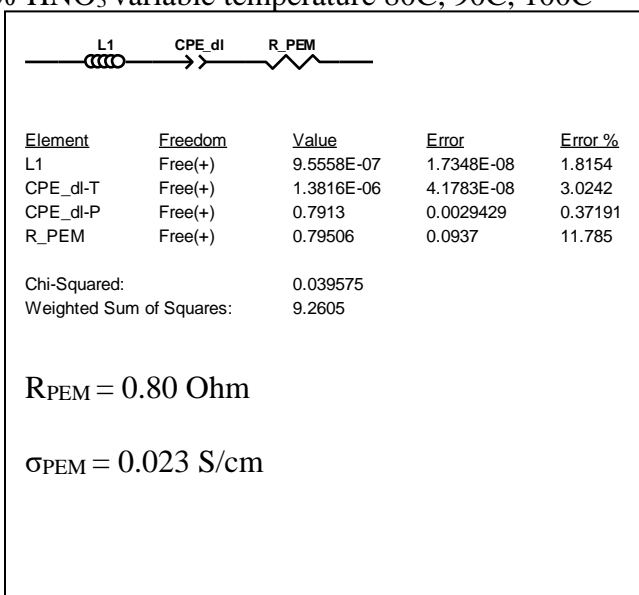
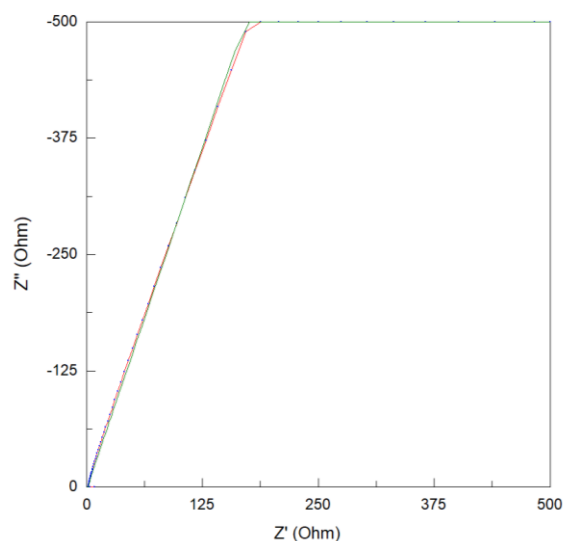


Figure B.14- EIS Au 2-point probe analysis of sample 8112016PCTFE-16 grafted with 5-vinylpyridine and acid treated with 5% HNO_3 at 90C fit with an equivalent circuit model (left) Nyquist Plot (right) equivalent circuit model fit

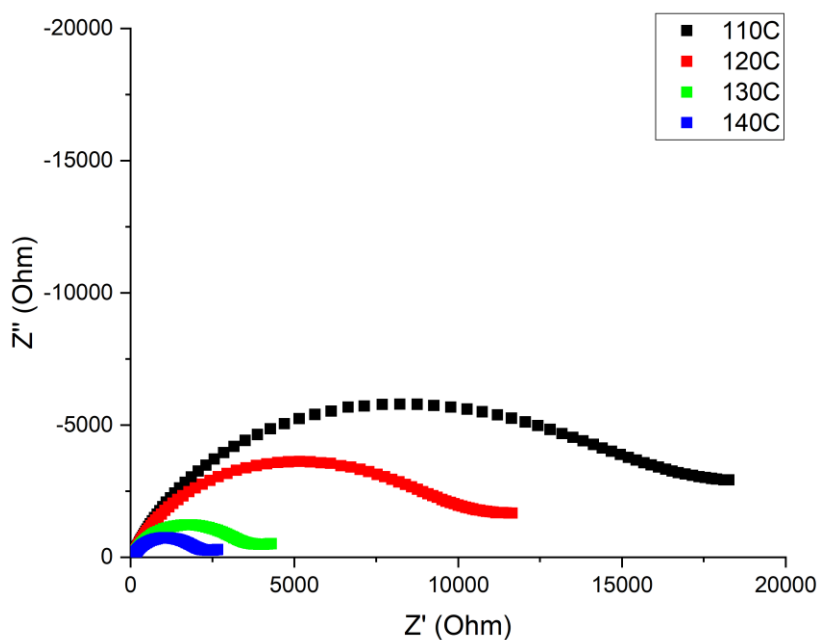


Figure B.15-Nyquist Plot of EIS Au 2-point probe analysis of sample 8112016PCTFE-16 grafted with 5-vinylpyridine and acid treated with 5% HNO_3 variable temperature 110C, 120C, 130C, 140C

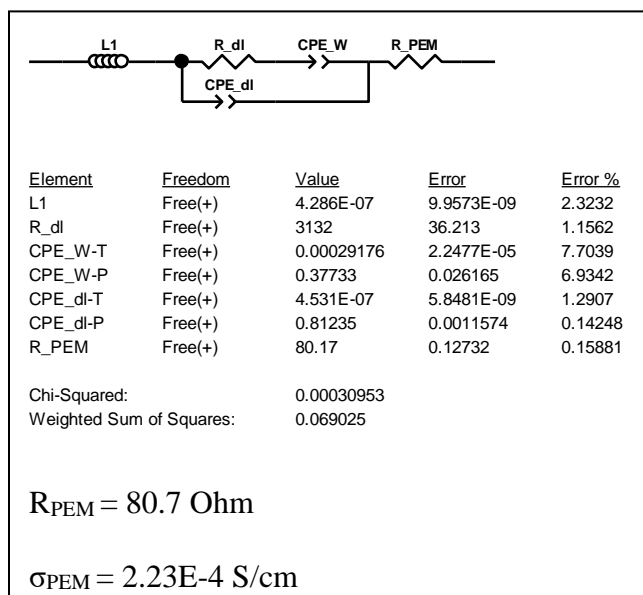
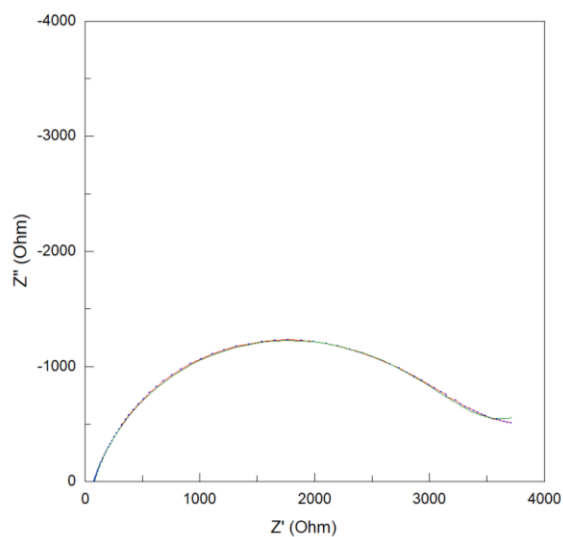


Figure B.16- EIS Au 2-point probe analysis of sample 8112016PCTFE-16 grafted with 5-vinylpyridine and acid treated with 5% HNO_3 at 130C fit with an equivalent circuit model (left) Nyquist Plot (right) equivalent circuit model fit

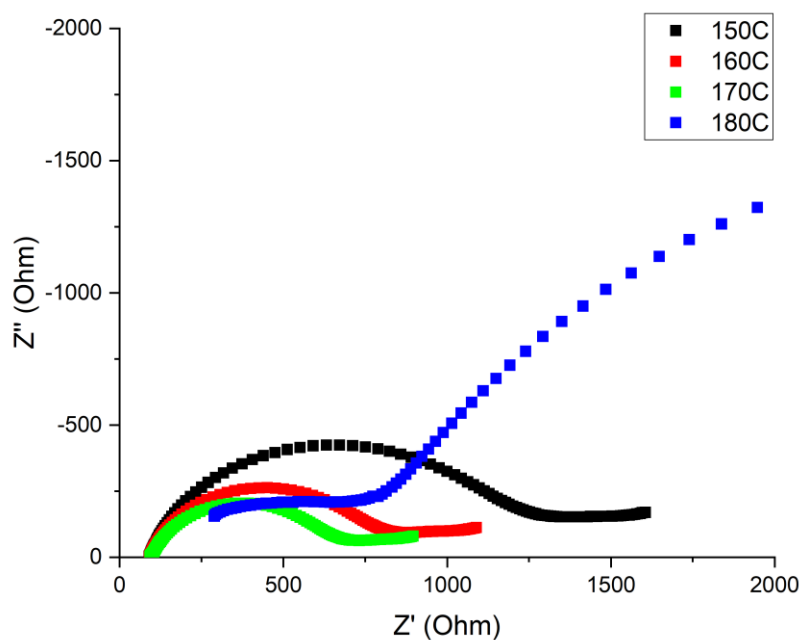


Figure B.17-Nyquist Plot of EIS Au 2-point probe analysis of sample 8112016PCTFE-16 grafted with 5-vinylpyridine and acid treated with 5% HNO₃ variable temperature 150C, 160C, 170C, 180C

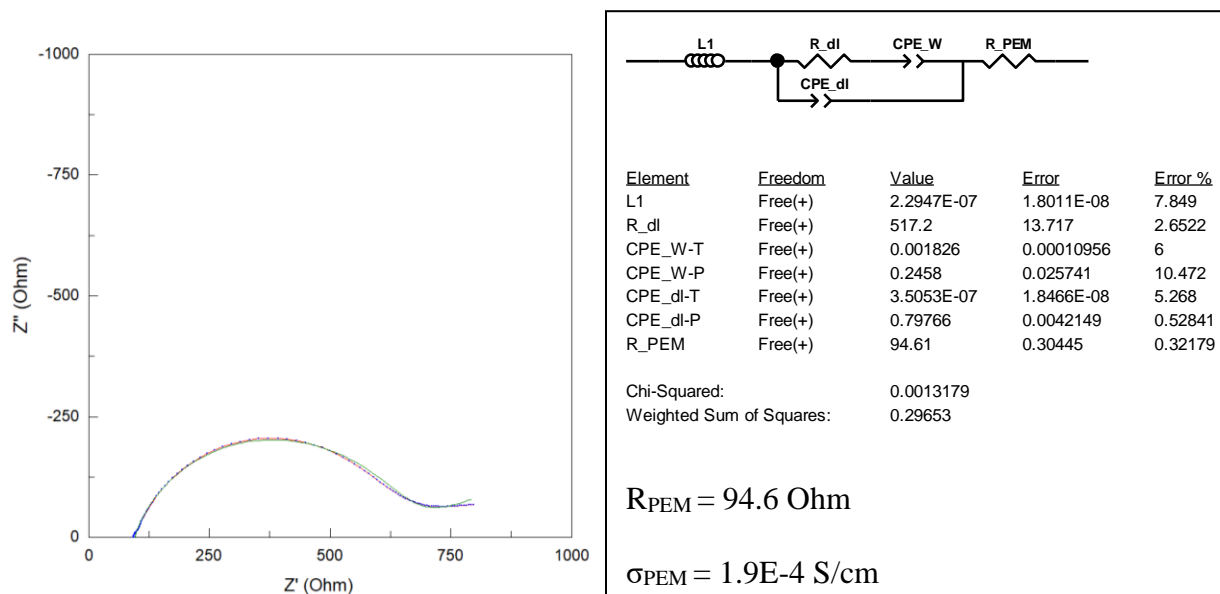


Figure B.18- EIS Au 2-point probe analysis of sample 8112016PCTFE-16 grafted with 5-vinylpyridine and acid treated with 5% HNO₃ at 170C fit with an equivalent circuit model (left) Nyquist Plot (right) equivalent circuit model fit

9102018PVF-13

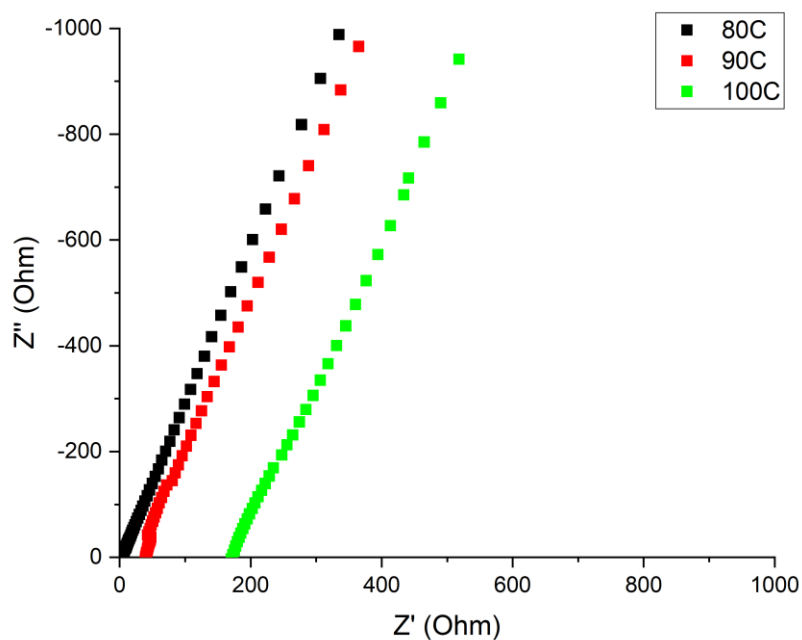


Figure B.19-Nyquist Plot of EIS Au 2-point probe analysis of sample 9102018PVF-13 grafted with 5-vinylpyridine and acid treated with 5% HNO_3 variable temperature 80C, 90C, 100C

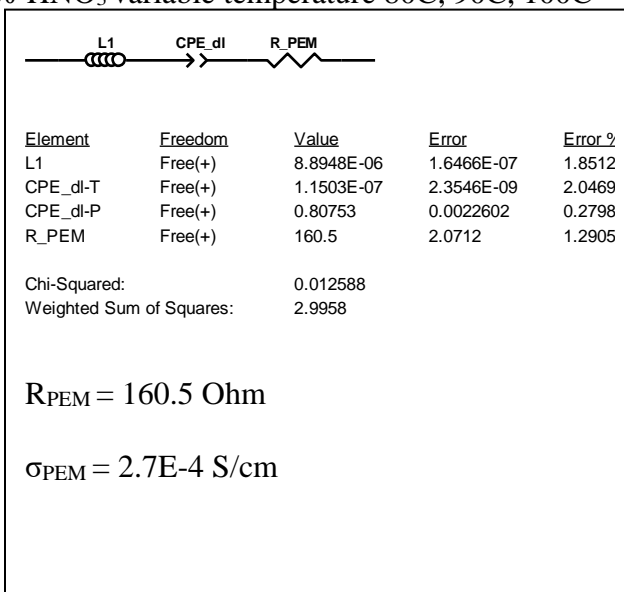
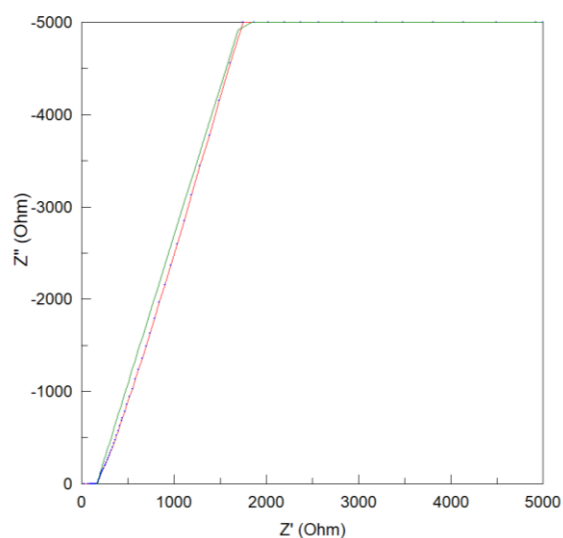


Figure B.20- EIS Au 2-point probe analysis of sample 9102018PVF-13 grafted with 5-vinylpyridine and acid treated with 5% HNO_3 at 100C fit with an equivalent circuit model (left) Nyquist Plot (right) equivalent circuit model fit

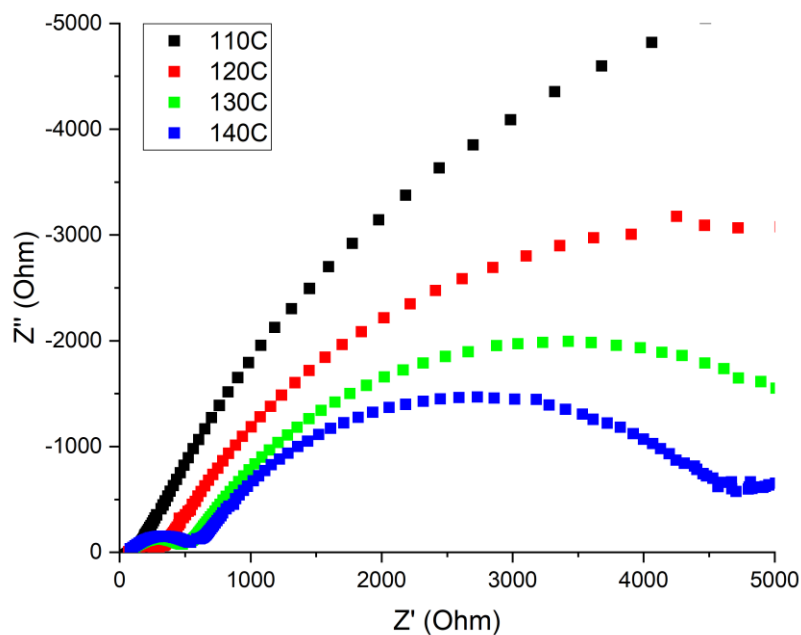


Figure B.21-Nyquist Plot of EIS Au 2-point probe analysis of sample 9102018PVF-13 grafted with 5-vinylpyridine and acid treated with 5% HNO₃ variable temperature 110C, 120C, 130C, 140C

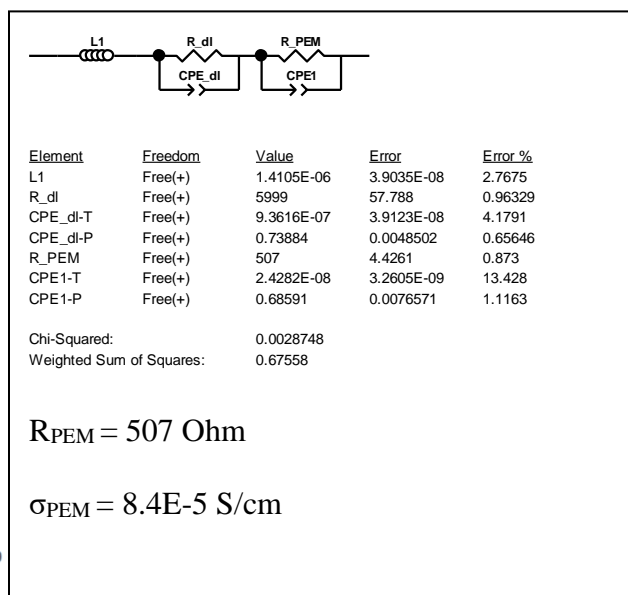
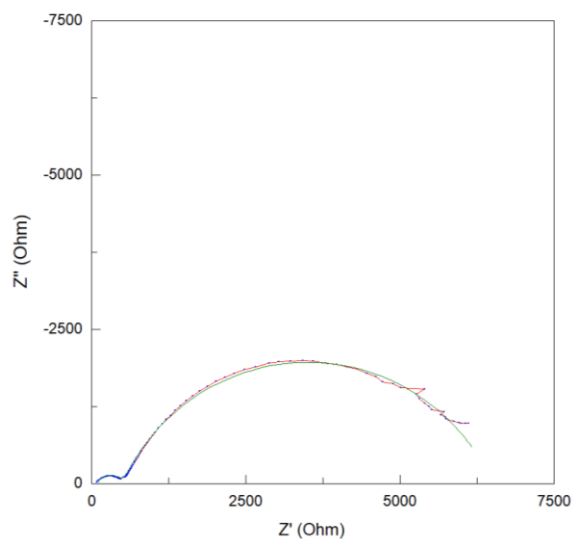


Figure B.22- EIS Au 2-point probe analysis of sample 9102018PVF-13 grafted with 5-vinylpyridine and acid treated with 5% HNO₃ at 130C fit with an equivalent circuit model (left) Nyquist Plot (right) equivalent circuit model fit

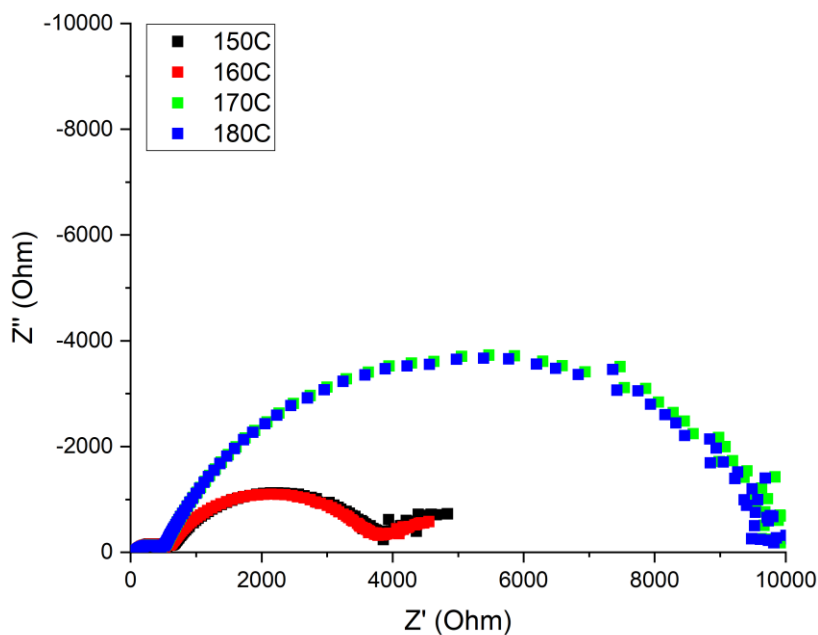


Figure B.23-Nyquist Plot of EIS Au 2-point probe analysis of sample 9102018PVF-13 grafted with 5-vinylpyridine and acid treated with 5% HNO_3 variable temperature 150C, 160C, 170C, 180C

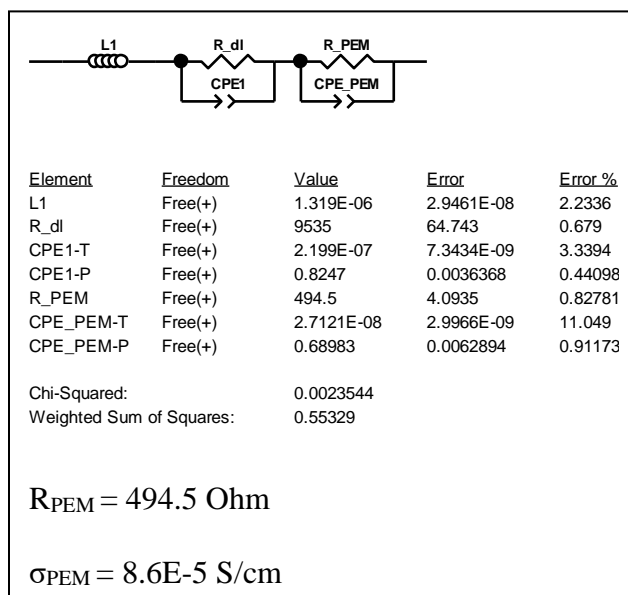
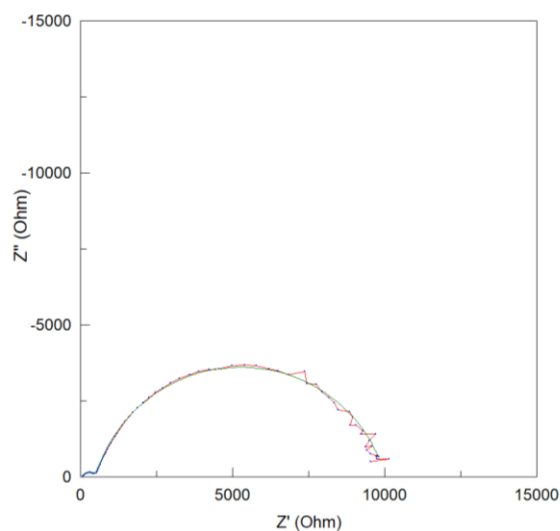


Figure B.24- EIS Au 2-point probe analysis of sample 9102018PVF-13 grafted with 5-vinylpyridine and acid treated with 5% HNO_3 at 180C fit with an equivalent circuit model (left) Nyquist Plot (right) equivalent circuit model fit

Au 2-Point Probe Summary: 5-vinylpyridine

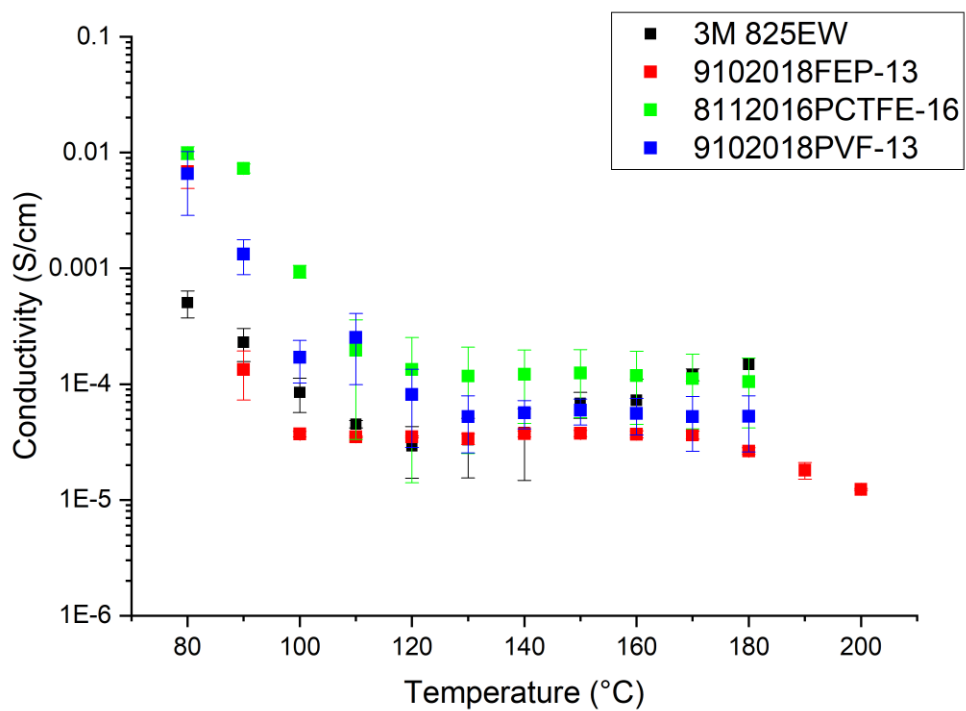


Figure B.25: EIS proton conductivity vs. temperature Au 2-Point Parallel Plate Capacitor Test Cell: (black) 3M 825EW Control, 4-vinylpyridine PEM: (red) 9102018FEP-13, (green) 8112016PCTFE-16, (blue), 9102018PVF-13; samples were acid treated with 5% HNO_3 , $n = 3$

9122018FEP-2Na

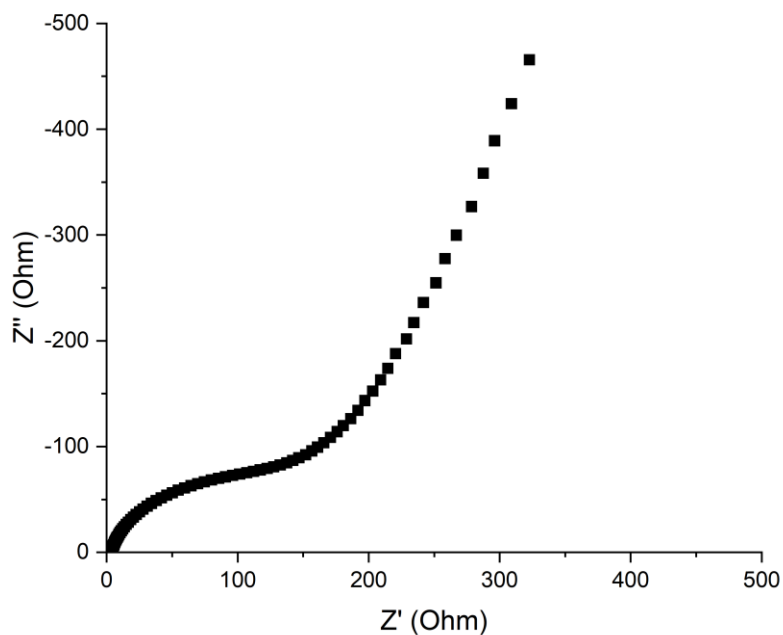


Figure B.26-Nyquist Plot of EIS Au 2-point probe analysis of sample 9122018FEP-2Na grafted with 4-vinylpyrimidine acid treated with 5% H_2SO_4 variable temperature 120C

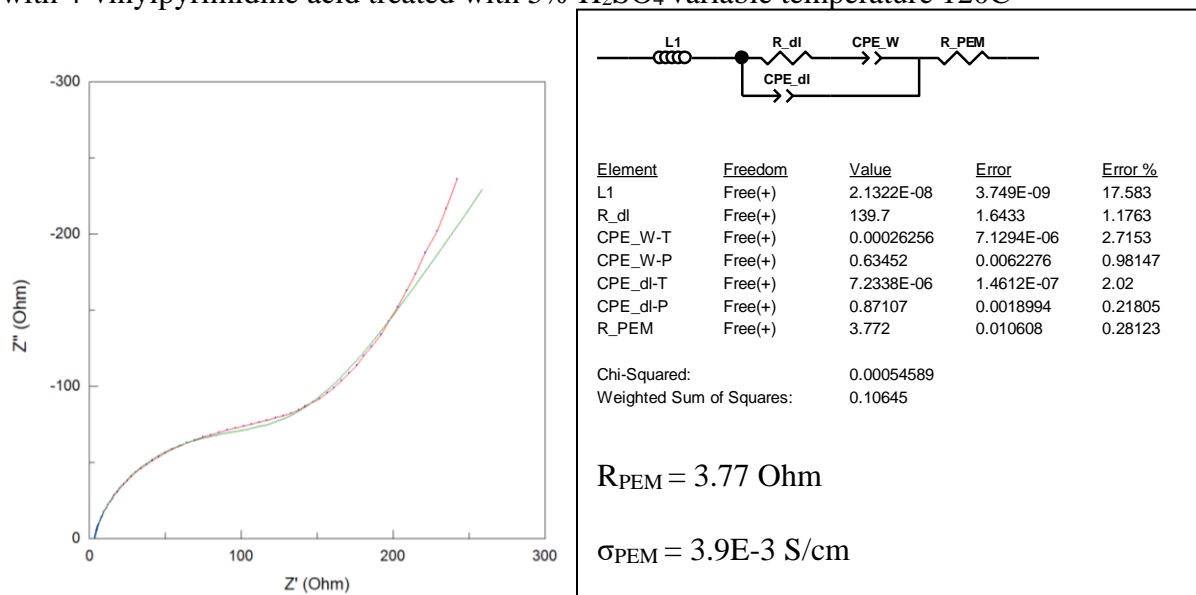


Figure B.27- EIS Au 2-point probe analysis of sample 9122018FEP-2Na grafted with 4-vinylpyrimidine acid treated with 5% H_2SO_4 at 120C fit with an equivalent circuit model (left) Nyquist Plot (right) equivalent circuit model fit

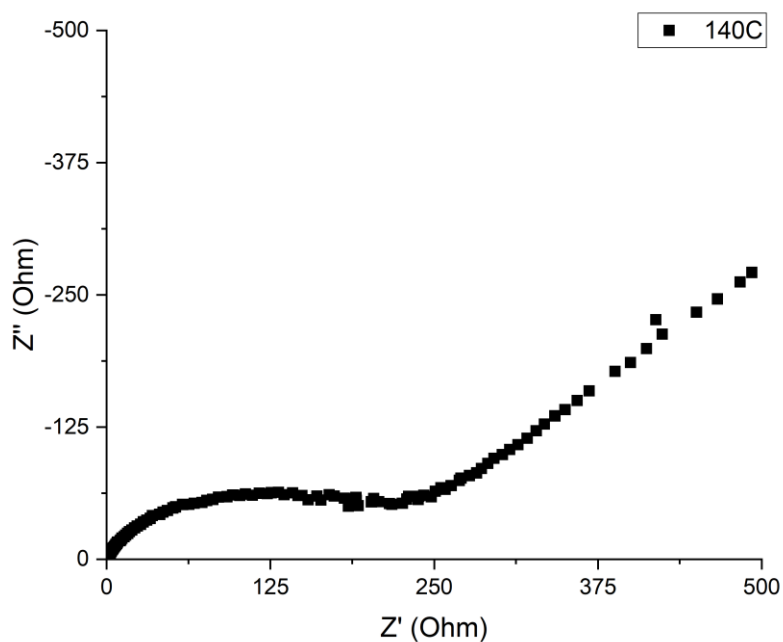


Figure B.28-Nyquist Plot of EIS Au 2-point probe analysis of sample 9122018FEP-2Na grafted with 4-vinylpyridine acid treated with 5% H_2SO_4 variable temperature 140C,

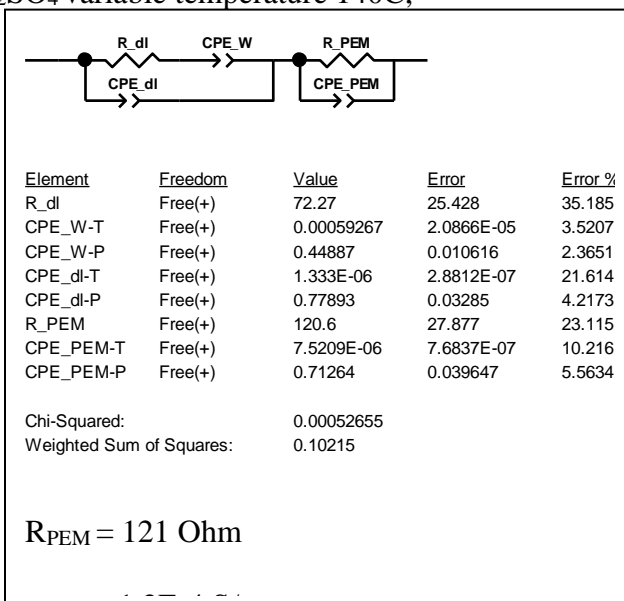
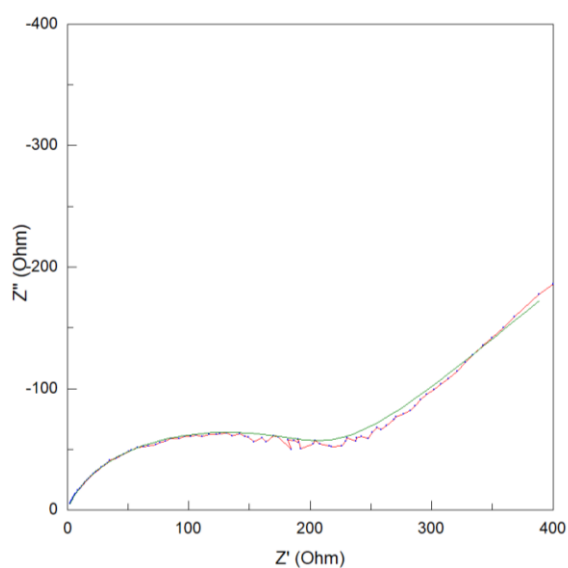


Figure B.29- EIS Au 2-point probe analysis of sample 9122018FEP-2Na grafted with 4-vinylpyrimidine acid treated with 5% H_2SO_4 at 140C fit with an equivalent circuit model (left) Nyquist Plot (right) equivalent circuit model fit

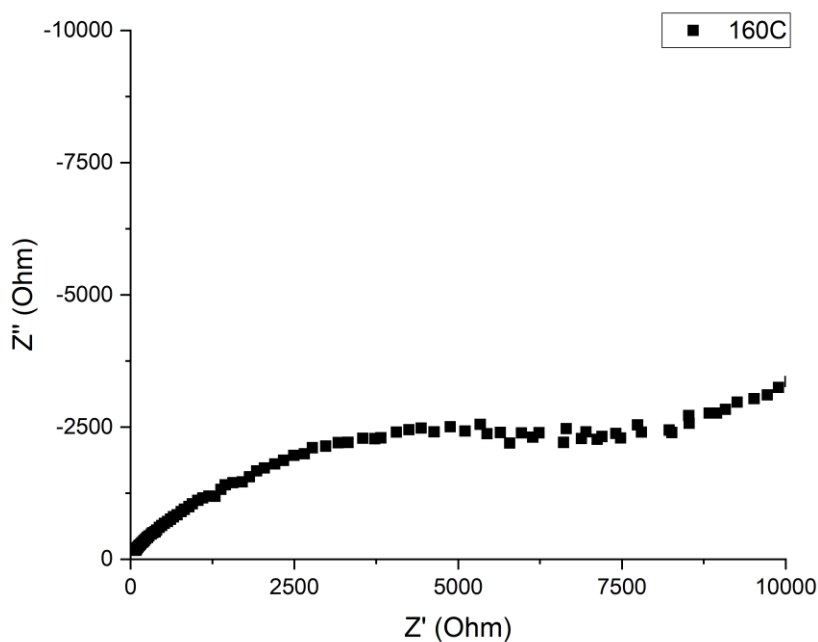


Figure B.30-Nyquist Plot of EIS Au 2-point probe analysis of sample 9122018FEP-2Na grafted with 4-vinylpyridine acid treated with 5% H_2SO_4 variable temperature 160C

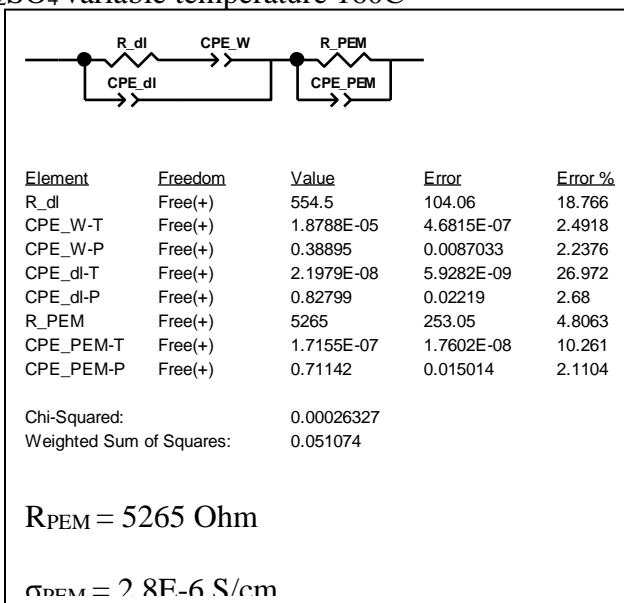
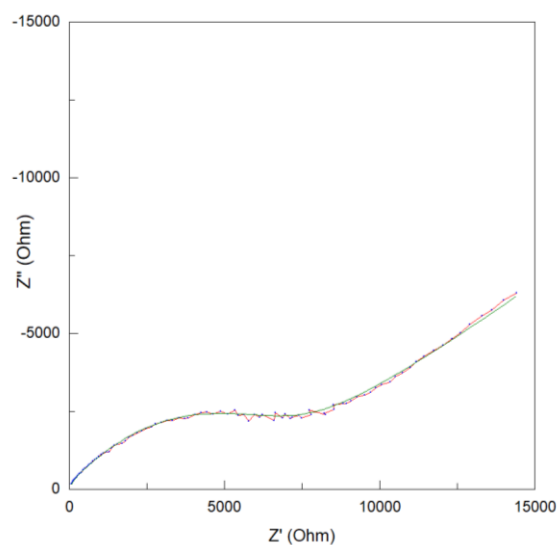


Figure B.31- EIS Au 2-point probe analysis of sample 9122018FEP-2Na grafted with 4-vinylpyrimidine acid treated with 5% H_2SO_4 at 160C fit with an equivalent circuit model (left) Nyquist Plot (right) equivalent circuit model fit

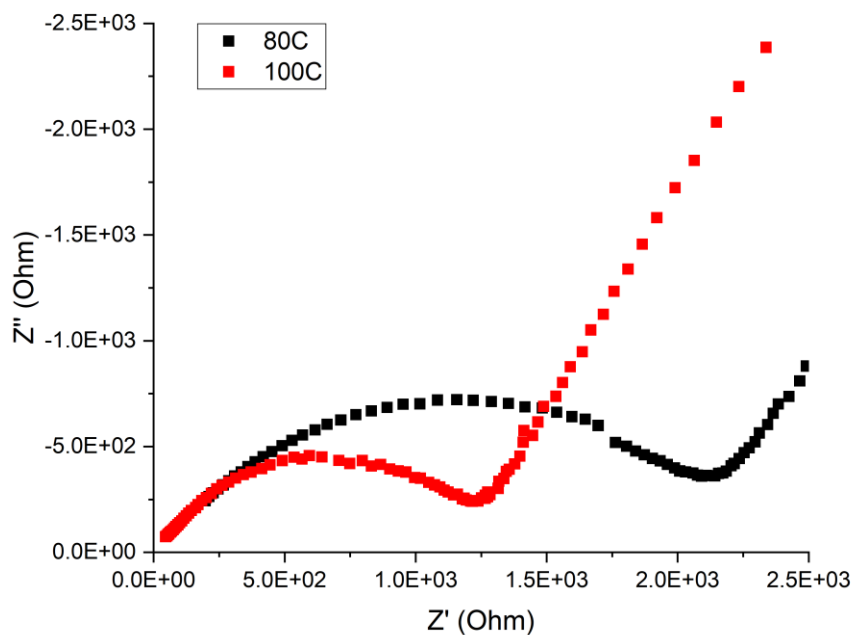


Figure B.32-Nyquist Plot of EIS Au 2-point probe analysis of sample 9122018FEP-2Na grafted with 4-vinylpyrimidine acid treated with 5% HNO₃ variable temperature 80C, 100C

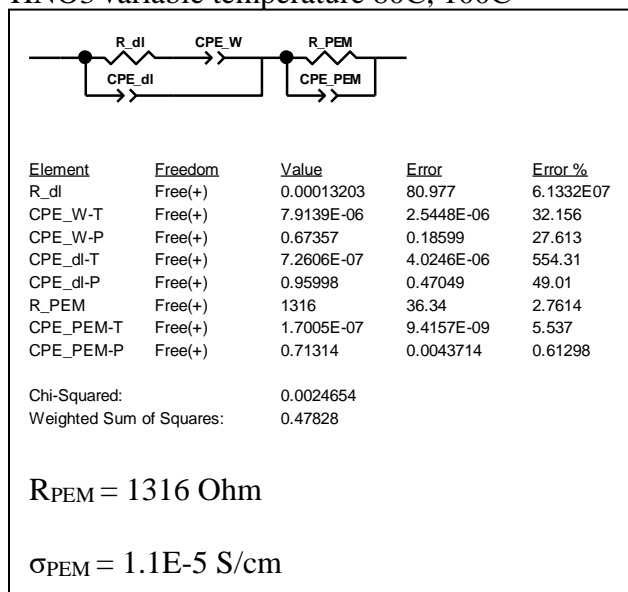
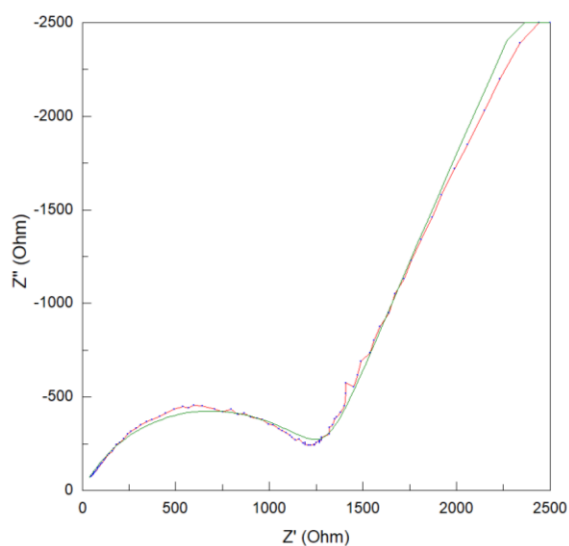


Figure B.33- EIS Au 2-point probe analysis of sample 9122018FEP-2Na grafted with 4-vinylpyrimidine acid treated with 5% H₂SO₄ at 100C fit with an equivalent circuit model (left) Nyquist Plot (right) equivalent circuit model fit

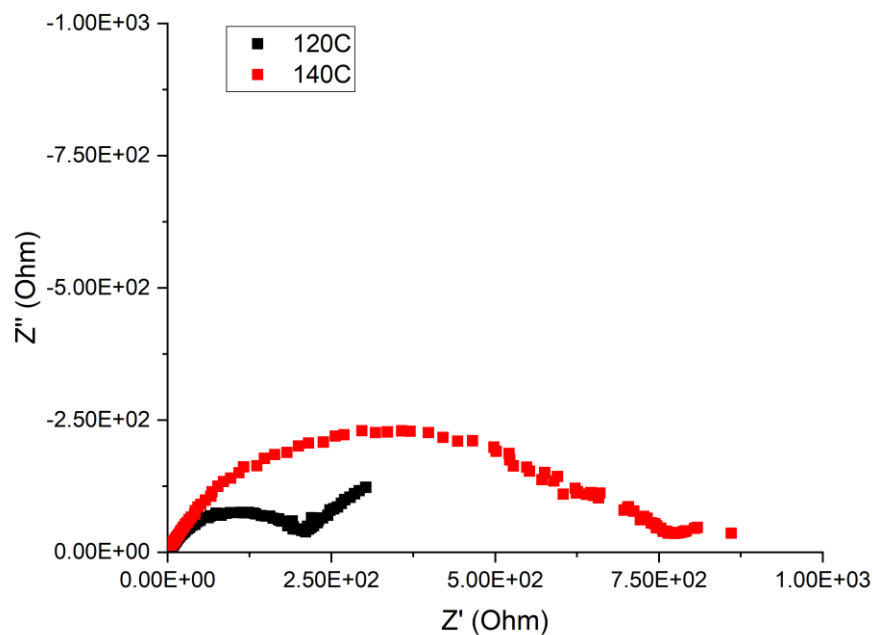


Figure B.34-Nyquist Plot of EIS Au 2-point probe analysis of sample 9122018FEP-2Na grafted with 4-vinylpyrimidine acid treated with 5% HNO₃ variable temperature 120C, 140C

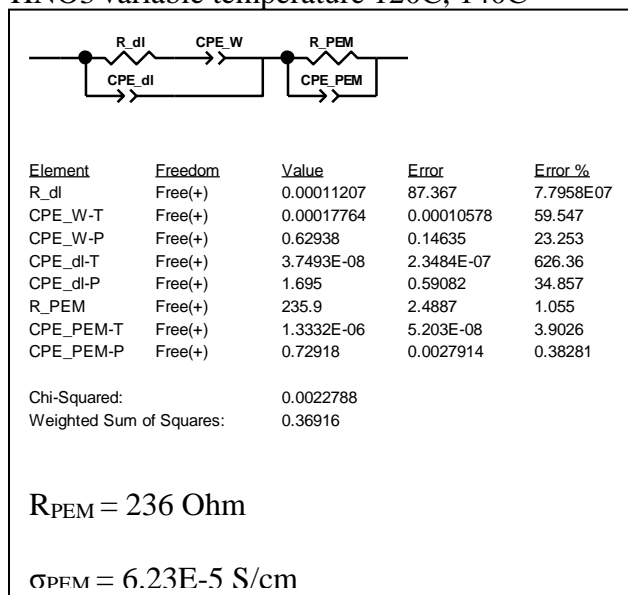
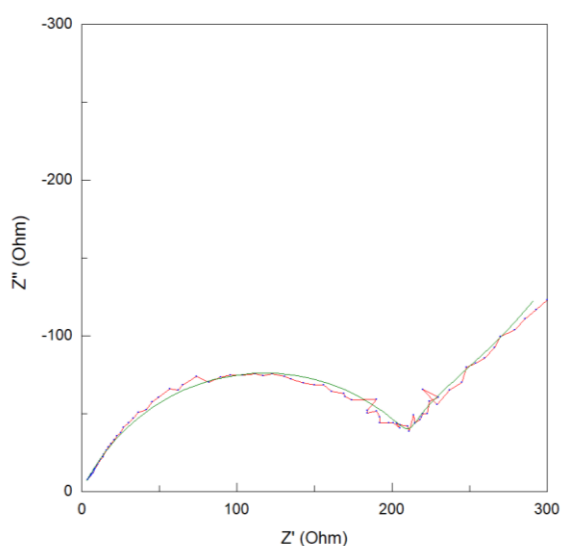


Figure B.35- EIS Au 2-point probe analysis of sample 9122018FEP-2Na grafted with 4-vinylpyrimidine acid treated with 5% HNO₃ at 120C fit with an equivalent circuit model (left) Nyquist Plot (right) equivalent circuit model fit

3222017PVF-1a

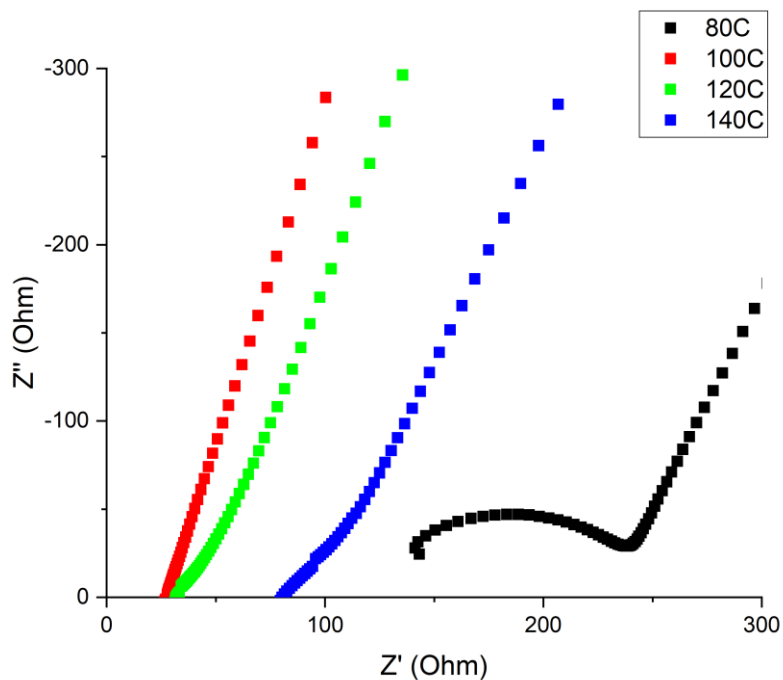


Figure B.36-Nyquist Plot of EIS Au 2-point probe analysis of sample 3222017PVF-1a grafted with 4-vinylpyrimidine acid treated with 5% HNO₃ variable temperature 80C, 100C, 120C, 140C

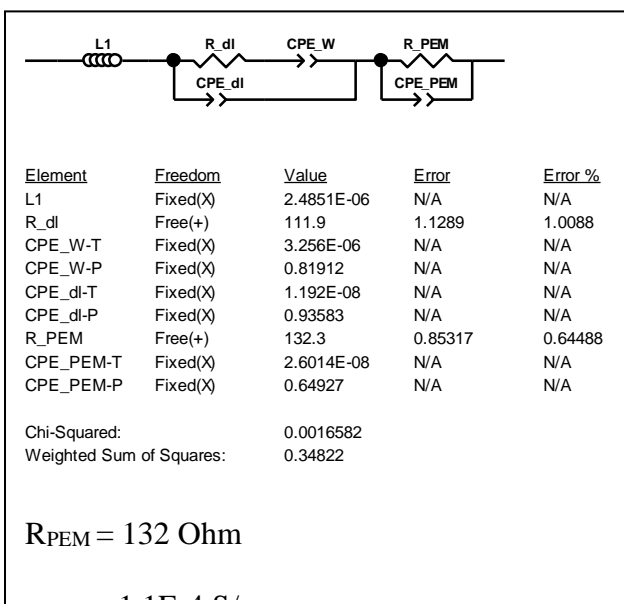
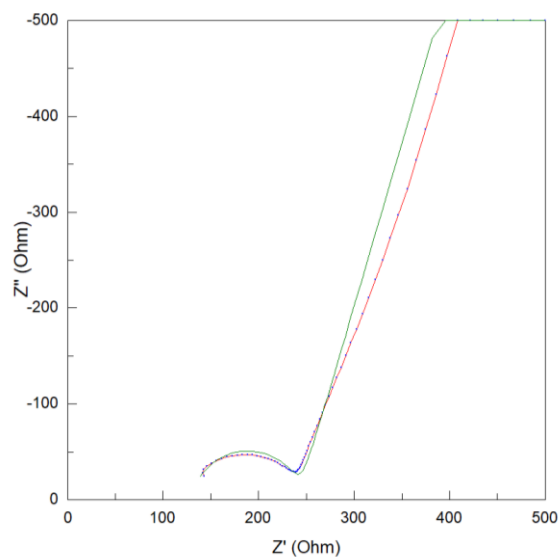


Figure B.37- EIS Au 2-point probe analysis of sample 3222017PVF-1a grafted with 4-vinylpyrimidine acid treated with 5% H₂SO₄ at 80C fit with an equivalent circuit model (left) Nyquist Plot (right) equivalent circuit model fit

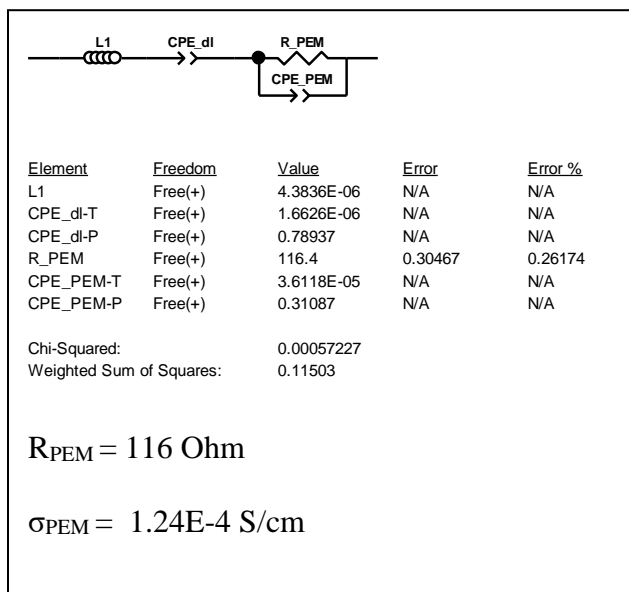
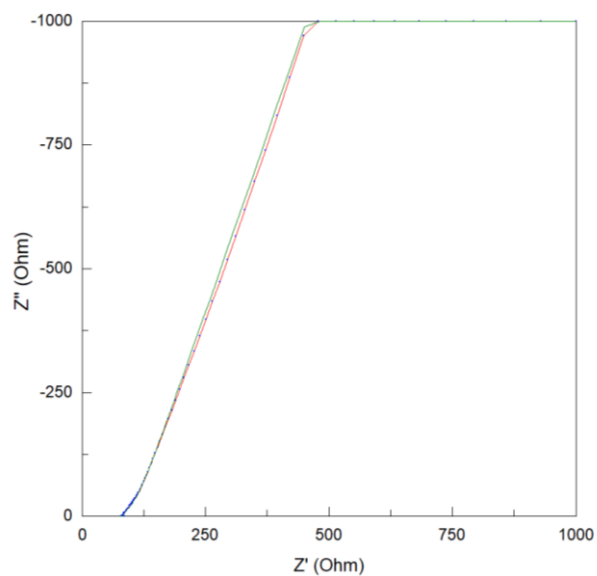


Figure B.38- EIS Au 2-point probe analysis of sample 3222017PVF-1a grafted with 4-vinylpyrimidine acid treated with 5% H_2SO_4 at 140C fit with an equivalent circuit model (left) Nyquist Plot (right) equivalent circuit model fit

Au 2-Point Probe Summary: 4-vinylpyrimidine

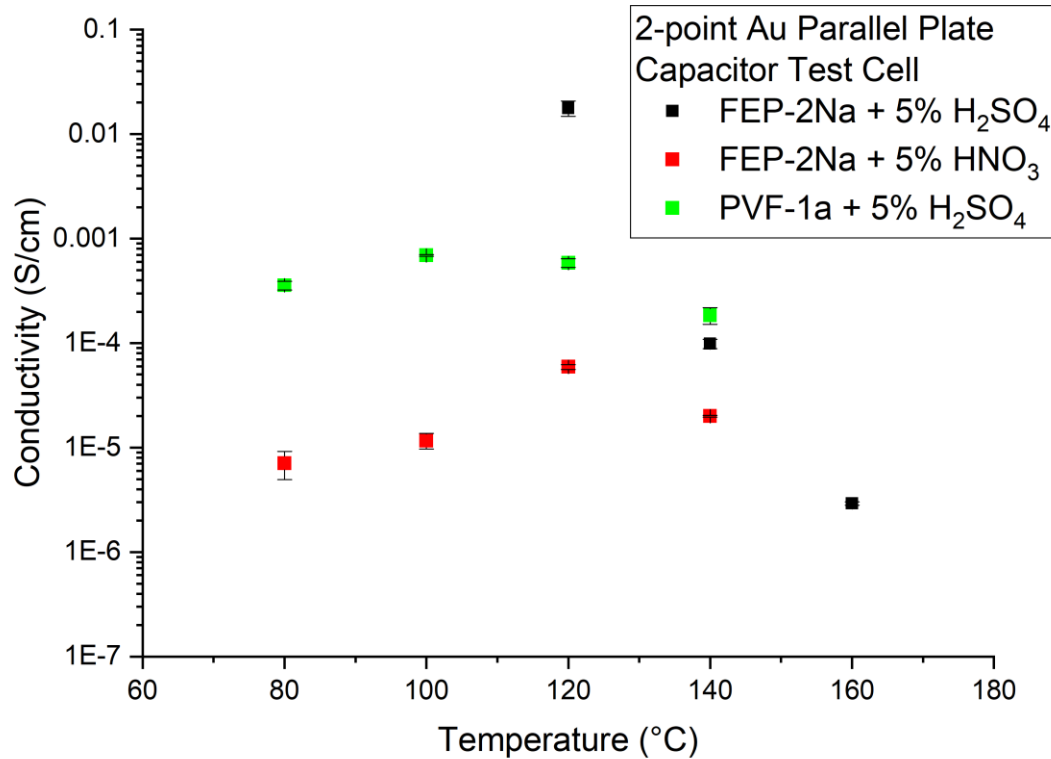


Figure B.39-EIS proton conductivity vs. temperature 2-Point Au Parallel Plate Capacitor Test Cell: 5-vinylpyrimidine (black) Sample 9122018FEP-2Na treated with 5% H₂SO₄ (red) Sample 9122018FEP-2Na treated with 5% HNO₃ (green) Sample 3222017PVF-1a treated with 5% H₂SO₄, n = 3

4-Pt Point Probe
3M 825EW Control

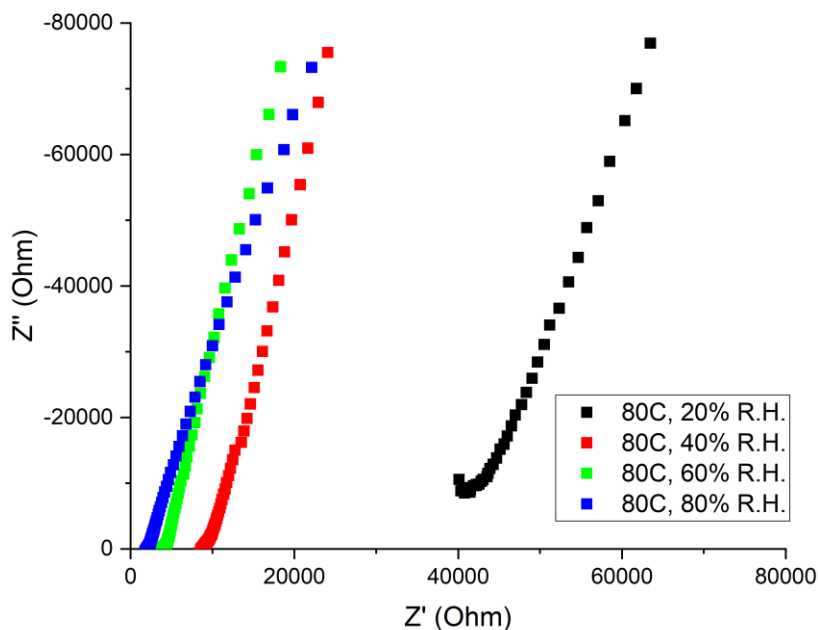


Figure C.1-Nyquist Plot of EIS Pt 4-point probe analysis of sample 3M 825EW Control grafted with 5-vinylpyridine acid treated with 5% HNO₃ variable temperature 80C: 20%, 40%, 60%, 80% R.H.

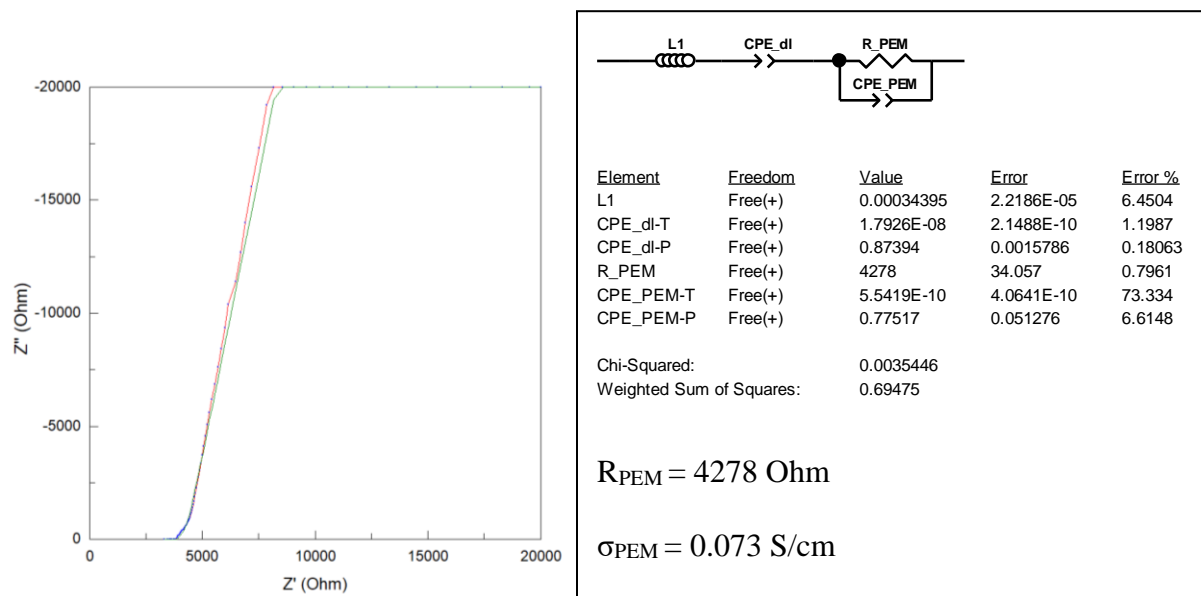


Figure C.2- EIS Pt 4-point probe analysis of sample 3M 825EW Control acid treated with 5% HNO₃ at 80C 60% R.H. fit with an equivalent circuit model (left) Nyquist Plot (right) equivalent circuit model fit

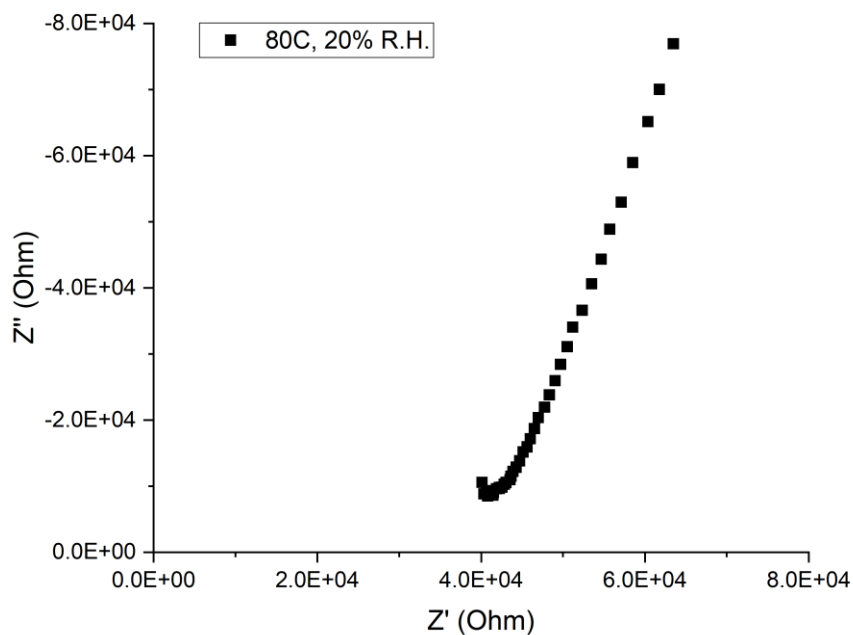


Figure C.3-Nyquist Plot of EIS Pt 4-point probe analysis of sample 3M 825EW Control grafted with 5-vinylpyridine acid treated with 5% HNO₃ variable temperature 80C,

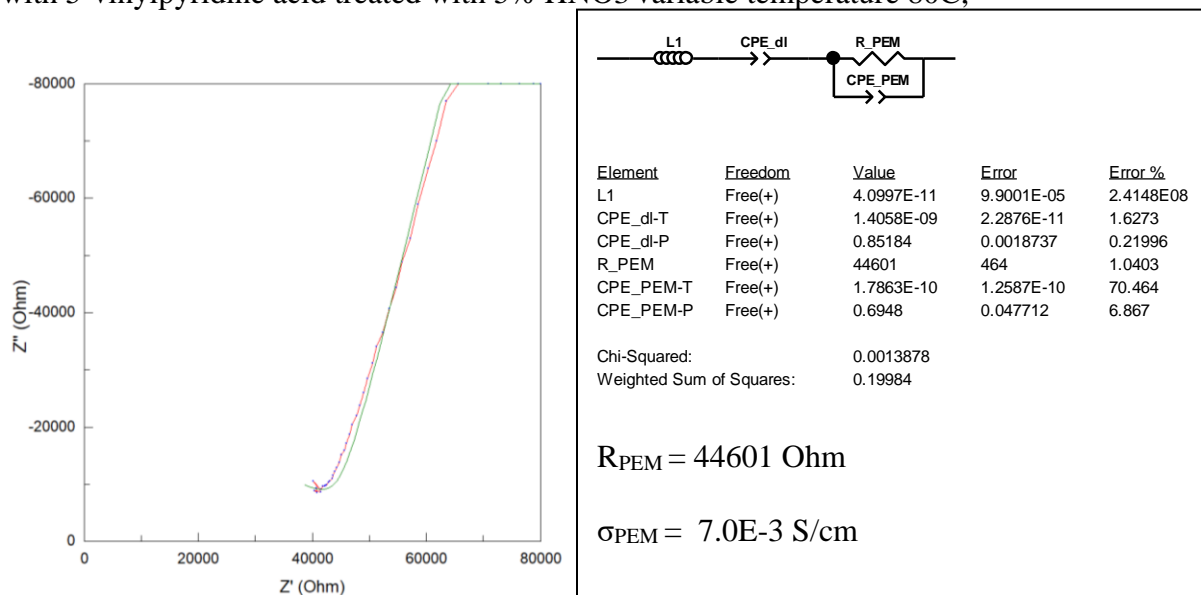


Figure C.4- EIS Pt 4-point probe analysis of sample 3M 825EW Control acid treated with 5% HNO₃ at 80C 20% R.H. fit with an equivalent circuit model (left) Nyquist Plot (right) equivalent circuit model fit

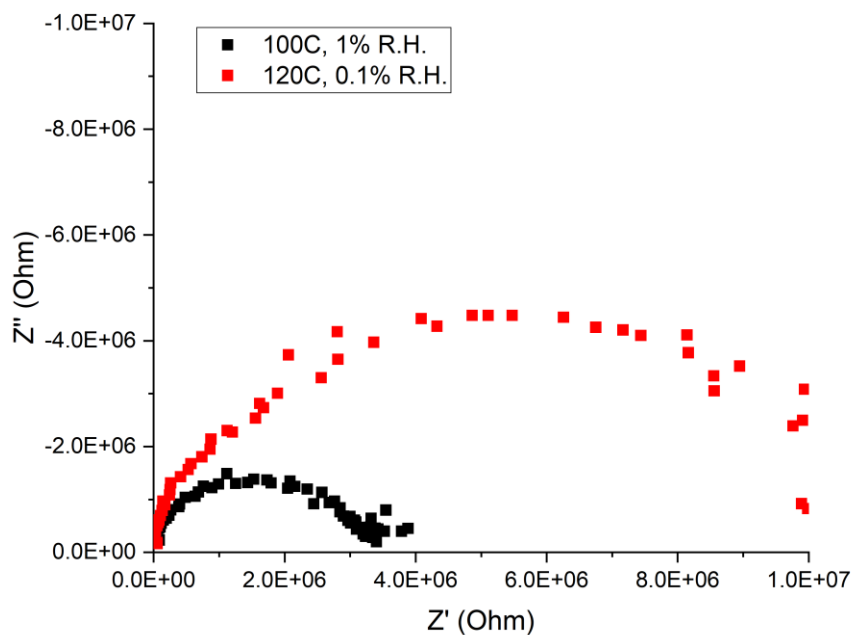


Figure C.5-Nyquist Plot of EIS Pt 4-point probe analysis of sample 3M 825EW Control grafted with 5-vinylpyridine acid treated with 5% HNO₃ variable temperature 100C, 120C

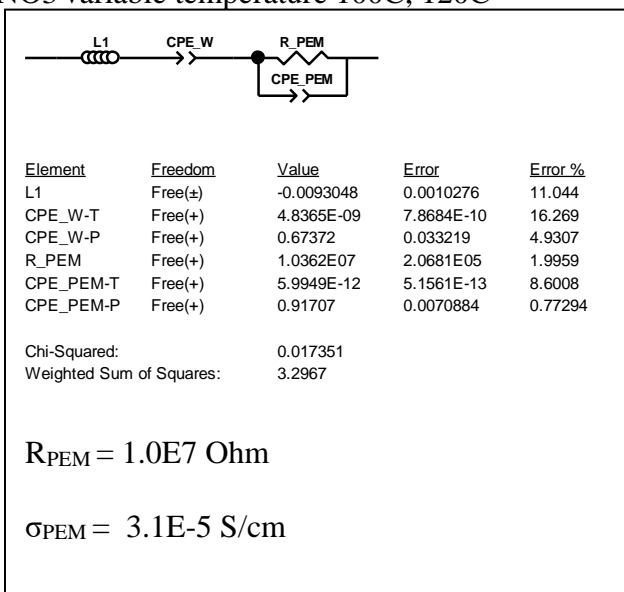
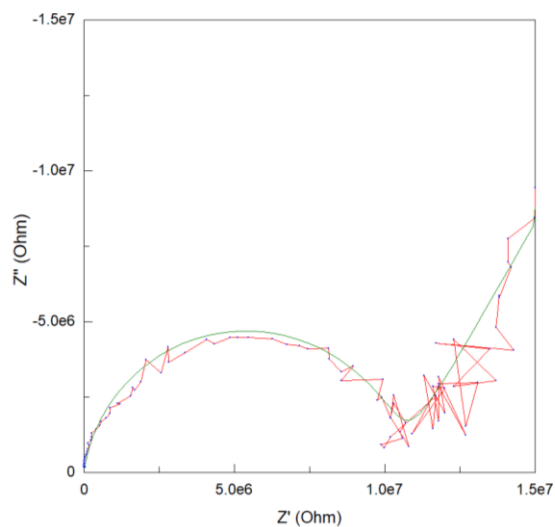


Figure C.6- EIS Pt 4-point probe analysis of sample 3M 825EW Control acid treated with 5% HNO₃ at 120C 0.1% R.H. fit with an equivalent circuit model (left) Nyquist Plot (right) equivalent circuit model fit

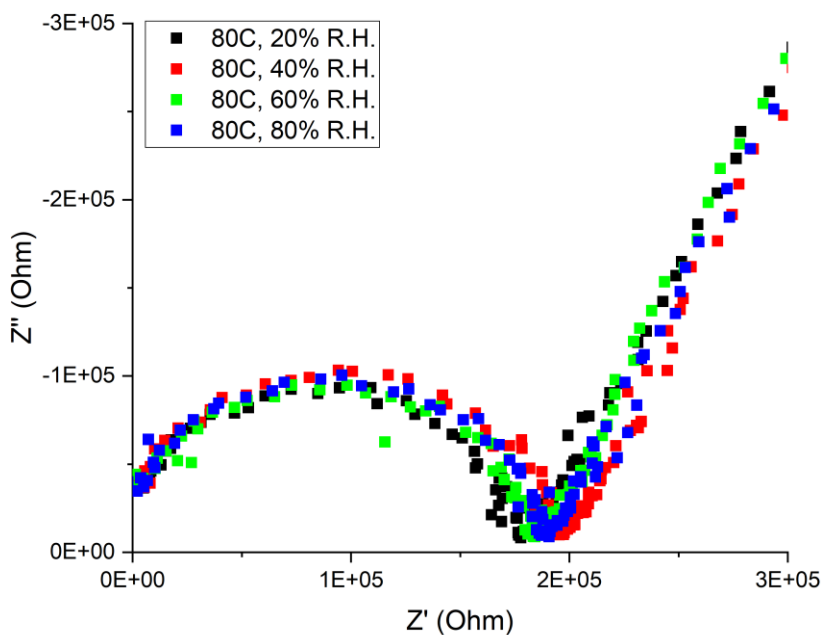


Figure C.7-Nyquist Plot of EIS Pt 4-point probe analysis of sample 322017FEP-1b grafted with 5-vinylpyridine and acid treated with 5% HNO₃ variable temperature 80C: 20%, 40%, 60%, 80% R.H.

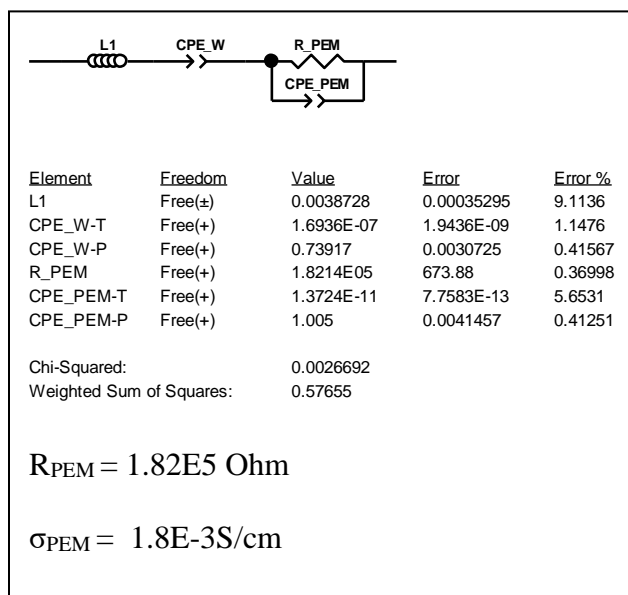
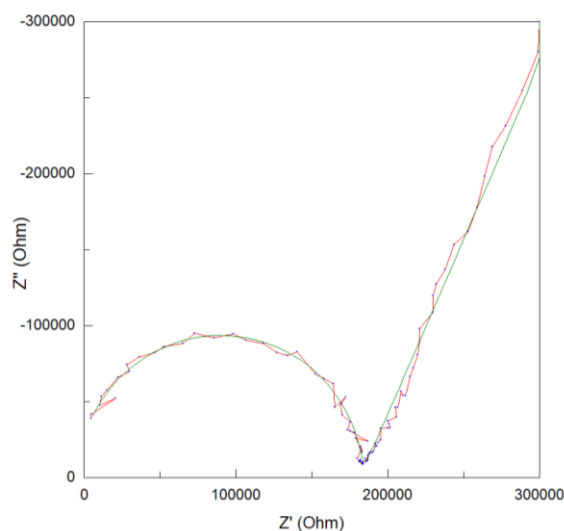


Figure C.8- EIS Pt 4-point probe analysis of sample 322017FEP-1b grafted with 5-vinylpyridine and acid treated with 5% HNO₃ at 80C 60% R.H. fit with an equivalent circuit model (left) Nyquist Plot (right) equivalent circuit model fit

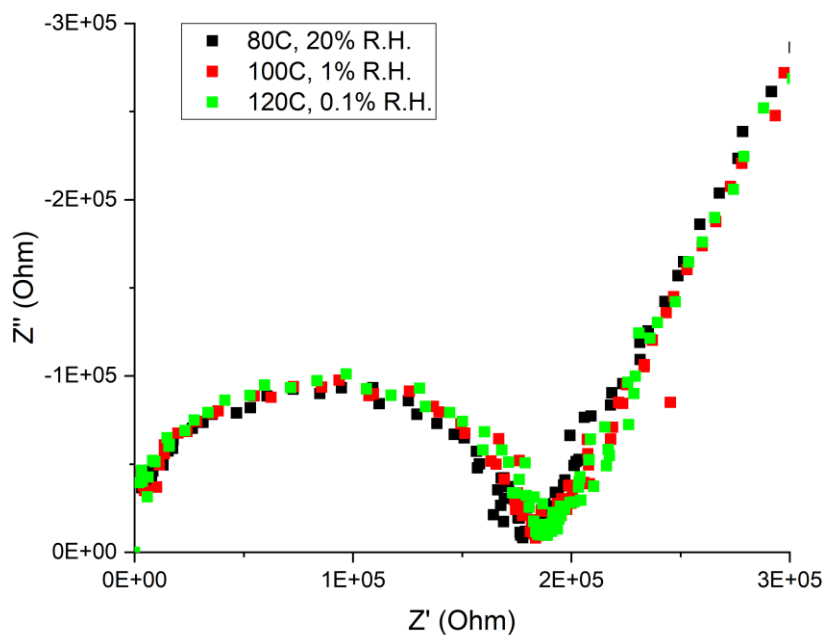


Figure C.9-Nyquist Plot of EIS Pt 4-point probe analysis of sample 322017FEP-1b grafted with 5-vinylpyridine and acid treated with 5% HNO₃ variable temperature 80C, 100C, 120C

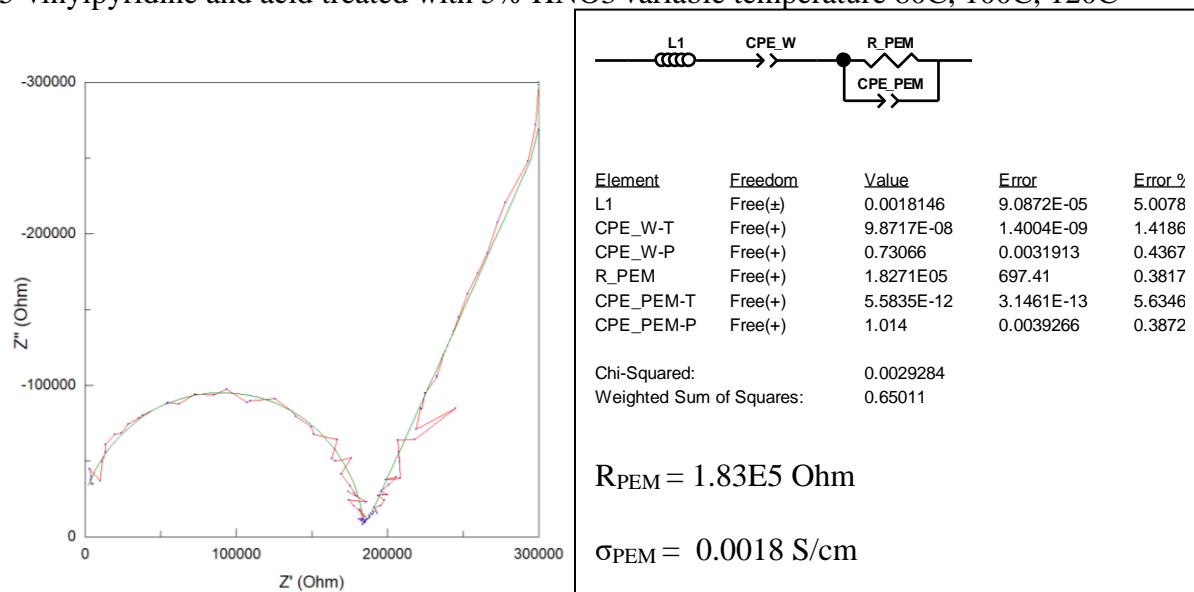


Figure C.10- EIS Pt 4-point probe analysis of sample 322017FEP-1b acid treated with 5% HNO₃ at 100C 1%R.H. fit with an equivalent circuit model (left) Nyquist Plot (right) equivalent circuit model fit

3222017PCTFE-3c

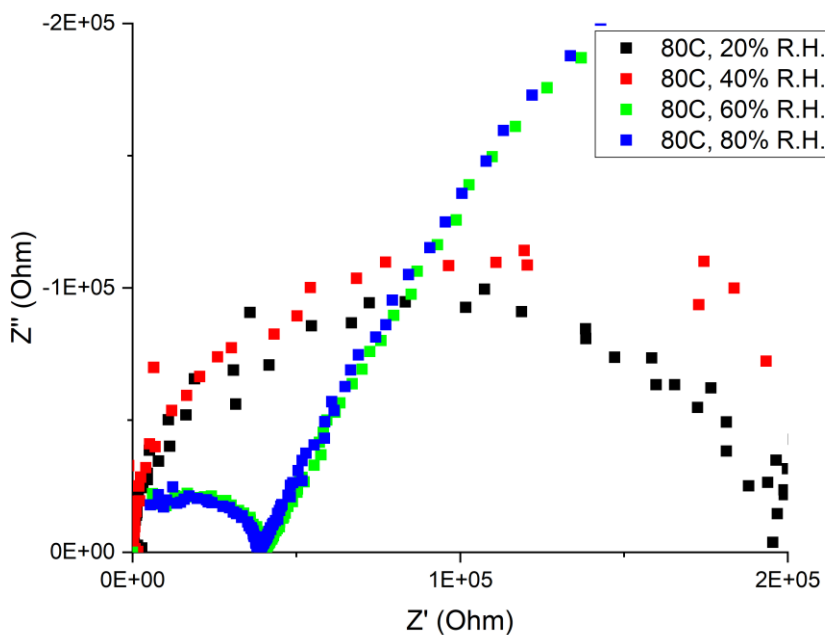


Figure C.11-Nyquist Plot of EIS Pt 4-point probe analysis of sample 322017PCTFE-3c grafted with 5-vinylpyridine and acid treated with 5% HNO₃ variable temperature 80C: 20%, 40%, 60%, 80% R.H.

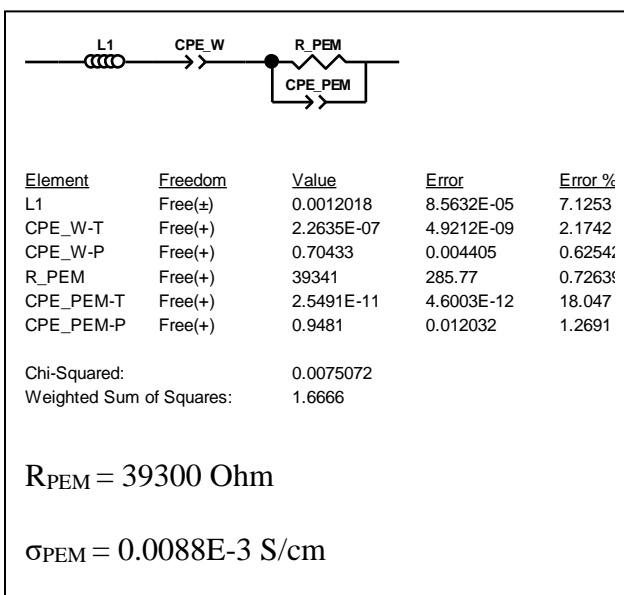
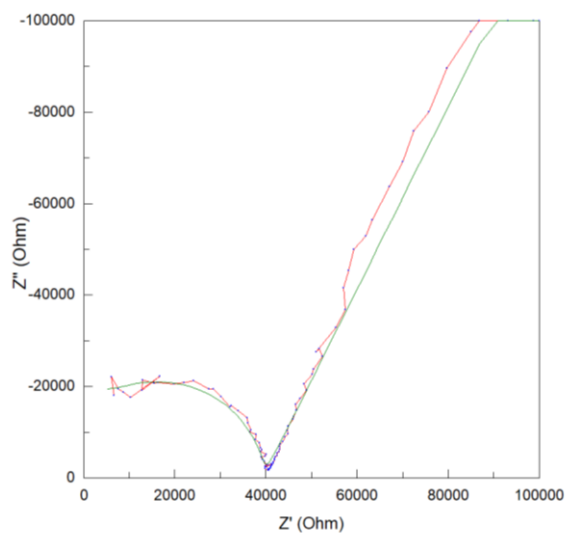


Figure C.12- EIS Pt 4-point probe analysis of sample 322017PCTFE-3c grafted with 5-vinylpyridine and acid treated with 5% HNO₃ at 80C 60% R.H. fit with an equivalent circuit model (left) Nyquist Plot (right) equivalent circuit model fit

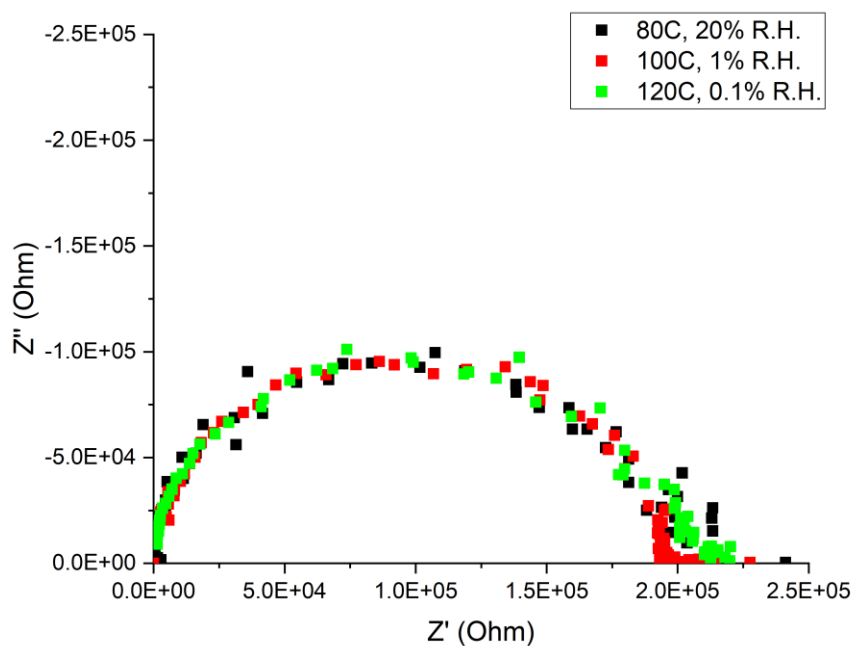


Figure C.13-Nyquist Plot of EIS Pt 4-point probe analysis of sample 322017PCTFE-3c grafted with 5-vinylpyridine and acid treated with 5% HNO₃ variable temperature 80C, 100C, 120C

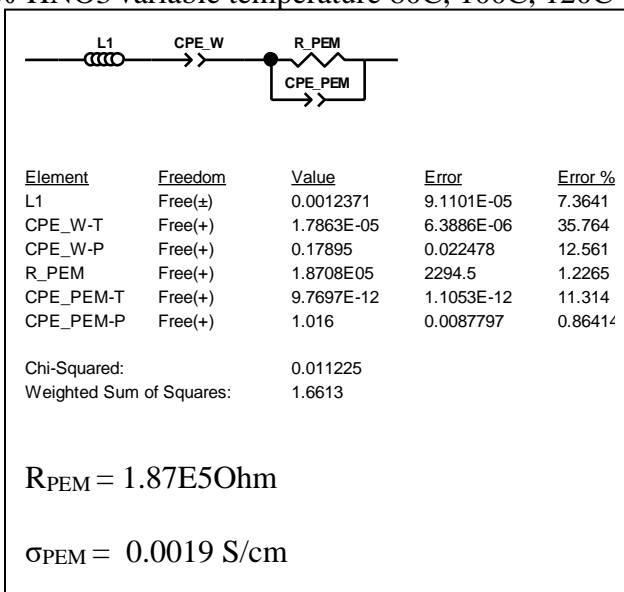
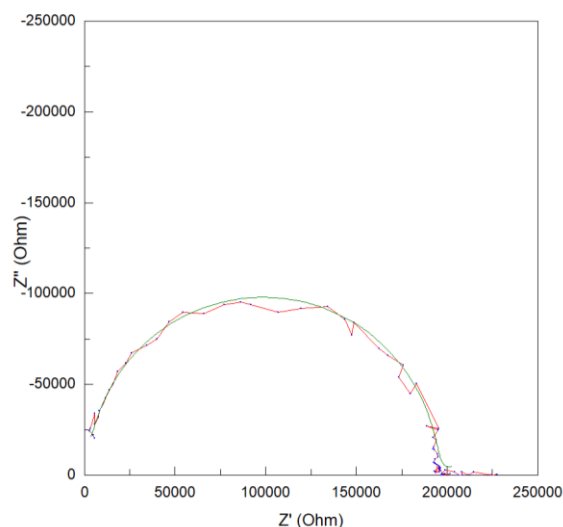


Figure C.14- EIS Pt 4-point probe analysis of sample 322017PCTFE-3c grafted with 5-vinylpyridine and acid treated with 5% HNO₃ at 100C 1% R.H. fit with an equivalent circuit model (left) Nyquist Plot (right) equivalent circuit model fit

322017PVF-1e

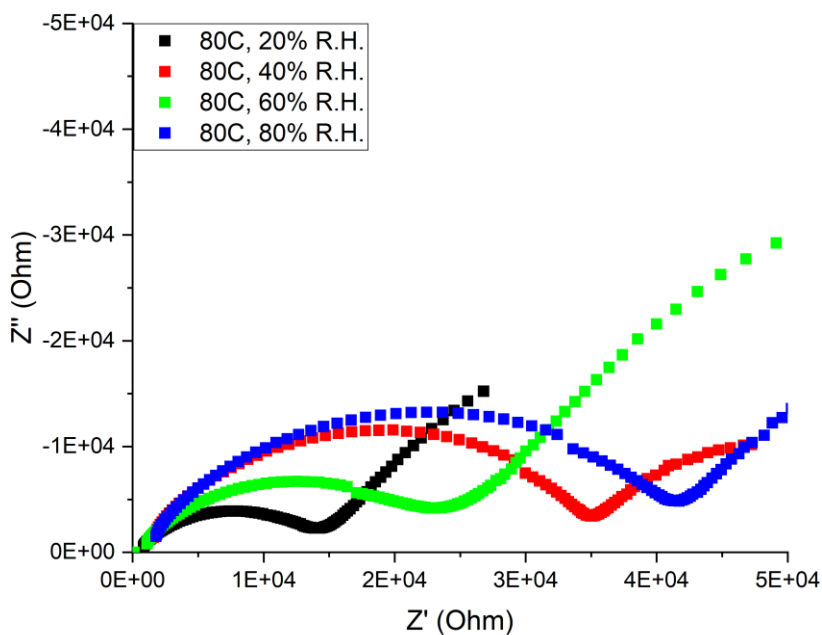


Figure C.15-Nyquist Plot of EIS Pt 4-point probe analysis of sample 322017PVF-1e grafted with 5-vinylpyridine and acid treated with 5% HNO₃ variable temperature 80C: 20%, 40%, 60%, 80% R.H.

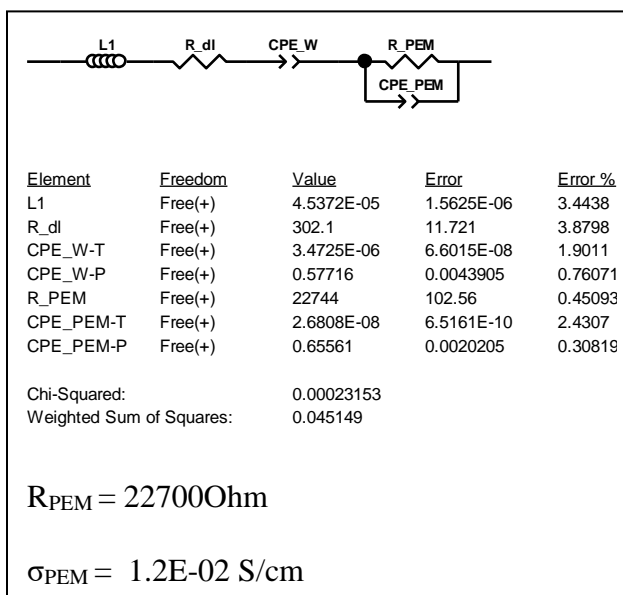
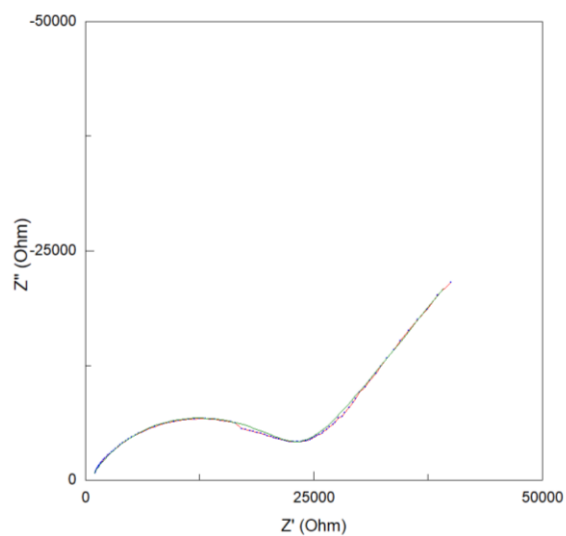


Figure C.16- EIS Pt 4-point probe analysis of sample 322017PVF-1e grafted with 5-vinylpyridine and acid treated with 5% HNO₃ at 80C 60% R.H. fit with an equivalent circuit model (left) Nyquist Plot (right) equivalent circuit model fit

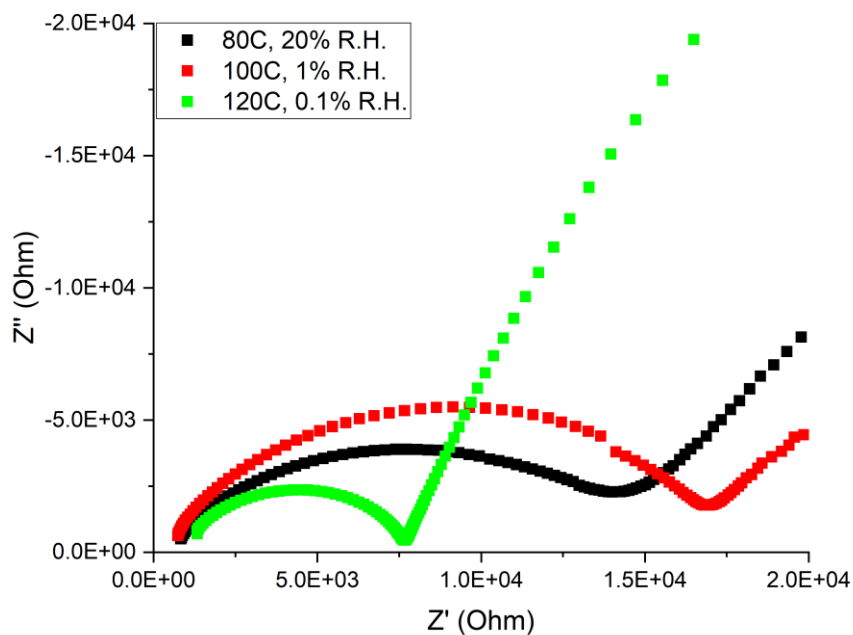


Figure C.17-Nyquist Plot of EIS Pt 4-point probe analysis of sample 322017PVF-1e grafted with 5-vinylpyridine and acid treated with 5% HNO₃ variable temperature 80C, 100C, 120C

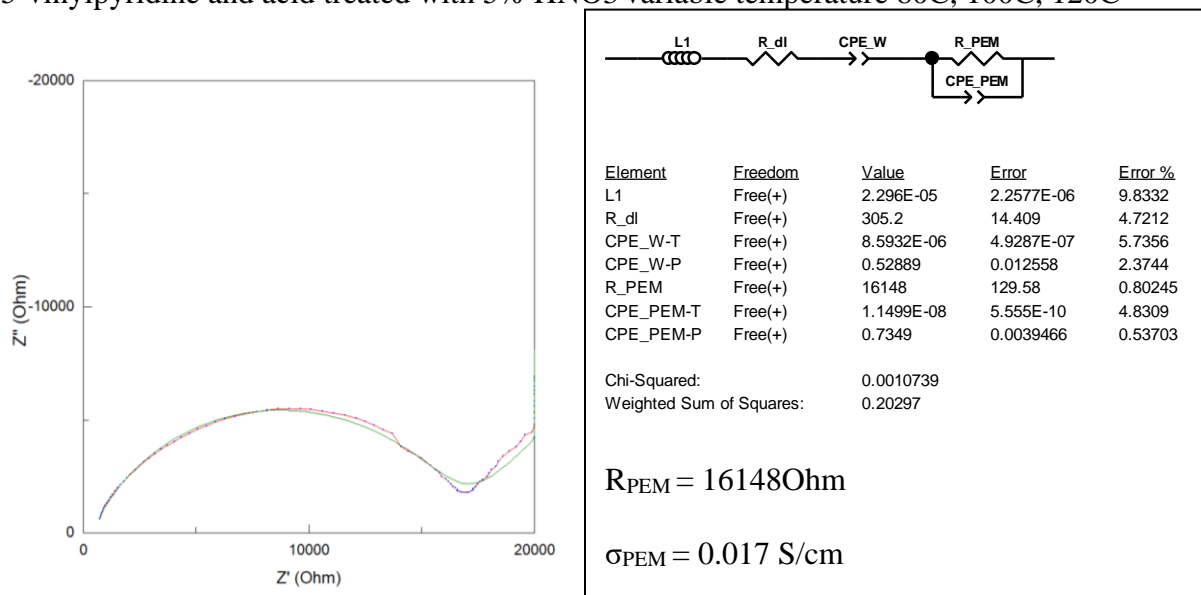


Figure C.18- EIS Pt 4-point probe analysis of sample 322017PVF-1e grafted with 5-vinylpyridine and acid treated with 5% HNO₃ at 100C 1% R.H. fit with an equivalent circuit model (left) Nyquist Plot (right) equivalent circuit model fit

Pt 4-Point Probe Summary: Humidity

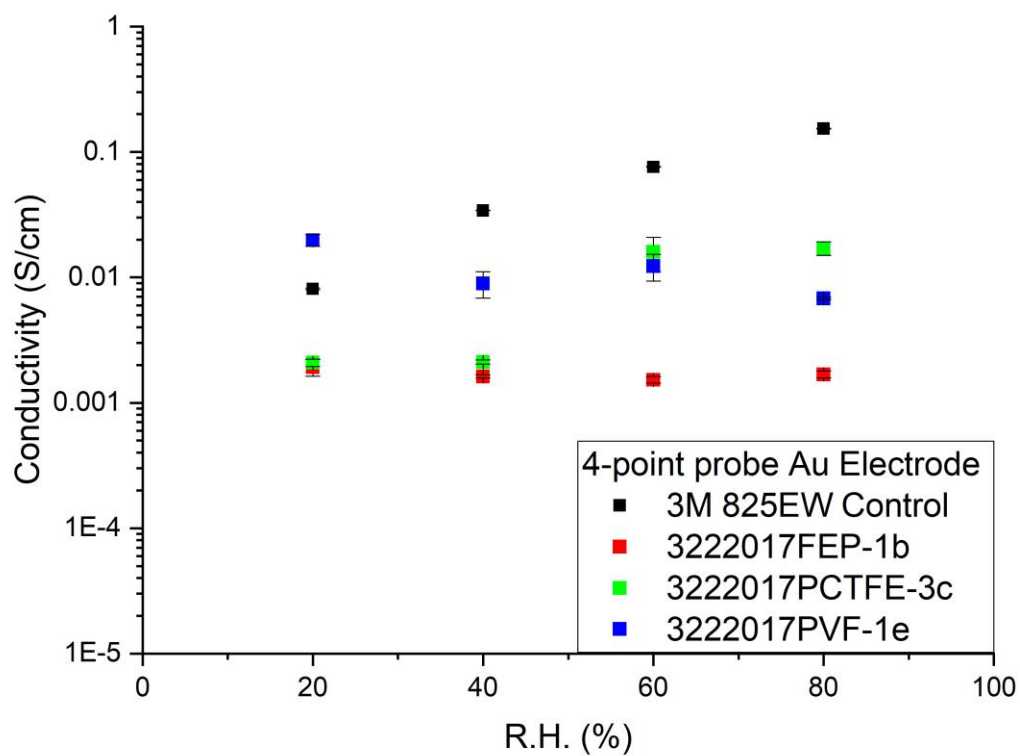


Figure C.19: EIS Proton conductivity as a function of relative humidity at 80°C treated with 5% HNO₃: (black) 3M 825EW Control; PEM were grafted with 5-vinylpyrimidine: (red) 3222017FEP-1b, (green) 322017PCTFE-3c, (blue) 3222017PVF-1e, n = 3

Pt 4-Point Probe Summary: Temperature

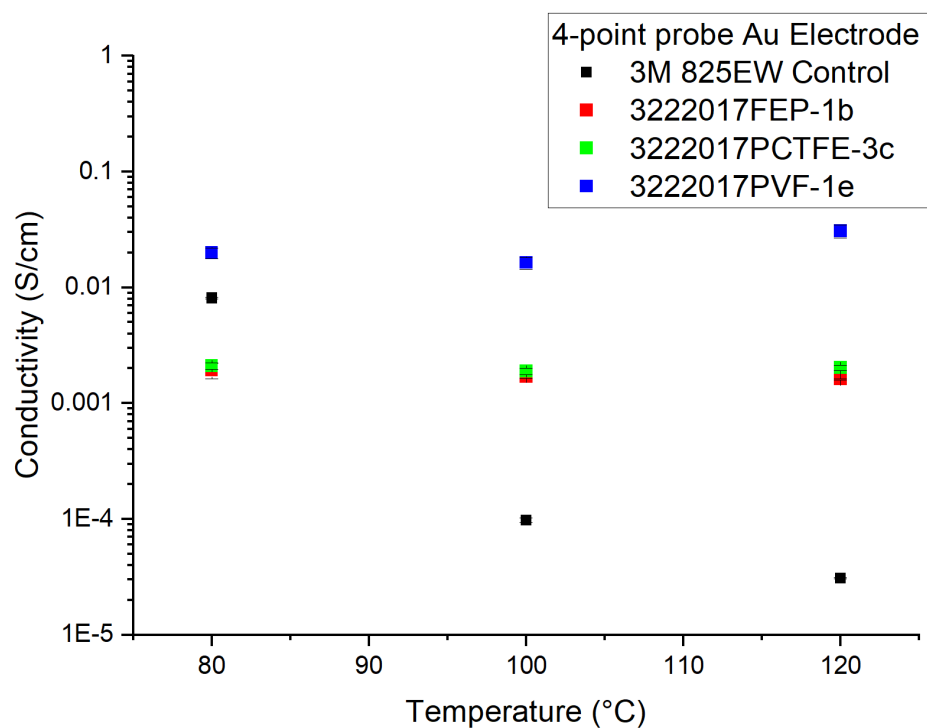


Figure C.20 - EIS proton conductivity as a function of temperature without humidity control treated with 5% HNO_3 : (black) 3M 825EW Control; PEM grafted with 5-vinylpyrimidine: (red) 3222017FEP-1b, (green) 322017PCTFE-3c, (blue) 3222017PVF-1e, $n = 3$

Results/Discussion EIS Analysis

In summary the equivalent circuit model changes due to the membrane testing conditions which causes the significant components of the proton conductivity and the

time constants to shift. Sometimes components also become less significant to the fit as they overlap each other making them indistinguishable. As the temperature rises from 25°C to 100°C the membrane which were loaded wet dehydrates significantly impacting the mobility of protons in the membrane. At this temperature range the proton conductive mechanism is forced to shift from a diffusive mechanism to proton hopping between ionic liquid groups. At approximately 120°C is the glass transition temperature of the grafted ionic liquid groups which is why there is a significant change in the EIS data. At higher temperatures, above 150°C, the substrates of the PEM approaches their melting point causing a decrease in proton conductivity. For other membranes the proton conductivity increases through thermal activation if the structure is stable. The EIS models that were used for fitting the data are subsets of the general model which was selected to represent the electrochemical system of the PEM and the EIS test cell that was used.

The membranes composed of 5-vinylpyridine showed a higher degree of humidity dependence. Whereas, the membranes composed of 4-vinylpyrimidine demonstrated proton hopping under anhydrous conditions. The membrane substrate significantly impacted the thermal stability of the membrane and its behavior under EIS testing. The more amorphous the substrate the higher the proton conductivity but the lower the thermal stability. The amount of crosslinking, degree and density of grafting also significantly impacts the proton conductivity which will be further studied.

Appendix B: DRT Analysis of EIS Data

When developing new materials for electrical applications, it is important to evaluate the electrochemical impedance spectroscopy equivalent circuit model to separate charge kinetics within the system. Through distribution of relaxation time (DRT) analysis it is possible to distinguish between electrochemical ion transport, surface chemical reactions, and gas diffusion from the EIS spectrum. DRT allows for the separation of electrochemical reactions, by their time constants, that are present within an EIS spectrum.[133] These are real and imaginary electrochemical components which make up the equivalent circuit used to model the EIS data. For polymer electrolyte membrane fuel cells these peaks are due to mobility of charges in the membrane and the reactions at the electrodes. The DRT analysis was performed on the EIS data using software DRTools run with Matlab.[134] A summary of the DRT analysis of a promising ionic liquid membrane is described in the following paragraph using the data from Figure A.1 to Figure A.3. This section contains Figure A.4 to Figure A.17 of the DRT analysis of the EIS data for my thesis.

Significant shifts in the DRT plots reveal changes in proton conductivity kinetics and proton conductive mechanism of the membrane. These shifts were observed under variable temperature and humidity conditions. Figure 1 shows that for the 3M 825EW control. One of these shifts in DRT was observed at 100°C in which, the membranes dehydrate, changing the medium of proton conductivity from water to functional groups in the membranes. This transition can be most clearly seen in Figure 2 with the peak at 0.4s(2.5Hz) which represents proton diffusion in the membrane. This was observed by the significant decrease in the mass transport peak which correlates to proton diffusion and a significant drop in proton conductivity across the membranes. However ionic liquids synthesized with 5-vinylpyrimidine were still able to operate under these anhydrous conditions, maintaining conductivity. The sample PVF-1e shown in Figure 14 and Figure 15 maintained its proton conductivity the best at 120°C under anhydrous conditions. The DRT analysis supports the electrochemical models that were used to fit the EIS data and determination of proton conductivity.

An example of the DRT analysis of the Pt 4-point probe EIS measurements is shown for sample 322017PVF-1e which was grafted with 5-vinylpyrimidine and exhibited anhydrous proton conductivity at temperatures above 100°C. The EIS data as a function of temperature is depicted in Figure A.1. The DRT analysis of the EIS data is depicted in Figure A.2 the peak of interest for the conductivity is between ~0.01-0.1s response times. It was observed that as temperature increases, and humidity decreased, the response time decreased. This shift could indicate a new proton conductive mechanism transitioning similar to what was seen in Figure 2. This frequency region corresponds to the conductivity between functional groups rather than mass diffusion. This supports the Grotthuss mechanism, with proton hopping between ionic liquid groups in the PEM. The proton conductivity was modeled using the equivalent circuit model shown in Figure A.1 and the proton conductivity of the membrane was determined from R_{PEM} . The proton conductivity as a function of temperature was plotted in Figure A.3, the proton conductivity of 322017PVF-1e was tested to be 0.031 S/cm at 120°C. This research shows that the ionic liquid monomer is a suitable medium to produce PEM that can be proton conductive under anhydrous conditions. Radiation grafting provides a high degree of versatility

in grafting ionic liquid monomers customizing PEM membranes and controlling their composition.

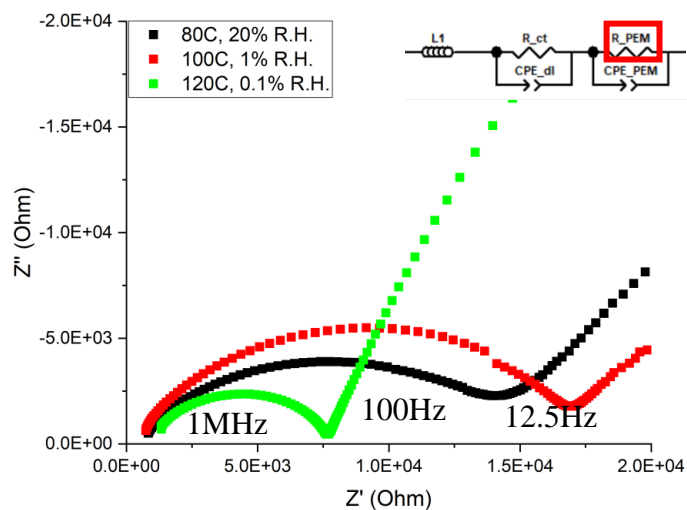


Figure A.1-Nyquist Plot of EIS Pt 4-point probe analysis of sample 322017PVF-1e grafted with 5-vinylpyridine and acid treated with 5% HNO₃ variable temperature 80C, 100C, 120C

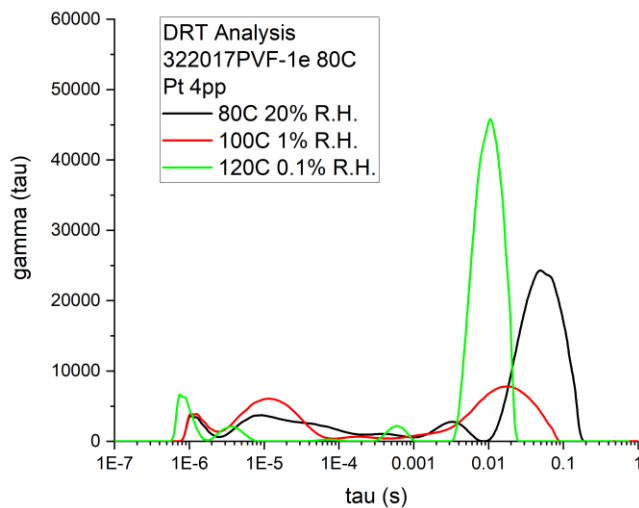


Figure A.2-DRT analysis of EIS data of 322017PVF-1a for variable temperatures 80C, 100C, 120C

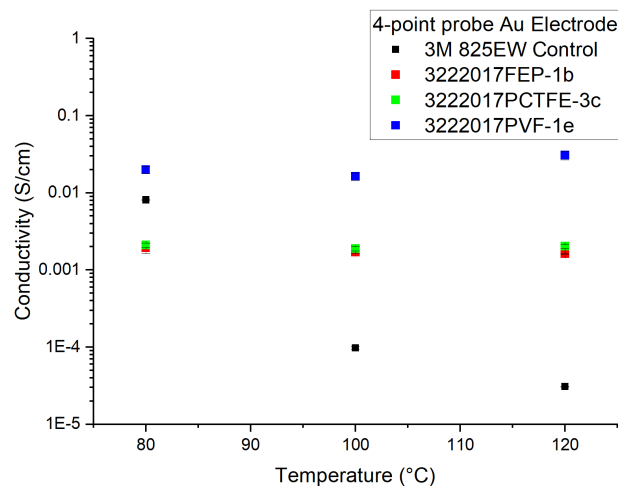


Figure A.3 - EIS proton conductivity as a function of temperature without humidity control treated with 5% HNO_3 : (black) 3M 825EW Control; PEM grafted with 5-vinylpyrimidine: (red) 3222017FEP-1b, (green) 322017PCTFE-3c, (blue) 3222017PVF-1e, $n = 3$

DRT DATA: 2-Point probe EIS data:

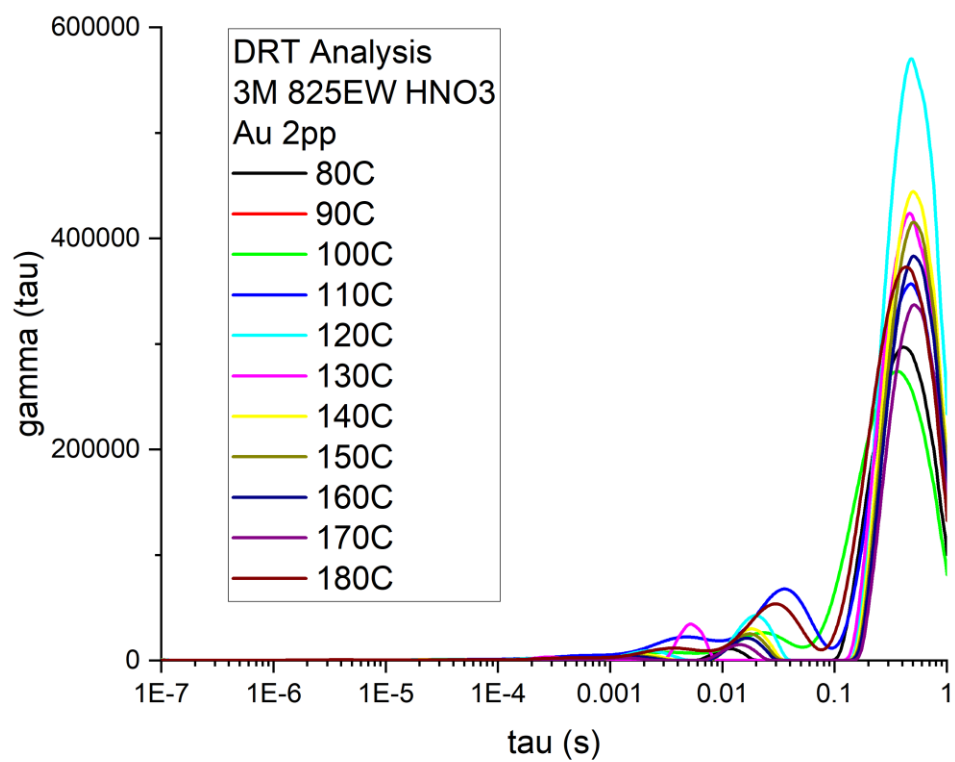


Figure A.4- DRT analysis of EIS data of 3M 825EW control for variable temperatures

PEM synthesized with Monomer_4-Vinylpyridine:

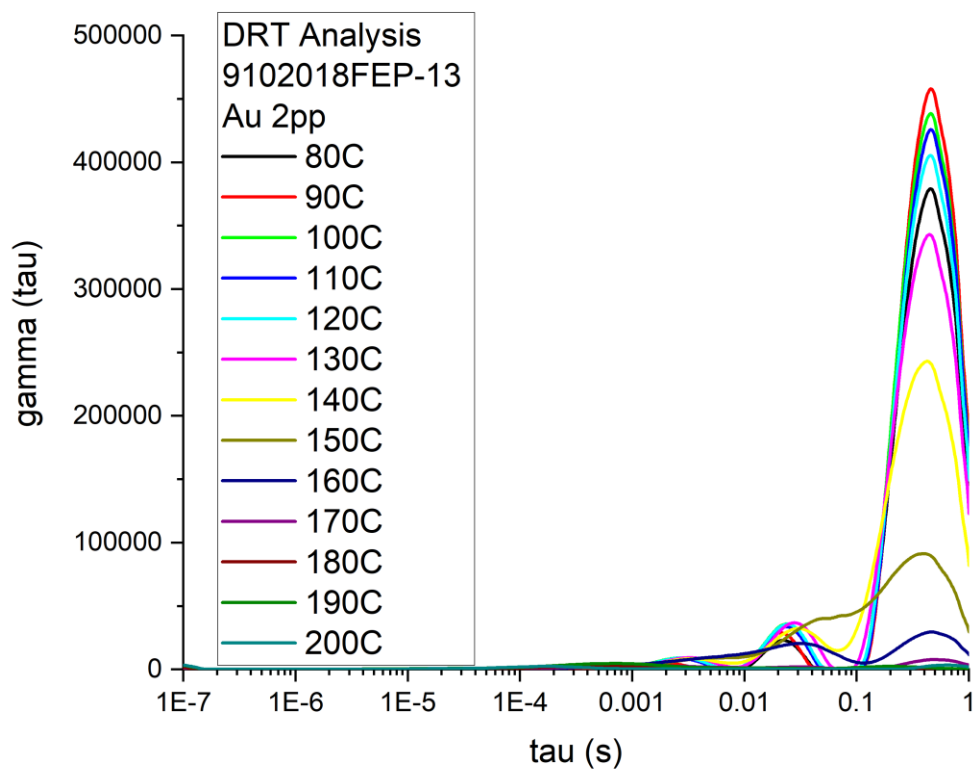


Figure A.5-DRT analysis of EIS data of 9102018FEP-13 for variable temperatures

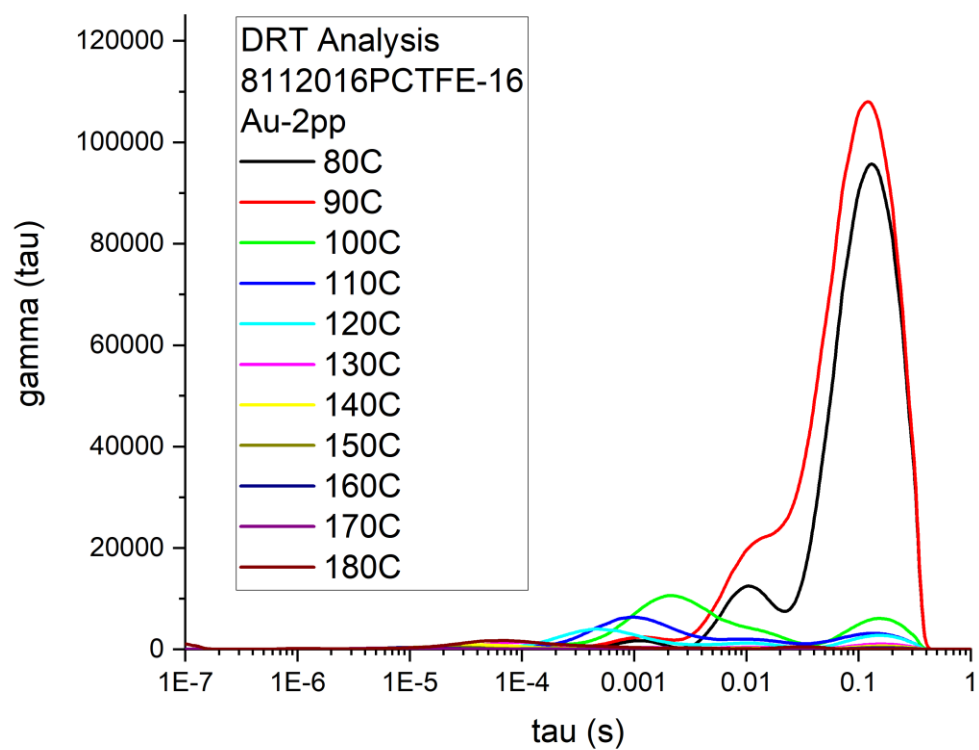


Figure A.6 DRT analysis of EIS data of 8112016PCTFE-16 for variable temperatures

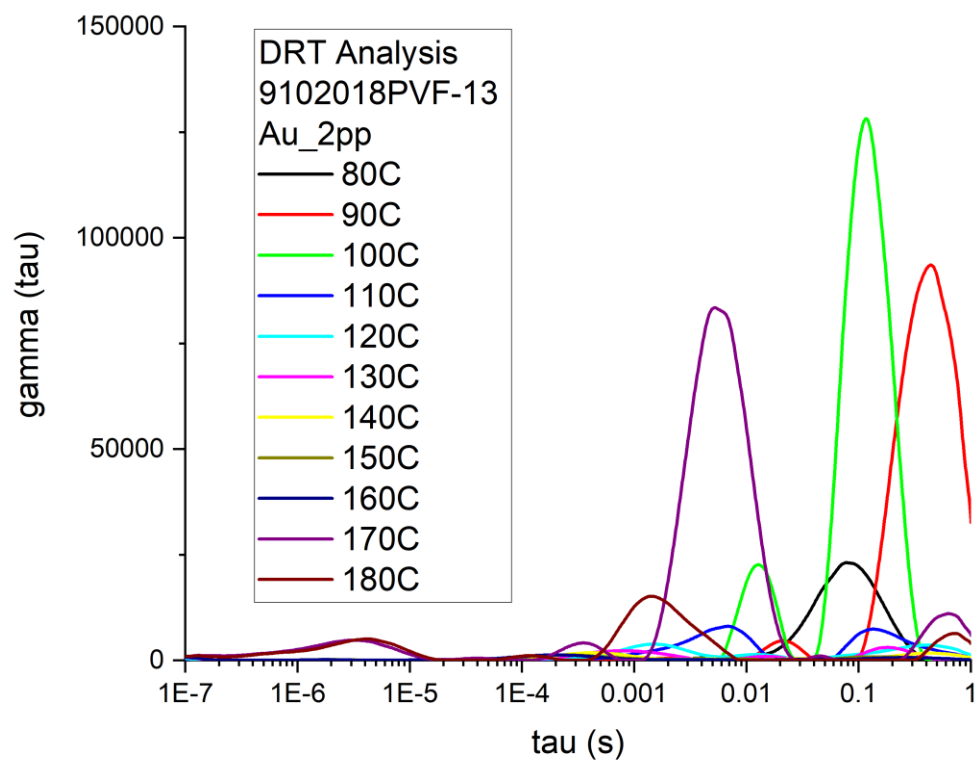


Figure A.7- DRT analysis of EIS data of 9102018PVF-13 for variable temperatures

PEM synthesized with Monomer_5-Vinylpyrimidine:

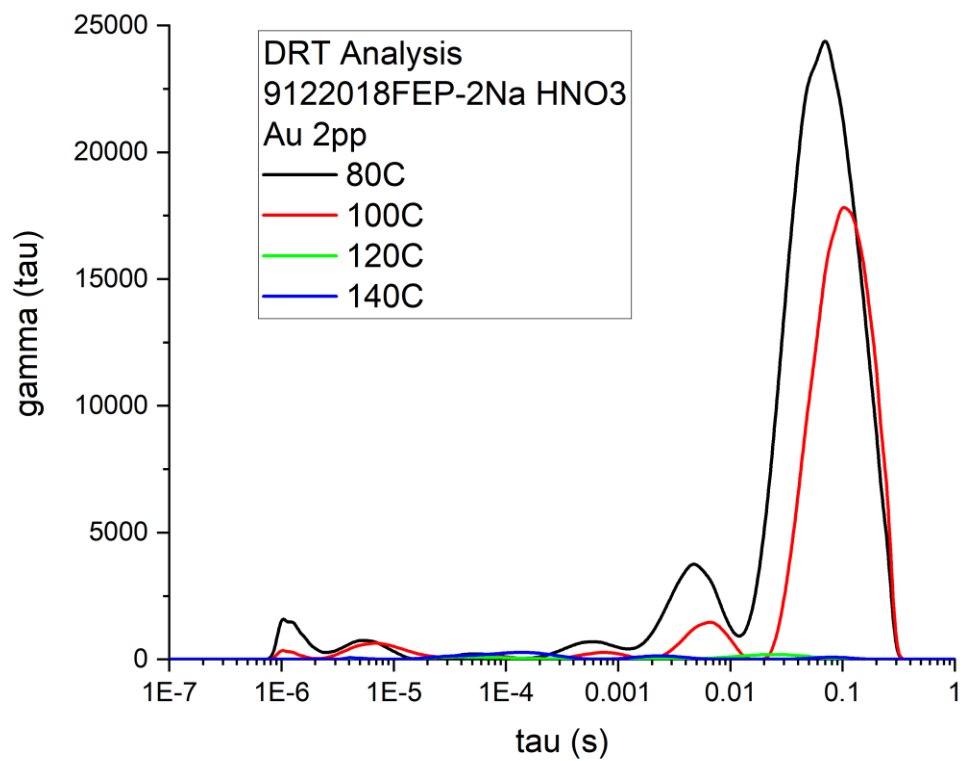


Figure A.8- DRT analysis of EIS data of 9102018FEP-2Na for variable temperatures

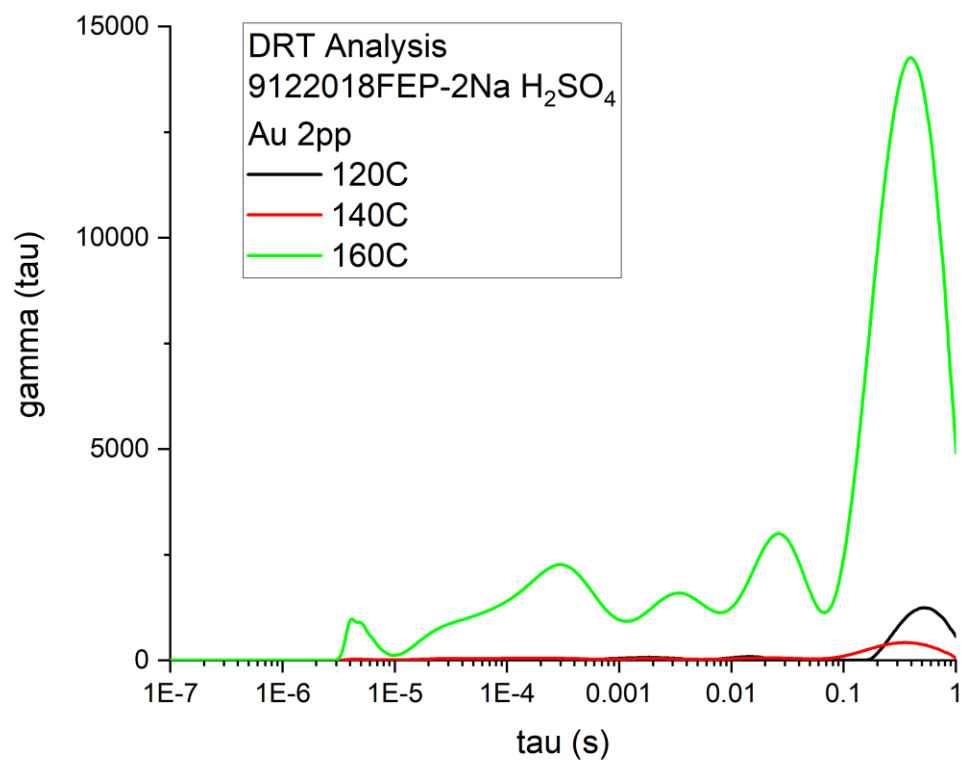


Figure A.9- DRT analysis of EIS data of 9102018FEP-2N for variable temperatures

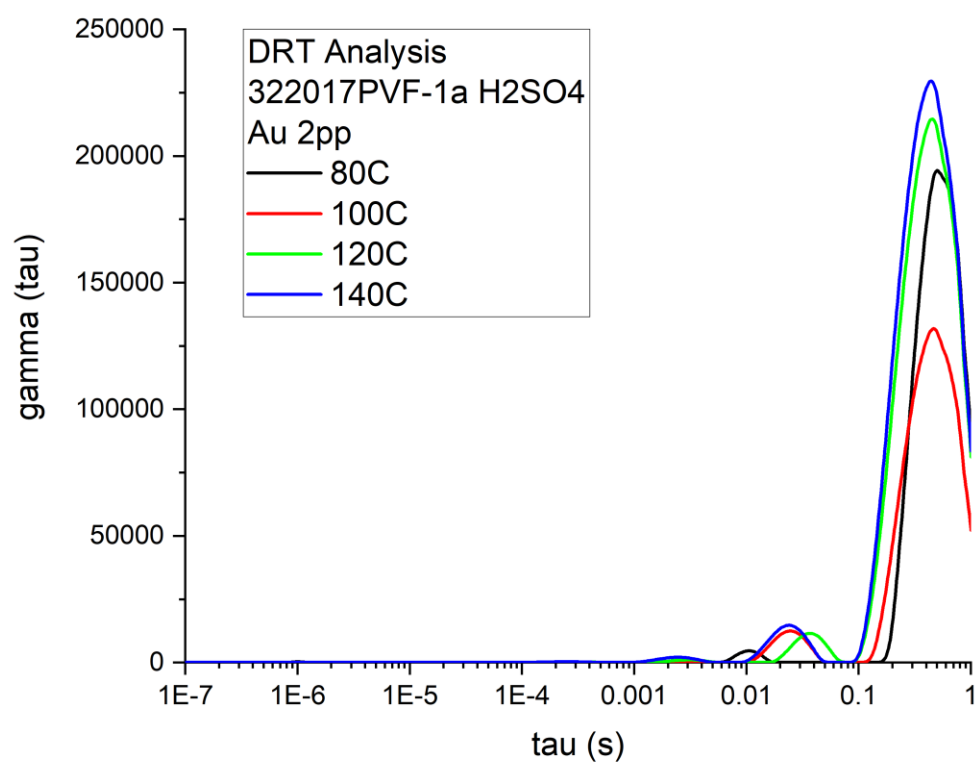


Figure A.10- DRT analysis of EIS data of 322017PVF-1a for variable temperatures

4-Point probe DRT Analysis

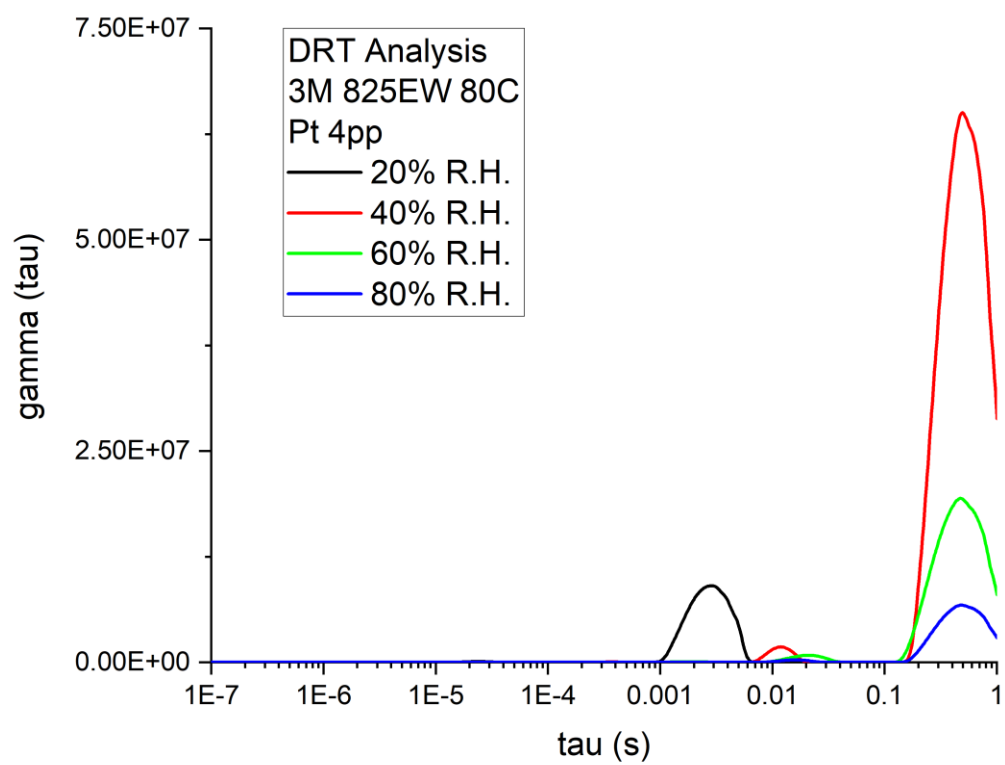


Figure A.11- DRT analysis of EIS data of 3M 825EW control for variable humidity

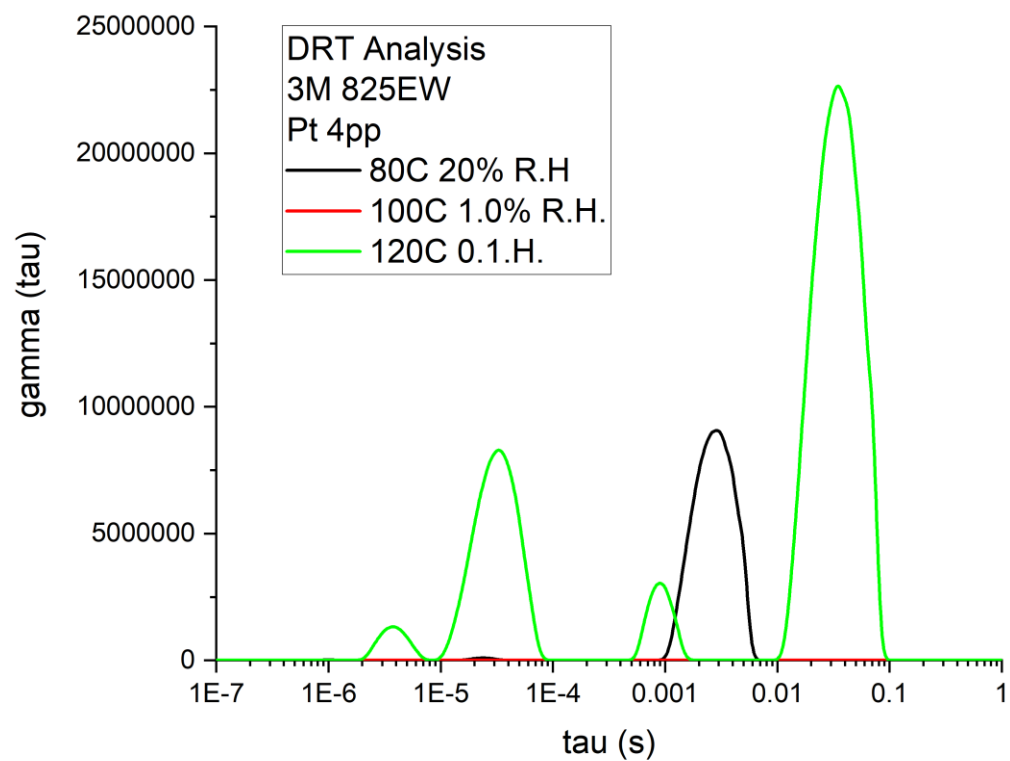


Figure A.12- DRT analysis of EIS data of 3M 825EW control for variable temperature

PEM synthesized with Monomer_5-Vinylpyrimidine:

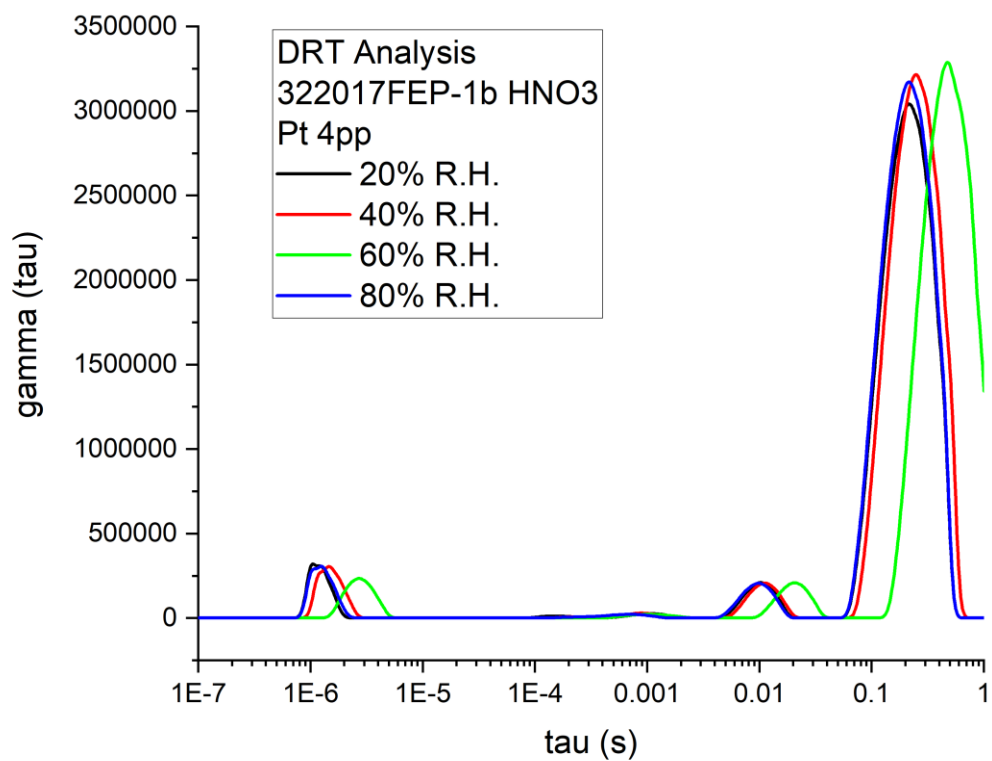


Figure A.13-DRT analysis of EIS data of 322017FEP-1b for variable humidity

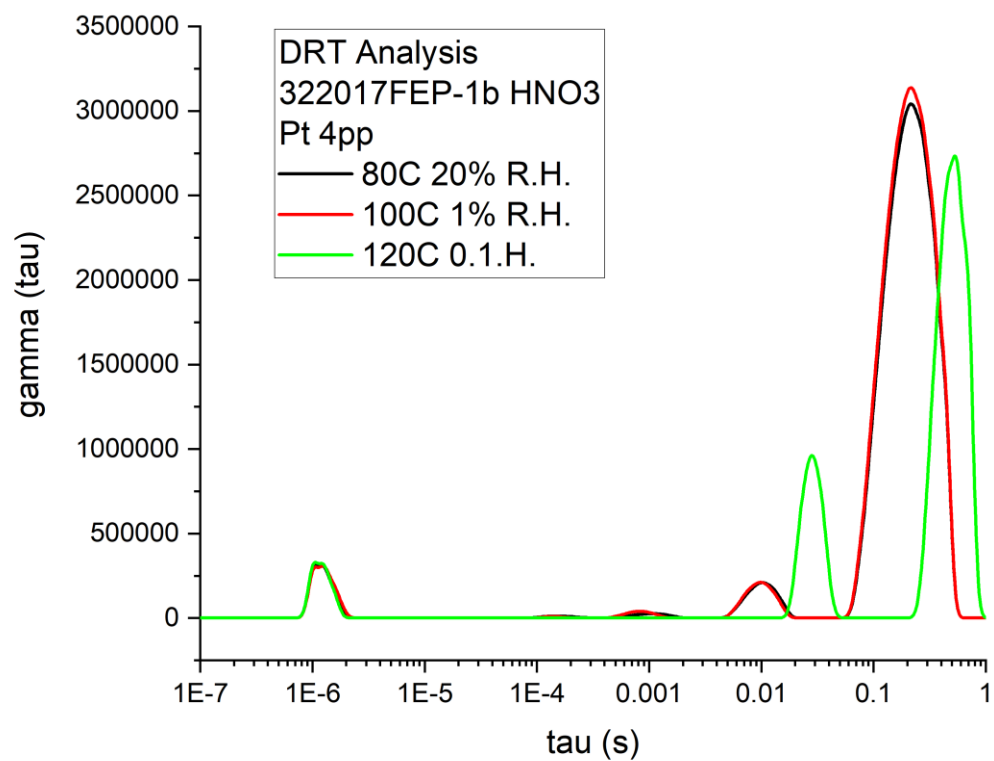


Figure A.14 DRT analysis of EIS data of 322017FEP-1b for variable temperature

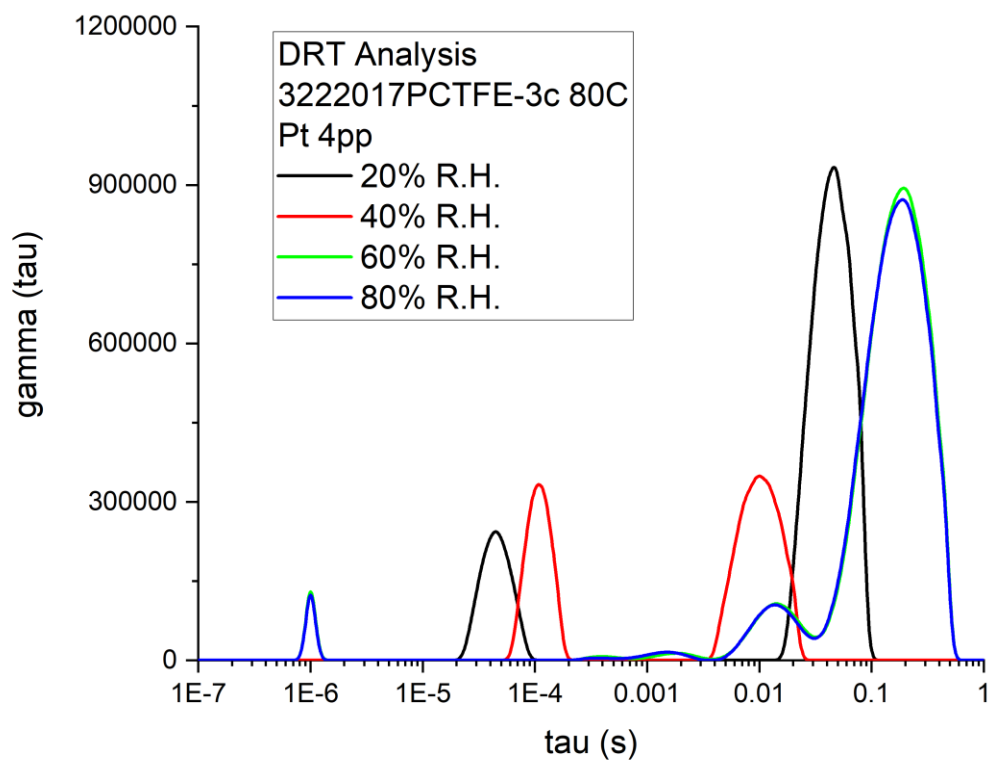


Figure A.14- DRT analysis of EIS data of 3222017PCTFE-3c for variable humidity

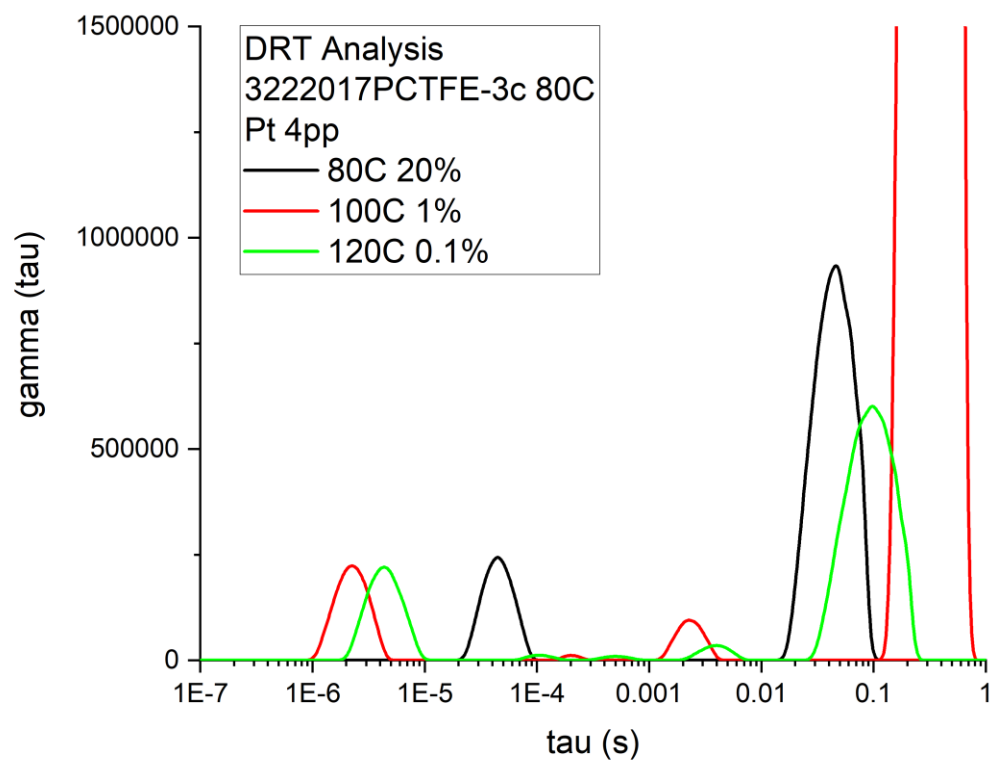


Figure A.15 DRT analysis of EIS data of 3222017PCTFE-3c for variable temperature

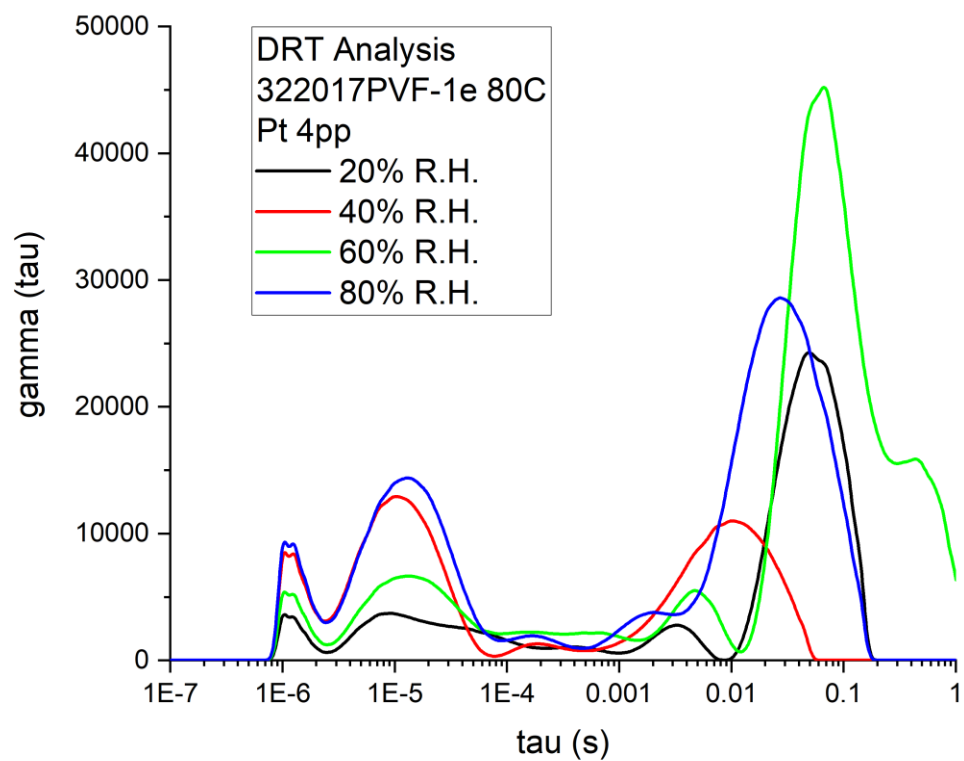


Figure A.16 DRT analysis of EIS data of 3222017PVF-1e for variable humidity

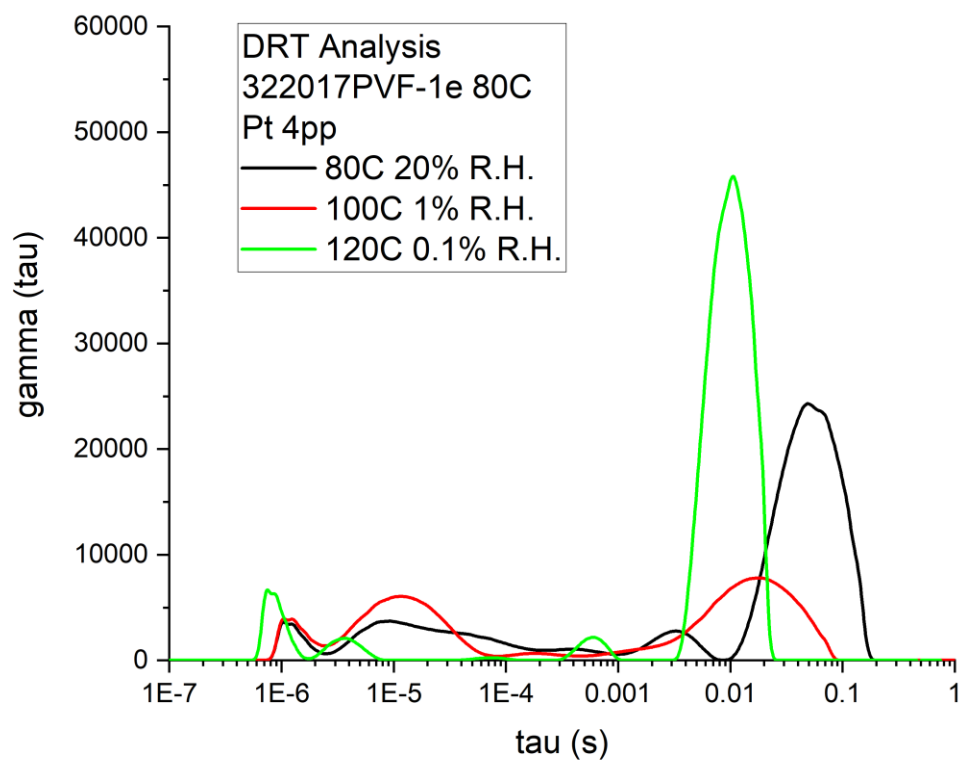


Figure A.17- Figure A.16 DRT analysis of EIS data of 3222017PVF-1e for variable temperature

List of References

- [1] M. Gali, A. Lewandowski, I. St, Ionic liquids as electrolytes, 51 (2006) 5567–5580. doi:10.1016/j.electacta.2006.03.016.
- [2] J.C. An, A. Weaver, B. Kim, A. Barkatt, D. Poster, W.N. Vreeland, J. Silverman, M. Al-Sheikhly, Radiation-induced synthesis of poly(vinylpyrrolidone) nanogel, Polymer (Guildf). 52 (2011) 5746–5755. doi:10.1016/j.polymer.2011.09.056.
- [3] S. Solomon, G. Plattner, R. Knutti, P. Friedlingstein, Irreversible climate change due to carbon dioxide emissions, (2009).
- [4] P.M. Cox, R.A. Betts, C.D. Jones, S.A. Spall, Acceleration of global warming due to carbon-cycle feedbacks in a coupled climate model, 408 (2000) 184–187.
- [5] A.A. Franco, Polymer Electrolyte Fuel Cells : Science, Applications, and Challenges, Pan Stanford Publishing, 2013.
- [6] P. Grimes, Historical Pathways for Fuel Cells The New Electric Century, (n.d.).
- [7] P.B.L. Chaurasia, Y. Ando, T. Tanaka, Regenerative fuel cell with chemical reactions, Energy Convers. Manag. 44 (2003) 611–628.
- [8] O.Z. Sharaf, M.F. Orhan, F. Segura, J.M. Andu, Fuel cells : History and updating . A walk along two centuries, Renew. Sustain. Energy Rev. 32 (2014) 810–853. doi:10.1016/j.rser.2014.01.012.
- [9] A.B. Stambouli, E. Traversa, Solid oxide fuel cells (SOFCs): a review of an environmentally clean and efficient source of energy, 6 (2002) 433–455.
- [10] F.T. Bacon, Fuel cells, past, present and future, Electrochim. Acta. 14 (1969) 569–585.
- [11] W.T. Grubb, L.W. Niedrach, Batteries with Solid Ion-Exchange Membrane

- Electrolytes, J. Electrochem. Soc. 107 (1960) 131.
- [12] F.C. Today, Fuel Cell Electric Vehicles : The Road Ahead, (2013).
http://www.fuelcelltoday.com/media/1711108/fuel_cell_electric_vehicles_-_the_road_ahead_v3.pdf.
- [13] O.Z. Sharaf, M.F. Orhan, An overview of fuel cell technology : Fundamentals and applications, Renew. Sustain. Energy Rev. 32 (2014) 810–853.
doi:10.1016/j.rser.2014.01.012.
- [14] P. Howard, C.J. Greenhill, Ballard PEM Fuel Cell Powered ZeV Bus, SAE Tech. Pape 931817. (1993) 10. doi:10.4271/931817.
- [15] P. Wolfram, N. Lutsey, Electric vehicles : Literature review of technology costs and carbon emissions, Int. Counc. CLEAN Transp. (2016).
doi:10.13140/RG.2.1.2045.3364.
- [16] H.C. November, Hydrogen scaling up, (2017).
- [17] W.C. Lattin, V.P. Utgikar, Transition to hydrogen economy in the United States: A 2006 status report, Int. J. Hydrogen Energy. 32 (2007) 3230–3237.
doi:10.1016/j.ijhydene.2007.02.004.
- [18] S. Dunn, Hydrogen futures : toward a sustainable energy system, 27 (2002) 235–264.
- [19] G.W. Crabtree, M.S. Dresselhaus, M. V Buchanan, G.W. Crabtree, M.S. Dresselhaus, M. V Buchanan, The Hydrogen Economy, 39 (2007).
doi:10.1063/1.1878333.
- [20] G. Locatelli, M. Mancini, N. Todeschini, Generation IV nuclear reactors: Current status and future prospects, Energy Policy. 61 (2013) 1503–1520.

doi:10.1016/j.enpol.2013.06.101.

- [21] X.L. Yan, R. Hino, Nuclear Hydrogen Production Handbook, CRC Press, Boca Raton, 2011.
- [22] J. et al. Chang, A STUDY OF A NUCLEAR HYDROGEN PRODUCTION DEMONSTRATION PLANT, Nucl. Eng. Technol. 37 (2007).
- [23] H. Pu, Polymers for PEM Fuel Cells, John Wiley and Sons, Hoboken, New Jersey, 2014.
- [24] S. Tsushima, K. Teranishi, S. Hirai, Experimental Elucidation of Proton Conducting Mechanism in a Polymer Electrolyte Membrane of Fuel Cell by Nuclei Labeling MRI, ECS Trans. 3 (2006) 91–96. doi:10.1149/1.2356127.
- [25] K.D. Kreuer, Proton conductivity: Materials and applications, Chem. Mater. 8 (1996) 610–641. doi:10.1021/cm950192a.
- [26] P. Choi, N.H. Jalani, R. Datta, Thermodynamics and Proton Transport in Nafion, (2005). doi:10.1149/1.1859814.
- [27] H. Sun, M. Yu, Z. Li, S. Almheiri, A molecular dynamic simulation of hydrated proton transfer in perfluorosulfonate ionomer membranes (Nafion 117), J. Chem. 2015 (2015). doi:10.1155/2015/169680.
- [28] I.N. Levine, Physical Chemistry, 2nd ed., New York, 1978.
- [29] N. Agmon, The Grotthuss mechanism, Chem. Phys. Lett. 244 (1995) 456–462. doi:10.1016/0009-2614(95)00905-J.
- [30] O. Markovitch, N. Agmon, Structure and Energetics of the Hydronium Hydration Shells, J. Phys. Chem. A Lett. 111 (2007) 2253–2256. doi:10.1021/jp068960g.
- [31] M. Eikerling, A.A. Kornyshev, A.M. Kuznetsov, J. Ulstrup, S. Walbran,

- Mechanisms of proton conductance in polymer electrolyte membranes, *J. Phys. Chem. B.* 105 (2002) 3646–3662. doi:10.1021/jp003182s.
- [32] T. Thampan, S. Malhotra, H. Tang, R. Datta, Modeling of Conductive Transport in Proton-Exchange Membranes for Fuel Cells, *J. Electrochem. Soc.* 147 (2000) 3242–3250.
- [33] D.E. Curtin, R.D. Lousenberg, T.J. Henry, P.C. Tangeman, M.E. Tisack, Advanced materials for improved PEMFC performance and life, *J. Power Sources.* 131 (2004) 41–48. doi:10.1016/j.jpowsour.2004.01.023.
- [34] B.N. Kim, D.H. Lee, S.W. Lee, D.H. Han, Improvement of polymer electrolyte membrane by radiation-induced grafting of styrene onto FEP film with subsequent sulfonation, *Korean J. Chem. Eng.* 25 (2008) 1212–1220. doi:10.1007/s11814-008-0201-4.
- [35] X. Cheng, Z. Shi, N. Glass, L. Zhang, J. Zhang, D. Song, Z.S. Liu, H. Wang, J. Shen, A review of PEM hydrogen fuel cell contamination: Impacts, mechanisms, and mitigation, *J. Power Sources.* 165 (2007) 739–756. doi:10.1016/j.jpowsour.2006.12.012.
- [36] S. Bose, T. Kuila, T. Xuan, H. Nguyen, N. Hoon, Progress in Polymer Science Polymer membranes for high temperature proton exchange membrane fuel cell : Recent advances and challenges, *Prog. Polym. Sci.* 36 (2011) 813–843. doi:10.1016/j.progpolymsci.2011.01.003.
- [37] J.J. Baschuk, X.L. R, Carbon monoxide poisoning of proton exchange membrane fuel cells, *Int. J. Energy Res.* 713 (2001) 695–713. doi:10.1002/er.713.
- [38] Q. Li, R. He, J.-A. Gao, J.O. Jensen, N.J. Bjerrum, The CO Poisoning Effect in

- PEMFCs Operational at Temperatures up to 200°C, *J. Electrochem. Soc.* 150 (2003) A1599. doi:10.1149/1.1619984.
- [39] J. Zhang, Z. Xie, J. Zhang, Y. Tang, C. Song, T. Navessin, Z. Shi, D. Song, H. Wang, D.P. Wilkinson, Z.S. Liu, S. Holdcroft, High temperature PEM fuel cells, *J. Power Sources*. 160 (2006) 872–891. doi:10.1016/j.jpowsour.2006.05.034.
- [40] R.L. Clough, High-energy radiation and polymers : A review of commercial processes and emerging applications, 185 (2001) 8–33.
- [41] P.J. Flory, *Principles of Polymer Chemistry*, Cornell University Press, 1953.
- [42] A.G. Chmielewski, Progress in radiation processing of polymers, *Nucl. Instruments Methods Phys. Res. B*. 236 (2005) 44–54. doi:10.1016/j.nimb.2005.03.247.
- [43] R.J. Woods, A.K. Pikaev, *Applied Radiation Chemistry Radiation Processing*, John Wiley and Sons, New York, N.Y., 1994.
- [44] M.R. Cleland, L.A. Parks, S. Cheng, Applications for radiation processing of materials, *Nucl. Instruments Methods Phys. Res. B*. 208 (2003) 66–73. doi:10.1016/S0168-583X(03)00655-4.
- [45] J.W.T. Spinks, R.J. Woods, *An Introduction to Radiation Chemistry*, Wiley, New York, 1964.
- [46] D. Feldman, Polymer History, *Des. Monomers Polym.* 11 (2008) 1–15. doi:10.1163/156855508X292383.
- [47] G. Choppin, J.-O. Liljenzin, J. Rydberg, C. Ekberg, *Radiochemistry and Nuclear Chemistry*, Elsevier, 2013.
- [48] E. Giannetti, Thermal stability and bond dissociation energy of fluorinated

- polymers : A critical evaluation, 126 (2005) 625–632.
doi:10.1016/j.jfluchem.2005.01.008.
- [49] S. Le Caë, Water Radiolysis: Influence of Oxide Surfaces on H₂ Production under Ionizing Radiation, *Water*. 3 (2011) 235–253. doi:10.3390/w3010235.
- [50] R. Farhataziz, *Radiation Chemistry: Principles and Applications*, VCH Publisher, New York, N.Y., 1987.
- [51] E.L. Alpen, *Radiation Biophysics*, 2nd ed., Academic Press, San Diego, 1998.
- [52] G. Nelson, D. Rewy, *Gamma-Ray Interactions with Matter*, (1909).
- [53] J.F. Watts, *An Introduction to Surface Analysis by Electron Spectroscopy*, Oxford University Press, 1990.
- [54] R. Mehnert, *Review of industrial applications of electron accelerators*, (1996).
- [55] J.D. Bourland, *Radiation Oncology Physics*, 3rd ed., Elsevier, 2012.
www.sciencedirect.com/science/article/pii/B9781437716375000067.
- [56] A. Chapiro, Chemical Modification in Irradiated Polymers, *Nucl. Instruments Methods Phys. Res. B*. 32 (1988) 111–114.
- [57] J.S. Forsythe, D.J.T. Hill, Radiation chemistry of fluoropolymers, *Prog. Polym. Sci.* 25 (2000) 101–136. doi:10.1016/S0079-6700(00)00008-3.
- [58] V.Y. Kabanov, RADIATION INDUCED GRAFT POLYMERIZATION IN THE USSR, 33 (1989).
- [59] S.D. Smith, S.D. Alexandratos, Ion-Selective Polymer-supported Reagents, *Solvent Extration Ion Exch.* 18 (2000).
- [60] L. Gubler, S.A. Gürsel, G.G. Scherer, Radiation grafted membranes for polymer electrolyte fuel cells, *Fuel Cells*. 5 (2005) 317–335. doi:10.1002/fuce.200400078.

- [61] M.M. Nasef, Radiation-Grafted Membranes for Polymer Electrolyte Fuel Cells : Current Trends and Future Directions, (2014). doi:10.1021/cr4005499.
- [62] A.B. Kim, A. Weaver, M. Chumakov, I.M. Pazos, L. Dianne, B. Kim, A. Weaver, M. Chumakov, I.M. Pazos, D.L. Poster, K. Gaskell, Mechanisms and Characterization of the Pulsed Electron-Induced Grafting of Styrene onto Poly (tetrafluoroethylene-co- hexafluoropropylene) to Prepare a Polymer Electrolyte Membrane Mechanisms and Characterization of the Pulsed Electron-Induced Grafting, *Radiat. Res.* 190 (2018) 309–321. doi:10.1667/RR15006.1.
- [63] A. Bhattacharya, B.N. Misra, Grafting : a versatile means to modify polymers Techniques , factors and applications, 29 (2004) 767–814. doi:10.1016/j.progpolymsci.2004.05.002.
- [64] V.T. Stannett, Section 2.2. co-polymerization and grafting, 35 (1990) 82–87.
- [65] R. Bouchet, Proton conduction in acid doped polybenzimidazole, *Solid State Ionics.* 118 (1999) 287–299. doi:10.1016/S0167-2738(98)00466-4.
- [66] L. Gubler, Polymer Design Strategies for Radiation-Grafted Fuel Cell Membranes, (2014). doi:10.1002/aenm.201300827.
- [67] B.N. Kim, D.H. Lee, D.H. Han, Thermal, mechanical and electrical properties on the styrene-grafted and subsequently sulfonated FEP film induced by electron beam, *Polym. Degrad. Stab.* 93 (2008) 1214–1221. doi:10.1016/j.polymdegradstab.2008.01.034.
- [68] V.Y. Kabanov, Preparation of Polymer Membranes for Fuel Cells by Radiation Graft Polymerization 1, 38 (2004) 83–91.
- [69] K.D. Kreuer, On the development of proton conducting polymer membranes for

- hydrogen and methanol fuel cells, *J. Memb. Sci.* 185 (2001) 29–39.
doi:10.1016/S0376-7388(00)00632-3.
- [70] K.D. Kreuer, a. Fuchs, M. Ise, M. Spaeth, J. Maier, Imidazole and pyrazole-based proton conducting polymers and liquids, *Electrochim. Acta.* 43 (1998) 1281–1288.
doi:10.1016/S0013-4686(97)10031-7.
- [71] C. Ke, J. Li, X. Li, Z. Shao, B. Yi, Protic ionic liquids: an alternative proton-conducting electrolyte for high temperature proton exchange membrane fuel cells, *RSC Adv.* 2 (2012) 8953. doi:10.1039/c2ra21378h.
- [72] R. Marschall, M. Sharifi, M. Wark, Microporous and Mesoporous Materials Proton conductivity of imidazole functionalized ordered mesoporous silica : Influence of type of anchorage , chain length and humidity, *Microporous Mesoporous Mater.* 123 (2009) 21–29. doi:10.1016/j.micromeso.2009.03.019.
- [73] J.S. Wainright, Acid-Doped Polybenzimidazoles: A New Polymer Electrolyte, *J. Electrochem. Soc.* 142 (1995) L121. doi:10.1149/1.2044337.
- [74] M. Díaz, A. Ortiz, I. Ortiz, Progress in the use of ionic liquids as electrolyte membranes in fuel cells, *J. Memb. Sci.* 469 (2014) 379–396.
doi:10.1016/j.memsci.2014.06.033.
- [75] D.R. MacFarlane, N. Tachikawa, M. Forsyth, P.C. Pringle, Jennifer M. Howlett, G.D. Elliott, J.H. Davis Jr., M. Watanabe, P. Simon, A. Angell, Energy Applications of Ionic Liquids, *Energy Environ. Sci.* 7 (2014).
doi:10.1039/c3ee42099j.
- [76] J.F. Wishart, Energy applications of ionic liquids, *R. Soc. Chem.* 2 (2009) 956–961. doi:10.1039/b906273d.

- [77] S. Yi, F. Zhang, W. Li, C. Huang, H. Zhang, M. Pan, Anhydrous elevated-temperature polymer electrolyte membranes based on ionic liquids, *J. Memb. Sci.* 366 (2011) 349–355. doi:10.1016/j.memsci.2010.10.031.
- [78] A. Noda, S. Mitsushima, M. Watanabe, S. Engineering, Brønsted acid – base ionic liquids and their use as new materials for anhydrous proton conductors, (2003) 938–939.
- [79] T.L. Greaves, C.J. Drummond, Protic ionic liquids: Properties and applications, *Chem. Rev.* 108 (2008) 206–237. doi:10.1021/cr068040u.
- [80] E.C.S. Transactions, T.E. Society, Proton Exchange membranes for high temperature fuel cells: Equivalent weight and end group effects on conductivity Manale Maalouf, 25 (2009) 1473–1481.
- [81] S.R. Narayanan, S.P. Yen, L. Liu, S.G. Greenbaum, Anhydrous proton-conducting polymeric electrolytes for fuel cells, *J. Phys. Chem. B.* 110 (2006) 3942–3948. doi:10.1021/jp054167w.
- [82] Q. Li, J. Oluf, R.F. Savinell, N.J. Bjerrum, Progress in Polymer Science High temperature proton exchange membranes based on polybenzimidazoles for fuel cells, *Prog. Polym. Sci.* 34 (2009) 449–477. doi:10.1016/j.progpolymsci.2008.12.003.
- [83] W. Qian, J. Texter, F. Yan, Frontiers in poly(ionic liquid)s: syntheses and applications, *Chem. Soc. Rev.* (2017) 1124–1159. doi:10.1039/c6cs00620e.
- [84] M. Doyle, S.K. Choi, G. Proulx, High-Temperature Proton Conducting Membranes Based on Perfluorinated Ionomer Membrane-Ionic Liquid Composites, *J. Electrochem. Soc.* 147 (2000) 34. doi:10.1149/1.1393153.

- [85] V. Di Noto, E. Negro, J. Sanchez, C. Iojoiu, S. Chimiche, V. Uni, Structure-Relaxation Interplay of a New Nanostructured Membrane Based on Tetraethylammonium Trifluoromethanesulfonate Ionic Liquid and Neutralized Nafion 117 for High-Temperature Fuel Cells, *J. Am. Chem. Soc.* 3 (2010) 2183–2195.
- [86] C. Schmidt, T. Glück, G. Schmidt-naake, Modification of Nafion Membranes by Impregnation with Ionic Liquids, *Chem. Engineering Technol.* (2008) 13–22. doi:10.1002/ceat.200700054.
- [87] E. Cho, J.-S. Park, S.S. Sekhon, G.-G. Park, T.-H. Yang, W.-Y. Lee, C.-S. Kim, S.-B. Park, A Study on Proton Conductivity of Composite Membranes with Various Ionic Liquids for High-Temperature Anhydrous Fuel Cells, *J. Electrochem. Soc.* 156 (2009) B197. doi:10.1149/1.3031406.
- [88] M. Armand, F. Endres, D.R. MacFarlane, H. Ohno, B. Scrosati, Ionic-liquid materials for the electrochemical challenges of the future, *Nat. Mater.* 8 (2009) 621–629. doi:10.1038/nmat2448.
- [89] H. Zhang, W. Wu, J. Wang, T. Zhang, B. Shi, J. Liu, Enhanced anhydrous proton conductivity of polymer electrolyte membrane enabled by facile ionic liquid-based hopping pathways, *J. Memb. Sci.* 476 (2015) 136–147. doi:10.1016/j.memsci.2014.11.033.
- [90] A.S. Amarasekara, Acidic Ionic Liquids, *Chem. Rev.* 116 (2016) 6133–6183. doi:10.1021/acs.chemrev.5b00763.
- [91] J. Belieres, C.A. Angell, Protic Ionic Liquids : Preparation , Characterization , and Proton Free Energy Level, (2007) 4926–4937. doi:10.1021/jp067589u.

- [92] M.S. Miran, H. Kinoshita, T. Yasuda, A. Bin, H. Susan, Hydrogen bonds in protic ionic liquids and their correlation with physicochemical properties w, ChemComm. (2011) 12676–12678. doi:10.1039/c1cc14817f.
- [93] J. Stoimenovski, E.I. Izgorodina, D.R. Macfarlane, Ionicity and proton transfer in protic ionic liquids, Phys. Chem. Chem. Phys. (2010). doi:10.1039/c0cp00239a.
- [94] W. Tatara, M.J. Wo, J. Lindgren, M. Probst, Theoretical Study of Structures , Energies , and Vibrational Spectra of the Imidazole - Imidazolium System, J. Phys. Chem. A. (2003) 7827–7831. doi:10.1021/jp030065z.
- [95] M. Yoshizawa, W. Xu, C.A. Angell, Ionic Liquids by Proton Transfer : Vapor Pressure , Conductivity , and the Relevance of ΔpK_a from Aqueous Solutions, (2003) 15411–15419. doi:10.1021/ja035783d.
- [96] M.D. Green, T.E. Long, Designing Imidazole-Based Ionic Liquids and Ionic Liquid Monomers for Emerging Technologies, Polym. Rev. 49 (2009) 291–314.
- [97] T. Yasuda, M. Watanabe, Protic ionic liquids : Fuel cell applications, Mater. Res. Soc. (2015). doi:10.1557/mrs.2013.153.
- [98] T.J. Schmidt, K. Simbeck, G.G. Scherer, Influence of Cross-Linking on Performance of Radiation-Grafted and Sulfonated FEP 25 Membranes in H₂-O₂ PEFC, J. Electrochem. Soc. 152 (2005) A93. doi:10.1149/1.1829412.
- [99] M. Park, REVIEW RADIATION CROSSLINKING OF FLUOROPOLYMERS- A REVIEW, 45 (1995) 159–174.
- [100] DuPont, TeflonTM FEP, Bull. Inf. (n.d.) 1–10.
- [101] HydroBlock[®] P-Series TR Film -, (2013) 2013.
- [102] Fluorotherm, PCTFE Properties, (2019). <https://www.fluorotherm.com/technical->

information/materials-overview/pctfe-properties/.

- [103] DuPont, DuPont TM Tedlar ® Polyvinyl Fluoride (PVF) Films, (n.d.) 1–4.
- [104] J. Chen, M. Asano, Y. Maekawa, M. Yoshida, Suitability of some fluoropolymers used as base films for preparation of polymer electrolyte fuel cell membranes, 277 (2006) 249–257. doi:10.1016/j.memsci.2005.10.036.
- [105] J. Lu, F. Yan, J. Texter, Advanced applications of ionic liquids in polymer science, Prog. Polym. Sci. 34 (2009) 431–448. doi:10.1016/j.progpolymsci.2008.12.001.
- [106] T.R. Ralph, Proton exchange membrane fuel cells, Platin. Met. Rev. 41 (1997) 102–113. doi:10.1016/j.vacuum.2006.03.029.
- [107] D.E. Plastics, Stanyl PA46 General Information, 2005. https://cgtec.eu/wp-content/uploads/Stanyl_brochure_02.pdf.
- [108] F.B. Bateman, Medical-Industrial Radiation Facility, NIST/Tools & Instruments. (2017). <https://www.nist.gov/laboratories/tools-instruments/medical-industrial-radiation-facility>.
- [109] ISO/ASTM 51607:2013: Practice for use of the alanine-EPR dosimetry system, (n.d.). <https://www.iso.org/standard/62955.html>.
- [110] T.R. Dargaville, G.A. George, D.J.T. Hill, A.K. Whittaker, High energy radiation grafting of fluoropolymers, Prog. Polym. Sci. 28 (2003) 1355–1376. doi:10.1016/S0079-6700(03)00047-9.
- [111] R.E. Florin, L.A. Wall, Gamma Irradiation of Fluorocarbon Polymers *, 65 (1961) 375–387.
- [112] Y. Tabata, A. Oshima, Temperature Dependence of Radiation Effects on Polymers, Macromol. Symp. 143 (1999) 337–358.

- [113] H.-P. Brack, H.G. Buhner, L. Bonorand, G.G. Scherer, Grafting of pre-irradiated poly(ethylene--tetrafluoroethylene) films with styrene: influence of base polymer film properties and processing parameters, *J. Mater. Chem.* 10 (2000) 1795–1803. doi:10.1039/b001851l.
- [114] J. Jiang, R. t. Weber, Bruker EPR Spectrometer User's Manual Advanced Operations, 2000.
- [115] J.E. Wilson, Radiation Chemistry of Monomers, Polymers, and Plastics, Marcel Dekker Inc., M. Dekker: New York, 1974.
- [116] Gamry Instruments, Basics of Electrochemical Impedance Spectroscopy, (n.d.). <https://www.gamry.com/application-notes/EIS/basics-of-electrochemical-impedance-spectroscopy/>.
- [117] J.Z. Xiao-Zi Yuan, Chaojie Song, Haijiang Wang, EIS Diagnosis for PEM Fuel Cell Performance, 2010. doi:10.1007/978-1-84882-846-9_5.
- [118] Z. Xie, C. Song, B. Andreaus, T. Navessin, Z. Shi, J. Zhang, S. Holdcroft, Discrepancies in the measurement of ionic conductivity of PEMs using two- and four probe AC impedance spectroscopy, *J. Electrochem. Soc.* 153 (2006) 173–178.
- [119] I. Pivac, F. Barbir, Inductive phenomena at low frequencies in impedance spectra of proton exchange membrane fuel cells e A review, *J. Power Sources.* 326 (2016) 112–119. doi:10.1016/j.jpowsour.2016.06.119.
- [120] C.H. Lee, H.B. Park, Y.M. Lee, R.D. Lee, Importance of Proton Conductivity Measurement in Polymer Electrolyte Membrane for Fuel Cell Application, *Ind. Eng. Chem. Res.* 44 (2005) 7617–7626. doi:10.1021/ie0501172.
- [121] K. Schmidt-Rohr, Q. Chen, Parallel cylindrical water nanochannels in Nafion fuel-

- cell membranes, (2007). doi:10.1038/nmat2074.
- [122] S.K. Young, S.F. Trevino, N.C. Beck Tan, Small-angle neutron scattering investigation of structural changes in Nafion membranes induced by swelling with various solvents, *J. Polym. Sci. Part B Polym. Phys.* 40 (2002) 387–400. doi:10.1002/polb.10092.
- [123] G. Gebel, O. Diat, Neutron and X-ray Scattering: Suitable Tools for Studying Ionomer Membranes, *Fuel Cells*. 5 (2005) 261–276. doi:10.1002/fuce.200400080.
- [124] NIST, NG7 SANS - Small Angle Neutron Scattering, (2018).
<https://www.nist.gov/ncnr/ng7-sans-small-angle-neutron-scattering>.
- [125] S.Y. Pshezhetskii, A.G. Kotov, V.K. Milinchuk, V.A. Roginskii, V.I. Tupikov, *EPR of Free Radicals in Radiation Chemistry*, John Wiley & Sons, New York, 1974.
- [126] E. LOVEJOY, M. BRO, G. BOWERS, CHEMISTRY OF RADIATION
CROSSLINKING OF BRANCHED FLUOROCARBON RESINS, *J. Appl. Polym. Sci.* 9 (1965) 401-. doi:10.1002/app.1965.070090201.
- [127] P. Gehringer, E. Proksch, P. Krenmayr, RADIOLYSIS OF
PERFLUOROMETHYLCYCLOHEXANE. 1. RADIOLYTIC PRODUCTS., *Int. J. Radiat. Phys. Chem.* 5 (1973) 113–125.
- [128] E.R. Clark, K. Flunder, J.R. Darwent, A.F. Gaines, B. Demirci, A.C. Jones, Fluorescence of Pyridine Extracts of Coals, *Energy and Fuels*. 1 (1987) 392–397. doi:10.1021/ef00005a003.
- [129] A.M.S. Galante, O.L. Galante, L.L. Camposa, Study on application of PTFE, FEP and PFA fluoropolymers on radiation dosimetry, *Nucl. Instruments Methods Phys.*

- Res. Sect. A Accel. Spectrometers, Detect. Assoc. Equip. 619 (2010) 177–180.
doi:10.1016/j.nima.2009.10.103.
- [130] M.I. Zaki, M. a. Hasan, F. a. Al-Sagheer, L. Pasupulety, In situ FTIR spectra of pyridine adsorbed on SiO₂-Al₂O₃, TiO₂, ZrO₂ and CeO₂: General considerations for the identification of acid sites on surfaces of finely divided metal oxides, Colloids Surfaces A Physicochem. Eng. Asp. 190 (2001) 261–274.
doi:10.1016/S0927-7757(01)00690-2.
- [131] D. Lim, H. Tsukada, A. Shigematsu, T. Yamada, K. Otsubo, E. Alexander, A.G. Stepanov, D.I. Kolokolov, M. Maesato, H. Kitagawa, Ammonia as Proton Conducting Medium Confined in Porous Materials Ammonia as proton conducting medium confined in porous materials, ChemRxiv. (2018).
doi:10.26434/chemrxiv.7319273.v1.
- [132] Y. Huang, A.M. Hussain, I.A. Robinson, E.D. Wachsman, Nanointegrated, High-Performing Cobalt-Free Bismuth-Based Composite Cathode for Low-Temperature Solid Oxide Fuel Cells, ACS Appl. Mater. Interfaces. 10 (2018) 28635–28643.
doi:10.1021/acsami.8b08911.
- [133] M.A. Danzer, Generalized Distribution of Relaxation Times Analysis for the Characterization of Impedance Spectra, (2019) 1–16.
- [134] T.H. Wan, M. Saccoccio, C. Chen, F. Ciucci, Influence of the Discretization Methods on the Distribution of Relaxation Times Deconvolution: Implementing Radial Basis Functions with DRTtools, Electrochem. Acta. 184 (2015) 483–499.
- [135] A. Weiß, S. Schindler, S. Galbiati, M.A. Danzer, R. Zeis, Distribution of Relaxation Times Analysis of High-Temperature PEM Fuel Cell Impedance

Spectra, *Electrochim. Acta.* 230 (2017) 391–398.

doi:10.1016/j.electacta.2017.02.011.

- [136] A.C. Carreras, H.E. Andrada, ScienceDirect Dynamics and spatial distribution of water in Nafion 117 membrane investigated by NMR spin-spin relaxation vez, 3 (2018) 2–9. doi:10.1016/j.ijhydene.2018.03.124.
- [137] M. Heinzmann, A. Weber, E. Ivers-ti, Advanced impedance study of polymer electrolyte membrane single cells by means of distribution of relaxation times, 402 (2018) 24–33. doi:10.1016/j.jpowsour.2018.09.004.
- [138] S.J. Osborn, M.K. Hassan, G.M. Divoux, D.W. Rhoades, K.A. Mauritz, R.B. Moore, Glass Transition Temperature of Perfluorosulfonic Acid Ionomers, (2007) 3886–3890. doi:10.1021/ma062029e.
- [139] M.A. Travassos, V. V Lopes, R.A. Silva, A.Q. Novais, C.M. Rangel, Assessing cell polarity reversal degradation phenomena in PEM fuel cells by electrochemical impedance spectroscopy, *Int. J. Hydrogen Energy.* 38 (2013) 7684–7696. doi:10.1016/j.ijhydene.2013.01.132.

